AD-A069 729 ARIZONA UNIV TUCSON DEPT OF GEOSCIENCES F/G 8/7
ORIGIN AND DISTRIBUTION OF GRAVEL IN STREAM SYSTEM OF ARID REGI--ETC(U)
DEC 78 R GERSON, W B BULL, L H FLEISCHHAUER F49620-77-C-0115
UNCLASSIFIED AFOSR-TR-79-0681 NL

1 OF 3
AD
A069729

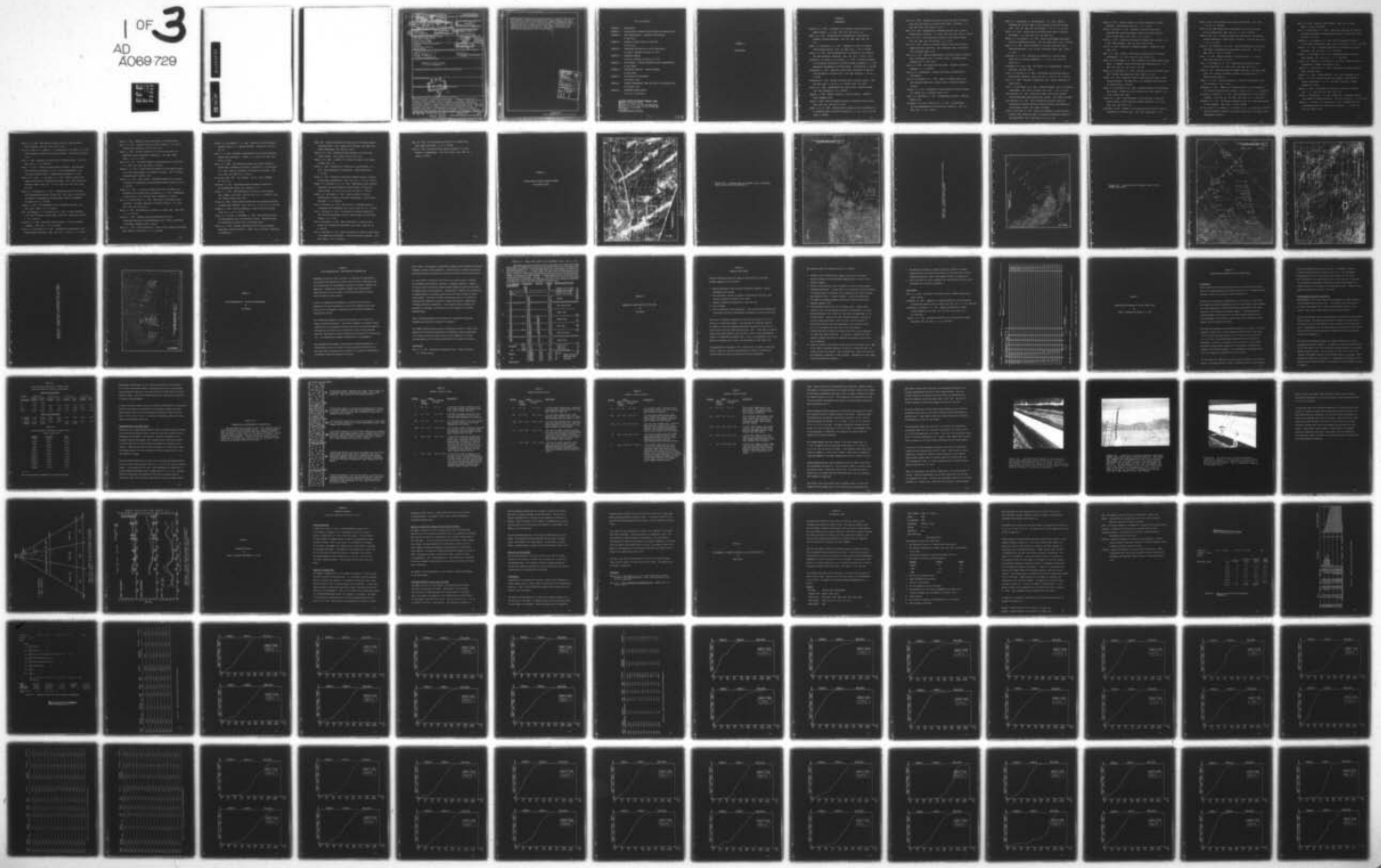

SECURITY CLASSIFICATION OF THIS PAGE (When Data Entered)

# REPORT DOCUMENTATION PAGE

READ INSTRUCTIONS BEFORE COMPLETING FORM

1. REPORT NUMBER: AFOSR-TR-79-0681
2. GOVT ACCESSION NO.
3. RECIPIENT'S CATALOG NUMBER

4. TITLE (and Subtitle): ORIGIN AND DISTRIBUTION OF GRAVEL IN STREAM SYSTEMS OF ARID REGIONS. Volume II. Appendices.

5. TYPE OF REPORT & PERIOD COVERED: Final repts.

6. PERFORMING ORG. REPORT NUMBER

7. AUTHOR(s): Ran Gerson, William B. Bull, Louis H. Fleischhauer, William C. Tucker, Jr., Lanny R. McHargue, Lenny Mayer, Ernest H.H. Shih

8. CONTRACT OR GRANT NUMBER(s): F49620-77-C-0115

9. PERFORMING ORGANIZATION NAME AND ADDRESS
Department of Geosciences
University of Arizona
Tucson, Arizona 85721

10. PROGRAM ELEMENT, PROJECT, TASK AREA & WORK UNIT NUMBERS
61102F 2309/A1

11. CONTROLLING OFFICE NAME AND ADDRESS
AFOSR/NP
Bolling AFB, Bldg.#410
Wash DC 20332

12. REPORT DATE: Dec 78

13. NUMBER OF PAGES: 187

14. MONITORING AGENCY NAME & ADDRESS (if different from Controlling Office): 240 p.

15. SECURITY CLASS. (of this report): unclassified

15a. DECLASSIFICATION/DOWNGRADING SCHEDULE

16. DISTRIBUTION STATEMENT (of this Report)

Approved for public release;
distribution unlimited.

17. DISTRIBUTION STATEMENT (of the abstract entered in Block 20, if different from Report)

18. SUPPLEMENTARY NOTES



19. KEY WORDS (Continue on reverse side if necessary and identify by block number)

20. ABSTRACT (Continue on reverse side if necessary and identify by block number)

The present study is concerned with production, transport and deposition of gravel in fluvial systems in hot arid regions. It attempts a definition of the variables affecting gravel origin, transport and deposition, assessment of significant changes in texture after deposition and evaluation of the compcsition of gravel buried in the upper alluvial section of depositional basins. The arid gemorphic environment is characterized by low precipitation, low rates of chemical weathering in most lithologic environments, high rates of mechanical weathering, scant vegetation and slow and sporadic soil development. General

DD FORM 1 JAN 73 1473 EDITION OF 1 NOV 65 IS OBSOLETE

UNCLASSIFIED

SECURITY CLASSIFICATION OF THIS PAGE (When Data Entered)

411 216

Climate-process framework places most hot deserts in regions receiving less than 150 mm/yr of mean annual precipitation. Major geomorphic processes and events, occurring in rocky deserts are: mechanical weathering; debris flows and wash on hillslopes; free wind activity, precipitation of salts in fractured and elastic rocks and soils, and floods. Differential areal geomorphic activity and differential runoff-sediment contribution are very strongly emphasized in the arid environment.

LIST OF APPENDICES

# APPENDIX A

# BIBLIOGRAPHY

## APPENDIX A

## BIBLIOGRAPHY


Bagnold, R. A., 1966. An approach to the sediment transport problem from general physics. U. S. Geol. Surv. Prof. Pap. 422-I, 37 p.

Baker, V. R., 1973. Paleohydrology and sedimentology of Lake Missoula flooding in eastern Washington. Geol. Soc. Amer. Spec. Publ. 144, 79 p.

Baker, V. R. and Ritter, D. F., 1975. Competence of rivers to transport coarse bedload material. Geol. Soc. Amer. Bull., v. 86, p. 975-978.

Beaty, C. B., 1970. Age and estimated rate of accumulation of an alluvial fan, White Mountains, California. Amer. Jour. Sci., v. 268, p. 50-77.

Birkeland, P. W., Burke, R. M. and Yount, J. C., 1976. Preliminary comments on late Cenozoic glaciations in the Sierra Nevada, in Mahaney, W. C. (ed.), Quaternary stratigraphy of the United States. Halstead Press, p. 283-295.

Blissenback, E., 1952. Relation of surface angle distribution to particle size distribution on alluvial fans. Jour. Sed. Petrology, v. 22, no. 1, p. 25-28.

Blissenback, E., 1954. Geology of alluvial fans in semiarid regions. Geol. Soc. Amer. Bull., v. 65, no. 2, p. 175-189, illus., Feb. 1954.

Bluck, B. J., 1964. Sedimentation on an alluvial fan in southern Nevada. Jour. Sed. Petrology, v. 34, p. 395-400.

Bogardi, J., 1974. Sediment transport in alluvial channels. Akademiai Kiado, Budapest, 826 p.

Brune, G., 1948. Rates of sediment production in midwestern United States. Soil. Cons. Serv. Tech Publ. 65, 40 p.

Brush, L. M., Jr., 1961. Drainage basins, channels and flow characteristics of selected streams in central Pennsylvania. U. S. Geol. Surv. Prof. Pap. 282-F, p. 145-181.

Bull, W. B., 1962. Relations of alluvial fan size and slope to drainage basin size and lithology in western Fresno County, California. U. S. Geol. Surv. Prof. Pap. 450-B, p. 51-53.

Bull, W. B., 1964. Geomorphology of segmented alluvial fans in western Fresno County, California. U. S. Geol. Surv. Prof. Pap. 352-E, p. 89-129.

Bull, W. B., 1973. Local base-level processes in arid fluvial systems. Geol. Soc. Amer. Abs. with Programs, v. 5, p. 562.

Bull, W. B., 1974. Effects of Holocene climate on arid fluvial systems, Whipple Mountains, California. Amer. Quaternary Assoc. 3rd Biennial Conf. Discussant Paper, p. 64.

Bull, W. B., 1977. Tectonic geomorphology of the Mojave Desert, California. Dept. of Geosciences, Univ. of Arizona, Tucson. Unpublished paper sponsored by U. S. Geol. Surv.

Bull, W. B., 1978. The alluvial-fan environment. Progress in Physical Geography, v. 1, p. 222-270.

Bull, W. B., in preparation. Tectonic and climatic geomorphology of arid regions.

Bull, W. B. and Schick, A. P., 1979. Impact of climatic change on an arid watershed, Nahal Yael, southern Israel. Quaternary Research, in press.

Carlson, F. R., 1974. Measurement of cobble abrasion in natural streams. M.S. Thesis, Univ. of Arizona, Tucson, 63 p.

Cooke. R. U. and Warren, A., 1973. Geomorphology in deserts. Batsford, London, 374 p.

Dalrymple, D. G., Cox, A. and Doell, R. R., 1965. Potassium-argon age and paleomagnetism of the Bishop Tuff, California. Geol. Soc. Amer. Bull., v. 76, p. 665-673.

Damon, P. E., Shafiqullah, M. and Scarborough, R. B., 1978. Revised chronology for critical stages in the evolution of the lower Colorado River. Geol. Soc. Amer. Abs. with Programs, v. 10, no. 3, p. 101-102.

Denny, C. S., 1965. Alluvial fans in the Death Valley region, California and Nevada. U. S. Geol. Surv. Prof. Pap. 466, 62 p.

Eberly, L. D. and Stanley, T. B., 1978. Cenozoic stratigraphy and geologic history of southwestern Arizona. Geol. Soc. Amer. Bull, v. 89, p. 932-940.

Emmett, W. W., 1976. Bedload transport in two large, gravel-bed rivers, Idaho and Washington. Proc. 3rd Fed. Inter-Agency Sedim. Symp., Denver, p. 4-114.

Fahnestock, R. K., 1963. Morphology and hydrology of a glacial stream, White River, Mt. Rainier, Washington. U. S. Geol. Surv. Prof. Pap. 422-A, 70 p.

Fairbridge, R. W. (ed.), 1968. The encyclopedia of geomorphology. Reinhold Book Corp., New York, 1295 p.

Flint, R. F. and Gale, W. A., 1958. Stratigraphy and radiocarbon dates at Searles Lake, California. Amer. Jour. Sci., v. 256, no. 10, p. 698-714.

Folk, R. L., 1974. Petrology of sedimentary rocks. Hemphil Publishing Co., Austin, 188 p.

Frye, J. C. and Willman, H. B., 1962. Morphostratigraphic units in Pleistocene stratigraphy. Amer. Assoc. Petroleum. Geol. Bull., v. 46, p. 112-113.

Fugro National, Inc., 1975. Geotechnical report, Yuma Proving Grounds/ Luke-Williams Bombing and Gunnery Range, Arizona. Cons. Report for SAMSO.

Fugro National, Inc., 1976. Soils engineering and seismic refraction investigation, Multiple Aim-Point Validation Program, Luke Bombing and Gunnery Range, Arizona. Cons. Report for SAMSO.

Gerson, R. and Inbar, M., 1974. Reviews and summaries of Israeli research projects. The International Symp. on Present-day Geomorphic Processes in Arid Environments. Zeit. Geom. Suppl. Bd. 21, p. 1-40.

Gerson, R., 1977. Sediment transport for desert watersheds in erodible materials. Earth Surface Processes, v. 2, p. 343-361.

Gerson, R. and Yair, A., 1974. Geomorphic evolution of some desert watersheds and certain paleoclimatic implications (Santa Katherina area, southern Sinai). Zeit. Geom., v. 19, p. 66-82.

Gessler, J., 1971. Beginning and ceasing of sediment motion, in Shen, H. W. (ed.), River mechanics. Wat. Res. Publ., Fort Collins.

Graf, W. H., 1971. Hydraulics of sediment transport. McGraw-Hill, New York, 513 p.

Hack, J. T., 1957. Studies of longitudinal stream profiles in Virginia and Maryland. U. S. Geol. Surv. Prof. Pap. 294-B, 97 p.

Hadley, R. F. and Schumm, S. A., 1961. Hydrology of the Upper Cheyenne River basin: B. sediment sources and drainage basin characteristics. U. S. Geol. Surv. Wat. Sup. Pap. 1531, p. 137-198.

Hadley, R. F. and Shown, L. M., 1976. Relation of erosion to sediment yield. Proc. 3rd Fed. Inter-Agency Sed. Conf., Denver, p. 1-139.

Hawley, J. W., 1975. Quaternary history of Dona Ana County region, south-central New Mexico. New Mexico Geol. Soc. Guidebook, 26th Field Conf. Las Cruces County, p. 139-150.

Hawley, J. W. and Wilson, W. E., 1965. Quaternary geology of the Winnemucca area, Nevada. Nevada Univ. Desert Research Inst. Tech. Report 5, 66 p., illus., tables, geol. maps.

Helley, E. J., 1969. Field measurement of the initiation of large bed particle motion in Blue Creek near Klamath, California. U. S. Geol. Surv. Prof. Pap. 562-G, 19 p.

Hjulström, F., 1935. Studies on the morphological activities of rivers as illustrated by the River Fyris. Geol. Inst. Upsala Bull., v. 25.

Hooke, R. leB., 1967. Processes on arid region alluvial fans. Jour. Geol., v. 75, no. 4, p. 438-460.

Hooke, R. leB., 1968. Steady-state relationships on arid region alluvial fans in closed basins. Amer. Jour. Sci., v. 266, p. 609-629.

Hooke, R. leB., 1972. Geomorphic evidence for Late-Wisconsin and Holocene tectonic deformation in Death Valley, California. Geol. Soc. Amer. Bull., v. 83, p. 2073-2098.

Hooke, R. leB. and Rohrer, L. W., 1977. Relative erodibility of source-area rock types as determined from second-order alluvial fans. Geol. Soc. Amer. Bull., v. 88, p. 1177-1182.

Hunt, C. B., 1969. Geologic history of the Colorado River. U. S. Geol. Surv. Prof. Pap. 669-C, p. 59-130.

Hunt, C. B. and Mabey, D. R., 1966. Stratigraphy and structure, Death Valley, California. U. S. Geol. Surv. Prof. Pap. 494-A, 162 p.

Inbar, M., 1977. Bedload movement and channel morphology in the Upper Jordon River. Ph.D. Dissert. The Hebrew University of Jerusalem, 204 p. (in Hebrew, English summary).

Inman, D. L., 1949. Sorting of sediments in light of fluid mechanics. Jour. Sed. Petrology, v. 19, p. 51-70.

Kellerhals, R., 1971. Comments on an improved method for size distribution of stream bed gravel by Luna B. Leopold. Wat. Res. Res., v. 7, p. 1045-1047.

Kellerhals, R. and Bray, D. I., 1971. Sampling procedures for coarse fluvial sediments. Proc. Amer. Soc. Civ. Eng., Jour. Hydr. Div., p. 1165-1179.

Krumbein, W. C., 1937. The effects of abrasion on the size, shape and roughness of rock fragments. Jour. Geol., v. 49, p. 420-482.

Ku, T-L, Bull, W. B., Freeman, S. T. and Knauss, K. G., in preparation, $Th^{230}/U^{234}$ dating of pedogenic carbonates in gravelly desert soils of the Vidal Valley, southeastern California.

Lane, E. W., 1955. Design of stable channels. Amer. Soc. Civ. Eng. Trans., v. 120, p. 1234-1260.

Lane, E. W. and Carlson, E. J., 1953. Some factors affecting the stability of canals constructed in coarse granular material. Intern. Assoc. Hydr. Res. Proc., p. 37-48.

Langbein, W. B. and Schumm, S. A., 1958. Yield of sediment in relation to mean annual precipitation. Amer. Geoph. Union Trans., v. 39, p. 1076-1084.

Leopold, L. B., 1970. An improved method for size distribution of stream bed gravel. Wat. Res. Res., v. 6, p. 1357-1366.

Leopold, L. B. and Emmett, W. W., 1976. Bedload measurements, East Fork River, Wyoming. Nat. Acad. Sci., v. 73, p. 1000-1004.

Leopold, L. B., Wolman, M. G. and Miller, J. P., 1964. Fluvial processes in geomorphology. Freeman, San Francisco, 522 p.

Longwell, C. R. and Flint, R. F., 1962. Introduction to physical geology. Wiley, New York, 504 p.

Mabbutt, J. A., 1977. Desert landforms. M.I.T. Press, Cambridge, 340 p.

Mackin, J. H., 1963. Rational and empirical methods of investigation in geology, in Albriton, C. A., Jr., The fabric of geology. Freeman, Stanford, p. 135-163.

Maddock, T., 1969. The behavior of straight open channels with movable beds. U. S. Geol. Surv. Prof. Pap. 622-A, 70 p.

Merriam, R. and Bischoff, J. L., 1975. Bishop Ash: a widespread volcanic ash extended to southern California. Jour. Sed. Petrology, v. 45, p. 207-211.

Metzger, D. G., Loeltz, D. S. and Irelna, B., 1973. Geohydrology of the Parker-Blythe-Cibola area, Arizona and California. U. S. Geol. Surv. Prof. Pap. 486-G, 130 p.

Miller, J. P., 1958. High mountain streams, State Bur. Mines and Miner. Res., New Mexico Inst. Min. Tech., Mem. 4, 53 p.

Nie, N. H., Hull, C. H., Jenkins, J. G., Steinbrenner, K. and Bent, D. H., 1975. SPSS, Statistical Package for the Social Sciences. McGraw-Hill, New York, 675 p.

Nevin, C., 1946. Competency of moving water to transport debris. Geol. Soc. Amer. Bull., v. 57, p. 651-674.

Novak, I. D., 1973. Predicting coarse sediment transport. The Hjulström curve revisted, in Morisawa, M. (ed.), Fluvial geomorphology. New York State University Publ. in Geomorphology, Binghamton, p. 13-25.

Osborn, M. B., Lane, L. J. and Kagan, R. S., 1971. Models of spacial and temporal distribution of thunderstorm rainfall. Proc. Symp. Statistical Hydrology, Tucson, Sept. 1971. U.S.D.A. Agric. Res. Ser., Misc. Publ. No. 1275.

Osborn, H. B. and Renard, K. G., 1970. Thunderstorm runoff on the Walnut Gulch experimental watershed, Arizona, USA. Proc. Symp. on the Results of Research on Representative and Experimental Basins, IASH-UNESCO, Wellington (N.Z.), p. 455-464.

Peltier, L., 1950. The geographical cycle in periglacial regions. Ann. Amer. Assoc. Geogr., v. 4, p. 214-236.

Peng, T-H, Goddard, J. G. and Broecker, W. S., 1978. A direct comparison of $^{14}C$ and $^{230}Th$ ages at Searles Lake, California. Quaternary Research, v. 9, p. 319-329.

Plumley, W. J., 1948. Black Hills terrace gravels: a study in sediment transport. Jour. Geol., v. 56, p. 526-577.

Porter, S. C. and Denton, G. H., 1967. Chronology of neoglaciation in the North American Cordillera. Amer. Jour. Sci., v. 265, no. 3, p. 177-210.

Raisz, E., 1957. Landforms of the United States, 6th Revised Edition.

Rana, S. A., 1971. Sediment sorting in alluvial channels. M.Sc. Thesis, Colorado State University, Fort Collins, 114 p.

Rognon, P., 1967. Climatic influences on the African Hogar during the Quaternary, based on geomorphic observations. Ann. Amer. Assoc. Geogr., v. 57, p. 115-157.

Rubey, W. W., 1937. The forces required to move particles on a stream bed. U. S. Geol. Surv. Prof. Pap. 189-E, p. 121-141.

Schenker, A. R., 1977. Particle-size distribution of late Cenozoic gravels on an arid region piedmont, Gila Mountains, Arizona. Univ. of Arizona. Unpublished Masters thesis, 118 p.

Schick, A. P., 1970. Desert floods. IAHS-UNESCO Symposium on the Results of Research on Representative and Experimental Basins, Wellington (N.Z.), p. 478-492.

Schick, A. P., 1977. A tentative sediment budget for an extremely arid Watershed in the southern Negev, in Doehring, O. D. (ed.), Geomorphology in arid regions. Proc. 8th Geom. Symp., Binghamton, p. 139-164.

Scott, K. M. and Gravlee, G. C., 1968. Flood surge on the Rubicon River, California - hydrology, hydraulics and boulder transport. U. S. Geol. Surv. Prof. Pap. 422-M, 40 p.

Sharon, D., 1972. The spottiness of rainfall in a desert area. Jour. Hydr., v. 17, p. 161-175.

Shields, A., 1936. Anwendung der ahnlichkeitsmochanik und der turbulenzorschung auf die geschiebebewegung: Mitt. Preuss. Versuchsanst. F. Wasserbau. Schiffbau, Heft 26, Berlin.

Shulits, S., 1936. Fluvial morphology in terms of scope, abrasion and bedload. Amer. Geophys. Union Trans., v. 17, p. 440-444.

Slatyer, R. O. and Mabbutt, J. A., 1964. Hydrology of arid and semiarid regions, in Chow, V. T., Applied hydrology. McGraw-Hill, New York, Sec. 24.

Smith, G. I., 1962. Subsurface stratigraphy of Late Quaternary deposits, Searles Lake, California: a summary. U. S. Geol. Surv. Prof. Pap. 450-C, p. 65-69.

Smith, G. I., 1968. Late Quaternary geologic and climatic history of Searles Lake, southeastern California, in Morrison, R. B. and Wright, H. E. (eds.), Means of correlation of Quaternary successions. Utah Univ. Press, Salt Lake City, p. 293-310.

Soil Survey Staff, 1975. Soil taxonomy. U.S.D.A., Agric. Handbook No. 436, 754 p.

Sternberg, H., 1875. Untersuchungen über das Längen und Querprofil geschiebeführender Flüsse. Zeit. Bauwesen, v. 25

Straub, L. G., 1935. Some observations of sorting of river sediments. Amer. Geophys. Union Trans., 16th Ann. Mtg. Pt. 2, p. 463-467, 6 Figs., Nat. Research Council, Aug. 1935.

Stuiver, M., 1964. Carbon isotopic distribution and correlated chronology of Searles Lake sediments. Amer. Jour. Sci., v. 262, no. 3, p. 377-392.

Sundborg, A., 1956. The river Klarälven, a study of fluvial processes. Geogr. Ann., v. 38, p. 127-316.

Tucker, W. C., Steiner, E. and Budden, T., 1974. Rock descriptions from the Sheep Mountain area, Gila Mountains, Arizona. Unpublished paper for Geosciences 350 course, Univ. of Arizona, Tucson.

Tucker, W. C., 1979. Geologic reconnaissance of the Aguila Mountains quadrangle, Arizona (MS Thesis). Tucson, Univ. of Arizona. Manuscript in preparation.

USDA, 1973. Present and prospective technology for predicting sediment yield and sources. Proc. Sediment-Yield Workshop, USDA Sedim. Lab., Oxford, Mississippi, 1972, ARS-S-40, 285 p.

Wilson, E. D., 1933. Geology and mineral deposits of southern Yuma County, Arizona. Ariz. Bureau of Mines, Bull. 134.

Wilson, E. D., 1962. A résumé of the geology of Arizona, Ariz. Bureau of Mines, Bull. 171.

Wilson, L., 1969. Morphogenetic classification, in Fairbridge, R. W. (ed.), The encyclopedia of geomorphology. Rienhold Book Corp., p. 717-729.

Wilson, L., 1973. Variation of mean annual sediment yield as a function of mean annual precipitation. Amer. Jour. Sci., v. 273, p. 349-353.

Wolman, M. G. and Brush, L. M., Jr., 1961. Experimental study of factors controlling the size and shape of stream channels in coarse non-cohesive sands. U. S. Geol. Surv. Prof. Pap 382-G, p. 183-210.

Wolman, M. G. and Gerson, R., 1978. Relative scales of time and effectiveness of climate in watershed geomorphology. Earth Surface Processes, v. 3, p. 189-209.

Yair, A. and Gerson, R., 1974. Mode and rate of escarpment retrat in an extremely arid environment. Zeit. Geom., Suppl. Bd. 21, p. 202-215.

Yair, A. and Klein, M., 1973. The influence of surface properties on flow and erosion processes on debris covered slopes in an arid area. Catena, v. 1, p. 1-18.

Yair, A. and Lavee, H., 1974. Areal contribution to runoff on scree slopes in an extreme arid environment. Zeit. Geom., Suppl. Bd. 21, p. 106-121.

Yair, A. and Lavee, M., 1977. Areal contribution to runoff on scree slopes in an extreme arid environment: a simulated rainstorm experiment. Zeit. Geom. Suppl., v. 21, p. 106-121.

Yatsu, E., 1955. On the longitudinal profile of the graded river. Amer. Geoph. Union Trans., v. 36, p. 655-663.

Young, A., 1974. The rate of slope retreat, in Brown, E. M. (ed.), Progress in geomorphology. Inst. Brit. Geogr., Spec. Publ. No. 7, London, p. 65-78.

# APPENDIX B

## LOCATION MAPS OF STUDIED FLUVIAL SYSTEMS

## AND SAMPLING SITES

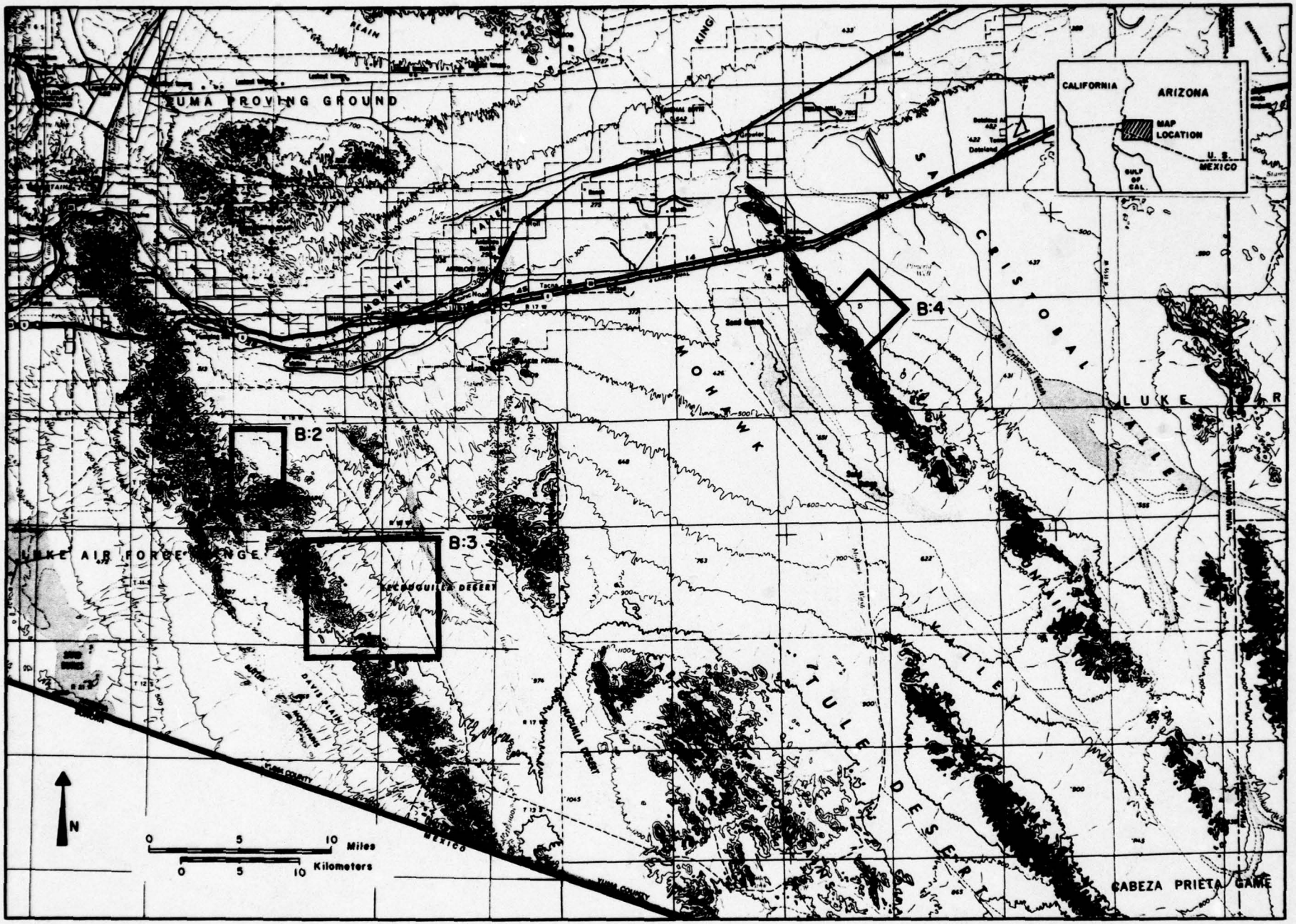


Figure B-1 Location map of studied areas in southwestern Arizona.

Figure B-2 Location map of sampled sites in Boulder Wash, northern Gila Mountains.

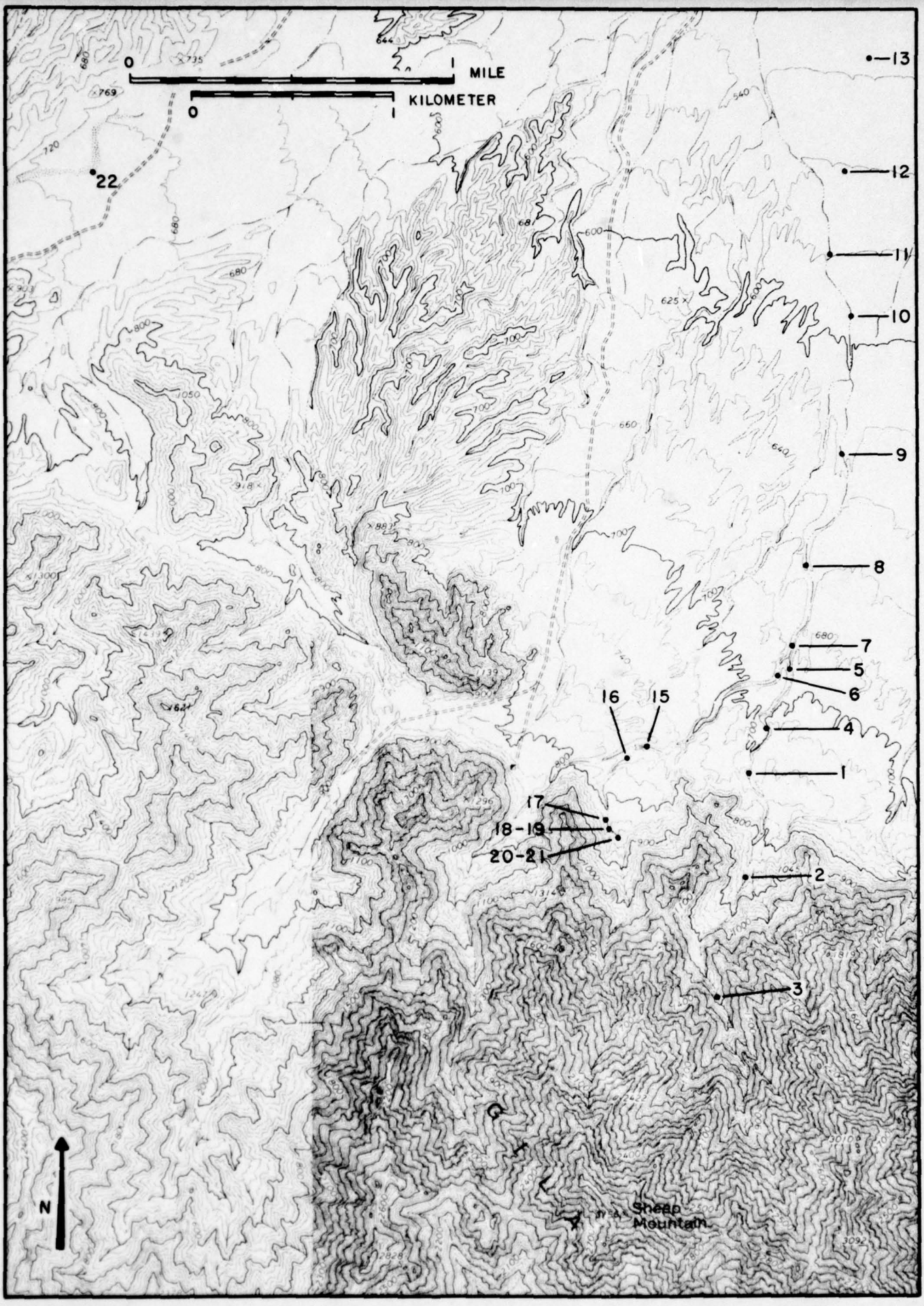
0
1
MILE
0
1
KILOMETER
22
13
12
11
10
9
8
7
5
6
16
15
4
1
17
18-19
20-21
2
3
N
Sheep
Mountain

Figure B-3 Location map of sampled sites in Cipriano Pass area, southern Gila Mountains.

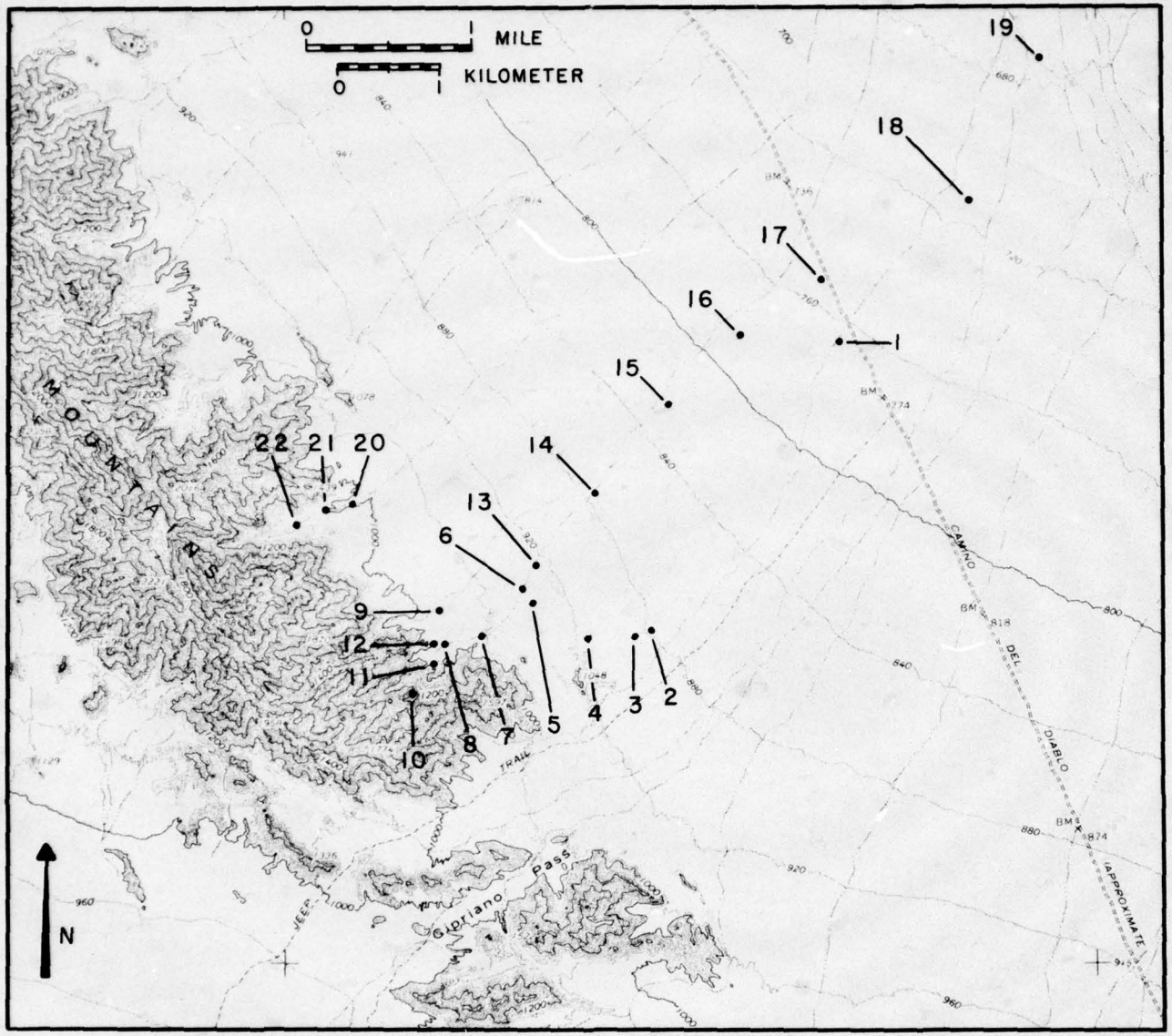
0 1 MILE
0 1 KILOMETER
MOUNTAINS
CAMINO DEL DIABLO
Gilpriano Pass
JEEP TRAIL
(APPROXIMATE)
N
1
2
3
4
5
6
7
8
9
10
11
12
13
14
15
16
17
18
19
20
21
22

Figure B-4 Location map of sampled sites in the Mohawk Mountains.

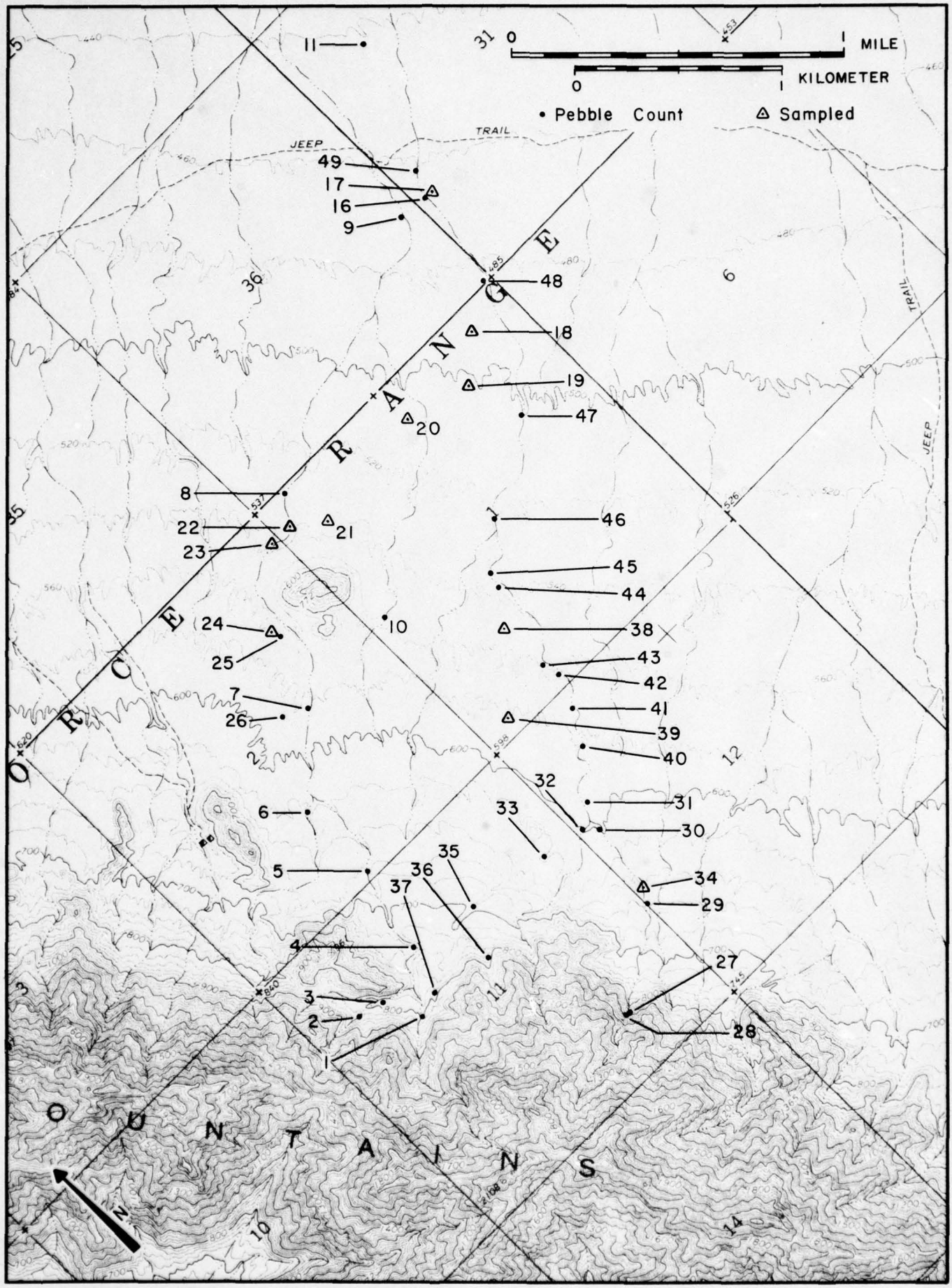
0 1 MILE
0 1 KILOMETER
• Pebble Count
△ Sampled
JEEP
TRAIL
49
17
16
9
11
48
18
19
47
20
8
22
23
21
46
45
44
24
25
10
38
43
42
41
7
26
39
40
6
5
4
3
2
1
32
31
33
30
35
36
37
34
29
27
28
R A N G E
O R O C E
O U N T A I N S
N

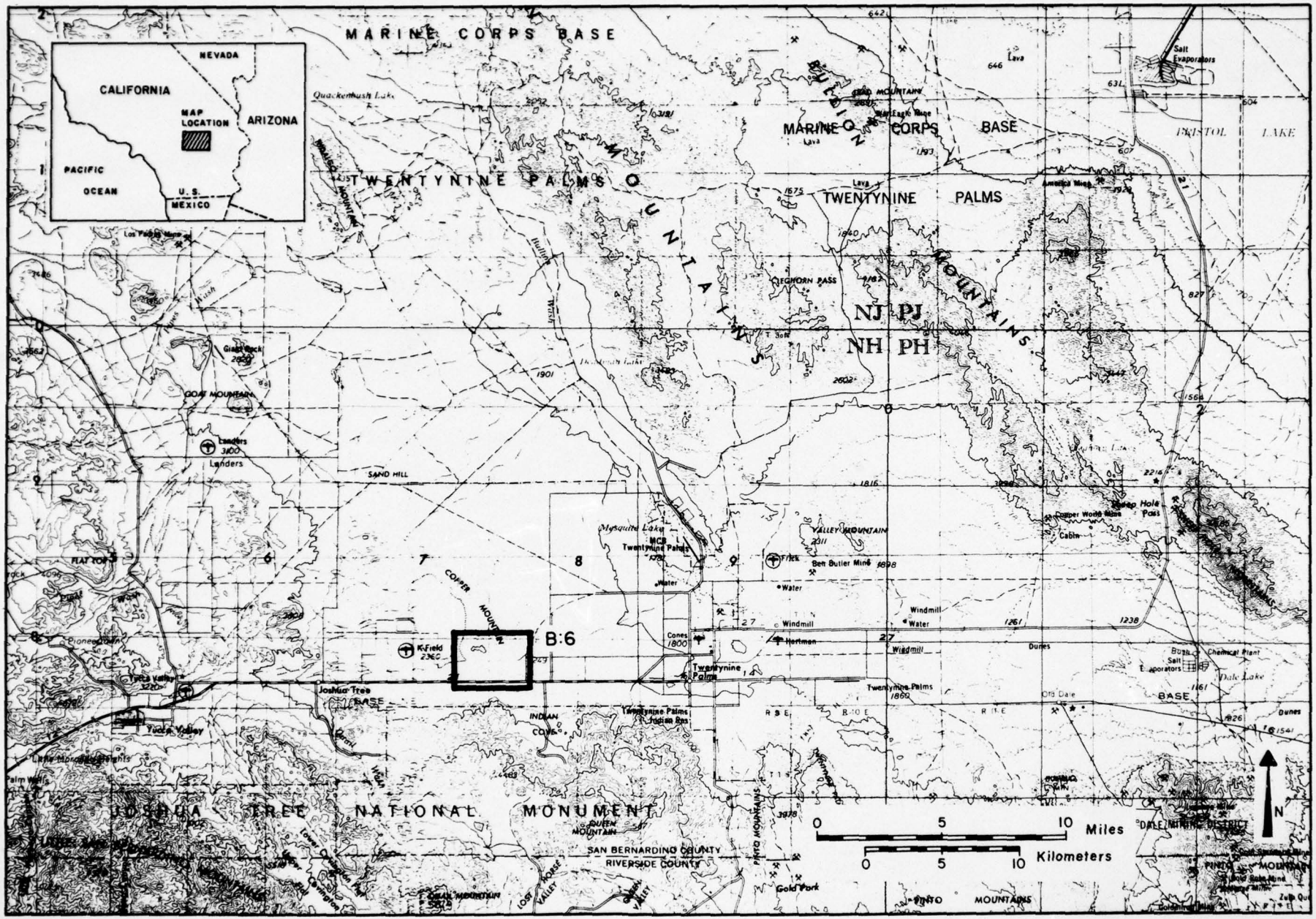


Figure B-5 Location map of study area in southern California.

Figure B-6 Location map of sampled sites in Copper Mountains (I-Bumble Bee; II-Tall Tale; III-Lost Home).

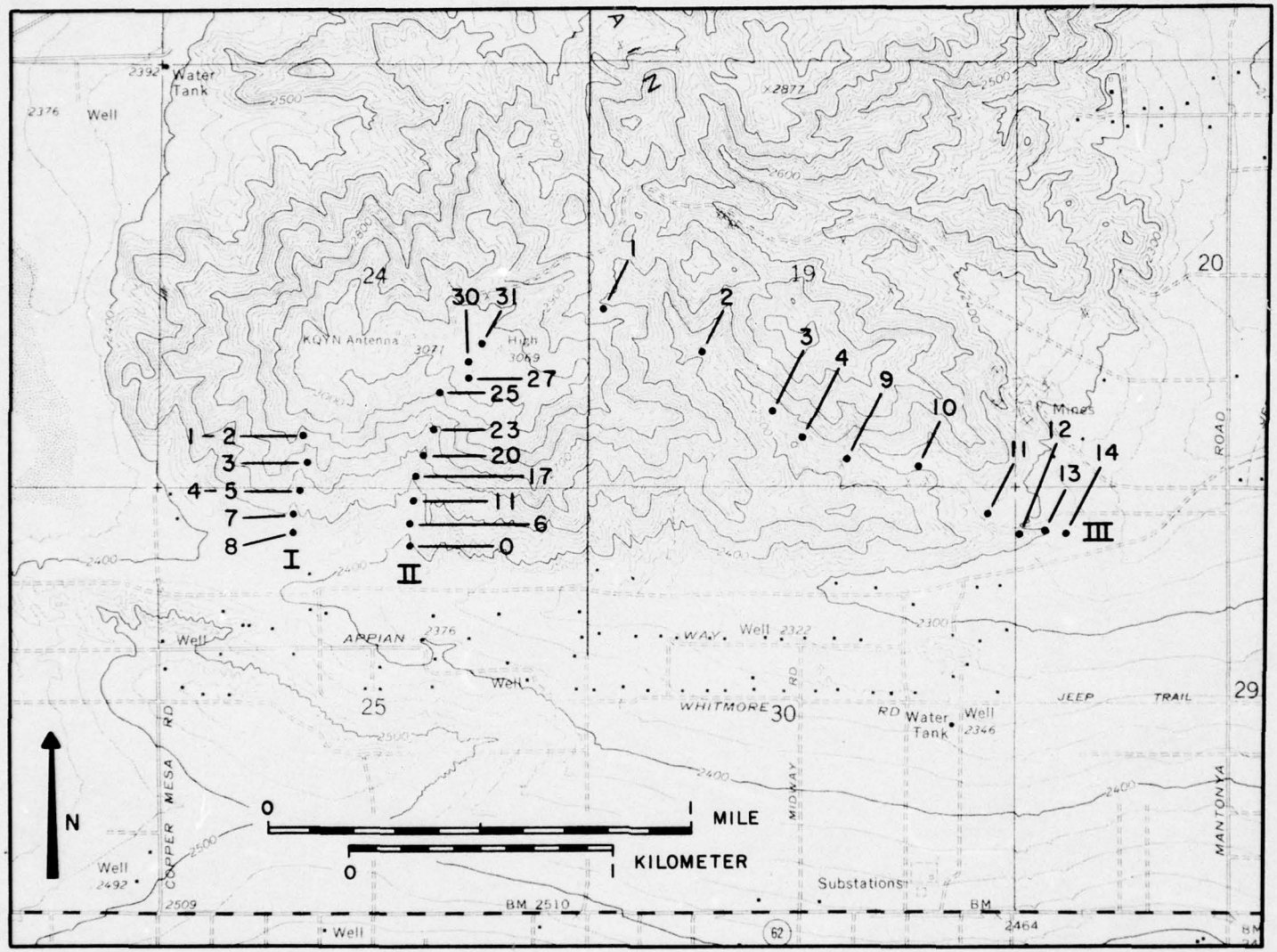
Water Tank
Well
KQYN Antenna
High 3069
3071
24
19
20
25
30
29
1
2
3
4
9
10
11
12
13
14
I
II
III
30
31
27
25
23
20
17
11
6
0
1-2
3
4-5
7
8
APPIAN
WAY
Well 2322
WHITMORE
RD
Water Tank
Well 2346
JEEP TRAIL
ROAD
COPPER MESA RD
MIDWAY RD
MANTONYA
Well 2492
Substations
BM 2510
BM 2464
Well
N
0
1
MILE
KILOMETER
62

# APPENDIX C

## SIZE CHARACTERISTICS: PRACTICAL CONSIDERATIONS

BY

RAN GERSON

# APPENDIX C

## SIZE CHARACTERISTICS - SOME PRACTICAL CONSIDERATIONS

Measurement of particle size in clastics is conducted for understanding the processes that produced the measured sizes and their distribution and for reconstructing the environmental conditions of sediment transport and deposition. Although many thousands of samples were characterized quantitatively all over the world, size distribution-process relationships for gravel is still obscure.

Criteria to characterize environments, on the basis of statistical measures of the size distribution, are still only moderately successful and are still not diagrastic enough for process-oriented assessements, especially for gravel.

The conventional approach to particle size analysis is to treat it as having a gaussian distribution. Statistical treatments of granular clastic sediments are on the assumption that most grain-size distributions approach log-normality and, hence, may be represented by mean size and standard deviation, describing the central tendency and the spread of the distribution cure. For definitions of sediment characteristics, see Appendix G.

Many sediments are polymodal, being mixtures of combined populations. In stream channels, this is a result of various processes operating at the same time (such as suspension and traction) and of mixture of superposition of sediments related to different flow events.

Still, there is no experience of population separation and subsequent statistical treatment of coarse fluvial sediments. Identification of component populations and relating their distributions to specific flow events have not been done yet.

It is not within the objectives and scope of the present report to develop the procedures and statistical treatment of polymodal population. However, it has to be kept in mind that treated sediment samples may deviate from ideal log-normal grain size distributions. Examinations of sediment size distributions of samples chosen in the present project shows that many of them are skewed and/or bimodal. The source of these characteristics may lie in production transportation, deposition, mixture of original populations, superposition of deposits and their combinations. Until sampling during transport and deposition is performed, one should not treat the samples in a process-oriented manner.

Hence, although misleading to some extent, the traditional statistical treatment was selected, as presented in Appendix G.

The commonly used grain-size scales are presented in Table C-3 (Folk, 1974). Because of the technical difficulties of sufficiently accurate measurement in the field of particles smaller than 8 mm (see Appendix D), we have included pebbles of 4 to 8 mm size range within the "granule" size class.

BIBLIOGRAPHY

Folk, R. L., 1974. Petrology of sedimentary rocks. Hemphil Publishing Co., Austin, 188 pp.

TABLE C-3: GRAIN SIZE SCALES FOR SEDIMENTS (Folk, 1974, p. 25)

The grade scale most commonly used for sediments is the Wentworth (1922) scale which is a logarithmic scale in that each grade limit is twice as large as the next smaller grade limit. The scale starting at 1mm and changing by a fixed ratio of 2 was introduced by J. A. Udden (1898), who also named the sand grades we use today. However, Udden drew the gravel/sand boundry at 1mm and used different terms in the gravel and mud divisions. For more detailed work, sieves have been constructed at intervals $\sqrt[2]{2}$ and $\sqrt[4]{2}$. The ϕ (phi) scale, devised by Krumbein, is a much more convenient way of presenting data than if the values are expressed in millimeters, and is used almost entirely in recent work.

| U. S. Standard Sieve Mesh # | Millimeters | Microns | Phi (ϕ) | Wentworth Size Class | |
|---|---|---|---|---|---|
| | 4096 | | -20 | | |
| | 1024 | | -12 | | |
| Use | 256 | | -10 | Boulder (-8 to -12ϕ) | GRAVEL |
| wire | 64 | | - 8 | Cobble (-6 to -8ϕ) | |
| squares | 16 | | -6 | Pebble (-2 to -6ϕ) | |
| 5 | 4 | | -4 | | |
| 6 | 3.36 | | -2 | | |
| 7 | 2.83 | | -1.75 | | |
| 8 | 2.38 | | -1.5 | Granule | |
| 10 | 2.00 | | -1.25 | | |
| 12 | 1.68 | | -1.0 | | |
| 14 | 1.41 | | -0.75 | | |
| 16 | 1.19 | | -0.5 | Very coarse sand | |
| 18 | 1.00 | | -0.25 | | |
| 20 | 0.84 | | 0.0 | | |
| 25 | 0.71 | | 0.25 | | |
| 30 | 0.59 | | 0.5 | Coarse sand | |
| 35 | 1/2 — 0.50 | 500 | 0.75 | | |
| 40 | 0.42 | 420 | 1.0 | | |
| 45 | 0.35 | 350 | 1.25 | | |
| 50 | 0.30 | 300 | 1.5 | Medium sand | |
| 60 | 1/4 — 0.25 | 250 | 1.75 | | |
| 70 | 0.210 | 210 | 2.0 | | |
| 80 | 0.177 | 177 | 2.25 | | |
| 100 | 0.149 | 149 | 2.5 | Fine sand | |
| 120 | 1/8 — 0.125 | 125 | 2,75 | | |
| 140 | 0.105 | 105 | 3.0 | | |
| 170 | 0.088 | 88 | 3.25 | | |
| 200 | 0.074 | 74 | 3.5 | Very fine sand | |
| 230 | 1/16 — 0.0625 | 62.5 | 3.75 | | |
| 270 | 0.053 | 53 | 4.0 | | |
| 325 | 0.044 | 44 | 4.25 | | |
| | 0.037 | 37 | 4.5 | Coarse silt | |
| | 1/32 — 0.031 | 31 | 4.75 | | |
| Analyzed | 1/64 0.0156 | 15.6 | 5.0 | | |
| | 1/128 0.0078 | 7.8 | 6.0 | Medium silt | |
| by | 1/256 0.0039 | 3.9 | 7.0 | Fine silt | |
| | 0.0020 | 2.0 | 8.0 | Very fine silt | MUD |
| Pipette | 0.00098 | 0.98 | 9.0 | | |
| | 0.00049 | 0.49 | 10.0 | Clay | |
| or | 0.00024 | 0.24 | 11.0 | (Some use 2μ or 9ϕ as the clay boundry) | |
| | 0.00012 | 0.12 | 12.0 | | |
| Hydrometer | 0.00006 | 0.06 | 13.0 | | |
| | | | 14.0 | | |

# APPENDIX D

## SAMPLING OF LOOSE CLASTICS IN THE FIELD

BY

RAN GERSON

# APPENDIX D

## SAMPLING LOOSE GRAVEL

Several difficulties arise when sampling representatively gravel-bed streams, especially in arid regions.

1. Spatial variations in bar and swale sedimentary landscape, lateral, longitudinal and vertical.
2. Time variations, related to frequency, magnitude and resulting superposition of gravel of different flow events.
3. Mixing of sedimentary populations in space and time.
4. Size of sample.
5. Field constraints in size measurement. These involve mainly difficulties in measuring partially exposed gravel and sampling of the top layer only.

Bulk sieve or volumetric sampling is by far the most accurate, but is not practical in gravel-bed channels. Grid sampling with frequency analysis by number is a practical sampling method which represents fairly well the surface layer of the bed (Kellerhals and Bray, 1971). Using tape, an operator walks along several parallel lines and picks a rock at every predetermined interval, as described by Leopold (1970). The B, or intermediate, axis of the particle is measured with a scale and registered on a form (Table D-4).

As demonstrated by Kellerhals (1971), conversion of the number of particles within a given size interval into percentage by weight of the same size fraction should be used for constructing the size distribution.

The procedure used in the present project is as follows:

1. Decision on the interval between sampling sites along the stream. Straight reaches at the predetermined sampling point or close to them should be sampled.
2. Stretch a tape along the reach and decide on interval of point samples (individual particles). In many cases, it is necessary, either for getting the required number of particles or for representing the reach to sample along parallel lines. In narrow channels, it may prove impractical.
3. The sample is considered complete when about 100 particles have been measured (Leopold, 1970).
4. Pick-up methods usually fail for the smaller sizes. Leopold (1970), considers 2 mm to be the smallest particle to be measured in the field, whereas Kellerhals (1971) points out that below 8 mm measurement is not accurate enough. Granule sizes pose a measuring problem. One may try to pick up particles between 2 and 8 mm, but it would be better to follow the 8 mm limit for scale measurement in the field and include the 2 to 8 mm fraction with the sand in the sieve analysis.
5. Granules and sand are analyzed by sieves, which also aid in separating the fines from coarser materials. Dry sieving is suggested for loose clastics, whereas wet sieving is essential for aggregated clastics that are not cemented.
6. Fines are treated in this report collectively as silt and sand sizes. Most of the fines in surficial materials, as well as in buried sections, are within the silt size classes. Only in buried soils, salts, silts and clay are separated, in addition to sand and gravel. Procedures for these separations are described in Appendix F.

7. The materials fractioned to number of particles (gravel) or weights (sands and fines) are treated statistically to find mean sizes, sorting (standard deviation), using a SPSS computer program (see Appendix G).
8. Grain size scale for clastic sediments are used according to Folk (1974). Definitions are presented in Appendix C.

BIBLIOGRAPHY

Folk, R. L., 1974. Petrology of sedimentary rocks. Hemphil Publishing Co., Austin, 188 pp.

Kellerhals, R., 1971. Comments on an improved method for size distribution pf stream bed gravel by Luna B. Leopold. Wat. Res. Res., v. 7, pp. 1045-1047.

Kellerhals, R. and Bray, D. I., 1971. Sampling procedures for coarse fluvial sediments, Proc. Amer. Soc. Civ. Eng., Jour. Hydr. Div., pp. 1165-1179.

Leopold, L. B., 1970. An improved method for size distribution of stream bed gravel. Wat. Res. Res., v. 6, pp. 1357-1366.

SITE NAME: _____ SAMPLE NO.: _____ DATE: _____ LITHOLOGY: _____

SAMPLED BY: _____

| SIEVE OPENING, mm | MEAN SIZE OF FRACTION $\bar{D}$, mm | NO. OF ROCKS N | % OF $\Sigma N$ | % SMALLER | FREQ. $x\bar{D}$ | | |
|---|---|---|---|---|---|---|---|
| 4096 | 5016 | | | | | | 4096 |
| 2896 | 3556 | | | | | | 2896 |
| 2048 | 2504 | | | | | | 2048 |
| 1448 | 1778 | | | | | | 1448 |
| 1024 | 1252 | | | | | | 1024 |
| 724 | 889 | | | | | | 724 |
| 512 | 632 | | | | | | 512 |
| 362 | 453 | | | | | | 362 |
| 256 | 303 | | | | | | 256 |
| 181 | 214 | | | | | | 181 |
| 128 | 152 | | | | | | 128 |
| 91 | 107 | | | | | | 91 |
| 64 | 76 | | | | | | 64 |
| 45 | 54 | | | | | | 45 |
| 32 | 38 | | | | | | 34 |
| 22.6 | 26.8 | | | | | | 22.6 |
| 16 | 19 | | | | | | 16 |
| 11.3 | 13.4 | | | | | | 11.3 |
| 8 | 9.5 | | | | | | 8 |
| 5.6 | 6.6 | | | | | | 5.6 |
| 4 | 4.7 | | | | | | 4 |
| 2.8 | 3.5 | | | | | | 2.8 |
| 2 | 2.4 | | | | | | 2 |
| < 2 | | | | | | | < 2 |
| | | $\Sigma N =$ | | | $\Sigma =$ | | |

_____ _____, $\bar{x} = \frac{\Sigma \text{FREQ. } x\bar{D}}{100\ \%} =$ _____

MAXIMUM SIZE OBSERVED (TEN LARGEST) _____

Table D-4 Sampling chart for loose gravel.

# APPENDIX E

## DESCRIPTION AND SAMPLING OF THE MX TRENCH WALLS

BY

LANNY R. McHARGUE AND ERNEST H. H. SHIH

APPENDIX E

DESCRIPTION AND SAMPLING OF THE MX TRENCH WALLS

INTRODUCTION

The MX 20,000 ft (6,096 m) Demonstration Trench trends NE from the eastern flank of the Mohawk mountains and transects nearly all of its piedmont slope. The exact location of the trench is shown in Appendix K.

Sections of the trench wall approximately 3m (10 ft) and 6 m (20 ft) deep were exposed by trenching operations along its entire length, which afforded an unusual opportunity to observe depositional and pedogenic trends along nearly all of the Mohawk-San Cristobal piedmont. A reconnaissance and sampling program of some sections of the trench enabled observations of the stratigraphy, soil properties, and particle size distribution as they ranged along the length of the trench.

The trench was excavated by two different machines in two steps: the first excavated a trench 2.8 m (9.19 ft) deep with vertical walls in the lower 1.23 m (4.04 ft) and walls angled out at $35^{o}$ from vertical in the upper 1.57 m (5.15 ft); the second machine excavated the vertical walls an additional 3 m (9.84 ft) to a depth of 5.8 m (19.03 ft). Due to safety regulations, detail sample gathering and stratigraphic description was limited to the shallow excavation. Only photographic reconnaissance and spoil pile sampling was possible with the deep trench.

In this report, all reference to position along the length of the trench is given in the survey engineers' format: hundreds of feet plus feet distance

from the northeasterly origin of the trench. For example, a station 1,050 feet from the origin is written as 10 + 50 ft. The photography accompanying the text is scaled with a measuring tape in feet which, due to the angle of the upper trench walls, is not true depth. References to units given in photographic captions are in tape measure depth since these are merely for the purpose of illustrating the units. However, stratigraphic descriptions are given in true depth.

RECONNAISSANCE, SAMPLING & DESCRIPTION

Reconnaissance of the trench consisted of photography and sample gathering from the trench walls and spoil pile. Two personnel from the University of Arizona took samples while a third took photographs from the ground surface. An air force representative acted as safety observer.

Access to the shallow trench was made possible by lowering an 18 foot ladder into the trench. Two personnel then moved the ladder to the other side of the trench to set up a wide measuring tape on the far wall for photographic scale. Approximately 2 kg (4.4 lbs) samples were obtained with hand trowels from each distinct horizon and placed in sample bags for later laboratory analysis (see Appendix F).

The results of laboratory analysis are listed in Tables E3a & b and are graphically depicted in Figure E4. In addition, the general characteristics of the trench walls, its color, consistency, horizon boundaries, and maximum particle sizes were noted. In the interval 74 + 54 to 193 + 90 ft, four complete stratigraphic sections of the shallow trench are described. These are given in Tables E6, E7, E8 and E9. A generalized stratigraphic column, showing the most salient features of each distinct unit and boundary is given in Table E5.

TABLE E3a

Clay and Ca-salt percentages of samples taken above and below the erosional unconformity

Above the unconformity

| Horizon & Subhorizon | Section A (Station 74+54) Ca-Salts | Clay | Section B (Station 94+12) Ca-Salts | Clay | Section C (Station 142+75) Ca-Salts | Clay | Section D (Station 193+90) Ca-Salts | Clay |
|---|---|---|---|---|---|---|---|---|
| V | 5.09 | 3.78 | | | | | | |
| VI | 4.64 | 4.93 | 4.01 | 5.30 | 4.46 | 1.63 | 15.33 | 4.87 |
| VII | 4.12 | 3.25 | 5.15 | 0.93 | 1.83 | 12.42 | 20.07 | 5.37 |
| VIII | 29.82 | 18.57 | 2.95 | 2.65 | 5.93 | 17.78 | 5.73 | 2.99 |

Below the unconformity

| | | | | | | | | |
|---|---|---|---|---|---|---|---|---|
| IX (upper) | 27.73 | 13.20 | 11.85 | 8.42 | 4.85 | 18.82 | 29.67 | 9.89 |
| (lower) | 1.91 | 12.49 | 10.82 | 11.21 | | | | |
| X (upper) | 23.57 | 24.14 | 11.85 | 10.75 | 8.99 | 22.99 | 24.79 | 5.67 |
| (lower) | 26.72 | 35.89 | | | 12.24 | 14.83 | | |

TABLE E3b

Clay and Ca-salt percentages of samples taken from the spoil pile

| Station | Ca-Salts | Clay |
|---|---|---|
| 32+00 | 12.85 | 23.32 |
| 43+50 | 16.91 | 10.82 |
| 55+00 | 11.39 | 15.79 |
| 73+00 | 28.86 | 37.14 |
| 94+00 | 13.81 | 13.57 |
| 114+00 | 13.14 | 11.50 |
| 135+00 | 16.82 | 11.01 |
| 148+00 | 27.74 | 8.97 |
| 158+00 | 32.68 | 14.25 |
| 168+42 | 23.65 | 10.87 |
| 176+85 | 30.18 | 13.82 |
| Average | 20.73 | 15.55 |

---

E17 is the graphical presentation of trends along trench

Photographic reconnaissance of the trench was performed with a Hasselblad 6 x 6 cm (2¼ in sq) format camera. Photographs were taken of the described sections along the far wall of the trench and also of other areas of interest along the trench. Much of the maximum particle size data given in Figure E17 is based on this photography.

In order to obtain a general idea of the sediment characteristics of the deeper portion of the trench not accessible by other methods, samples were taken from the spoil pile of the second excavator approximately every 1,000 feet from 32 + 00 ft to 176 + 85 ft. The results of laboratory analysis of these samples are tabulated in Table E3b.

CHARACTERISTICS OF THE TRENCH WALLS

Excavation of the trench exposed numerous layers of sediments deposited during the Pleistocene and Holocene epochs, along with erosional surfaces and soils formed upon the sediments. Soil horizons, erosional unconformities and boundaries between stratigraphic units remained roughly parallel throughout the entire length of the trench without any noticeable divergence or convergence. There may have been a slight divergence of the upper units toward the mountain front, but, due to planation by surface grading activity, this was difficult to assess.

The major feature exposed in the trench was an erosional unconformity between units IX and VIII which occurred from 1.5 to 2 m (5 to 8 ft) below the leveled surface. (see Figures E12, E13, E14) This unconformity was abrupt and its surface undulated irregularly with a maximum relief of 1 m (3 ft). Generally, sediments found above the unconformity were loose to slightly cohesive, clasts were large, and the colors ranged from dull orange to bright reddish

Figure E-5

GENERALIZED STRATIGRAPHIC DESCRIPTION

The description was based on the four complete section descriptions from the shallow trench. Depth measurements were converted from the measuring tape (marked in feet) and the slope of the walls to true depth in meters. Gravel content was estimated, but the texture of the fines was based on lab analysis. Values in the description for Ca-salts and clay were less than 6% for low, 6-16% for intermediate and greater than 16% for high.

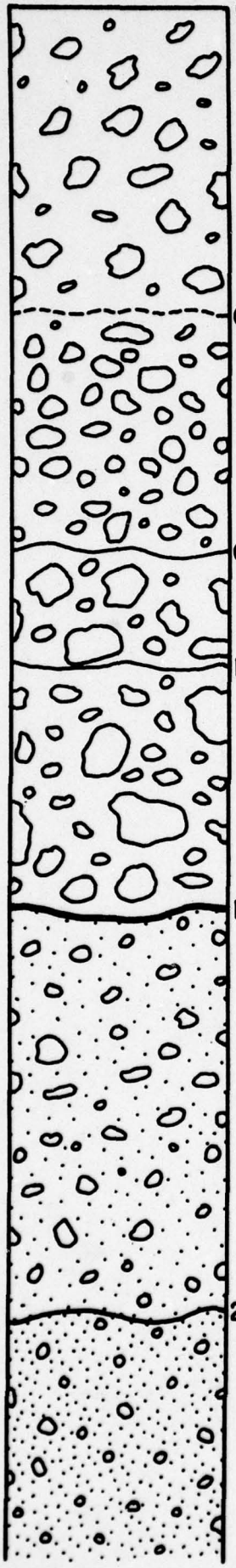


V — 5 YR 6/4 dull orange, (gravelly) silty sand, loose to soft, low in Ca-salts and clay, cut-and-fill in places, upper surface planed off. This horizon not found beyond Section A.

VI — 5 YR 6/4 dull orange to 5 YR 5/8 bright reddish brown, texture varies from (gravelly) silty sand to sandy (gravel), mostly low in Ca-salts and clay but can have intermediate values, upper boundary wavy and gradual.

VII — 5 YR 5/6 bright reddish brown, silty-sandy (gravel), loose mostly low in Ca-salts and clay but can have intermediate values, upper boundary wavy and diffuse.

VIII — 5 YR 7/4 dull orange to 5 YR 5/6 bright reddish brown, (gravelly) sandy mud to silty sandy (gravel), soft to slightly hard, few to no mottles, some discontinuous carbonate coatings on clasts, Ca-salts vary from low to high, and clay content low to intermediate, upper boundary wavy and clear to gradual.

IX — 5 YR 8/3 pale orange at the top of the horizon to 5 YR 5/4 dull reddish brown at some lower areas, (gravelly) muddy sand to silty sandy (gravel), hard, many to common distinct mottles, continuous carbonate coatings on clasts, Ca-salts intermediate to high and clay mostly intermediate, upper boundary wavy and abrupt.

X — 5 YR 8/3 pale orange to 5 YR 7/4 dull orange, (gravelly) mud to (gravelly) muddy sand, hard, many distinct mottles, continuous carbonate coatings which may decrease to bottom of horizon, Ca-salts and clay intermediate to high, upper boundary wavy and abrupt or broken.

TABLE E6

SECTION A (Station 74+54)

| Horizon | Depth (meters below surface) | Depth (feet readings on tape) | Description |
|---|---|---|---|
| V | (0 - .5) | (0 - 2) | 5 YR 6/4 dull orange, (gravelly) silty sand, loose to soft, max. particle size 4 cm, upper boundary planed off. |
| VI | (.5 - .9) | (2 - 3.5) | 5 YR 6/4 dull orange, (gravelly) silty sand, max. particle size 3 cm, loose to soft, upper boundary wavy and gradual. |
| VII | (.9 - 1.1 | (3.5 - 4.5) | 5 YR 6/4 dull orange, silty sandy (gravel), max. particle size 4 cm, loose, upper boundary wavy and diffuse. |
| VIII | (1.1 - 1.5) | (4.5 - 6.0) | 5 YR 7/4 dull orange, (gravelly) sandy mud, max. particle size 3 cm, slightly hard, discontinuous carbonate pebble coatings, upper boundary wavy and clear. |
| IX | (1.5 - 2.4) | (6.0 - 9.0) | 5 YR 8/3 pale orange at the upper part of horizon to 5 YR 5/4 dull reddish brown at the lower, (gravelly) silty sand at upper changing to (gravelly) sandy mud at lower, max. particle size (2-5 cm), hard, many distinct medium mottles near top decreasing to a few at the bottom, continuous calcium carbonate coatings, upper boundary abrupt and wavy. |
| X | (2.4 - 2.9+) | (9.0 - 10.5+) | 5 YR 8/3 pale orange at upper part of horizon to 5 YR 5/4 dull reddish brown at lower section, (gravelly) mud throughout most of the unit, max. particle size 2 cm, hard, many distinct medium mottles near top and slightly decreasing below, continuous carbonate coatings, upper boundary abrupt and wavy or broken. |

TABLE E7

SECTION B (Station 94+12)

| Horizon | Depth (meters below surface) | Depth (feet readings on tape) | Description |
|---|---|---|---|
| VI | (0 - .6) | (0 - 2.5 ) | 5 YR 5/8 bright reddish brown, (gravelly) silty sand, max. particle size 5 cm, soft, upper boundary planed off. |
| VII | (.6 - 1.1) | (2.5 - 4.5) | 5 YR 5/6 bright reddish brown, sandy (gravel), max. particle size 7 cm, loose, upper boundary wavy and gradual to clear. |
| VIII | (1.1 - 1.5) | (4.5 - 6.0) | 5 YR 5/6 bright reddish brown, (gravelly) sand, max. particle size 7 cm, some iron oxide coatings on sand and gravel, soft, upper boundary wavy and diffuse. |
| IX | (1.5 - 2.4) | (6.0 - 9.0) | 5 YR 6/4 dull orange, (gravelly) muddy sand, max. particle size 4 cm, many medium to fine mottles decreasing slightly to lower part of unit, there is an indistinct wavy broken band near 2.2 meters, hard, upper boundary abrupt and wavy. |
| X | (2.4 - 2.9+) | (9.0 - 10.5+) | 5 YR 7/4 dull orange (gravelly) muddy sand, max. particle size 5 cm, many medium mottles decreasing slightly downward, continuous carbonate coatings, hard, upper boundary wavy and abrupt or broken. |

TABLE E8

SECTION C (Station 142+75)

| Horizon | Depth (meters below surface) | Depth (feet readings on tape) | Description |
|---|---|---|---|
| VI | (0 - .9) | (0 - 3.5) | 5 YR 6/4 dull orange, (gravelly) sand, max. particle size 11 cm, soft to loose, upper boundary planed off. |
| VII | (.9 - 1.2) | (3.4 - 5) | 5 YR 5/6 bright reddish brown, muddy sandy (gravel) max. particle size 9 cm, soft to loose, no carbonate coatings, upper boundary wavy and diffuse. |
| VIII | (1.2 - 1.6) | (5.0 - 6.5) | 5 YR 5/6 bright reddish brown, (gravelly) muddy sand, max. particle size 5 cm, slightly hard, discontinuous carbonate coatings, some physical weathering of clasts, upper boundary wavy and gradual. |
| IX | (1.6 - 1.9) | (6.5 - 7.5) | 5 YR 6/4 dull orange, (gravelly) muddy sand, max. particle size 6 cm, hard, common medium distinct mottling, some continuous carbonate coatings, upper boundary wavy and clear or broken. |
| X | (1.9 - 2.6+) | (7.5 - 10.5+) | 5 YR 6/4 dull orange near the top to 5 YR 7/3 dull orange near the bottom, (gravelly) muddy sand, perhaps with more gravel near top of the unit, max. particle size 8 cm near top to 5 cm near bottom, hard, many medium distinct mottles, continuous carbonate coatings, the horizon may be broken down into subhorizons by a faint wavy boundary at 2.1 meters, upper boundary wavy and abrupt. |

TABLE E9

SECTION D (Station 193+90)

| Horizon | Depth (meters below surface) | Depth (feet readings on tape) | Description |
|---|---|---|---|
| VI | (0 - .5) | (0 - 2) | 5YR 5/4 dull reddish brown, silty sand (gravel), max. particle size 10 cm, soft, no carbonate coatings, upper boundary planed off. |
| VII | (0.5 - 1.1) | (2 - 4.5) | 5 YR 5/6 bright reddish brown, silty sandy (gravel), max. particle size 20 cm, loose, some discontinuous carbonate coatings, upper boundary wavy and diffuse. |
| VIII | (1.1 - 1.9) | (4.5 - 7.5) | 5 YR 4/6 reddish brown, silty sandy (gravel), max. particle size 39 cm, soft, few carbonate coatings, upper boundary wavy and gradual. |
| IX | (1.9 - 2.2) | (7.5 - 8.5) | 5 YR 6/4 dull orange, silty sandy (gravel), max. particle size 13 cm, hard, common medium distinct mottles, upper boundary wavy and abrupt. |
| X | (2.2 - 2.7+) | (8.5 - 10+) | 5 YR 8/4 pale orange, slightly sandy (gravel), max. particle size 12 cm, hard, many medium to fine distinct mottles, some redder lenses (or few mottles), upper boundary wavy and abrupt. |

brown. Those found below the unconformity were moderately indurated, clasts were smaller, the distinguishing colors ranged from pale orange to dull orange. A second major unconformity exposed only with the deeper excavation was found at a depth of about 4 m (14 ft). This surface was not accessible for study. The two erosional unconformities are shown in the oblique photo (Figure E12) taken near station 94 + 50.

Another prominent feature exposed in the trench was the presence of cut-and-fill structures found in several horizons of the trench. Figure E13 shows two different age cut-and-fill structures at station 83 +70 ft. Most of these structures were between .5 to 1.5 m deep (1.5 to 4.5 ft) and about 1.6 to 3 m (5 to 10 ft) wide. The larger cut-and-fill structure did not exceed 2 m (6 ft) in depth and 5 m (15 ft) in width. No systematic change in the magnitudes or frequencies of cut-and-fill structures along the length of the trench was detected.

The average maximum size clast exposed in the trench ranged from 1 cm (.4 in) in diameter near the beginning of the trench to 20 - 40 cm (7.9 to 15.7 in) near the end of the trench. A few anomalous sized clasts were found, for example, a 15 cm (5.9 in) basaltic clast found in essentially sandy mud sediments in the short demonstration trench in Stoval air field.

Average maximum particle size was generally one to two times larger above the unconformity than below it. This difference tended to increase toward the mountain front. Figure E14, taken at 143 + 00, shows the trend of greater rate of increase above the unconformity than below it, especially when compared to Figure E12.

The texture of the fine fraction of the sediments (sand, silt and clay) ranged from mud to muddy sand to silty sand below the unconformity and

muddy sand to mostly silty sand above the unconformity according to the textural names derived from Folk's (1974) ternary diagram. The fine fraction texture in the bottom of the deep trench, as indicated by the spoil pile samples, varied from muddy sand to silty sand. The plots of the fine fraction on the ternary diagram are given in Figure E16.

As seen in Figure E16, the fine fraction was generally coarser above the unconformity than below it, but these differences lessen approaching the mountain front. These trends reflect the complex influences of deposition and pedogenesis on clay and silt content.

Clay percentages ranged from less than 1 to 19% above the unconformity and averaged about 7% or less, below the unconformity, the range was from 5 to 30% and averaged about 13% or more. Spoil pile clay percentages ranged from 9 to 38% and averaged about 16%. However, these samples were obtained from an interval of the trench shifted downslope from the trench samples.

The Ca-salts, calcium carbonate and gypsum, like the clays, varied non-linearly and non-exponentially along the trench. These trends are shown graphically in Figure E17. Based on visual observation of the samples, gypsum crystal content seems to increase toward San Cristobal wash and with stratigraphic depth. No crystal gypsum was found in shallow trench samples beyond station 74 + 50 ft.

Above the unconformity, the Ca-salts ranged from 2 to 30% and averaged 9% or less. Below the unconformity, the Ca-salts ranged from 2 to 30% also but averaged 16% or more. The spoil pile had higher values of 11 to 33% and averaged 21%. Soluble salts, particularly the Na-salts, usually averaged

Figure E12 Oblique view SW showing a large section of the 20 feet deep trench near station 94+50. The major unconformity between unit VIII & IX can be seen as a wavy abrupt line below the change in slope. The erosional surface between units VII and VI above the change in slope marks an increase in larger particle sizes.

Figure E13 University of Arizona personnel obtaining sample from trench wall at Station 83+70 ft. The trench wall exposes two superimposed cut and fill structures. The younger cut is a wash filled in by recent grading operations and is offset laterally from the older cut and fill. At the measuring tape, unit VI extends from 0 to 2 ft; unit VII from 2 to 2.6 ft; unit VIII is the fill in the older cut, extending to 4.5 ft; unit IX from 4.5 to 8.1 ft; and unit X extends to the bottom. Note that these depths are not true depths.

Figure E14 Two University of Arizona personnel inspecting a section of trench wall at station 143+00. Note the increased size of maximum sized particles from Figures E12 and E13. This is especially apparent in the upper units.

below 1% of the total weight (data from short trench, Aguilas; Mohawk). The Mg-salts ranged about 2 to 8% of the Ca-salt values and averaged between 3 to 4% of the Ca-salts.

In conclusion, above the erosional unconformity or the top five feet of the trench, the clasts are larger and the percentage of clay and Ca-salts are lower while below the unconformity, the clay and Ca-salts percentages are higher but the maximum clasts sizes are smaller. Samples from the 20 foot trench spoil piles indicate little change in clay content but a slight increase of Ca-salts over that of the samples from just below the unconformity. These general trends suggest a greater degree of pedogenesis below the unconformity than above it and suggest that the unconformity is an erosional surface coincident with significant changes in depositional style and pedogenetic influences.

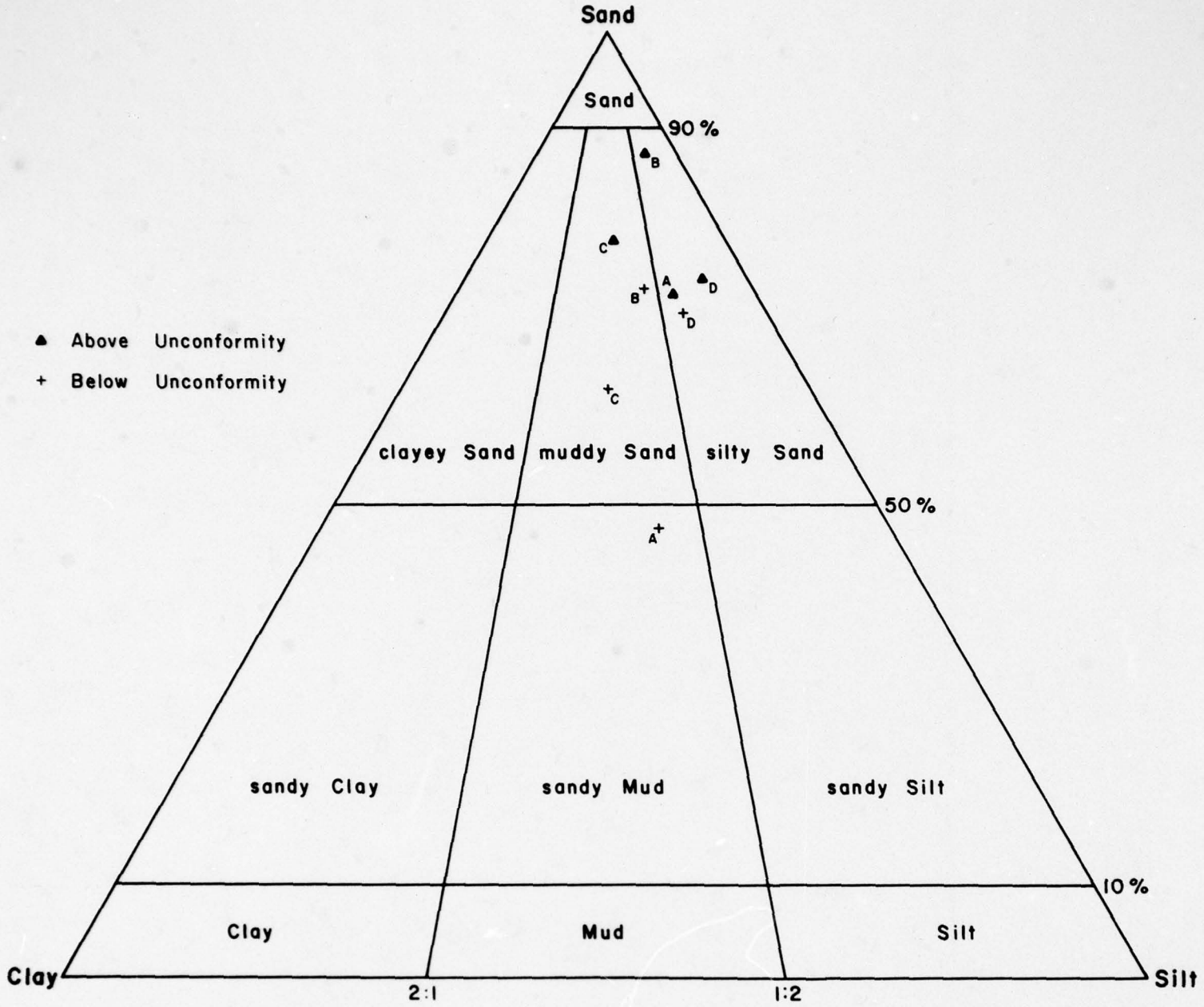


Figure E-16 Summary of the fine texture of sections A,B,C and D above and below the erosional unconformity (after Folk, 1974).

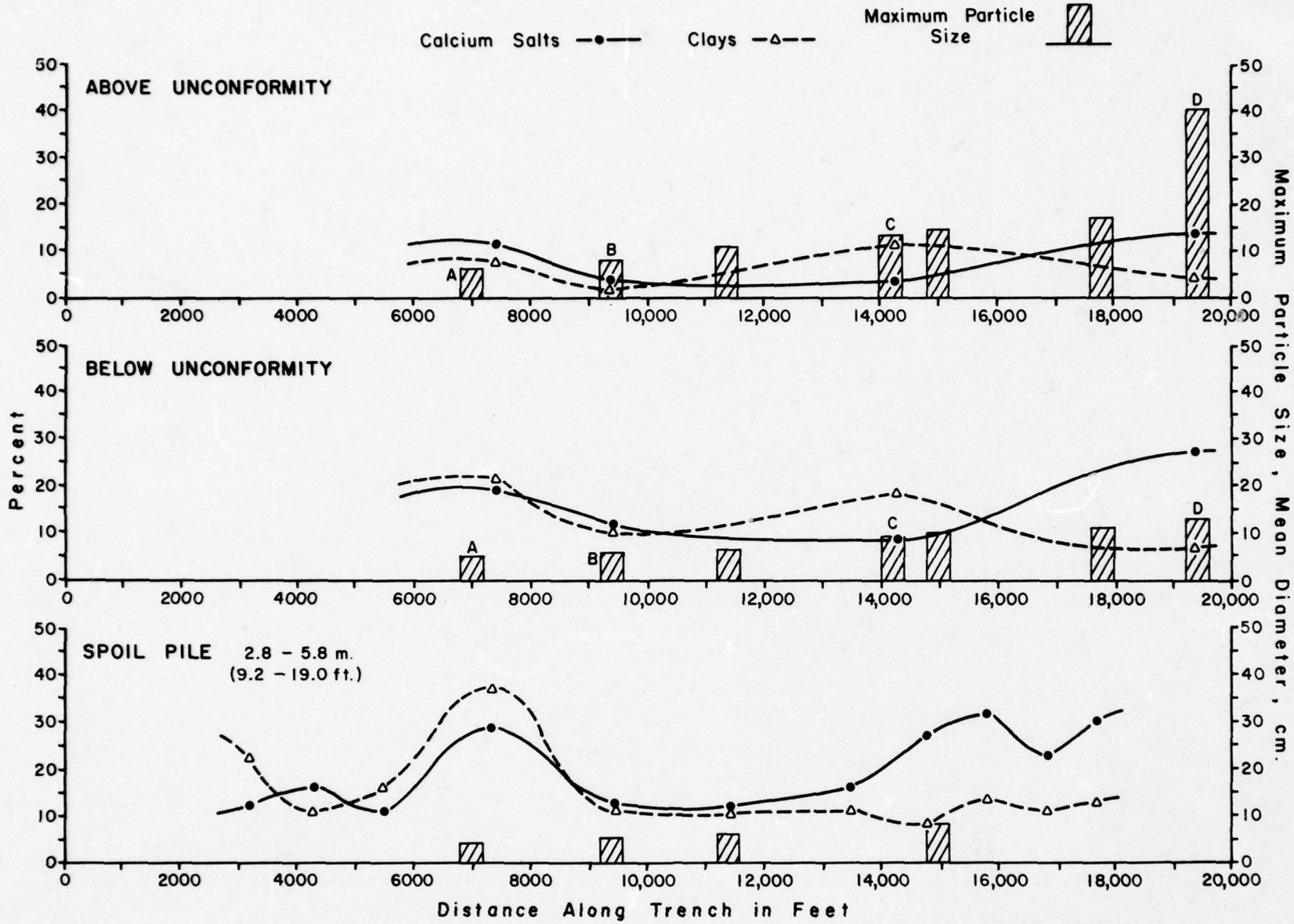


Figure E-17 Percent calcium, percent clay, and particle size trends along the trench for above the unconformity, below the unconformity, and spoil pile samples.

# APPENDIX F

## LABORATORY ANALYSIS

BY

LANNY R. McHARGUE AND ERNEST H. H. SHIH

APPENDIX F

# LABORATORY ANALYSIS

by Lanny R. McHargue and Ernest H.H. Shih

## INITIAL PROCEDURES

A sample of at least 0.5 kilo is obtained from the sampling site. If the sample is indurated, it is ground down by mortar and pestle. Gravel is sieved out by a -1 phi (2 mm) size screen. The fine portion is then divided by a sample splitter to obtain a representative sample of about 30 grams. This is then placed in a preweighed 50 ml beaker. At this point, the number of the beaker and its empty weight is recorded on the sample data sheet. The samples are then placed in an oven to dry for two hours at 105°C and then placed in a dessicator until cooled. The cooled samples are then weighed one at a time to a precision of $\pm$ .001 gm on a Mettler balance. These weights are recorded on the data sheet.

## REMOVAL OF SOLUBLE SALTS

The sample is removed from its 50 ml beaker and placed in a 1000 ml beaker filled with 900 ml of distilled water. It is allowed to settle overnight. After the solution has cleared, it is carefully siphoned off with a small aperture siphon so that the settled sample is not disturbed. (A good small aperture siphon is easily fashioned from a plastic laboratory hose and the glass tip of an eyedropper.) 300 ml of the solution is filtered and retained in a labeled polyethelene bottle, the remainder is discarded. The sample is then carefully transferred into a 150 ml preweighed beaker such that none of it is lost. This operation is performed with the aid of a rubber

policeman (a glass rod with a rubber spatula tip) and a squirt bottle of distilled water. The sample is then dried, cooled and weighed in the manner described above.

REMOVAL OF CALCIUM AND MAGNESIUM SALTS WITH EDTA SOLUTION

The sample is placed in a 1000 ml beaker with 500 ml of prepared EDTA solution at ph 11 (see Bodine and Fernald, 1973, for preparation procedures). This solution is boiled on a bunsen burner for one hour to remove most of the Ca-Mg-salts. It is then allowed to settle overnight or until cleared. Once cleared, the same procedure as outlined above is used to obtain a 300 ml sample of calcium and magnesium salts dissolved in solution for later analysis. To remove the remaining EDTA from the sample, the 1000 ml beaker containing the sample is filled with water, allowed to settle, and siphoned off. This is performed twice. The second time, a few drops of HCl may be added to help flocculate the clays so that they will settle from the solution.

The sample is then transferred to a 150 ml beaker, cooled and reweighed in the usual manner.

FRACTIONAL ANALYSIS OF CLAY, SALT, AND SAND

The sample, still in a 150 ml beaker, is mixed with distilled water containing 2.48 gm/liter of Calgon. This mixture is then stirred. With the aid of a rubber policeman and a squirt bottle of distilled water, the mixture is flushed out of the beaker and wet sieved through a 4 phi screen (.0625 mm) (Folk, 1974). The material which passes through the screen is the silt - clay fraction. This fraction is placed in a

1000 ml graduated cylinder and the cylinder is filled to the 1000 ml mark with a solution of Calgon and distilled water. This mixture is stirred thoroughly with a stirring rod and allowed to settle for 30 minutes. After 30 minutes, a 25 ml sample is withdrawn with a pipette from the upper 2 cm of the mixture and placed in a 50 ml beaker. This sample is the clay fraction.

The sand fraction remaining in the sieve is transferred into a 50 ml beaker. Both beakers containing sand and clay fractions are dried, cooled, and weighed in the usual fashion. In some cases, the sand sample is sieved further to obtain its size distribution (Folk, 1974).

ANALYSIS OF CATION CONTENT

The solutions retained in sections II and III are taken for atomic absorption (AA) analysis of sodium (Na), potassium (K), calcium (Ca), and magnesium (Mg). This analysis requires a separate cathode ray tube for each element and yields the results as ppm (parts per million) concentration of the soluble salt in solution.

CALCULATIONS

Calculations of the soluble salt content is based on the difference in weight between the dry, initial sample and the weight of the sample after section II. This is then divided into separate cation content with the results of the AA analysis.

The weight loss from section II to section III yields the amount of Ca and Mg salts in the sample. AA analysis gives the individual percentage of each element in the sample. These percentages must be changed by a

constant factor to obtain the true weight since dissolution of $CaSO_4$-$4H_2O$, $MgCO_3$ and $CaCO_3$ proceed at different rates. A conversion factor for one hour of boiling was derived from the graph (p. 1155) in Bodine and Fernald (1973).

Silt, sand, and clay percentages are based on the remainder of the sample after EDTA dissolution. These percentages are normalized to 100%. The sand fraction is obtained directly from weighing. The clay weight is calculated as 40 times the dry weight of the sample withdrawn by the pipette minus the weight of the added Calgon (2.48 gm). The weight of the silt is given by the subtraction of the sand and calculated clay weights from the weight of the sample after section III.

The sand, clay, and silt percentages are plotted on a ternary diagram (Folk, 1974) to obtain a textural name for the sample. The sample plots are shown in Figure E16.

REFERENCES

Bodine, M. W., and Fernald, T. H., 1973, EDTA dissolution of Gypsum, Anhydrite, and Ca-Mg carbonates: Jour. of Sed. Petrology, v. 43, no. 4, p. 1152-1156.

Folk, R. L., 1974, Petrology of Sedimentary Rocks: Hemphill Pub. Co., Austin, Texas.

APPENDIX G

# SIZE ANALYSIS: COMPUTER PROGRAMS FOR SIZE CHARACTERISTICS

BY

LARRY MAYER

APPENDIX G

SIZE ANALYSIS DATA

Following data collection in the field or laboratory, particle size information was punched on computer cards. The group of computer cards for each sample is called a data-subfile, while the group of data-subfiles for each sampling area is called a data-file. Two sets of computer programs were used to process the particle size data; Statistical Package for the Social Sciences (SPSS) and Frequency Plot (FRQPLT). Both are compatible with the University of Arizona's CDC Cyber computer.

SPSS (Nie and others, 1975) is an integrated system of computer programs that can perform various statistical operations. Statistical description of the particle size data was generated by using SPSS subprogram FREQUENCIES. FREQUENCIES is used by supplying a list of variables to be processed, their format in the input stream and a list of statistics desired (for a complete description of SPSS see Nie and others, 1975, SPSS, p. 1-34, 181-202).

The computer cards which inform SPSS what is to be done with the data are called control cards. Twelve control cards are needed to use FREQUENCIES in this study. An example of using SPSS subprogram FREQUENCIES is as follows:

Column 1

| | |
|---|---|
| RUN NAME | PARTICLE SIZE DISTRIBUTIONS |
| VARIABLE LIST | SAMPLE, CLASS, FREQ |
| SUBFILE LIST | BB01, BB02, BB03, BB04, BB05, BB06, BB07, BB08 |
| INPUT FORMAT | FIXED (1X, A4, 1X, F6.1, 2X, F2.0) |
| INPUT MEDIUM | CARD |

```
PRINT FORMATS    CLASS (1), FREQ (2)
WEIGHT           FREQ
RUN SUBFILES     EACH
FREQUENCIES      GENERAL = CLASS
OPTIONS          1, 3, 8
STATISTICS       ALL
READ INPUT DATA
```

Data-Subfiles Here

This sequence of cards tells SPSS that:

1. The identify of the run is "Particle Size Distribution"
2. The variables inputted are a sample code, size class, and frequency of the class.
3. The data-file consists of data-subfiles BB01, BB02, etc.
4. The format of the data on punched cards is:

| Variable | Columns | Format |
|---|---|---|
| SAMPLE | 2-5 | A4 |
| CLASS | 7-12 | F6.1 |
| FREQ | 15-16 | F2.0 |

5. The data is on punched cards.
6. CLASS and FREQ will be printed.
7. FREQ is to be weighted.
8. All the subfiles are to be processed.
9. The processing is to be done by FREQUENCIES; the data may be integer or decimal and is contained in variable 'class'.
10. Output options
11. All statistics availalbe in FREQUENCIES are to be printed.
12. Begin reading in the data.

The output from this run through SPSS will be a table listing of the class intervals, absolute frequency, relative frequency, and cumulative frequency of each subfile (see Figure G-5).

The particle size statistics for gravel samples are summarized in Tables G-8, 13, 21, 22, 40, 49, 59, 60, 61. The sample sizes for each sample locality are listed in Table G-11.

Graphic output of the distribution data was facilitated by writing a utility computer program in Fortran IV. The utility program, named FRQPLT, was written to be run on the University of Arizona's CDC Cyber computer in conjunction with a Calcomp drum plotter. FRQPLT accepts input data that is formatted to be run SPSS, thus avoiding extensive reformatting. The output is on two devices. The printed output consists of a listing of: the particles recount of each sample; the frequency of each phi interval; the cumulative frequency of each phi interval; a histogram of frequencies, and a histogram of cumulative frequencies. Output on the Calcomp plotter consists of a graph showing the cumulative frequency curve for each phi interval. The Calcomp output is formatted to provide two graphs per standard 8½ by 11 inch page. FRQPLT requires 52 K of memory for execution and compilation on the CDC Cyber computer. An example of the printed output is shown in Figure G-6. A listing of FRQPLT is provided below. In its present design, all phi categories must be filled with either a frequency or a zero. Thus, nineteeen cards are required for each sample.

In addition, a histogram of frequencies and the following statistics are printed (see Figure G-7):

Maximum - largest particle size recorded at a sample site.

Minimum - smallest particle size recorded at a sample site.

Mode - the particle size most frequently recorded at a sample site.

Median - the particle size category that lies on the 50th percentile. Half the sizes will lie above this value.

Mean - the central dendency of a sample site. Numerically the average value.

Variance - a measure of the dispersion of the data about the mean.

Standard Deviation - the square root of variance; another measure of dispersion about the mean value.

Skewness - measure of symmetry of particle size distribution. Positive values indicate a clustering towards the left while negative values indicate clustering towards the right.

Kurtosis - measure of peakedness of particle size distribution. Normal distribution have a zero value; positive Kurtosis indicates more peakedness while negative values indicate a flatter distribution curve.

06/07/78 FILE - NONAME - CREATED 06/07/78 PAGE 1

SUBFILE LHQ2

CLASS

| CATEGORY LABEL | CODE | ABSOLUTE FREQ | RELATIVE FREQ (PCT) | ADJUSTED FREQ (PCT) | CUM FREQ (PCT) |
|---|---|---|---|---|---|
| | 8.0 | 3 | 6.8 | 6.8 | 6.8 |
| | 11.3 | 4 | 9.1 | 9.1 | 15.9 |
| | 16.0 | 13 | 29.5 | 29.5 | 45.5 |
| | 22.6 | 8 | 18.2 | 18.2 | 63.6 |
| | 32.0 | 9 | 20.5 | 20.5 | 84.1 |
| | 45.0 | 5 | 11.4 | 11.4 | 95.5 |
| | 64.0 | 1 | 2.3 | 2.3 | 97.7 |
| | 128.0 | 1 | 2.3 | 2.3 | 100.0 |
| | TOTAL | 44 | 100.0 | 100.0 | |

Figure G-5 Sample of output from SPSS subprogram FREQUENCIES

| | BWTI | | | | HISTOGRAM | CUMULATIVE PERCENT |
|---|---|---|---|---|---|---|
| CODE | PHI | COUNT | FREQ | CUM FREQ | | |
| BWTI | -3.0 | 3.00 | 4.110 | 0.000 | I*** | I* I |
| BWTI | -3.5 | 2.00 | 2.740 | 4.110 | I** | I* I |
| BWTI | -4.0 | 8.00 | 10.959 | 6.849 | I******** | I** I |
| BWTI | -4.5 | 11.00 | 15.068 | 17.808 | I********** | I***** I |
| BWTI | -5.0 | 10.00 | 13.699 | 32.877 | I********** | I********* I |
| BWTI | -5.5 | 15.00 | 20.548 | 46.575 | I*************** | I************ I |
| BWTI | -6.0 | 9.00 | 12.329 | 67.123 | I******** | I********************* I |
| BWTI | -6.5 | 9.00 | 12.329 | 79.452 | I******** | I************************ I |
| BWTI | -7.0 | 2.00 | 2.740 | 91.781 | I** | I***************************** I |
| BWTI | -7.5 | 3.00 | 4.110 | 94.521 | I*** | I******************************* I |
| BWTI | -8.0 | 1.00 | 1.370 | 98.630 | I* | I********************************I |
| BWTI | -8.5 | 0.00 | 0.000 | 100.000 | I* | I********************************I |
| BWTI | -9.0 | 0.00 | 0.000 | 100.000 | I* | I********************************I |
| BWTI | -9.5 | 0.00 | 0.000 | 100.000 | I* | I********************************I |
| BWTI | -10.0 | 0.00 | 0.000 | 100.000 | I* | I********************************I |
| BWTI | -10.5 | 0.00 | 0.000 | 100.000 | I* | I********************************I |
| BWTI | -11.0 | 0.00 | 0.000 | 100.000 | I* | I********************************I |
| BWTI | -11.5 | 0.00 | 0.000 | 100.000 | I* | I********************************I |
| BWTI | -12.0 | 0.00 | 0.000 | 100.000 | I* | I********************************I |

THE STANDARD DEVIATION FOR LOCATION BWTI IS 2.36972 PHI : THE MEAN IS -5.80137 PHI

Figure G-6 Sample printed output from program FRQPLT

SUBFILE LHQ2

CLASS

```
     CODE
                I
      8.0 ******** (      3)
                I
                I
     11.3 *********** (      4)
                I
                I
     16.0 ********************************** (     13)
                I
                I
     22.6 ********************* (      8)
                I
                I
     32.0 ************************ (      9)
                I
                I
     45.0 ************* (      5)
                I
                I
     64.0 *** (      1)
                I
                I
    128.0 *** (      1)
                I
                I
                I.........I.........I.........I.........I.........I
                0         4         8         12        16        20
                FREQUENCY
```

| | | | | | |
|---|---|---|---|---|---|
| MEAN | 20.432 | STD ERR | 3.015 | MEDIAN | 21.775 |
| MODE | 16.000 | STD DEV | 19.999 | VARIANCE | 399.963 |
| KURTOSIS | 13.324 | SKEWNESS | 3.196 | RANGE | 120.000 |
| MINIMUM | 8.000 | MAXIMUM | 128.000 | SUM | 1163.000 |
| C.V. PCT | 75.661 | .95 C.I. | 20.352 | TO | 22.512 |

VALID CASES 44 MISSING CASES 0

Figure G-7 Sample of output from SPSS subprogram FREQUENCIES

| Sample Code | Maximum Category (mm) | Minimum Category (mm) | Mode (mm) | Median (mm) | Mean (mm) | Variance | Standard Deviation | Skewness | Kurtosis |
|---|---|---|---|---|---|---|---|---|---|
| BB01 | 632.0 | 9.5 | 54.0 | 108.9 | 181.5 | 28384.5 | 168.4 | 1.16 | 0.49 |
| BB02 | 303.0 | 9.5 | 152.0 | 55.9 | 87.8 | 5059.1 | 71.1 | 1.09 | 0.62 |
| BB03 | 889.0 | 9.5 | 303.0 | 107.5 | .55.0 | 22630.0 | 150.4 | 2.26 | 7.52 |
| BB04 | 632.0 | 9.5 | 38.0 | 107.2 | 183.8 | 34067.4 | 184.5 | 1.19 | 0.34 |
| BB05 | 453.0 | 9.5 | 19.0 | 53.0 | 82.1 | 8372.1 | 91.4 | 2.25 | 5.46 |
| BB06 | 632.0 | 9.5 | 76.0 | 75.8 | 126.6 | 18436.5 | 135.7 | 1.64 | 2.18 |
| BB07 | 453.0 | 9.5 | 19.0 | 52.9 | 88.6 | 10941.0 | 104.5 | 2.15 | 4.42 |
| BB08 | 303.0 | 9.5 | 54.0 | 54.3 | 81.6 | 5218.1 | 72.2 | 1.46 | 1.62 |

Table G-8 Particle Size Statistics for Bumble Bee Samples.

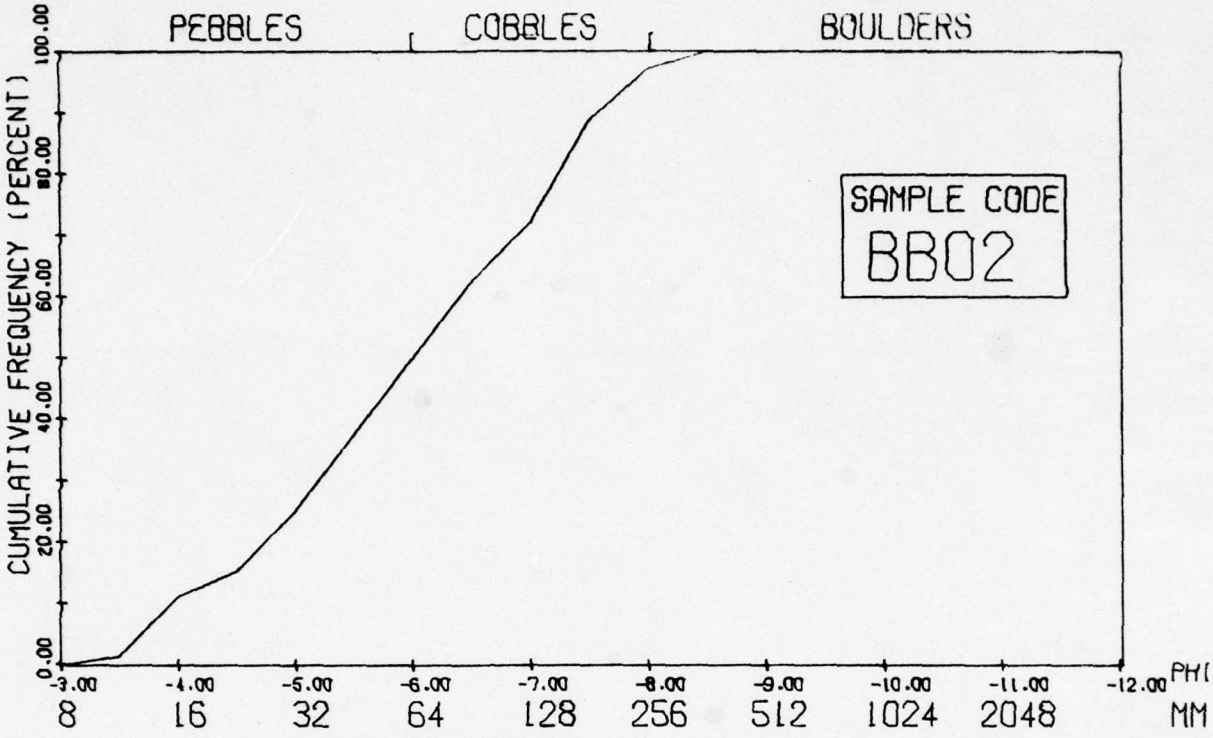
PEBBLES
COBBLES
BOULDERS
CUMULATIVE FREQUENCY (PERCENT)
100.00
80.00
60.00
40.00
20.00
0.00
SAMPLE CODE
BB02
-3.00
-4.00
-5.00
-6.00
-7.00
-8.00
-9.00
-10.00
-11.00
-12.00
PHI
8
16
32
64
128
256
512
1024
2048
MM

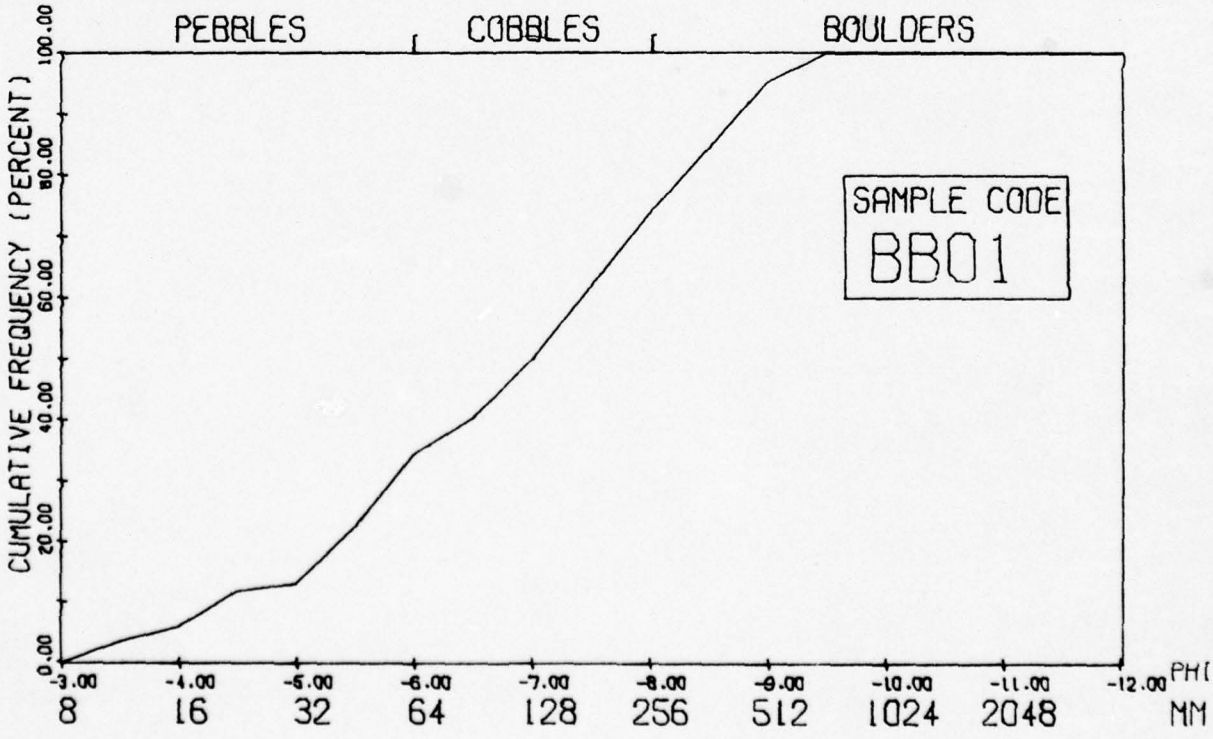
PEBBLES
COBBLES
BOULDERS
CUMULATIVE FREQUENCY (PERCENT)
100.00
80.00
60.00
40.00
20.00
0.00
SAMPLE CODE
BB01
-3.00
-4.00
-5.00
-6.00
-7.00
-8.00
-9.00
-10.00
-11.00
-12.00
PHI
8
16
32
64
128
256
512
1024
2048
MM

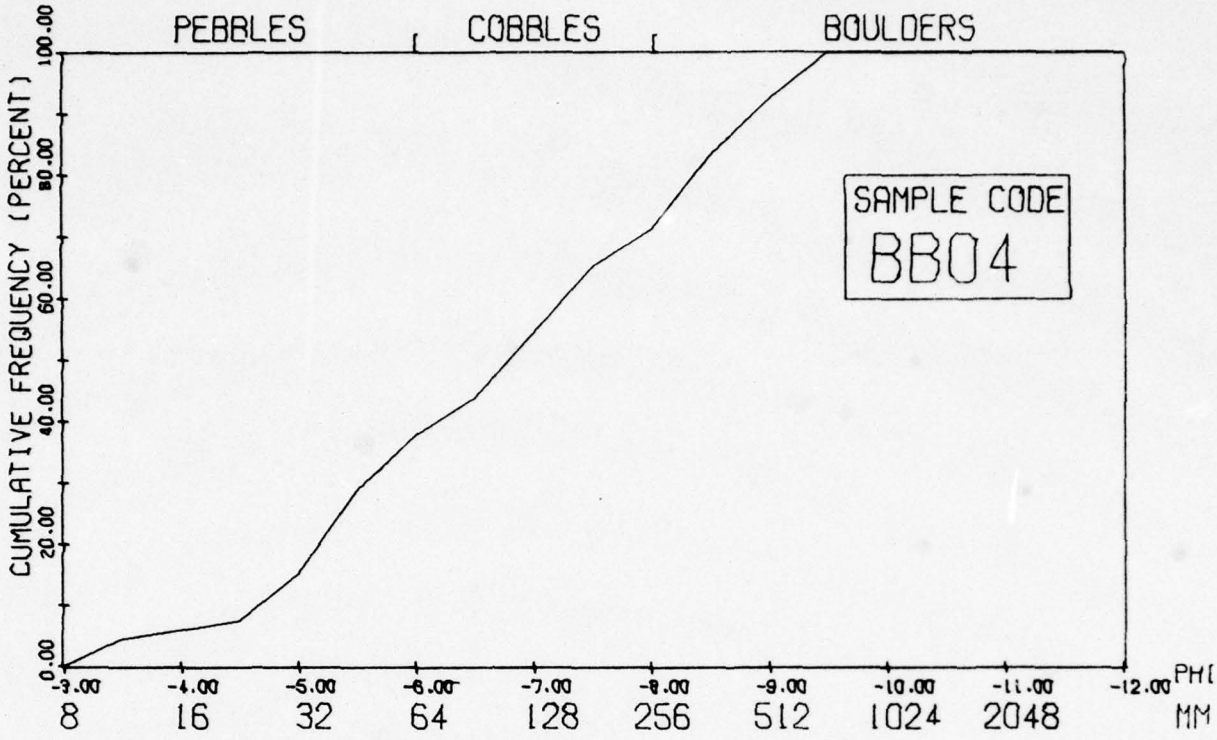
PEBBLES
COBBLES
BOULDERS
CUMULATIVE FREQUENCY (PERCENT)
0.00
20.00
40.00
60.00
80.00
100.00
SAMPLE CODE
BB04
-3.00
-4.00
-5.00
-6.00
-7.00
-8.00
-9.00
-10.00
-11.00
-12.00
PHI
8
16
32
64
128
256
512
1024
2048
MM

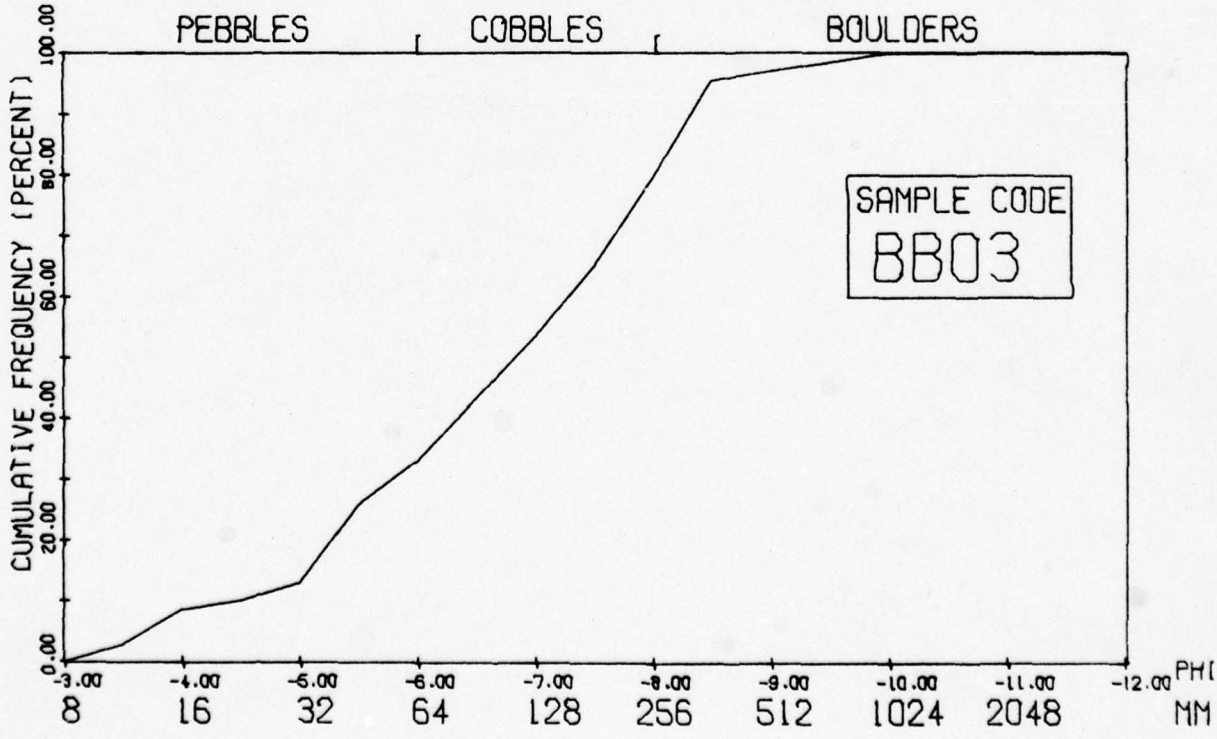
PEBBLES
COBBLES
BOULDERS
CUMULATIVE FREQUENCY (PERCENT)
0.00
20.00
40.00
60.00
80.00
100.00
SAMPLE CODE
BB03
-3.00
-4.00
-5.00
-6.00
-7.00
-8.00
-9.00
-10.00
-11.00
-12.00
PHI
8
16
32
64
128
256
512
1024
2048
MM

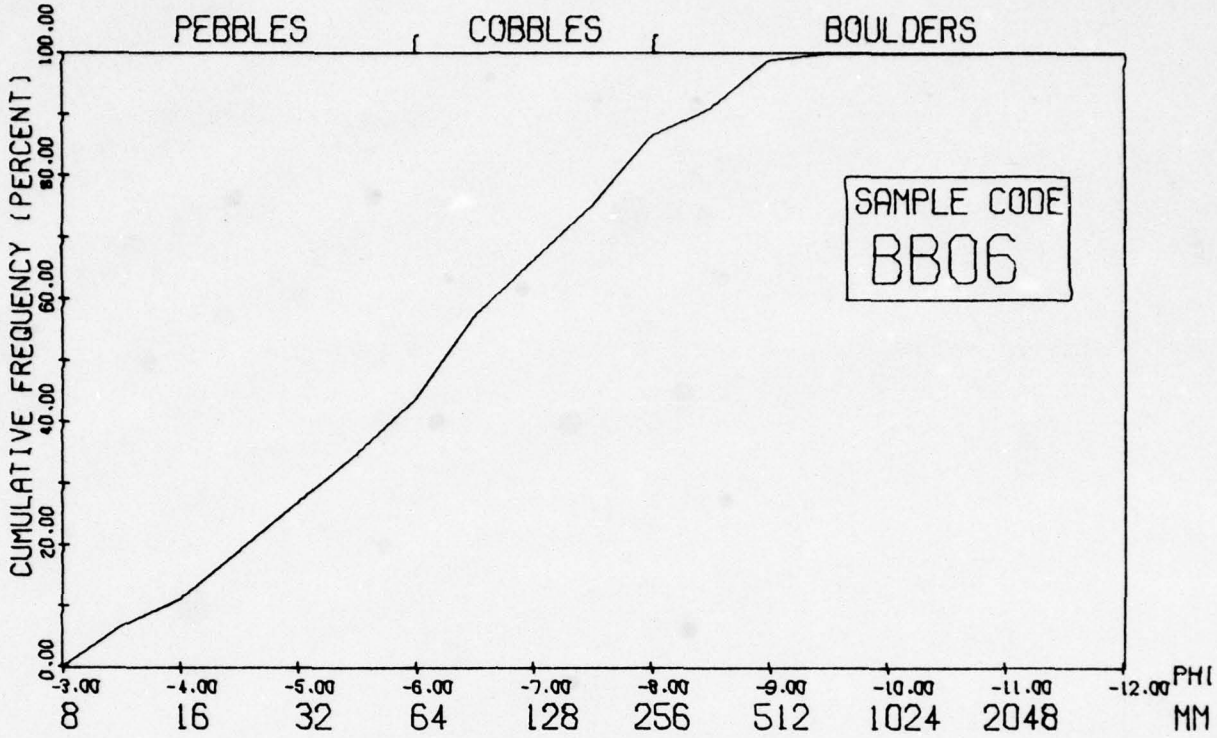
PEBBLES
COBBLES
BOULDERS
CUMULATIVE FREQUENCY (PERCENT)
0.00
20.00
40.00
60.00
80.00
100.00
SAMPLE CODE
BB06
-3.00
-4.00
-5.00
-6.00
-7.00
-8.00
-9.00
-10.00
-11.00
-12.00
PHI
8
16
32
64
128
256
512
1024
2048
MM

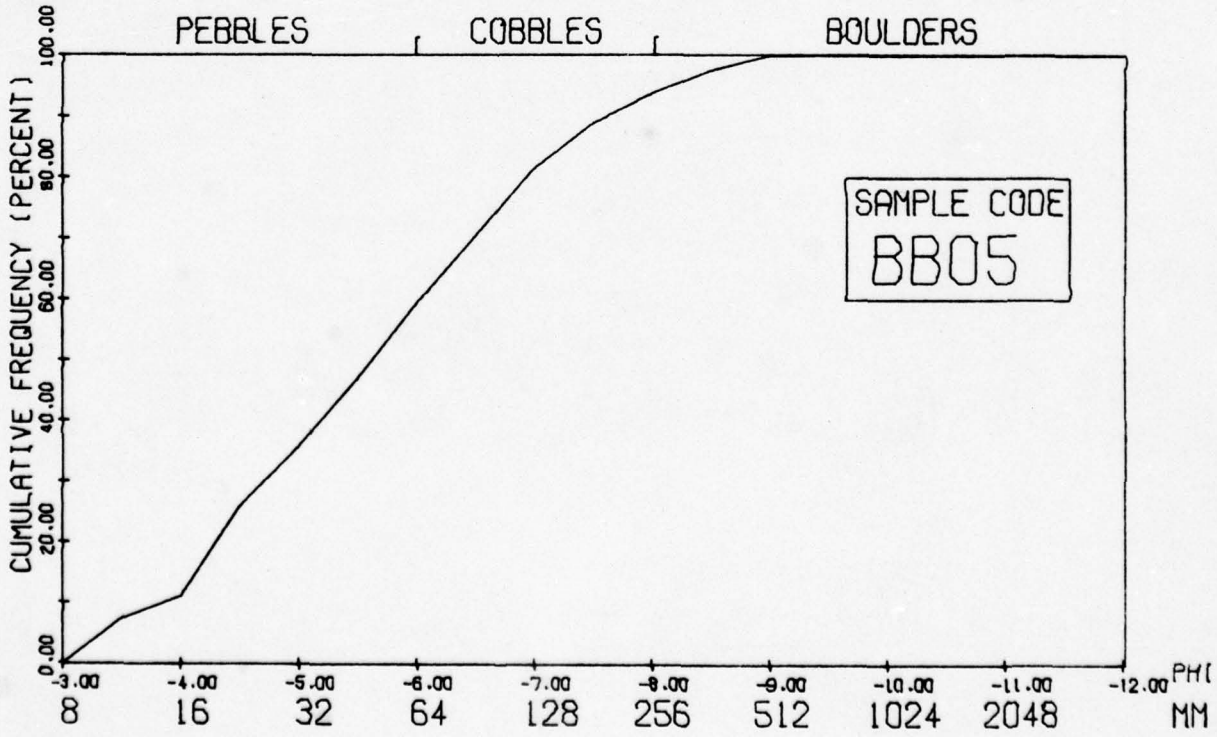
PEBBLES
COBBLES
BOULDERS
CUMULATIVE FREQUENCY (PERCENT)
0.00
20.00
40.00
60.00
80.00
100.00
SAMPLE CODE
BB05
-3.00
-4.00
-5.00
-6.00
-7.00
-8.00
-9.00
-10.00
-11.00
-12.00
PHI
8
16
32
64
128
256
512
1024
2048
MM

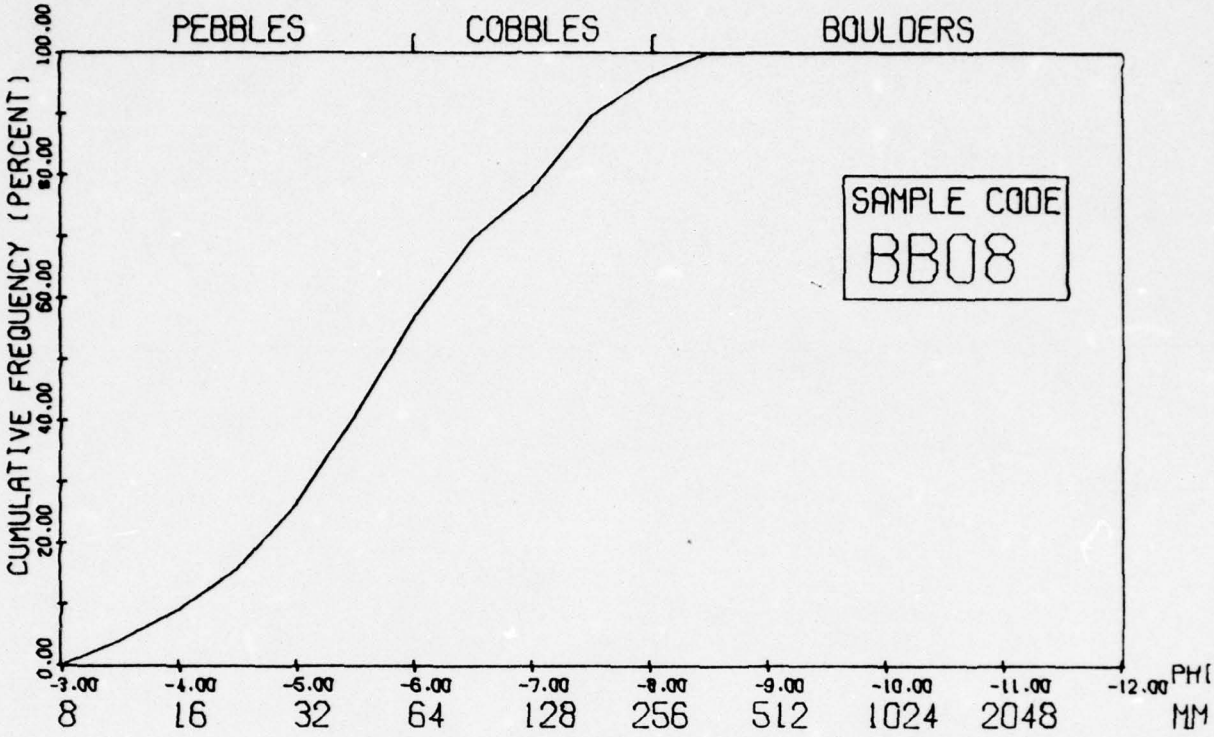
PEBBLES
COBBLES
BOULDERS
CUMULATIVE FREQUENCY (PERCENT)
0.00
20.00
40.00
60.00
80.00
100.00
SAMPLE CODE
BB08
-3.00
-4.00
-5.00
-6.00
-7.00
-8.00
-9.00
-10.00
-11.00
-12.00
PHI
8
16
32
64
128
256
512
1024
2048
MM

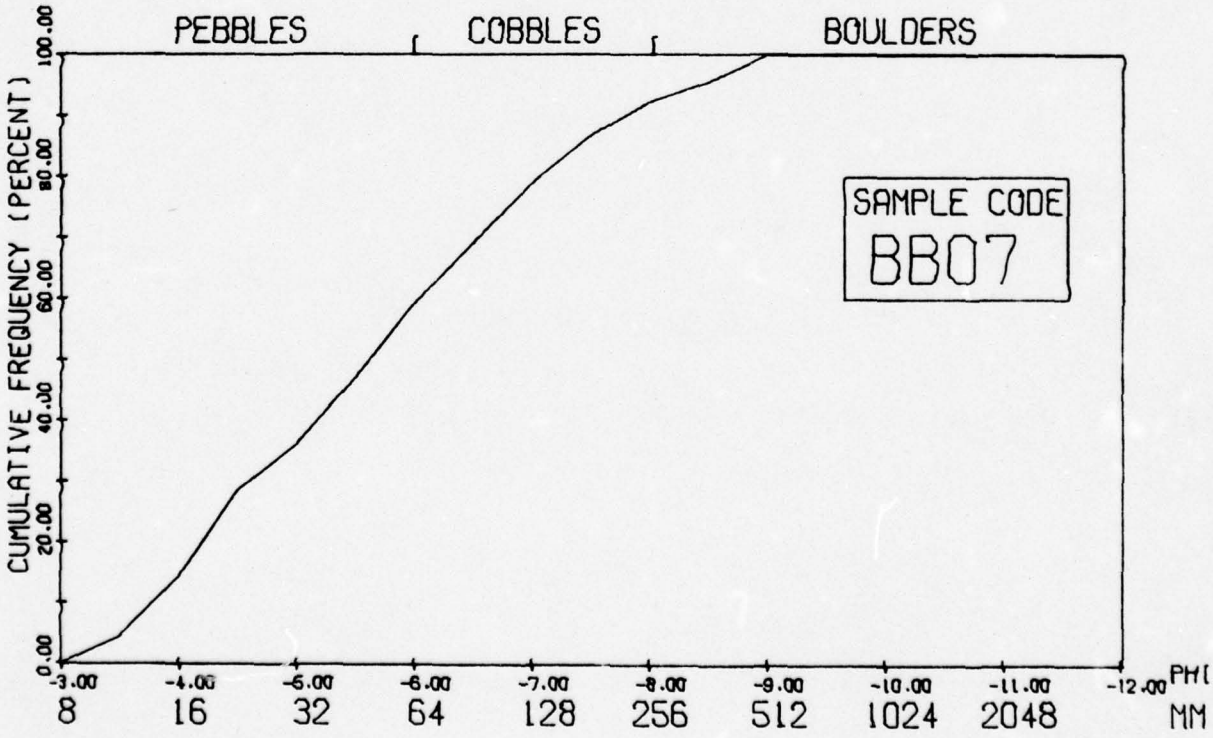
PEBBLES
COBBLES
BOULDERS
CUMULATIVE FREQUENCY (PERCENT)
0.00
20.00
40.00
60.00
80.00
100.00
SAMPLE CODE
BB07
-3.00
-4.00
-5.00
-6.00
-7.00
-8.00
-9.00
-10.00
-11.00
-12.00
PHI
8
16
32
64
128
256
512
1024
2048
MM

| SAMPLE CODE | MAXIMUM CATEGORY(mm) | MINIMUM Category(mm) | MODE (mm) | MEDIAN (mm) | MEAN (mm) | VARIANCE | STANDARD DEVIATION | SKEWNESS | KURTOSIS |
|---|---|---|---|---|---|---|---|---|---|
| LHBJ | 632.0 | 9.5 | 26.8 | 40.0 | 104.8 | 20438.4 | 143.0 | 2.46 | 5.93 |
| LH02 | 1252.0 | 9.5 | 76.0 | 53.1 | 124.7 | 50119.9 | 223.9 | 3.66 | 14.77 |
| LH03 | 107.0 | 9.5 | 13.4 | 18.2 | 30.5 | 687.5 | 26.2 | 1.49 | 1.50 |
| LH04 | 152.0 | 9.5 | 9.5 | 18.0 | 26.5 | 628.0 | 25.1 | 2.82 | 10.18 |
| LH09 | 632.0 | 9.5 | 9.5 | 26.6 | 86.4 | 24316.9 | 155.9 | 2.76 | 6.52 |
| LH10 | 453.0 | 9.5 | 19.0 | 27.7 | 46.7 | 4879.5 | 70.5 | 4.82 | 24.73 |
| LH11 | 1252.0 | 9.5 | 9.5 | 28.5 | 113.6 | 71968.3 | 268.3 | 3.83 | 13.50 |
| LH12 | 453.0 | 9.5 | 19.0 | 37.7 | 64.6 | 5687.8 | 75.4 | 2.92 | 11.07 |
| LH13 | 214.0 | 9.5 | 76.0 | 39.6 | 56.8 | 2573.2 | 50.7 | 1.50 | 2.00 |
| LH14 | 303.0 | 9.5 | 54.0 | 53.4 | 75.8 | 5886.1 | 76.7 | 1.46 | 1.34 |
| LH15 | 107.0 | 9.5 | 76.0 | 36.7 | 40.8 | 672.5 | 25.9 | 0.59 | -.73 |
| LHQ2 | 152.0 | 9.5 | 19.0 | 25.8 | 31.4 | 567.0 | 23.8 | 3.17 | 13.13 |
| LHQ3 | 889.0 | 9.5 | 76.0 | 76.4 | 139.2 | 40651.5 | 201.6 | 2.99 | 8.14 |

Table G-13 Particle Size Statistics for Lost Home Samples.

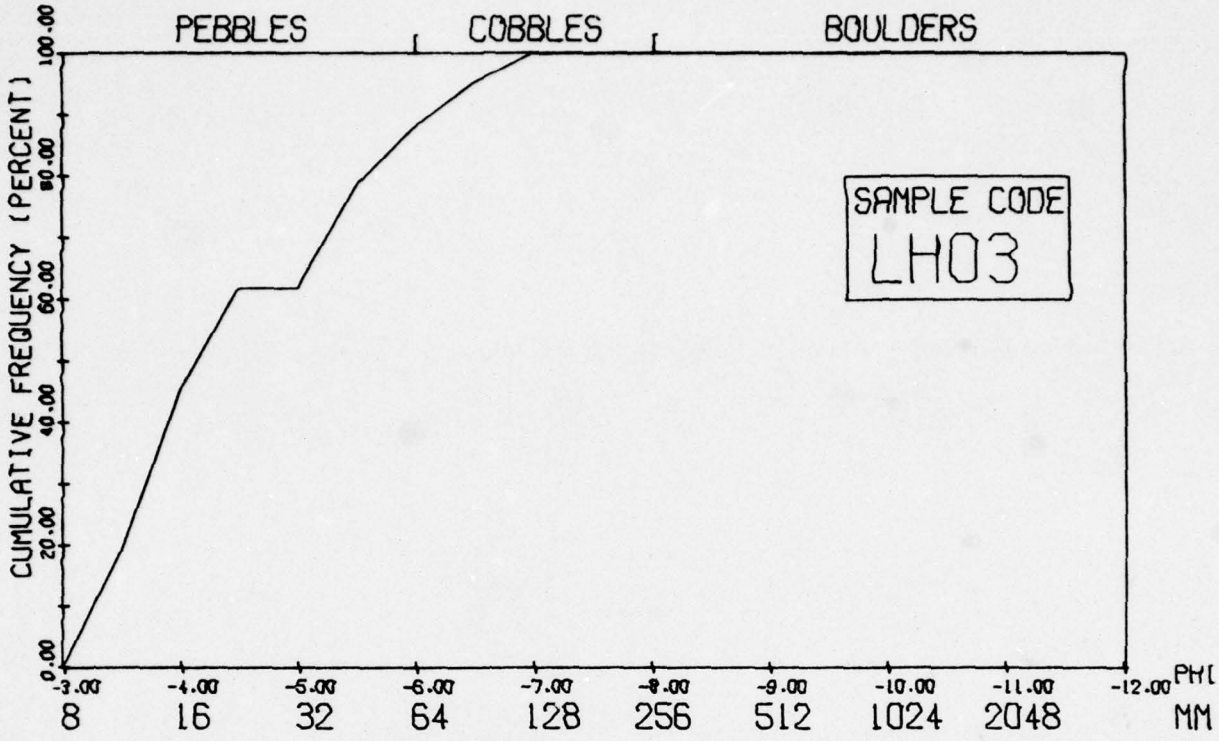
PEBBLES
COBBLES
BOULDERS
CUMULATIVE FREQUENCY (PERCENT)
100.00
80.00
60.00
40.00
20.00
0.00
SAMPLE CODE
LH03
-3.00
-4.00
-5.00
-6.00
-7.00
-8.00
-9.00
-10.00
-11.00
-12.00
PHI
8
16
32
64
128
256
512
1024
2048
MM

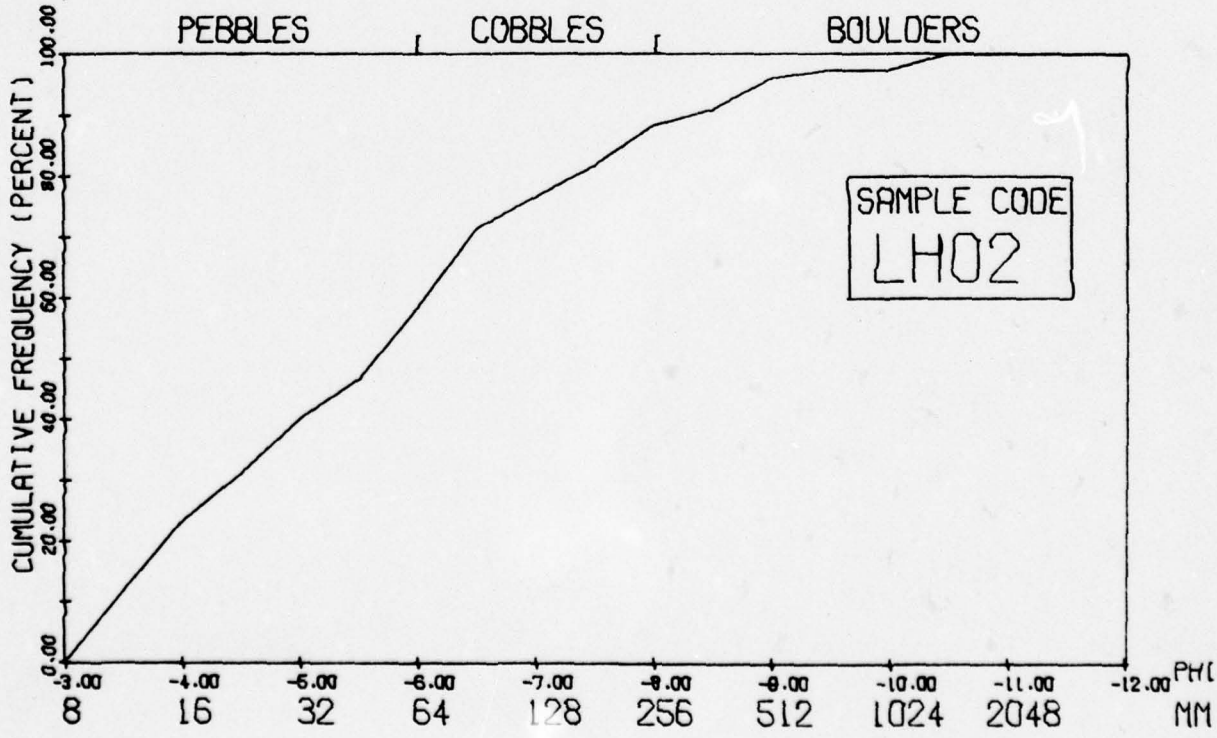
PEBBLES
COBBLES
BOULDERS
CUMULATIVE FREQUENCY (PERCENT)
100.00
80.00
60.00
40.00
20.00
0.00
SAMPLE CODE
LH02
-3.00
-4.00
-5.00
-6.00
-7.00
-8.00
-9.00
-10.00
-11.00
-12.00
PHI
8
16
32
64
128
256
512
1024
2048
MM

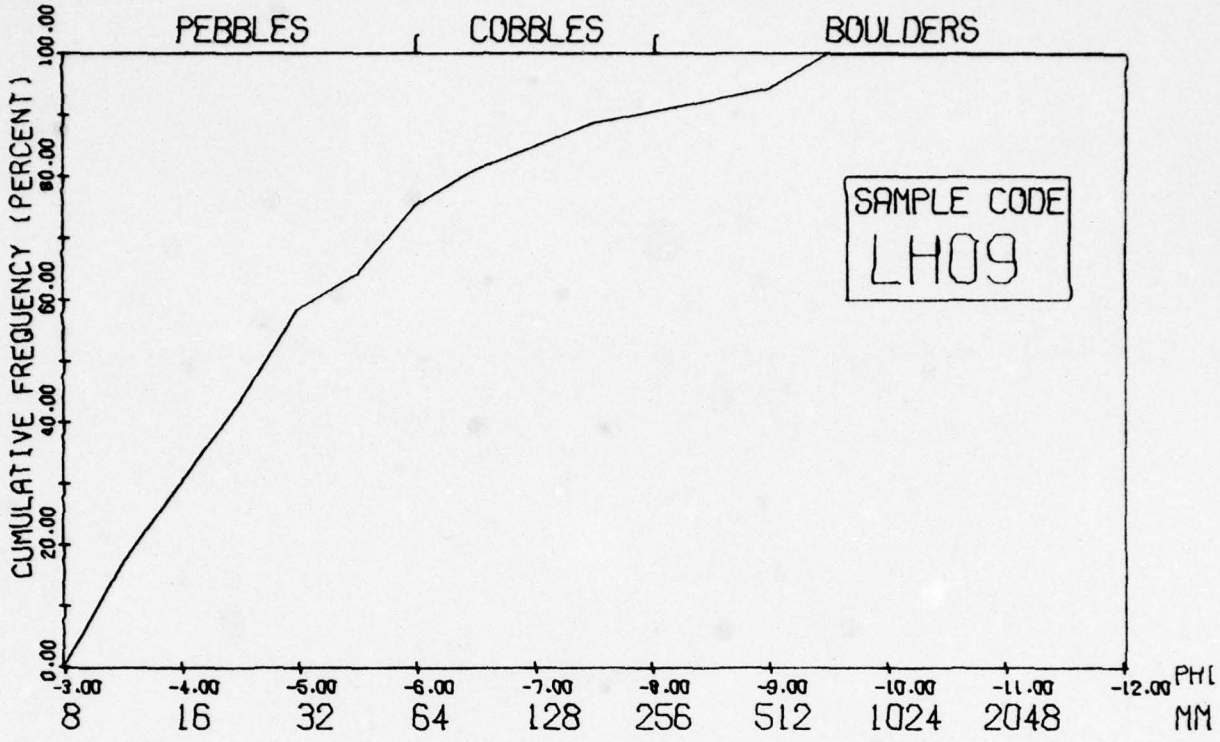
PEBBLES
COBBLES
BOULDERS
CUMULATIVE FREQUENCY (PERCENT)
100.00
80.00
60.00
40.00
20.00
0.00
SAMPLE CODE
LH09
-3.00
-4.00
-5.00
-6.00
-7.00
-8.00
-9.00
-10.00
-11.00
-12.00
PHI
8
16
32
64
128
256
512
1024
2048
MM

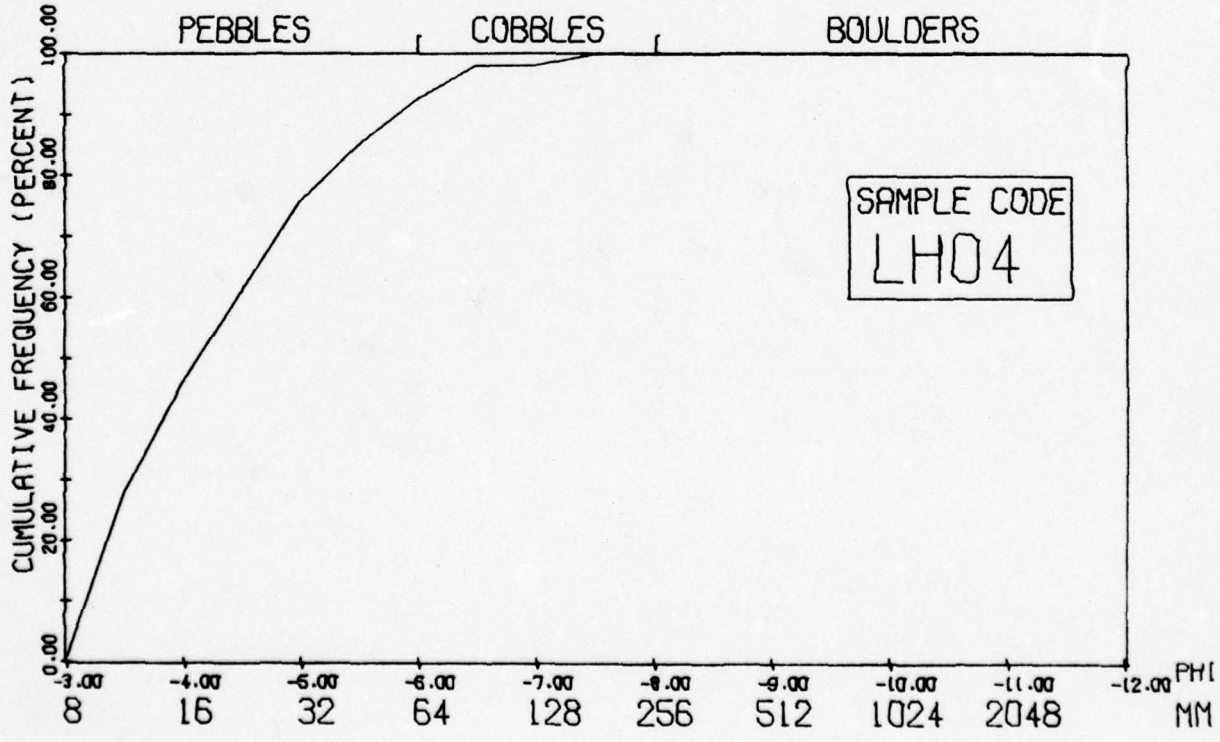
PEBBLES
COBBLES
BOULDERS
CUMULATIVE FREQUENCY (PERCENT)
100.00
80.00
60.00
40.00
20.00
0.00
SAMPLE CODE
LH04
-3.00
-4.00
-5.00
-6.00
-7.00
-8.00
-9.00
-10.00
-11.00
-12.00
PHI
8
16
32
64
128
256
512
1024
2048
MM

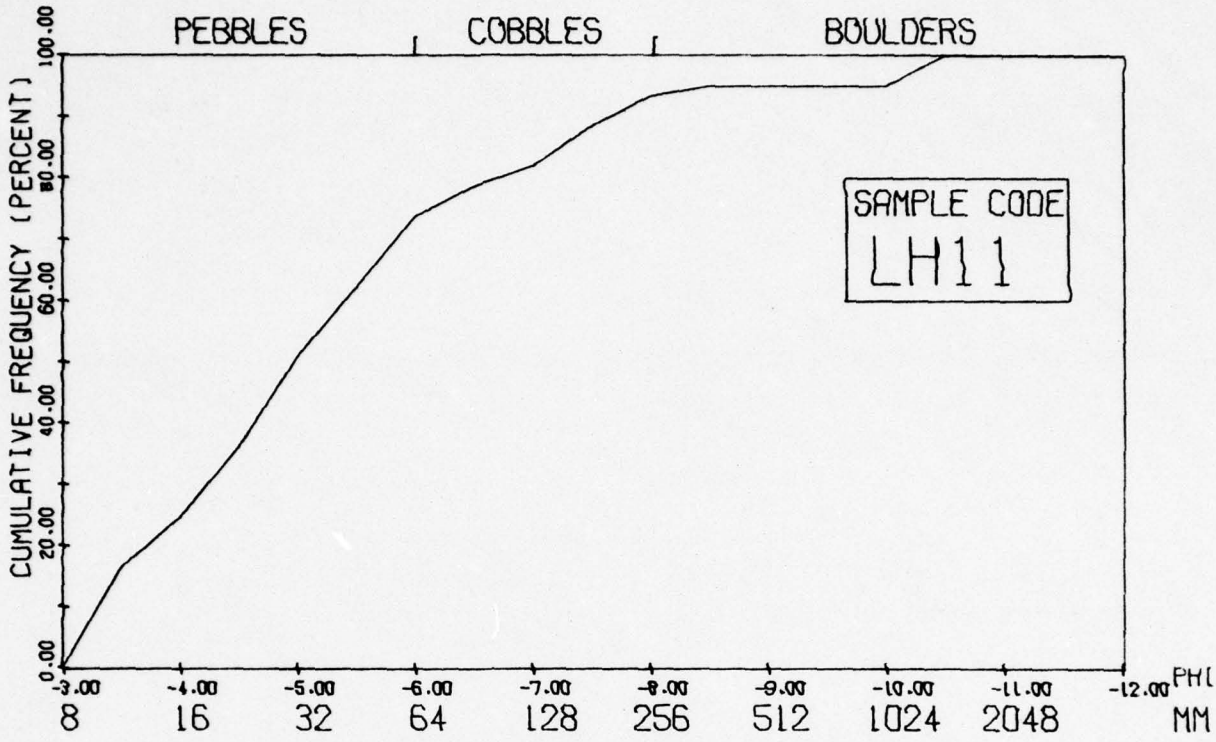
PEBBLES
COBBLES
BOULDERS
CUMULATIVE FREQUENCY (PERCENT)
0.00
20.00
40.00
60.00
80.00
100.00
SAMPLE CODE
LH11
-3.00
-4.00
-5.00
-6.00
-7.00
-8.00
-9.00
-10.00
-11.00
-12.00
PHI
8
16
32
64
128
256
512
1024
2048
MM

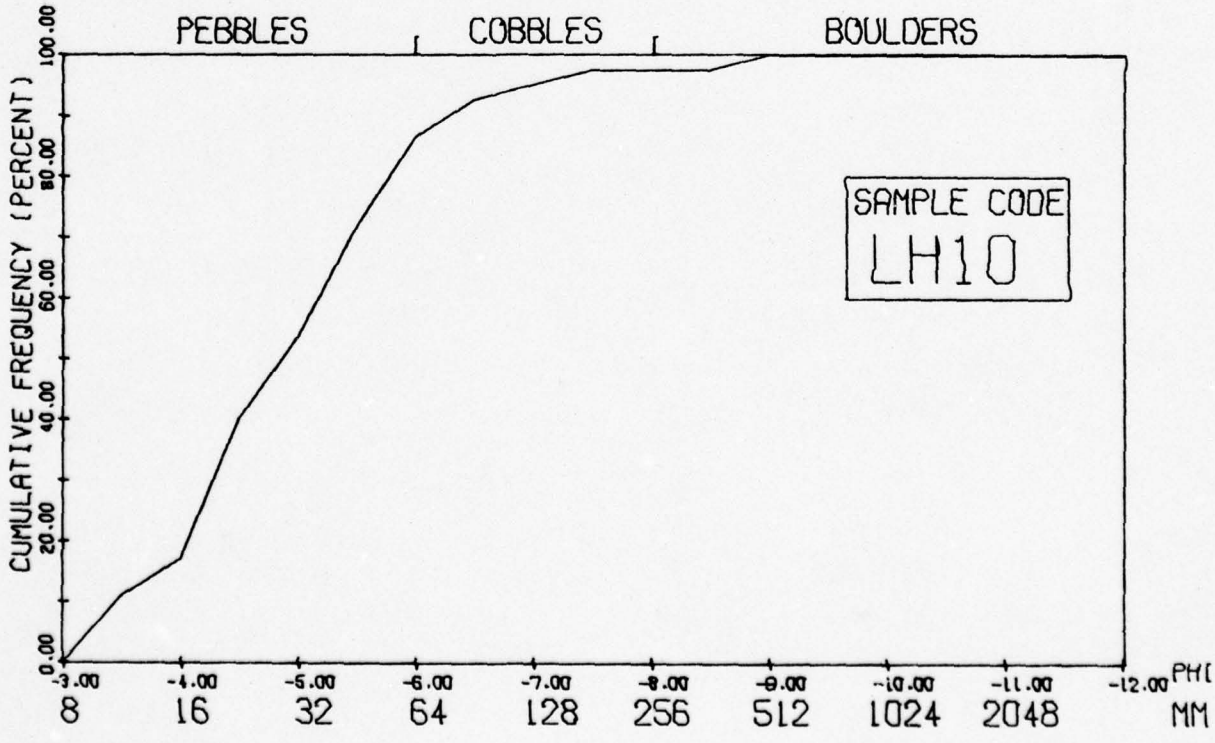
PEBBLES
COBBLES
BOULDERS
CUMULATIVE FREQUENCY (PERCENT)
0.00
20.00
40.00
60.00
80.00
100.00
SAMPLE CODE
LH10
-3.00
-4.00
-5.00
-6.00
-7.00
-8.00
-9.00
-10.00
-11.00
-12.00
PHI
8
16
32
64
128
256
512
1024
2048
MM

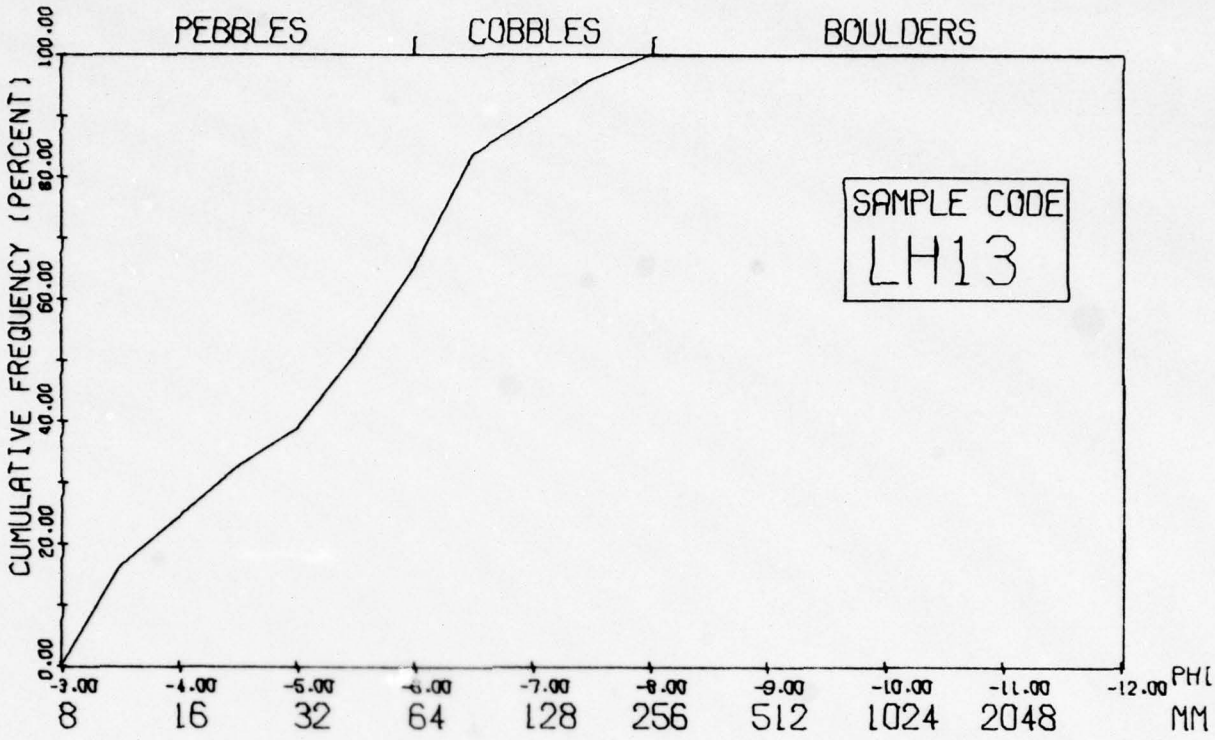
PEBBLES
COBBLES
BOULDERS
CUMULATIVE FREQUENCY (PERCENT)
0.00
20.00
40.00
60.00
80.00
100.00
SAMPLE CODE
LH13
-3.00
-4.00
-5.00
-6.00
-7.00
-8.00
-9.00
-10.00
-11.00
-12.00
PHI
8
16
32
64
128
256
512
1024
2048
MM

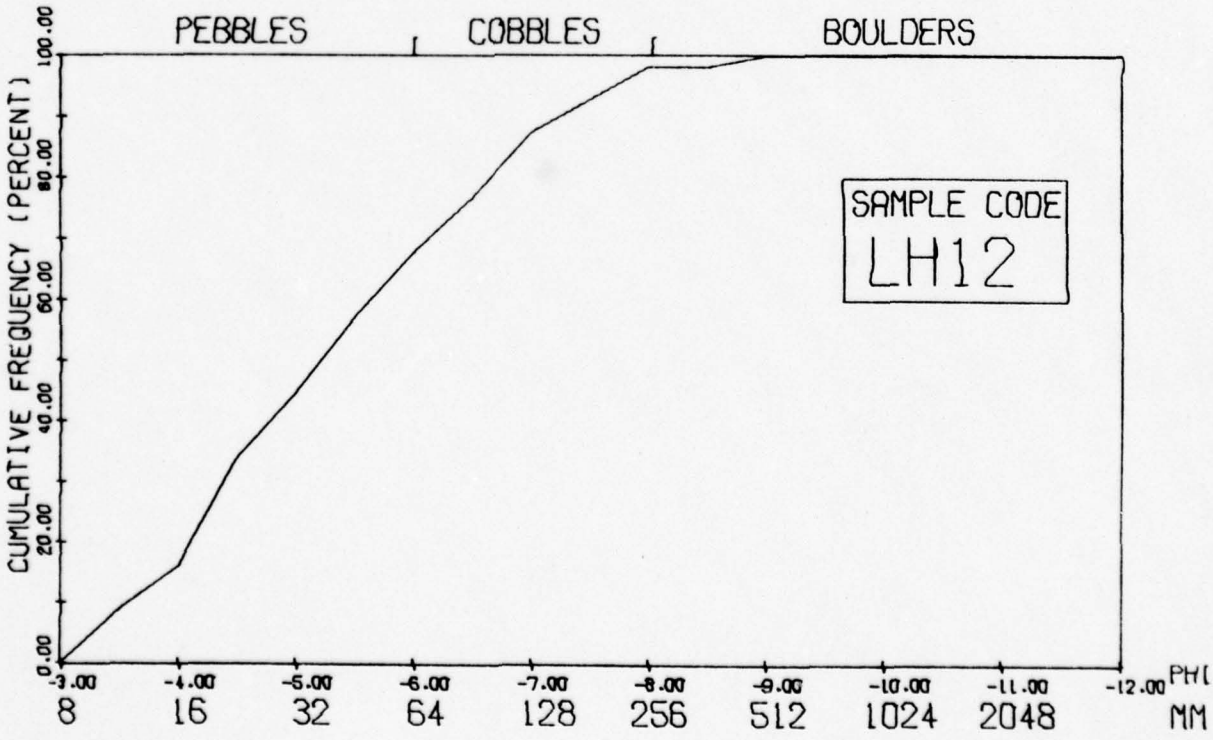
PEBBLES
COBBLES
BOULDERS
CUMULATIVE FREQUENCY (PERCENT)
0.00
20.00
40.00
60.00
80.00
100.00
SAMPLE CODE
LH12
-3.00
-4.00
-5.00
-6.00
-7.00
-8.00
-9.00
-10.00
-11.00
-12.00
PHI
8
16
32
64
128
256
512
1024
2048
MM

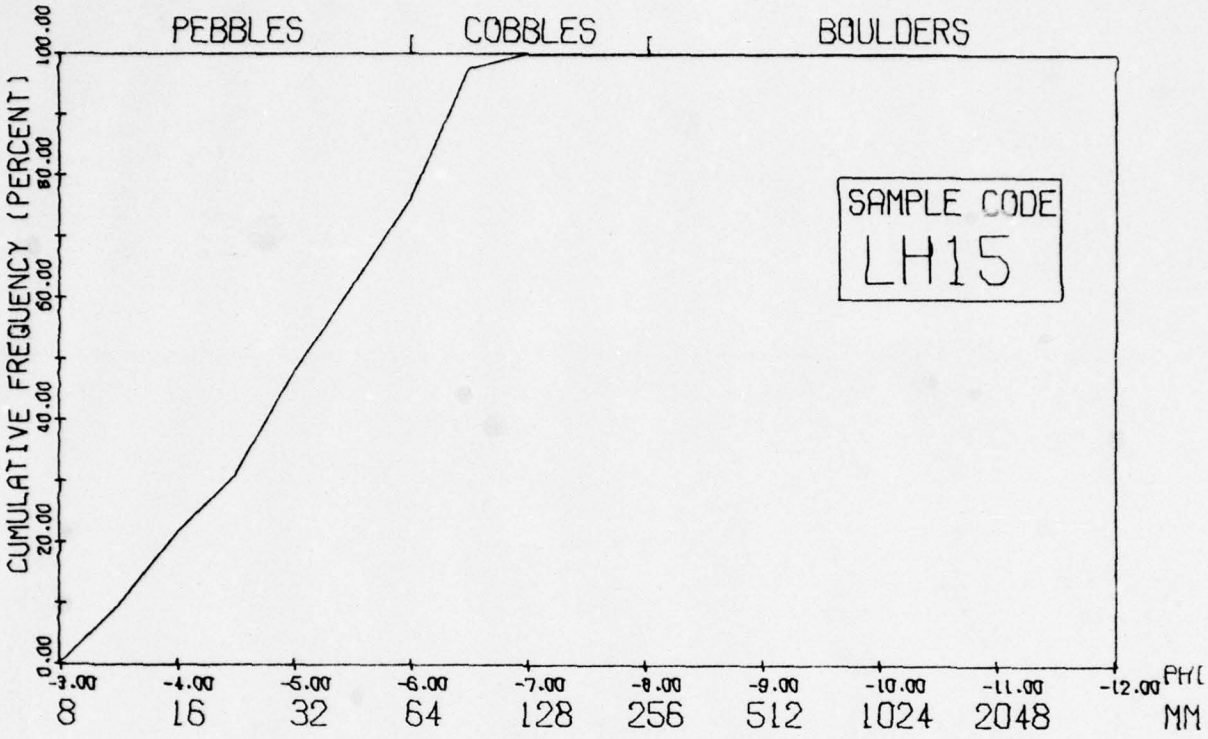
PEBBLES
COBBLES
BOULDERS
CUMULATIVE FREQUENCY (PERCENT)
100.00
80.00
60.00
40.00
20.00
0.00
SAMPLE CODE
LH15
-3.00
-4.00
-5.00
-6.00
-7.00
-8.00
-9.00
-10.00
-11.00
-12.00
PHI
8
16
32
64
128
256
512
1024
2048
MM

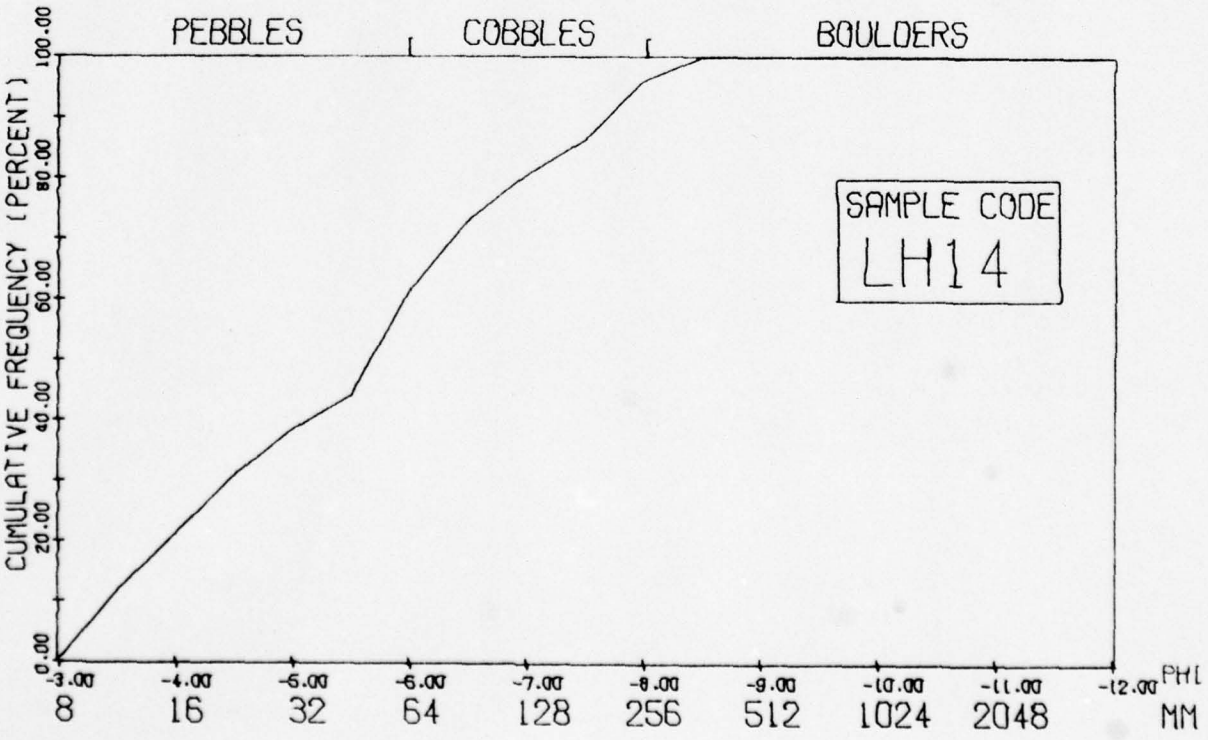
PEBBLES
COBBLES
BOULDERS
CUMULATIVE FREQUENCY (PERCENT)
100.00
80.00
60.00
40.00
20.00
0.00
SAMPLE CODE
LH14
-3.00
-4.00
-5.00
-6.00
-7.00
-8.00
-9.00
-10.00
-11.00
-12.00
PHI
8
16
32
64
128
256
512
1024
2048
MM

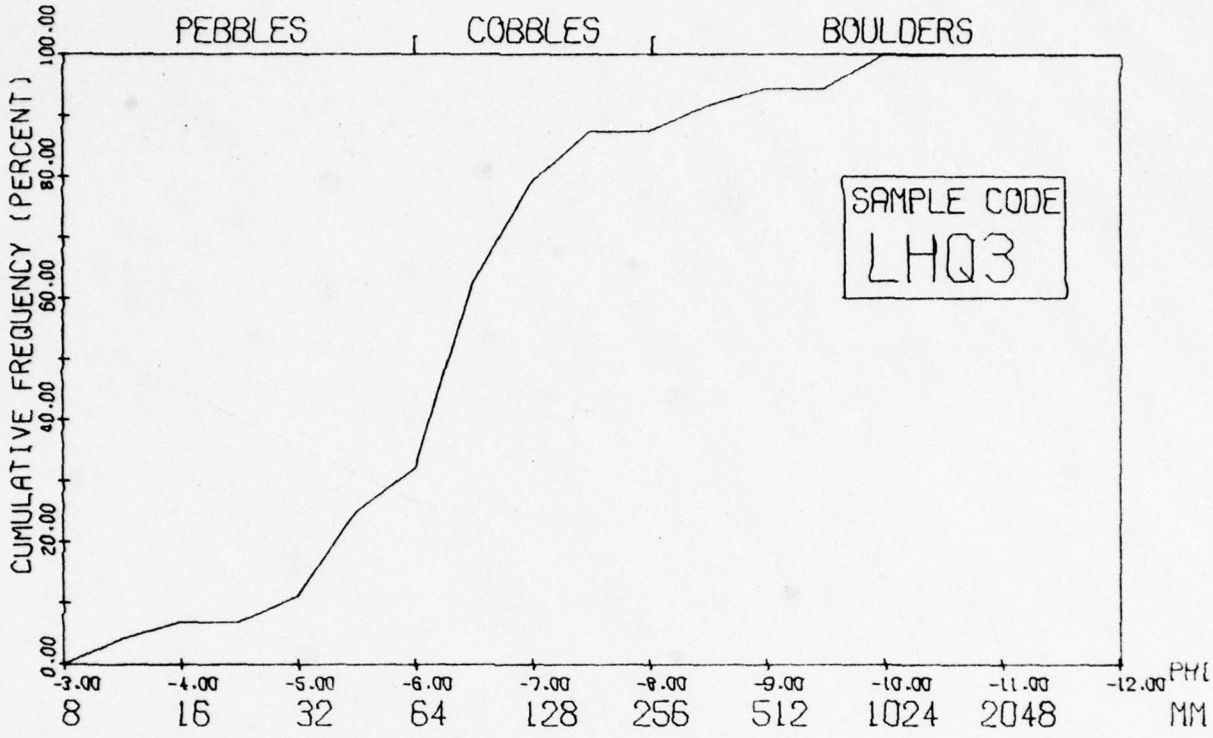
PEBBLES
COBBLES
BOULDERS
CUMULATIVE FREQUENCY (PERCENT)
0.00
20.00
40.00
60.00
80.00
100.00
SAMPLE CODE
LHQ3
-3.00
-4.00
-5.00
-6.00
-7.00
-8.00
-9.00
-10.00
-11.00
-12.00
PHI
8
16
32
64
128
256
512
1024
2048
MM

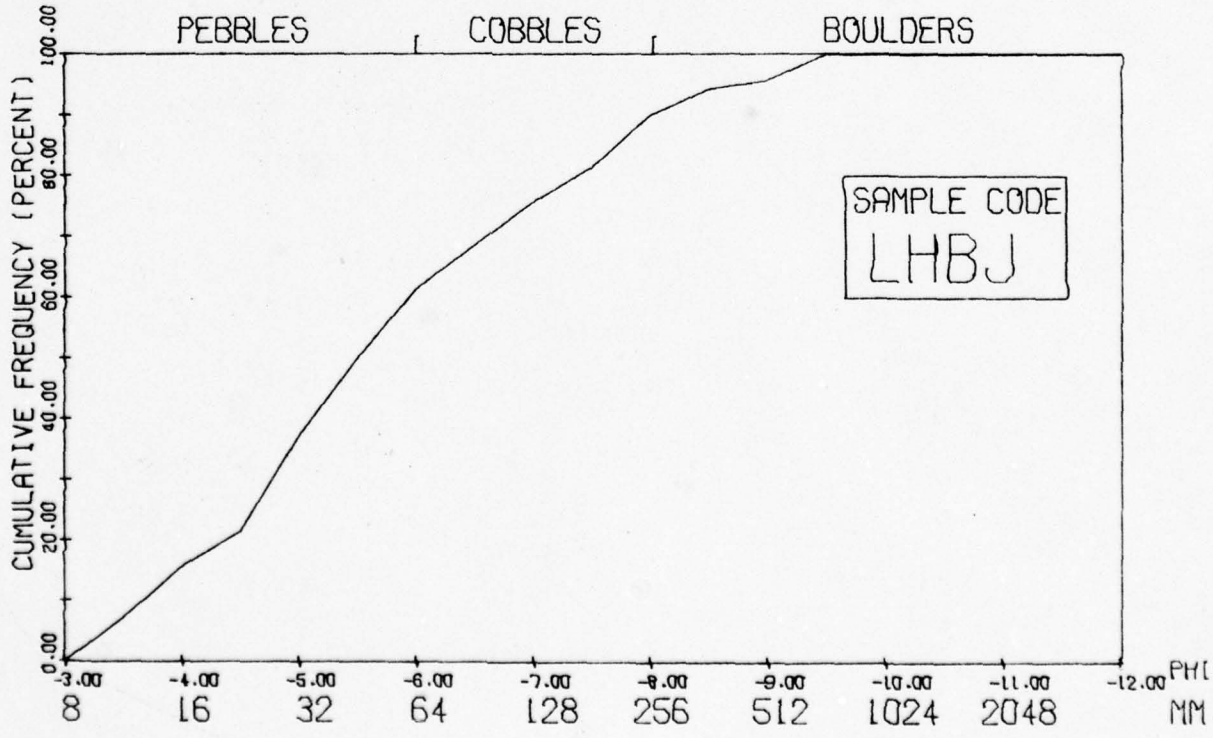
PEBBLES
COBBLES
BOULDERS
CUMULATIVE FREQUENCY (PERCENT)
0.00
20.00
40.00
60.00
80.00
100.00
SAMPLE CODE
LHBJ
-3.00
-4.00
-5.00
-6.00
-7.00
-8.00
-9.00
-10.00
-11.00
-12.00
PHI
8
16
32
64
128
256
512
1024
2048
MM

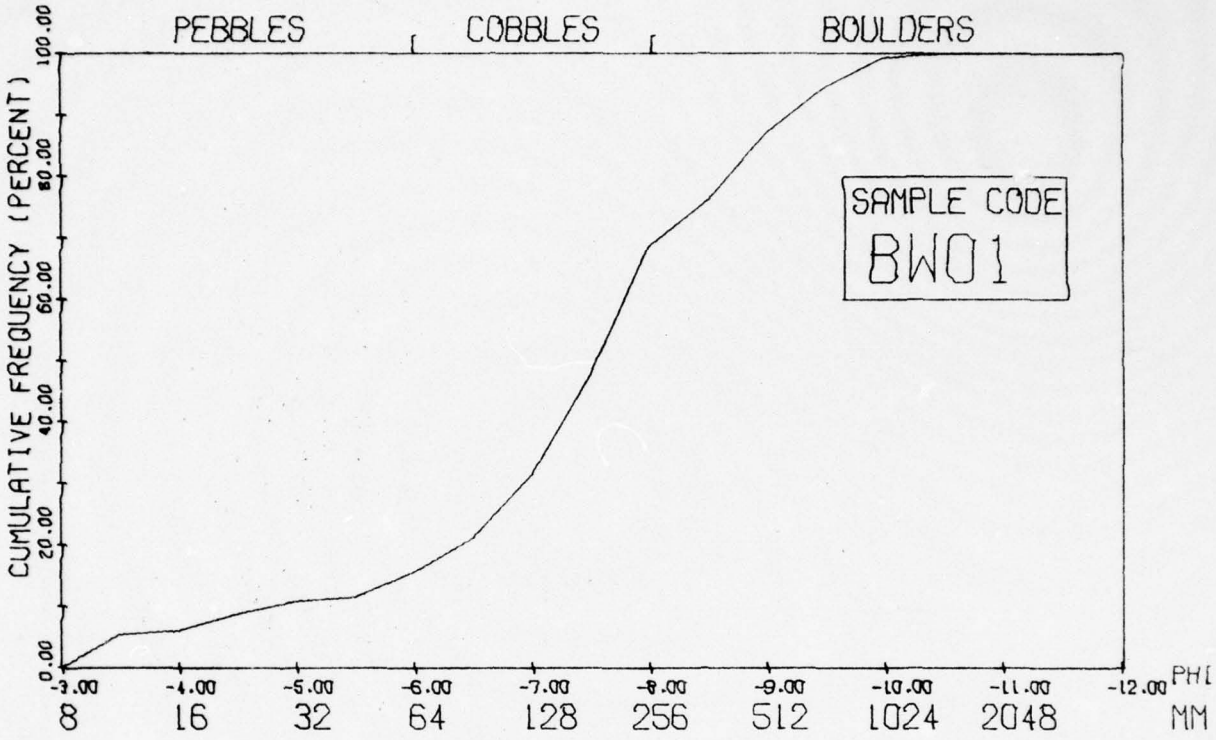
PEBBLES
COBBLES
BOULDERS
CUMULATIVE FREQUENCY (PERCENT)
100.00
80.00
60.00
40.00
20.00
0.00
SAMPLE CODE
BW01
-3.00
-4.00
-5.00
-6.00
-7.00
-8.00
-9.00
-10.00
-11.00
-12.00
PHI
8
16
32
64
128
256
512
1024
2048
MM

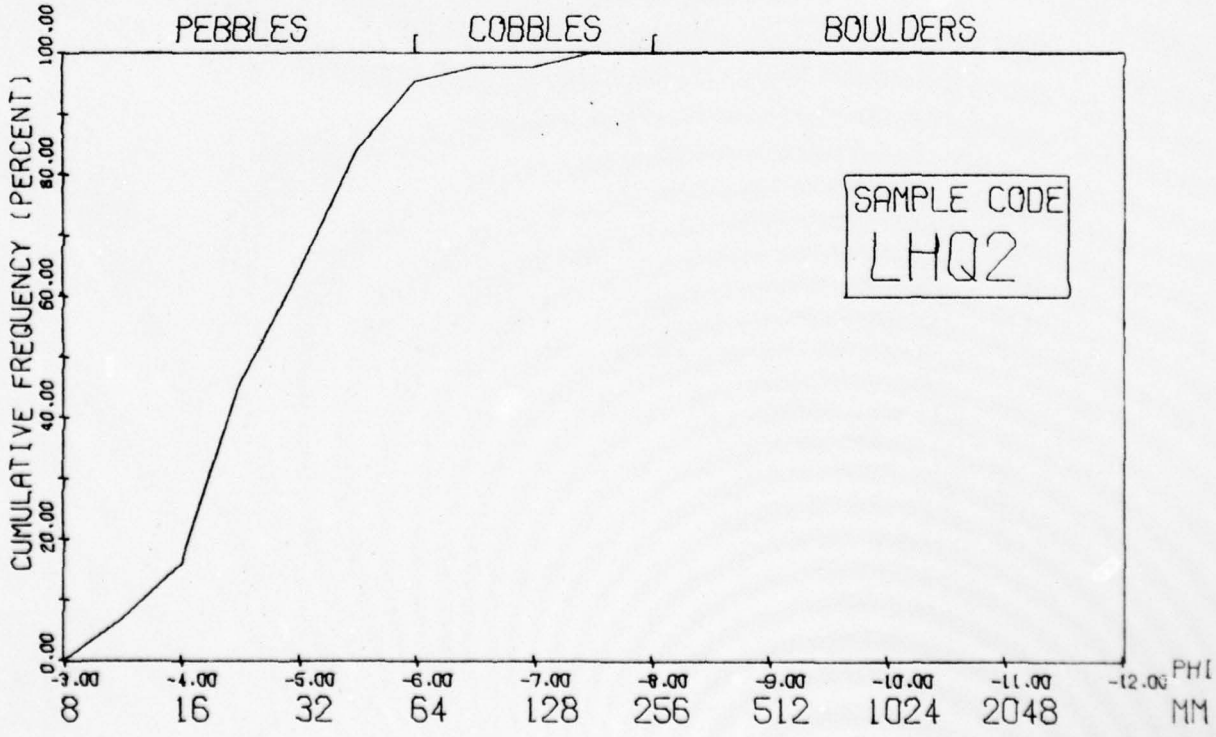
PEBBLES
COBBLES
BOULDERS
CUMULATIVE FREQUENCY (PERCENT)
100.00
80.00
60.00
40.00
20.00
0.00
SAMPLE CODE
LHQ2
-3.00
-4.00
-5.00
-6.00
-7.00
-8.00
-9.00
-10.00
-11.00
-12.00
PHI
8
16
32
64
128
256
512
1024
2048
MM

| Sample Code | Maximum Category (mm) | Minimum Category (mm) | Mode (mm) | Median (mm) | Mean (mm) | Variance | Standard Deviation | Skewness | Kurtosis |
|---|---|---|---|---|---|---|---|---|---|
| BW01 | 1252.0 | 9.5 | 214.0 | 212.4 | 259.2 | 55628.1 | 235.8 | 1.56 | 2.34 |
| BW02 | 1778.0 | 19.0 | 453.0 | 301.2 | 424.7 | 185025.8 | 430.1 | 1.63 | 2.16 |
| BW03 | 3556.0 | 26.8 | 303.0 | 300.7 | 505.1 | 324748.2 | 569.8 | 2.41 | 7.10 |
| BW05 | 889.0 | 9.5 | 107.0 | 107.3 | 191.4 | 44414.7 | 210.7 | 1.99 | 3.62 |
| BW06 | 889.0 | 9.5 | 214.0 | 155.6 | 207.5 | 24547.2 | 156.6 | 1.47 | 2.82 |
| BW07 | 632.0 | 9.5 | 303.0 | 109.7 | 162.6 | 19949.7 | 141.2 | 1.18 | 1.12 |
| BW08 | 453.0 | 9.5 | 54.0 | 76.6 | 113.0 | 8954.9 | 94.6 | 1.43 | 2.01 |
| BW09 | 303.0 | 9.5 | 54.0 | 75.1 | 92.4 | 5673.6 | 75.3 | 1.38 | 1.44 |
| BWXA | 107.0 | 9.5 | 19.0 | 19.5 | 28.8 | 545.6 | 23.3 | 1.73 | 2.69 |
| BWXB | 453.0 | 9.5 | 38.0 | 52.7 | 73.5 | 6170.3 | 78.5 | 2.98 | 10.48 |
| BW12 | 303.0 | 9.5 | 76.0 | 54.9 | 73.3 | 4082.0 | 63.8 | 1.94 | 4.14 |
| BW15 | 632.0 | 9.5 | 303.0 | 150.6 | 176.2 | 22666.1 | 150.5 | 1.04 | 0.46 |
| BW16 | 632.0 | 9.5 | 76.0 | 145.0 | 174.3 | 16499.7 | 128.4 | 1.29 | 1.51 |
| BW17 | 1778.0 | 19.0 | 453.0 | 299.4 | 340.4 | 85448.7 | 292.3 | 2.03 | 6.42 |
| BW18 | 632.0 | 9.5 | 152.0 | 107.7 | 150.5 | 16775.8 | 129.5 | 1.26 | 1.38 |
| BW19 | 889.0 | 13.4 | 152.0 | 109.1 | 170.3 | 27477.3 | 165.7 | 2.39 | 6.68 |

Table G-21 Particle Size Statistics for Boulder Wash Samples.

| Sample Code | Maximum Category (mm) | Minimum Category (mm) | Mode (mm) | Median (mm) | Mean (mm) | Variance | Standard Deviation | Skewness | Kurfosis |
|---|---|---|---|---|---|---|---|---|---|
| BW20 | 3556.0 | 76.0 | 889.0 | 862.8 | 828.8 | 474407.2 | 688.7 | 2.65 | 7.89 |
| BW2Y | 1252.0 | 9.5 | 632.0 | 631.1 | 558.7 | 150274.4 | 387.6 | 0.34 | -0.65 |
| BW22 | 303. | 9.5 | 76.0 | 74.2 | 76.3 | 2772.7 | 52.6 | 1.40 | 2.68 |
| BW30 | 303.0 | 9.5 | 26.8 | 38.1 | 53.6 | 2278.1 | 47.7 | 2.11 | 6.90 |
| BW31 | 453.0 | 9.5 | 107.0 | 53.8 | 73.7 | 5001.7 | 70.7 | 2.33 | 7.59 |
| BW32 | 76.0 | 9.5 | 19.0 | 25.6 | 28.8 | 222.9 | 14.9 | 1.22 | 1.22 |
| BW33 | 152.0 | 9.5 | 54.0 | 37.8 | 48.5 | 1434.9 | 37.8 | 1.30 | 1.16 |
| BWJ1 | 453.0 | 19.0 | 152.0 | 150.2 | 185.9 | 20723.8 | 143.9 | 0.89 | -0.55 |
| BWJ2 | 303.0 | 26.8 | 107.0 | 142.2 | 138.8 | 3569.0 | 59.7 | 0.58 | 0.24 |
| BWJ3 | 453.9 | 54.0 | 107.0 | 144.1 | 159.6 | 6928.7 | 83.2 | 1.71 | 3.39 |
| BWJ4 | 632.0 | 54.0 | 107.0 | 158.6 | 265.1 | 41213.2 | 203.0 | 0.90 | -0.75 |
| BWJ5 | 453.0 | 38.0 | 107.0 | 150.6 | 178.5 | 13490.7 | 116.1 | 1.35 | 1.03 |
| BWJ6 | 1252.0 | 152.0 | 214.0 | 453.0 | 525.2 | 99015.3 | 314.6 | 0.68 | -0.52 |
| BWJ7 | 1778.0 | 214.0 | 453.0 | 497.5 | 669.3 | 161543.0 | 401.9 | 1.23 | 0.65 |
| BWT8 | 1252.0 | 19.0 | 303.0 | 300.5 | 339.8 | 77570.0 | 278.5 | 1.39 | 1.67 |
| BWT1 | 453.0 | 9.5 | 54.0 | 38.3 | 53.4 | 3911.5 | 62.5 | 3.87 | 19.14 |
| BWTI | 303. | 9.5 | 54.0 | 52.7 | 62.8 | 2939.7 | 54.2 | 2.13 | 5.37 |

Table G-22 Particle Size Statistics for Boulder Wash Samples.

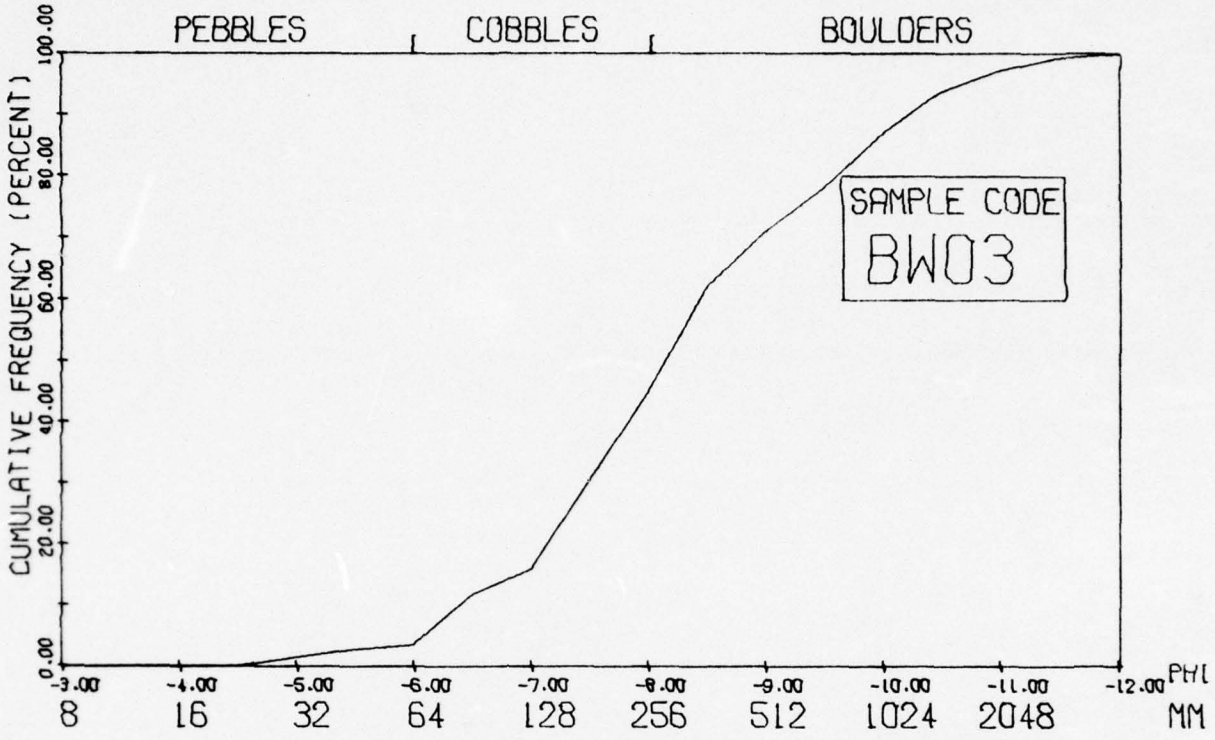
PEBBLES
COBBLES
BOULDERS
CUMULATIVE FREQUENCY (PERCENT)
0.00
20.00
40.00
60.00
80.00
100.00
SAMPLE CODE
BW03
-3.00
-4.00
-5.00
-6.00
-7.00
-8.00
-9.00
-10.00
-11.00
-12.00
PHI
8
16
32
64
128
256
512
1024
2048
MM

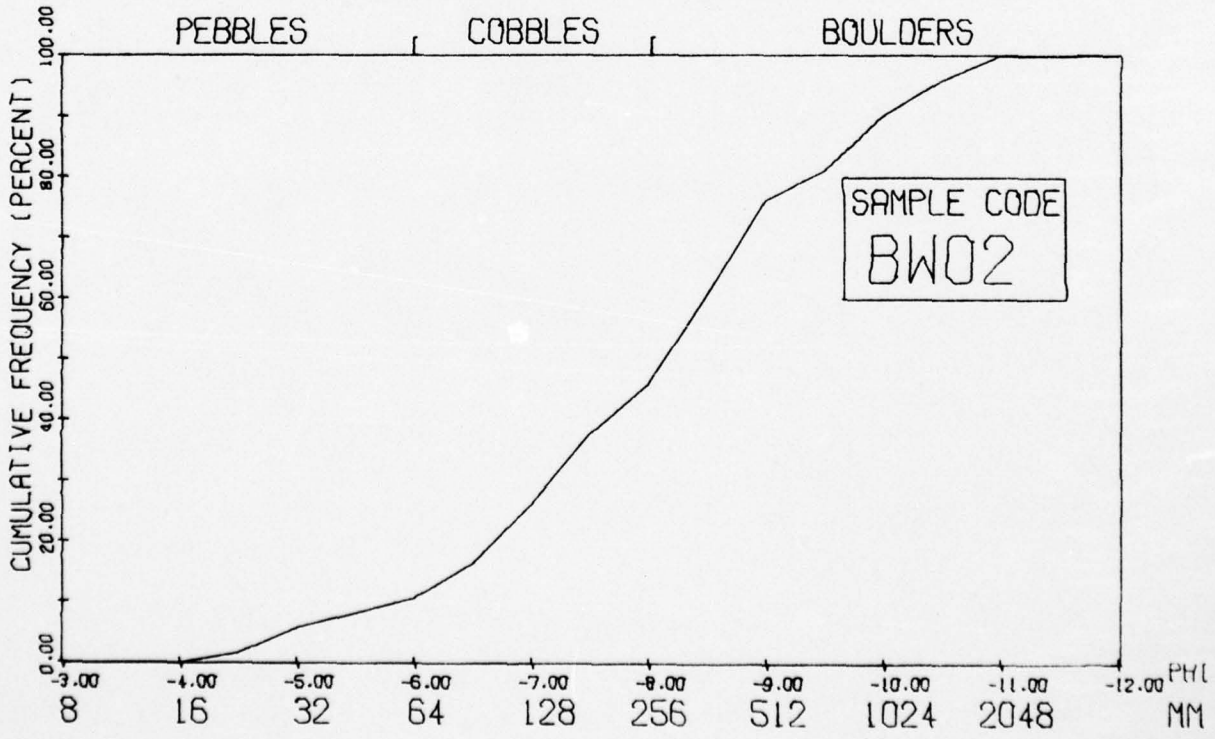
PEBBLES
COBBLES
BOULDERS
CUMULATIVE FREQUENCY (PERCENT)
0.00
20.00
40.00
60.00
80.00
100.00
SAMPLE CODE
BW02
-3.00
-4.00
-5.00
-6.00
-7.00
-8.00
-9.00
-10.00
-11.00
-12.00
PHI
8
16
32
64
128
256
512
1024
2048
MM

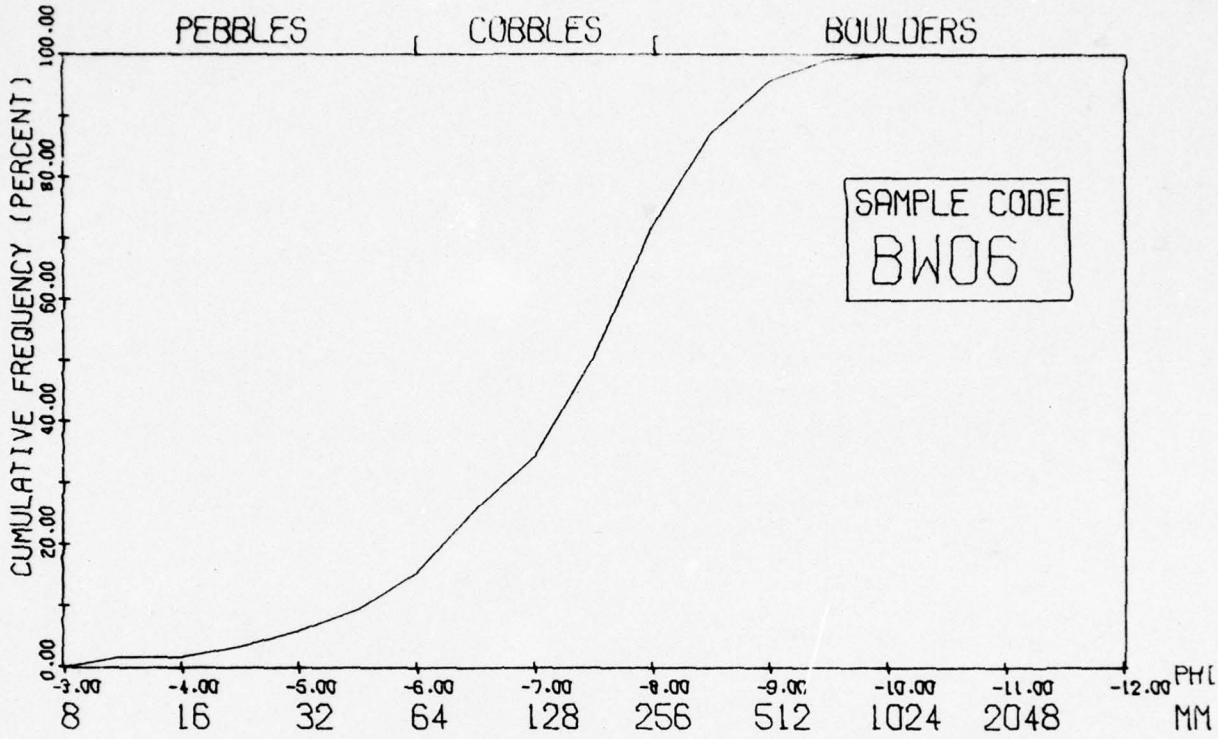
PEBBLES
COBBLES
BOULDERS
CUMULATIVE FREQUENCY (PERCENT)
0.00
20.00
40.00
60.00
80.00
100.00
SAMPLE CODE
BW06
-3.00
-4.00
-5.00
-6.00
-7.00
-8.00
-9.00
-10.00
-11.00
-12.00
PHI
8
16
32
64
128
256
512
1024
2048
MM

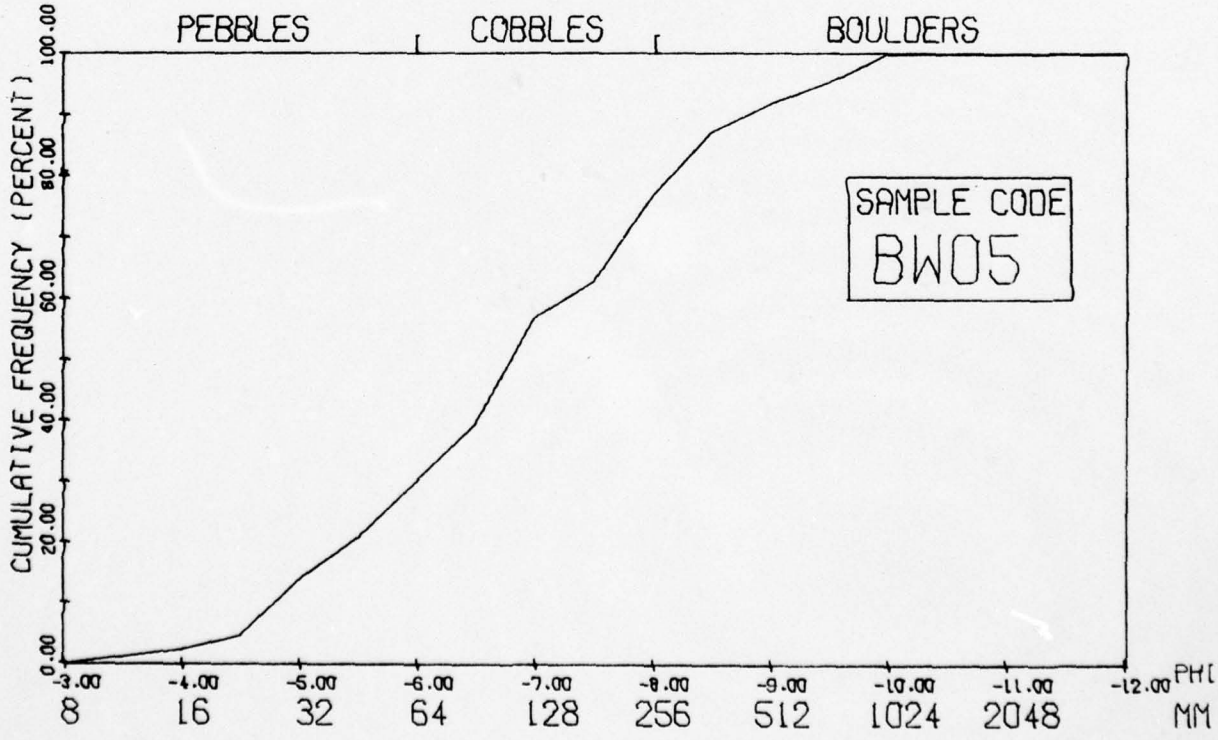
PEBBLES
COBBLES
BOULDERS
CUMULATIVE FREQUENCY (PERCENT)
0.00
20.00
40.00
60.00
80.00
100.00
SAMPLE CODE
BW05
-3.00
-4.00
-5.00
-6.00
-7.00
-8.00
-9.00
-10.00
-11.00
-12.00
PHI
8
16
32
64
128
256
512
1024
2048
MM

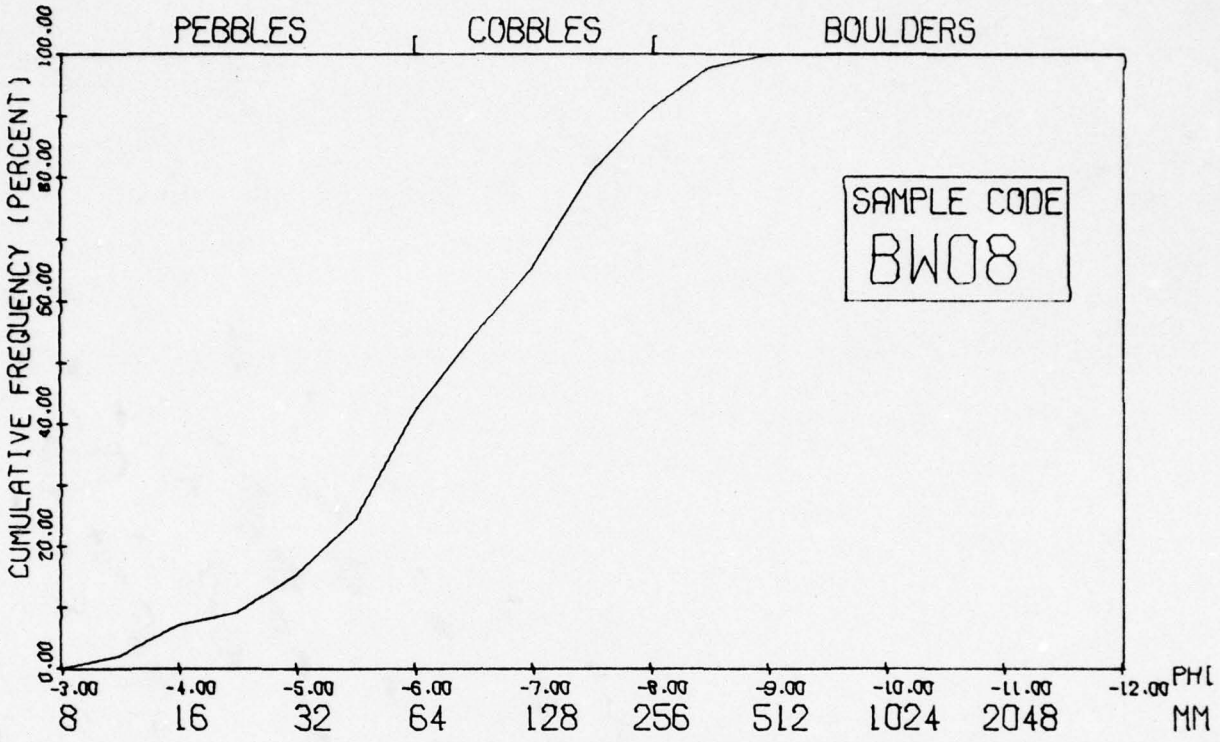
PEBBLES
COBBLES
BOULDERS
CUMULATIVE FREQUENCY (PERCENT)
0.00
20.00
40.00
60.00
80.00
100.00
SAMPLE CODE
BW08
-3.00
-4.00
-5.00
-6.00
-7.00
-8.00
-9.00
-10.00
-11.00
-12.00
PHI
8
16
32
64
128
256
512
1024
2048
MM

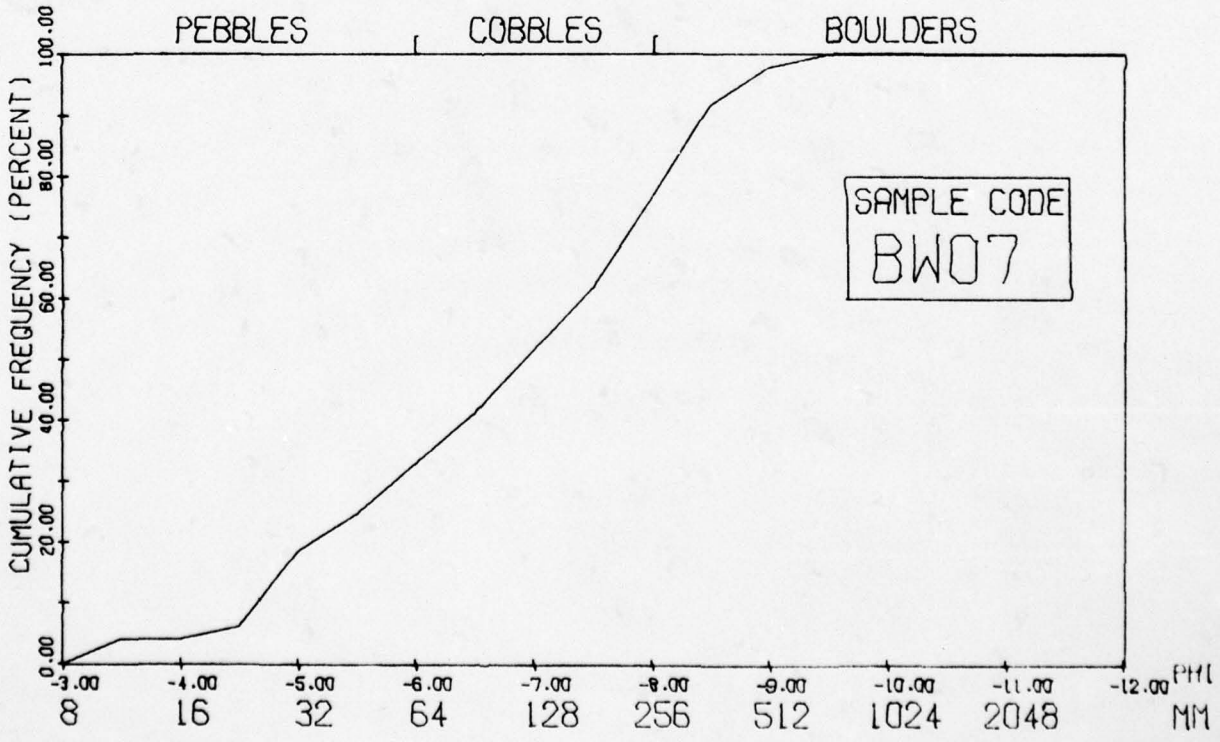
PEBBLES
COBBLES
BOULDERS
CUMULATIVE FREQUENCY (PERCENT)
0.00
20.00
40.00
60.00
80.00
100.00
SAMPLE CODE
BW07
-3.00
-4.00
-5.00
-6.00
-7.00
-8.00
-9.00
-10.00
-11.00
-12.00
PHI
8
16
32
64
128
256
512
1024
2048
MM

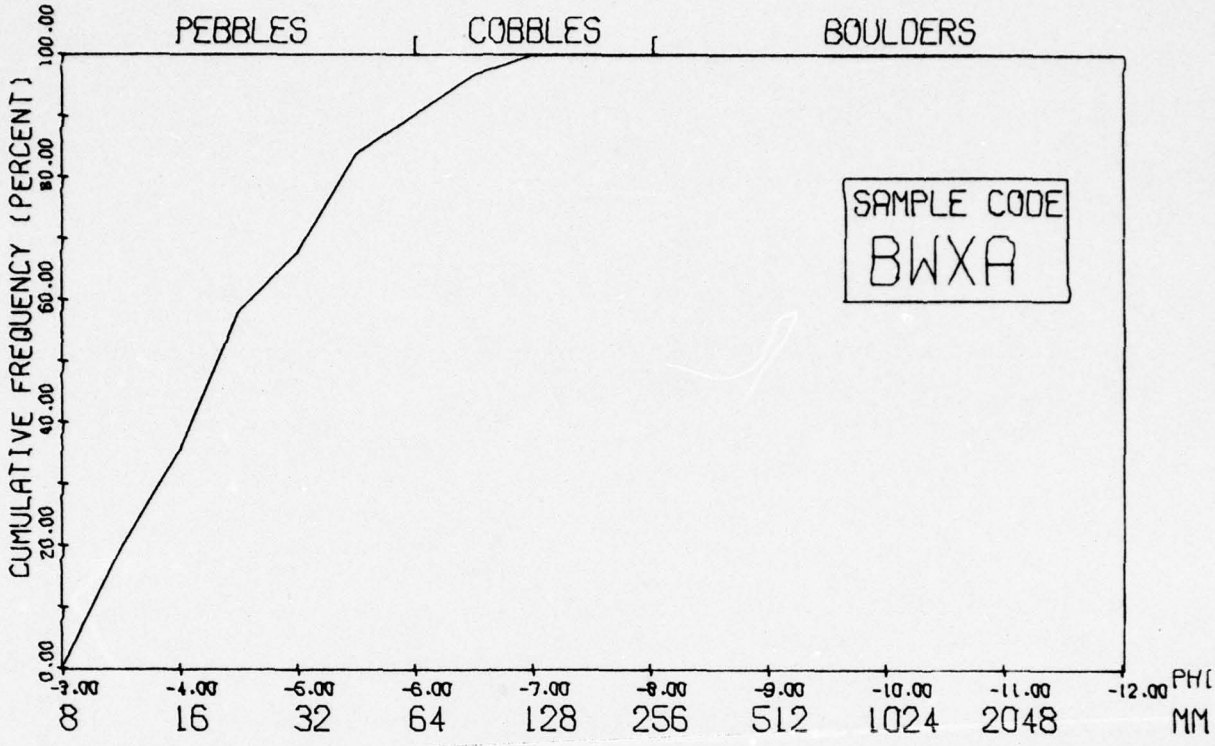
PEBBLES
COBBLES
BOULDERS
CUMULATIVE FREQUENCY (PERCENT)
0.00
20.00
40.00
60.00
80.00
100.00
SAMPLE CODE
BWXA
-3.00
-4.00
-5.00
-6.00
-7.00
-8.00
-9.00
-10.00
-11.00
-12.00
PHI
8
16
32
64
128
256
512
1024
2048
MM

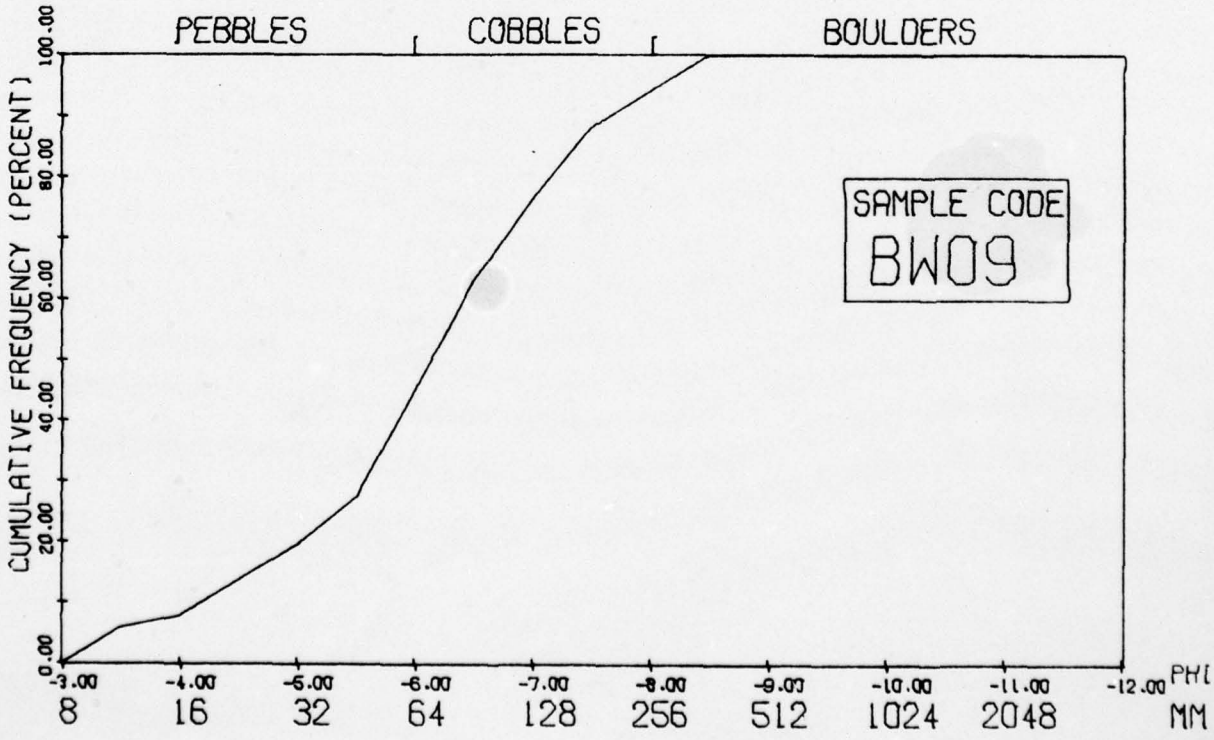
PEBBLES
COBBLES
BOULDERS
CUMULATIVE FREQUENCY (PERCENT)
0.00
20.00
40.00
60.00
80.00
100.00
SAMPLE CODE
BW09
-3.00
-4.00
-5.00
-6.00
-7.00
-8.00
-9.00
-10.00
-11.00
-12.00
PHI
8
16
32
64
128
256
512
1024
2048
MM

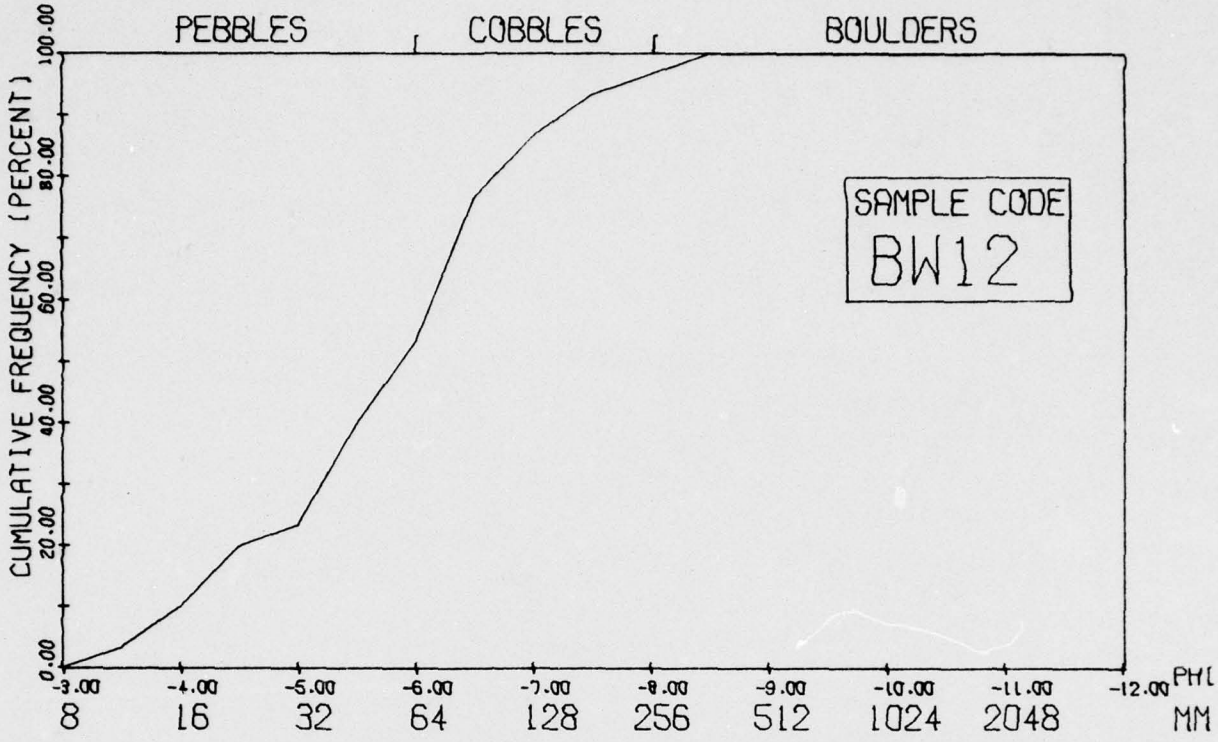
PEBBLES
COBBLES
BOULDERS
CUMULATIVE FREQUENCY (PERCENT)
0.00
20.00
40.00
60.00
80.00
100.00
SAMPLE CODE
BW12
-3.00
-4.00
-5.00
-6.00
-7.00
-8.00
-9.00
-10.00
-11.00
-12.00
PHI
8
16
32
64
128
256
512
1024
2048
MM

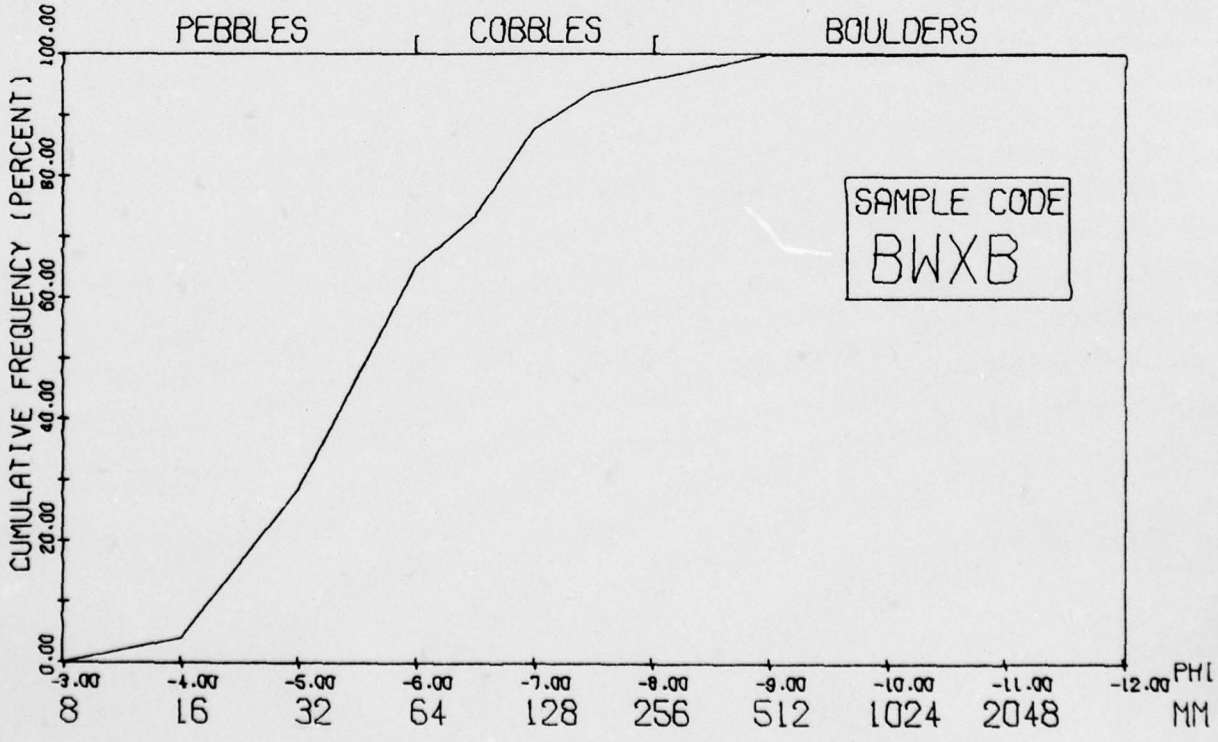
PEBBLES
COBBLES
BOULDERS
CUMULATIVE FREQUENCY (PERCENT)
0.00
20.00
40.00
60.00
80.00
100.00
SAMPLE CODE
BWXB
-3.00
-4.00
-5.00
-6.00
-7.00
-8.00
-9.00
-10.00
-11.00
-12.00
PHI
8
16
32
64
128
256
512
1024
2048
MM

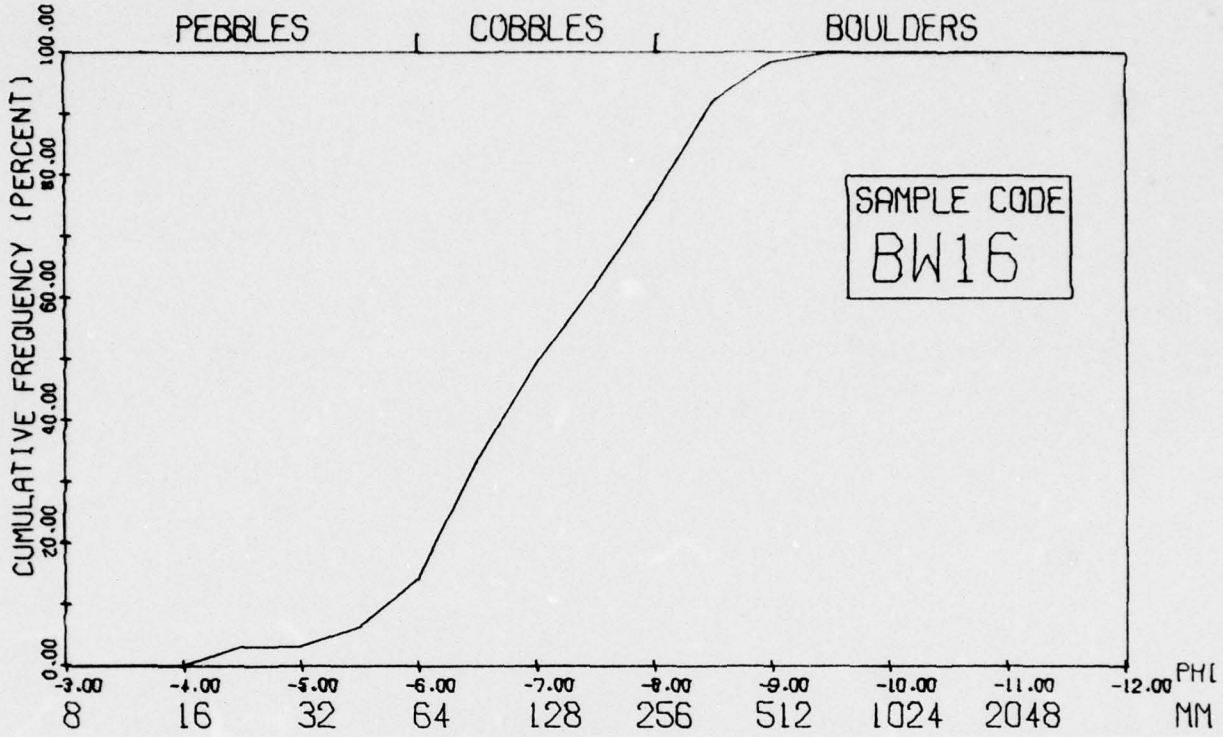
PEBBLES
COBBLES
BOULDERS
CUMULATIVE FREQUENCY (PERCENT)
0.00
20.00
40.00
60.00
80.00
100.00
SAMPLE CODE
BW16
-3.00
-4.00
-5.00
-6.00
-7.00
-8.00
-9.00
-10.00
-11.00
-12.00
PHI
8
16
32
64
128
256
512
1024
2048
MM

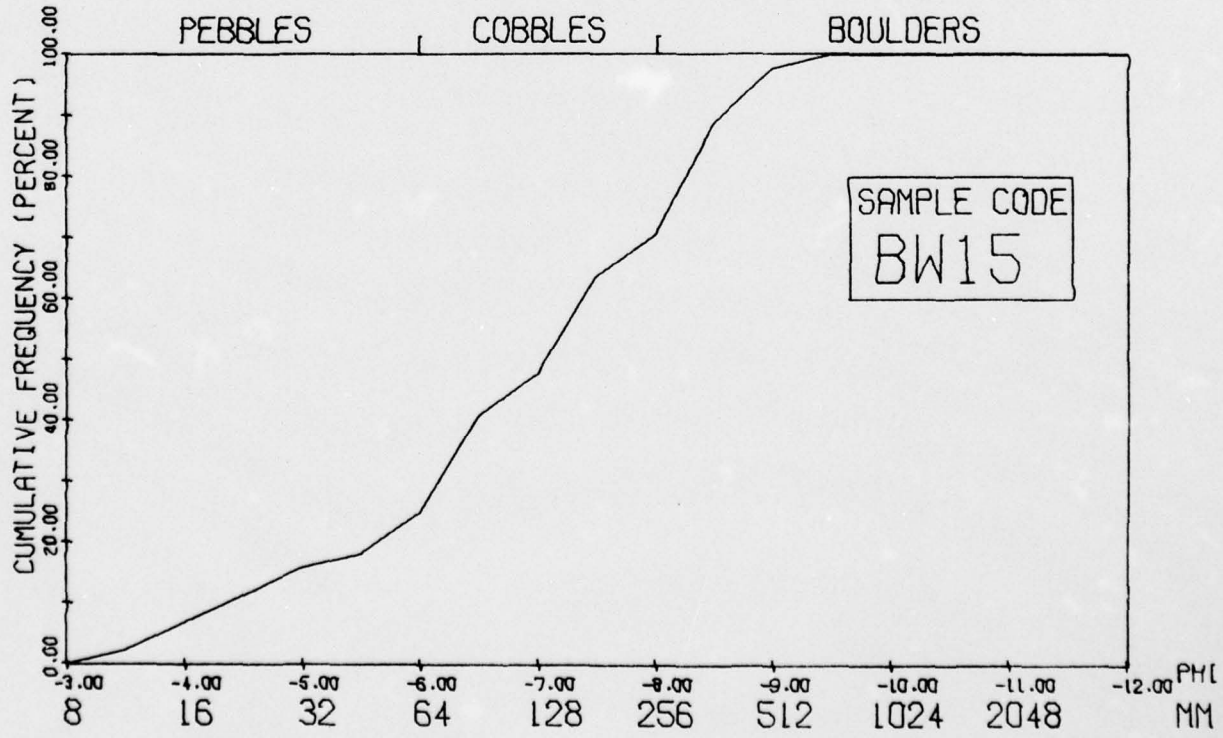
PEBBLES
COBBLES
BOULDERS
CUMULATIVE FREQUENCY (PERCENT)
0.00
20.00
40.00
60.00
80.00
100.00
SAMPLE CODE
BW15
-3.00
-4.00
-5.00
-6.00
-7.00
-8.00
-9.00
-10.00
-11.00
-12.00
PHI
8
16
32
64
128
256
512
1024
2048
MM

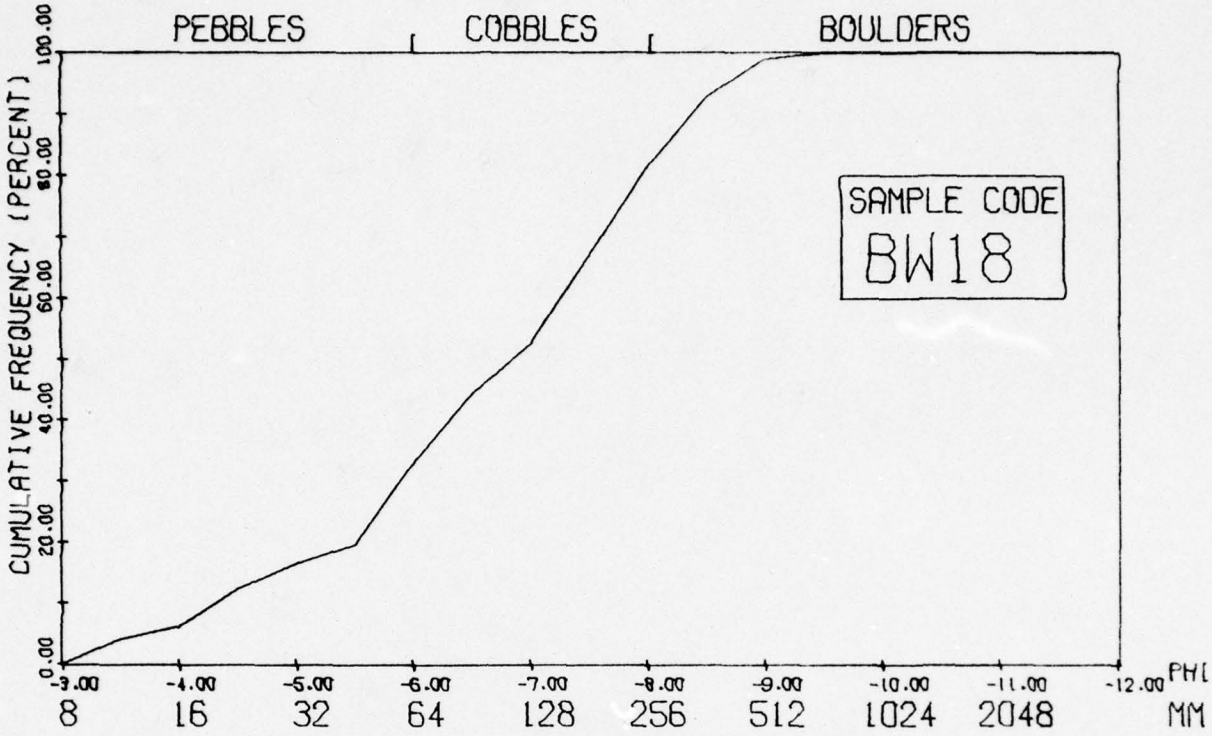
PEBBLES
COBBLES
BOULDERS
CUMULATIVE FREQUENCY (PERCENT)
100.00
80.00
60.00
40.00
20.00
0.00
SAMPLE CODE
BW18
-3.00
-4.00
-5.00
-6.00
-7.00
-8.00
-9.00
-10.00
-11.00
-12.00
PHI
8
16
32
64
128
256
512
1024
2048
MM

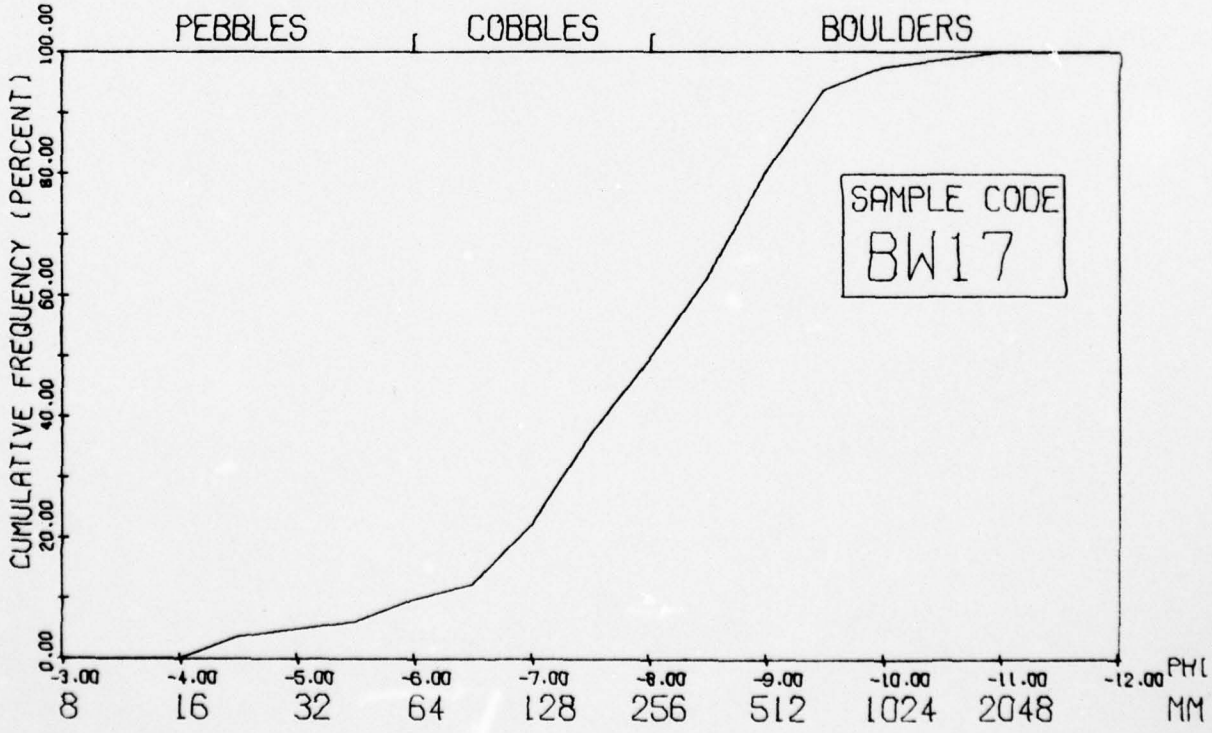
PEBBLES
COBBLES
BOULDERS
CUMULATIVE FREQUENCY (PERCENT)
100.00
80.00
60.00
40.00
20.00
0.00
SAMPLE CODE
BW17
-3.00
-4.00
-5.00
-6.00
-7.00
-8.00
-9.00
-10.00
-11.00
-12.00
PHI
8
16
32
64
128
256
512
1024
2048
MM

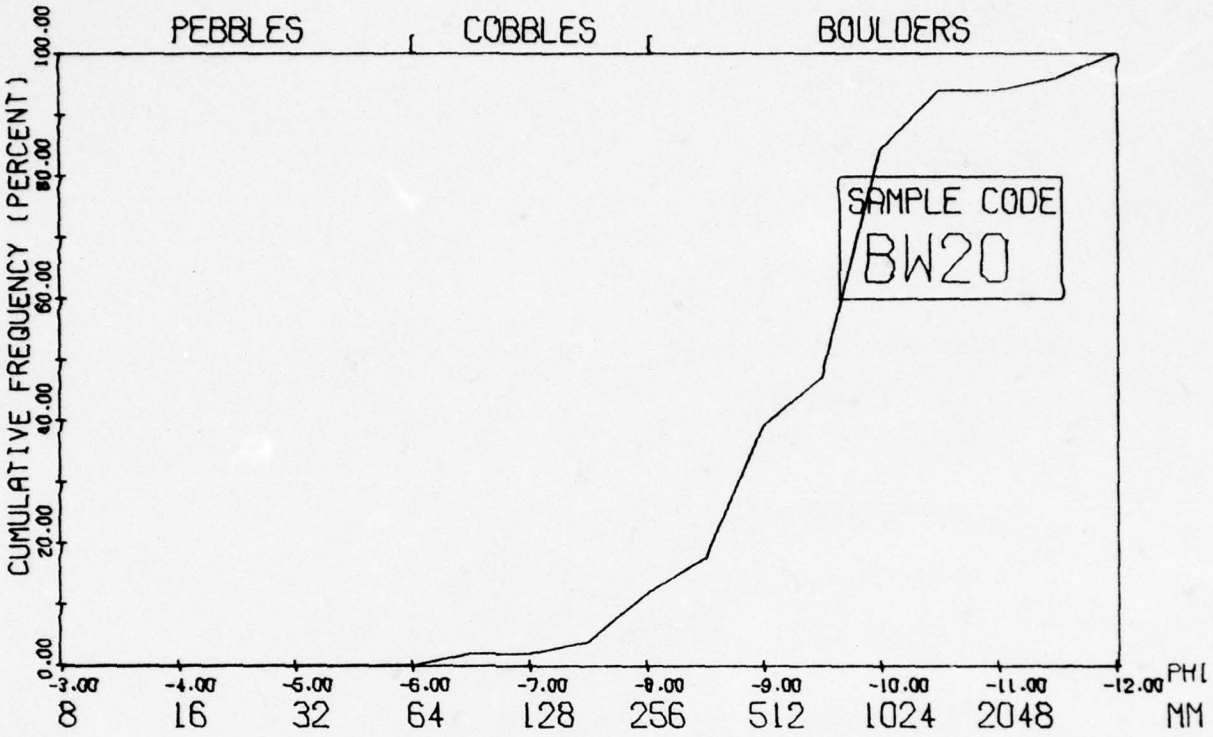
PEBBLES
COBBLES
BOULDERS
CUMULATIVE FREQUENCY (PERCENT)
100.00
80.00
60.00
40.00
20.00
0.00
SAMPLE CODE
BW20
-3.00
-4.00
-5.00
-6.00
-7.00
-8.00
-9.00
-10.00
-11.00
-12.00
PHI
8
16
32
64
128
256
512
1024
2048
MM

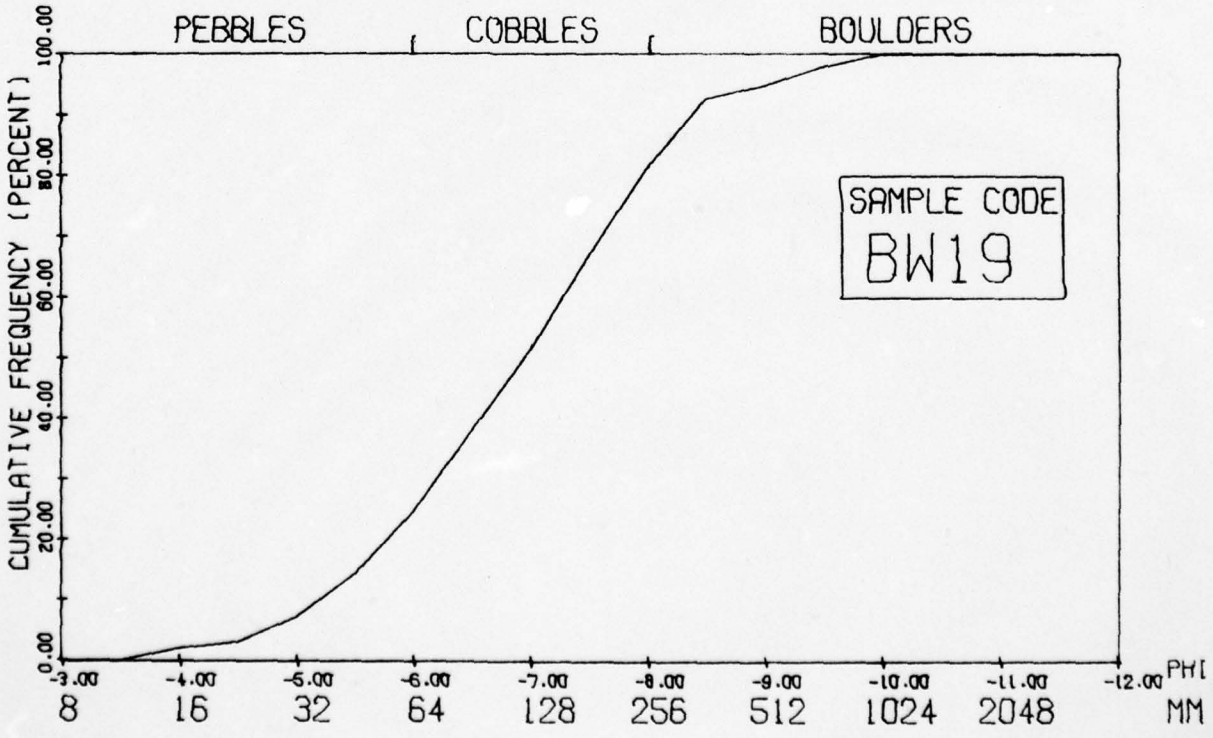
PEBBLES
COBBLES
BOULDERS
CUMULATIVE FREQUENCY (PERCENT)
100.00
80.00
60.00
40.00
20.00
0.00
SAMPLE CODE
BW19
-3.00
-4.00
-5.00
-6.00
-7.00
-8.00
-9.00
-10.00
-11.00
-12.00
PHI
8
16
32
64
128
256
512
1024
2048
MM

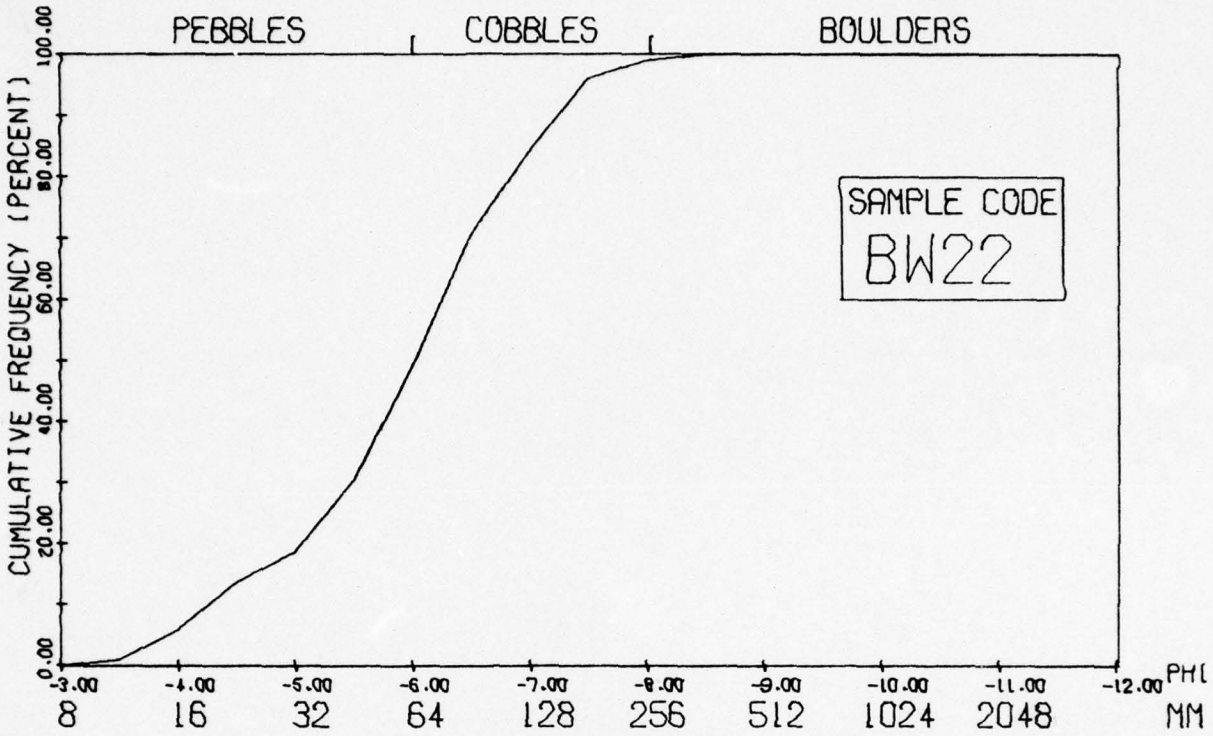
PEBBLES
COBBLES
BOULDERS
CUMULATIVE FREQUENCY (PERCENT)
0.00
20.00
40.00
60.00
80.00
100.00
SAMPLE CODE
BW22
-3.00
-4.00
-5.00
-6.00
-7.00
-8.00
-9.00
-10.00
-11.00
-12.00
PHI
8
16
32
64
128
256
512
1024
2048
MM

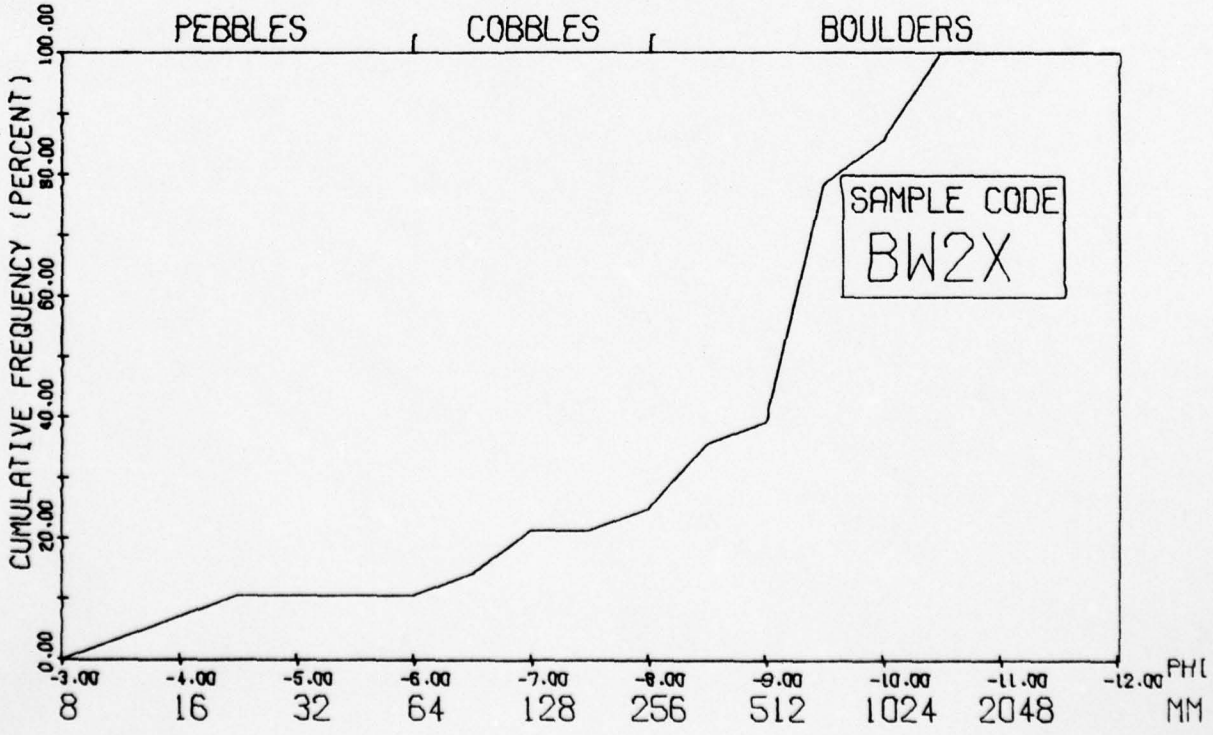
PEBBLES
COBBLES
BOULDERS
CUMULATIVE FREQUENCY (PERCENT)
0.00
20.00
40.00
60.00
80.00
100.00
SAMPLE CODE
BW2X
-3.00
-4.00
-5.00
-6.00
-7.00
-8.00
-9.00
-10.00
-11.00
-12.00
PHI
8
16
32
64
128
256
512
1024
2048
MM

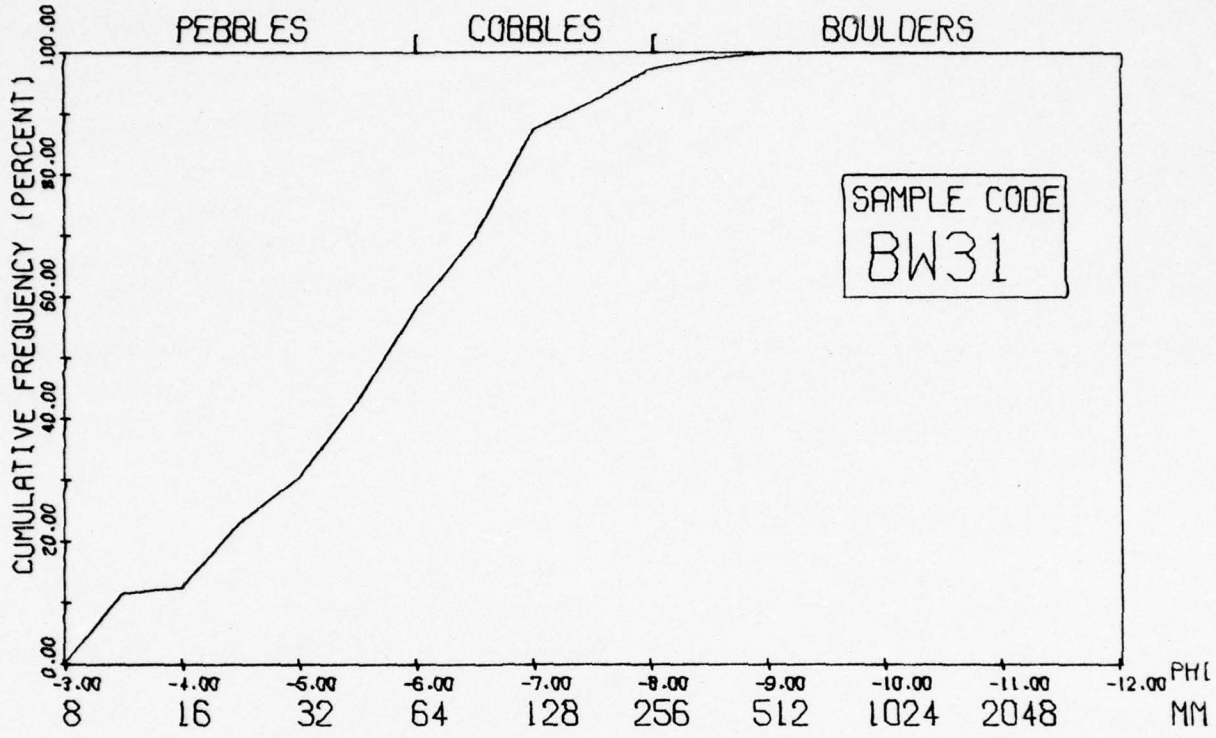
PEBBLES
COBBLES
BOULDERS
CUMULATIVE FREQUENCY (PERCENT)
100.00
80.00
60.00
40.00
20.00
0.00
SAMPLE CODE
BW31
-3.00
-4.00
-5.00
-6.00
-7.00
-8.00
-9.00
-10.00
-11.00
-12.00
PHI
8
16
32
64
128
256
512
1024
2048
MM

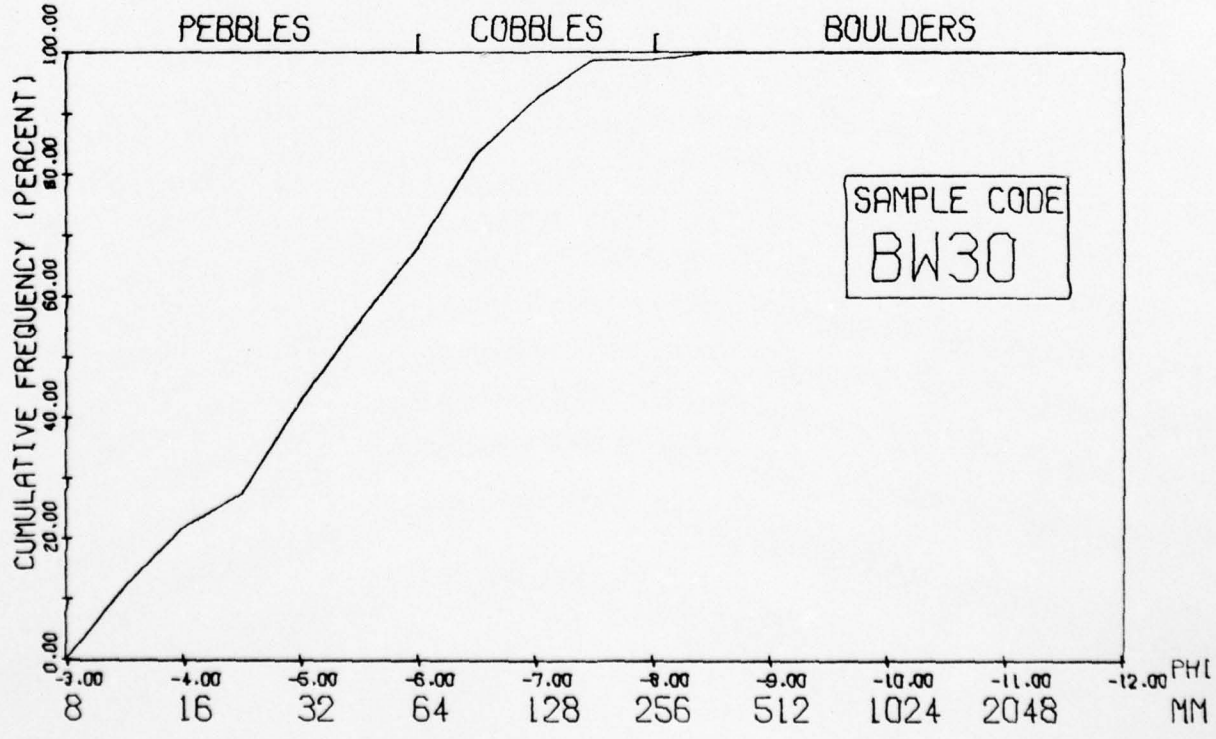
PEBBLES
COBBLES
BOULDERS
CUMULATIVE FREQUENCY (PERCENT)
100.00
80.00
60.00
40.00
20.00
0.00
SAMPLE CODE
BW30
-3.00
-4.00
-5.00
-6.00
-7.00
-8.00
-9.00
-10.00
-11.00
-12.00
PHI
8
16
32
64
128
256
512
1024
2048
MM

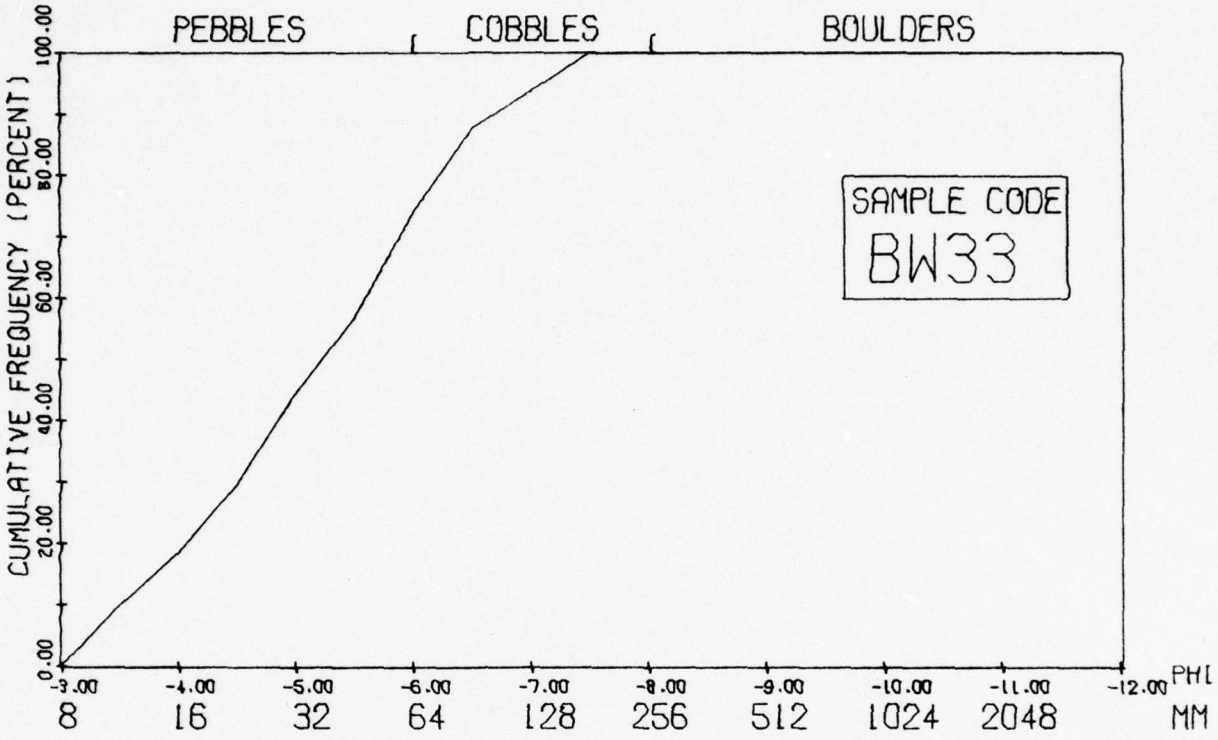
PEBBLES
COBBLES
BOULDERS
CUMULATIVE FREQUENCY (PERCENT)
100.00
80.00
60.00
40.00
20.00
0.00
SAMPLE CODE
BW33
-3.00
-4.00
-5.00
-6.00
-7.00
-8.00
-9.00
-10.00
-11.00
-12.00
PHI
8
16
32
64
128
256
512
1024
2048
MM

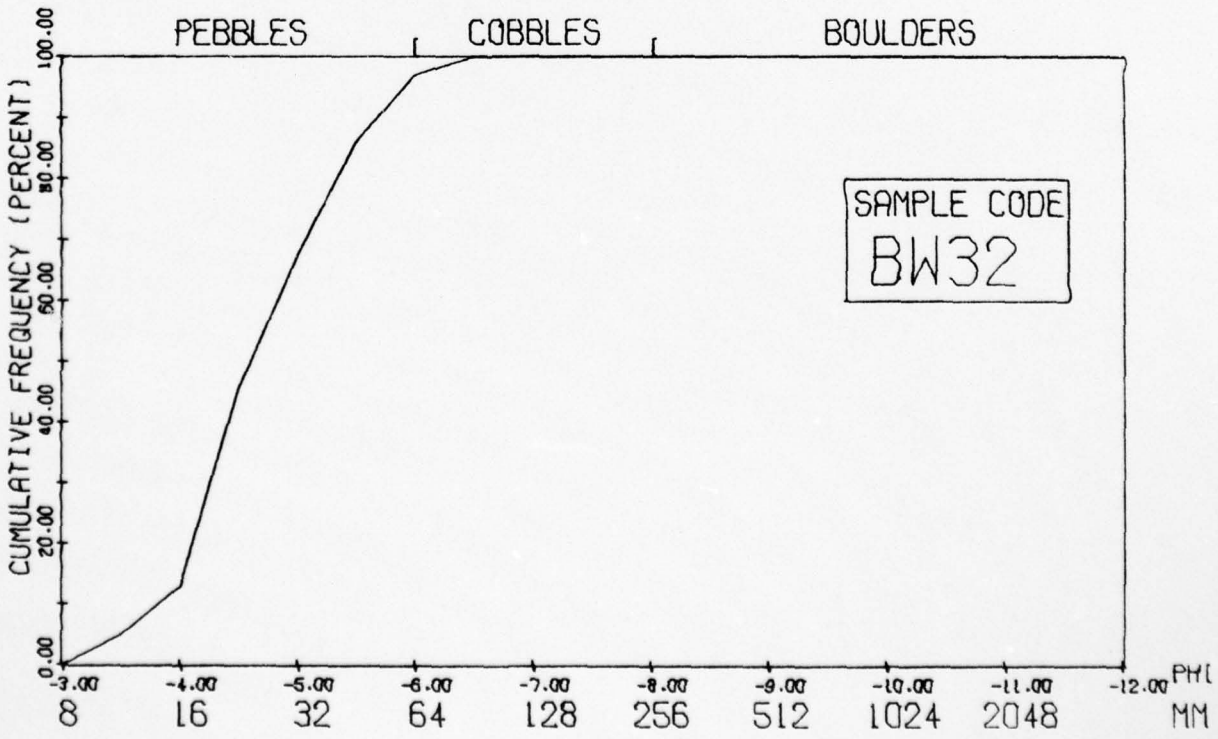
PEBBLES
COBBLES
BOULDERS
CUMULATIVE FREQUENCY (PERCENT)
100.00
80.00
60.00
40.00
20.00
0.00
SAMPLE CODE
BW32
-3.00
-4.00
-5.00
-6.00
-7.00
-8.00
-9.00
-10.00
-11.00
-12.00
PHI
8
16
32
64
128
256
512
1024
2048
MM

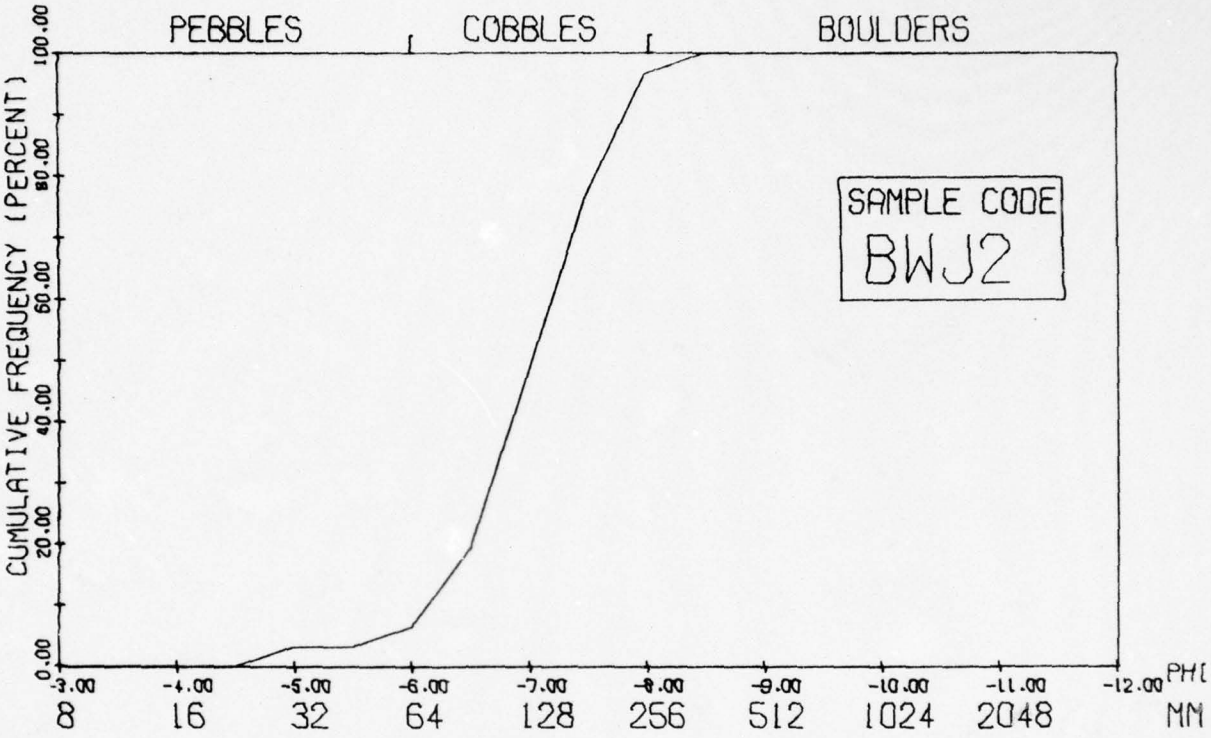
PEBBLES
COBBLES
BOULDERS
CUMULATIVE FREQUENCY (PERCENT)
0.00
20.00
40.00
60.00
80.00
100.00
SAMPLE CODE
BWJ2
-3.00
-4.00
-5.00
-6.00
-7.00
-8.00
-9.00
-10.00
-11.00
-12.00
PHI
8
16
32
64
128
256
512
1024
2048
MM

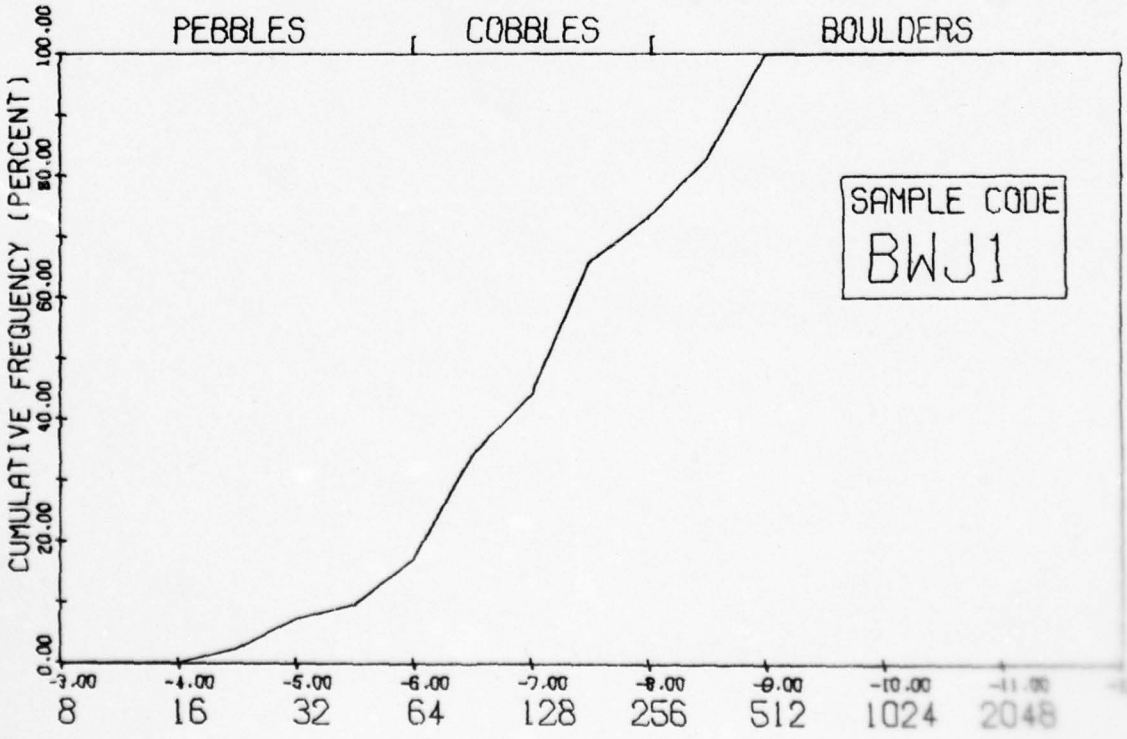
PEBBLES
COBBLES
BOULDERS
CUMULATIVE FREQUENCY (PERCENT)
0.00
20.00
40.00
60.00
80.00
100.00
SAMPLE CODE
BWJ1
-3.00
-4.00
-5.00
-6.00
-7.00
-8.00
-9.00
-10.00
-11.00
8
16
32
64
128
256
512
1024
2048

AD-A069 729 ARIZONA UNIV TUCSON DEPT OF GEOSCIENCES F/G 8/7
ORIGIN AND DISTRIBUTION OF GRAVEL IN STREAM SYSTEM OF ARID REGI--ETC(U)
DEC 78 R GERSON, W B BULL, L H FLEISCHHAUER F49620-77-C-0115
UNCLASSIFIED AFOSR-TR-79-0681 NL

2 OF 3
AD
A069729

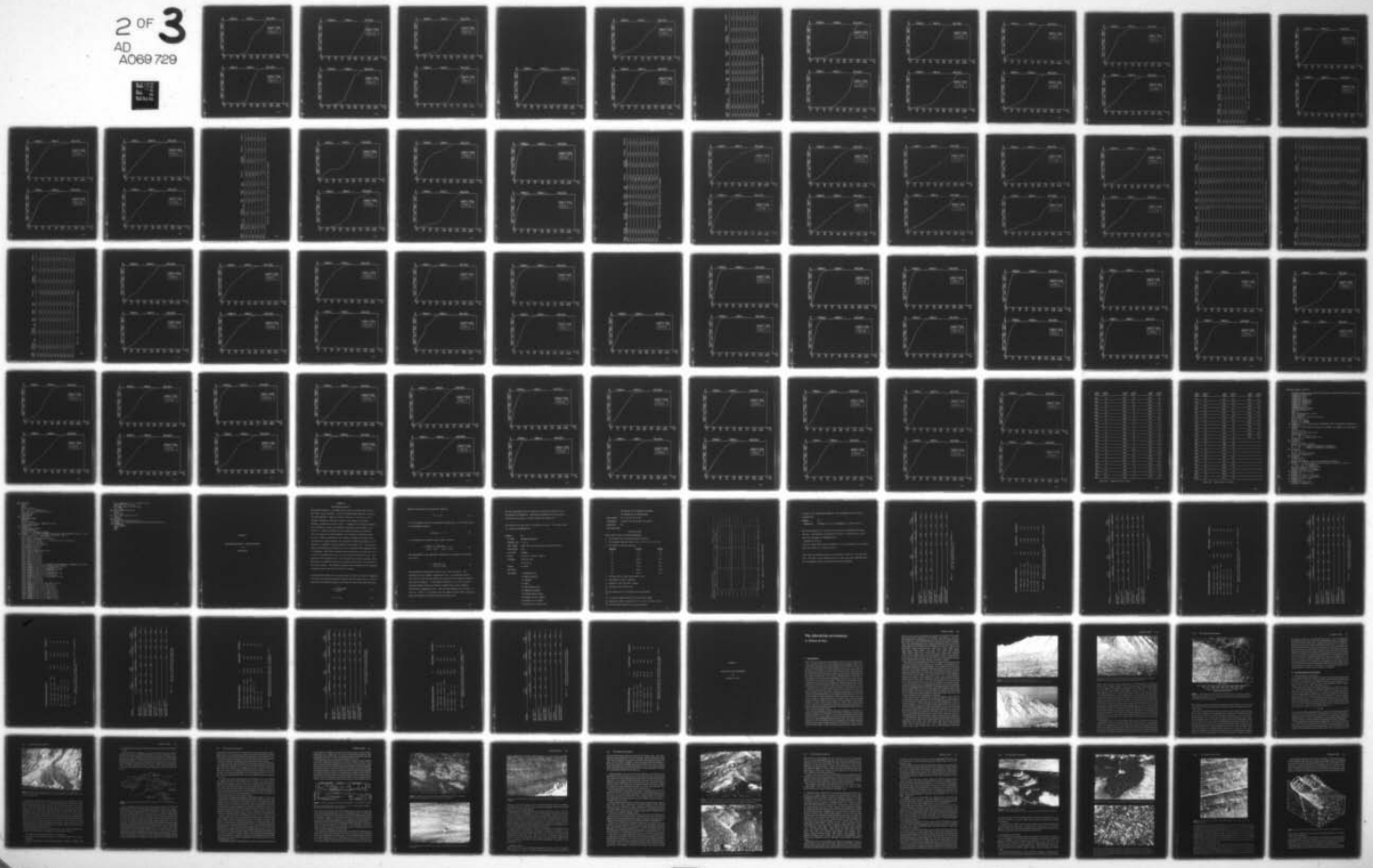

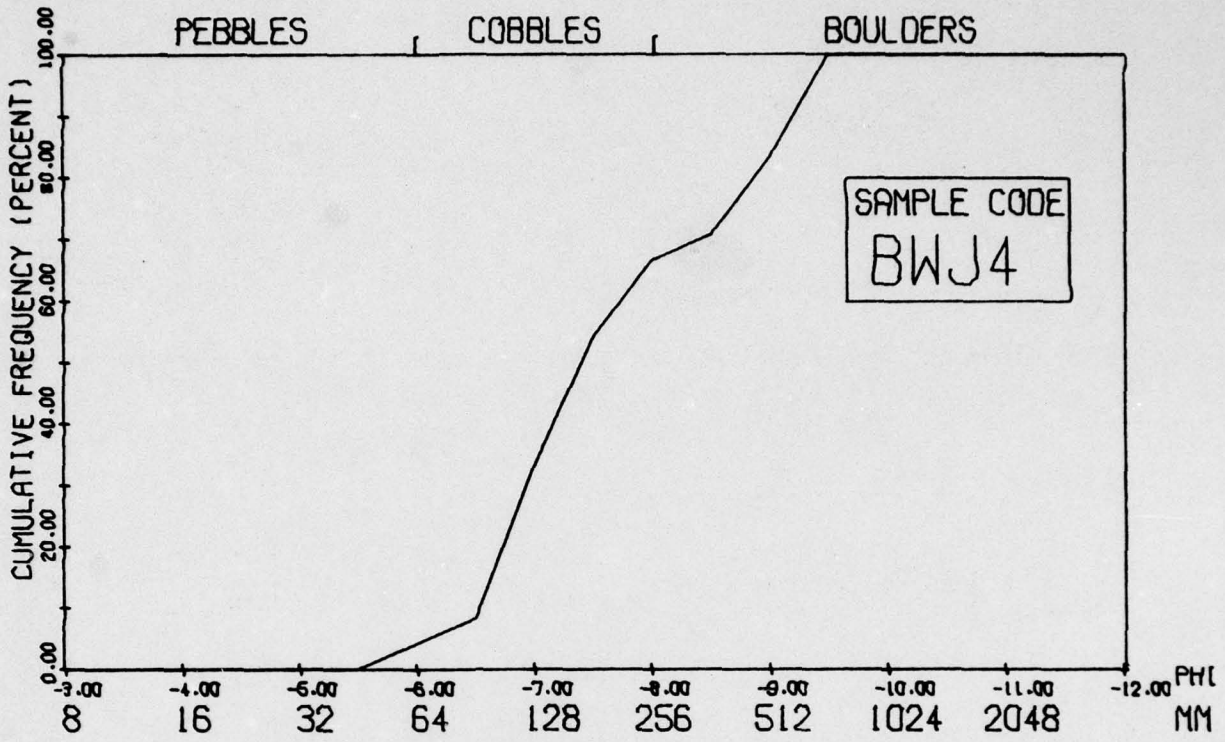
PEBBLES
COBBLES
BOULDERS
CUMULATIVE FREQUENCY (PERCENT)
100.00
80.00
60.00
40.00
20.00
0.00
SAMPLE CODE
BWJ4
-3.00
-4.00
-5.00
-6.00
-8.00
-7.00
-8.00
-9.00
-10.00
-11.00
-12.00
PHI
8
16
32
64
128
256
512
1024
2048
MM

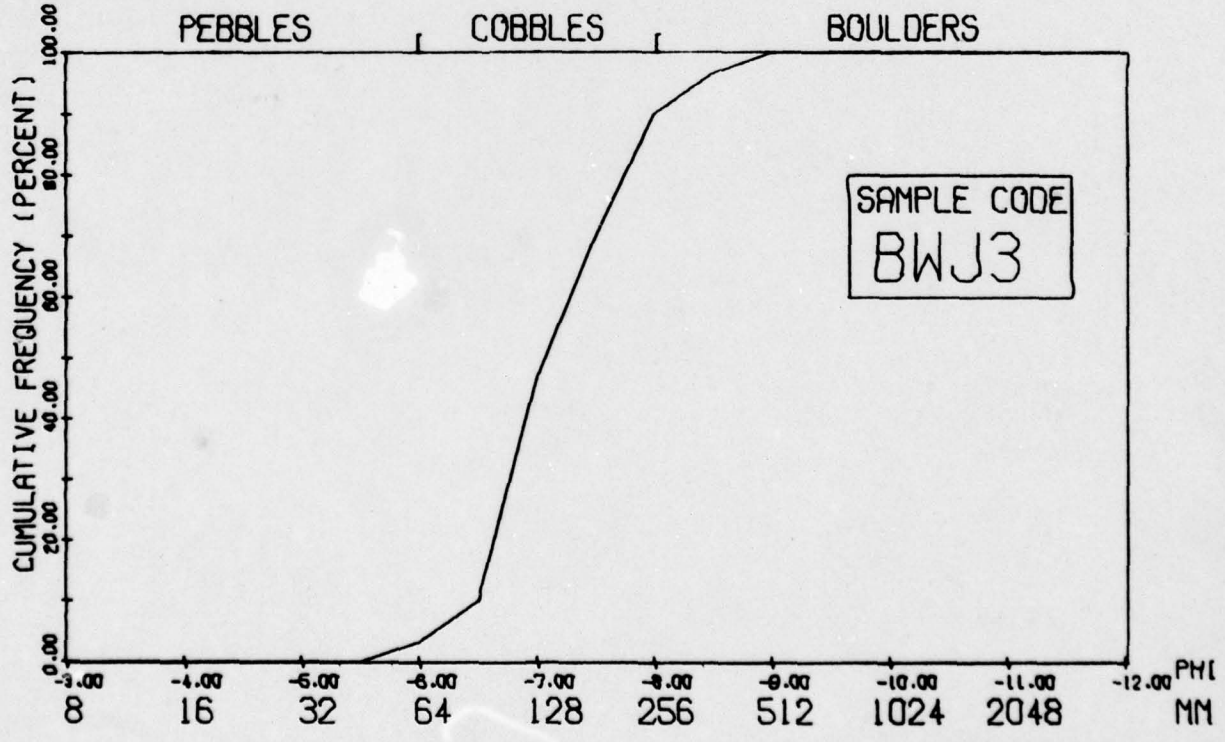
PEBBLES
COBBLES
BOULDERS
CUMULATIVE FREQUENCY (PERCENT)
100.00
80.00
60.00
40.00
20.00
0.00
SAMPLE CODE
BWJ3
-3.00
-4.00
-5.00
-6.00
-8.00
-7.00
-8.00
-9.00
-10.00
-11.00
-12.00
PHI
8
16
32
64
128
256
512
1024
2048
MM

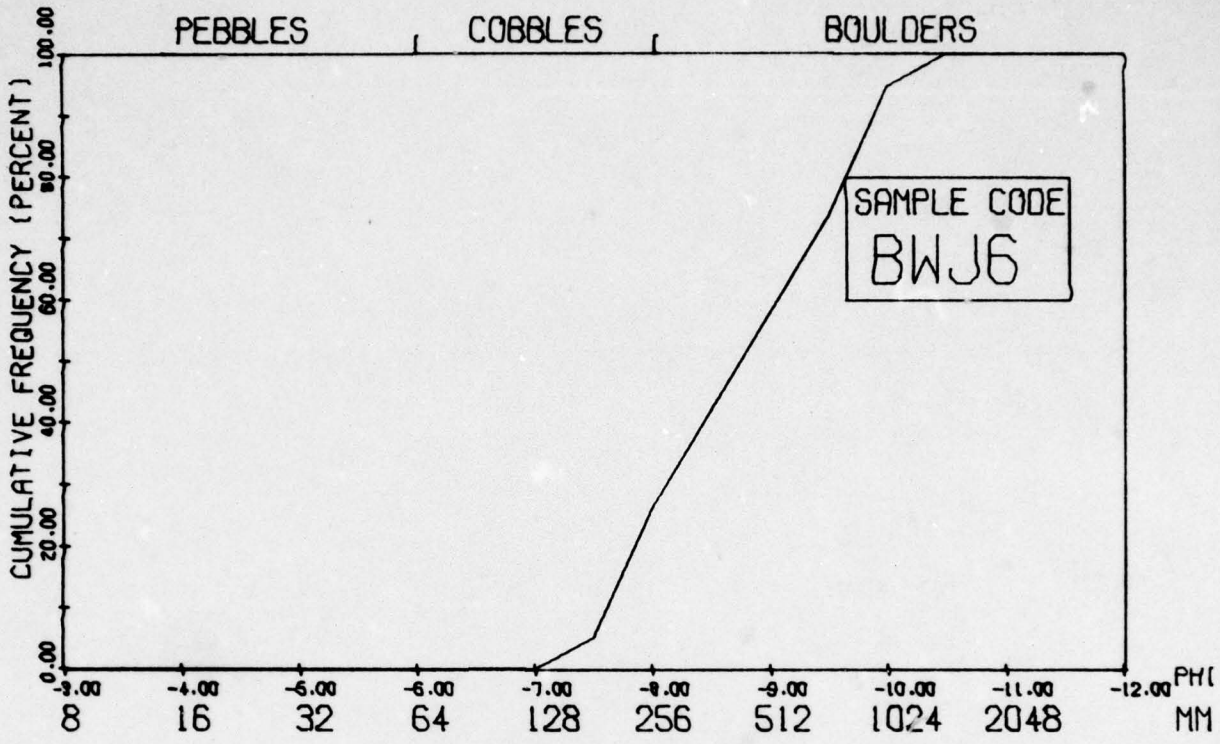
PEBBLES
COBBLES
BOULDERS
CUMULATIVE FREQUENCY (PERCENT)
100.00
80.00
60.00
40.00
20.00
0.00
SAMPLE CODE
BWJ6
-3.00
-4.00
-5.00
-6.00
-7.00
-8.00
-9.00
-10.00
-11.00
-12.00
PHI
8
16
32
64
128
256
512
1024
2048
MM

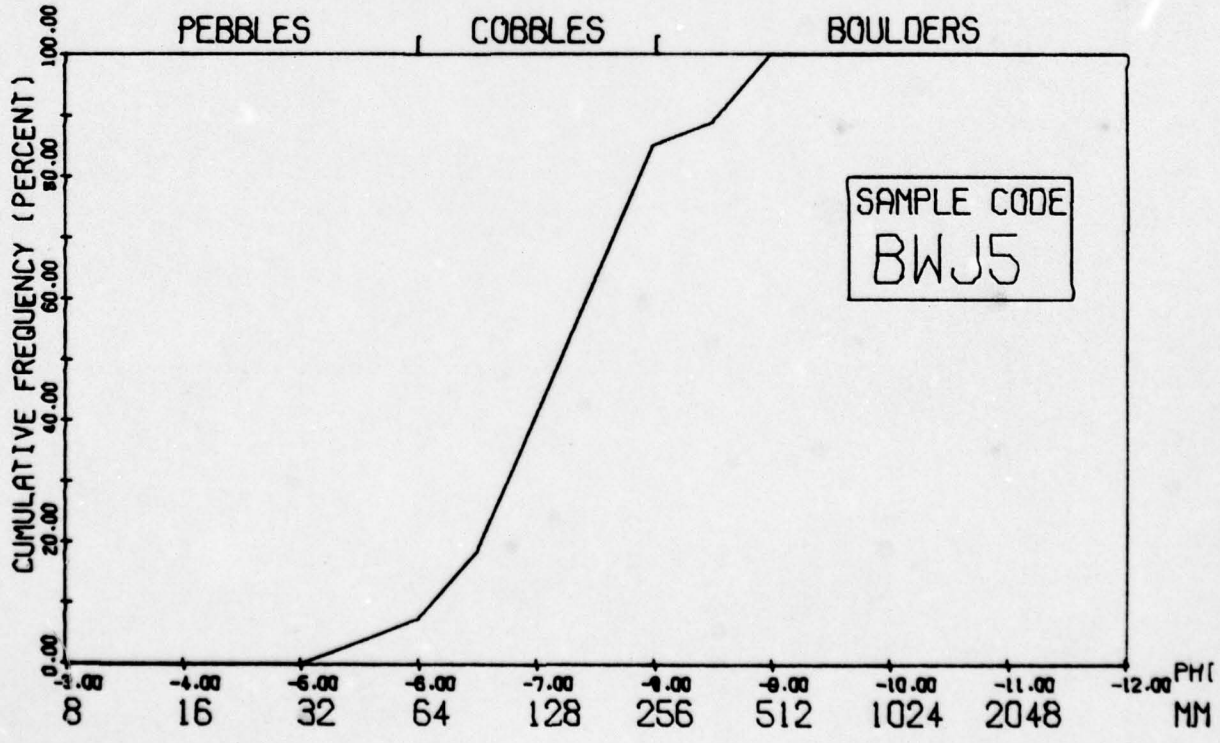
PEBBLES
COBBLES
BOULDERS
CUMULATIVE FREQUENCY (PERCENT)
100.00
80.00
60.00
40.00
20.00
0.00
SAMPLE CODE
BWJ5
-3.00
-4.00
-5.00
-6.00
-7.00
-8.00
-9.00
-10.00
-11.00
-12.00
PHI
8
16
32
64
128
256
512
1024
2048
MM

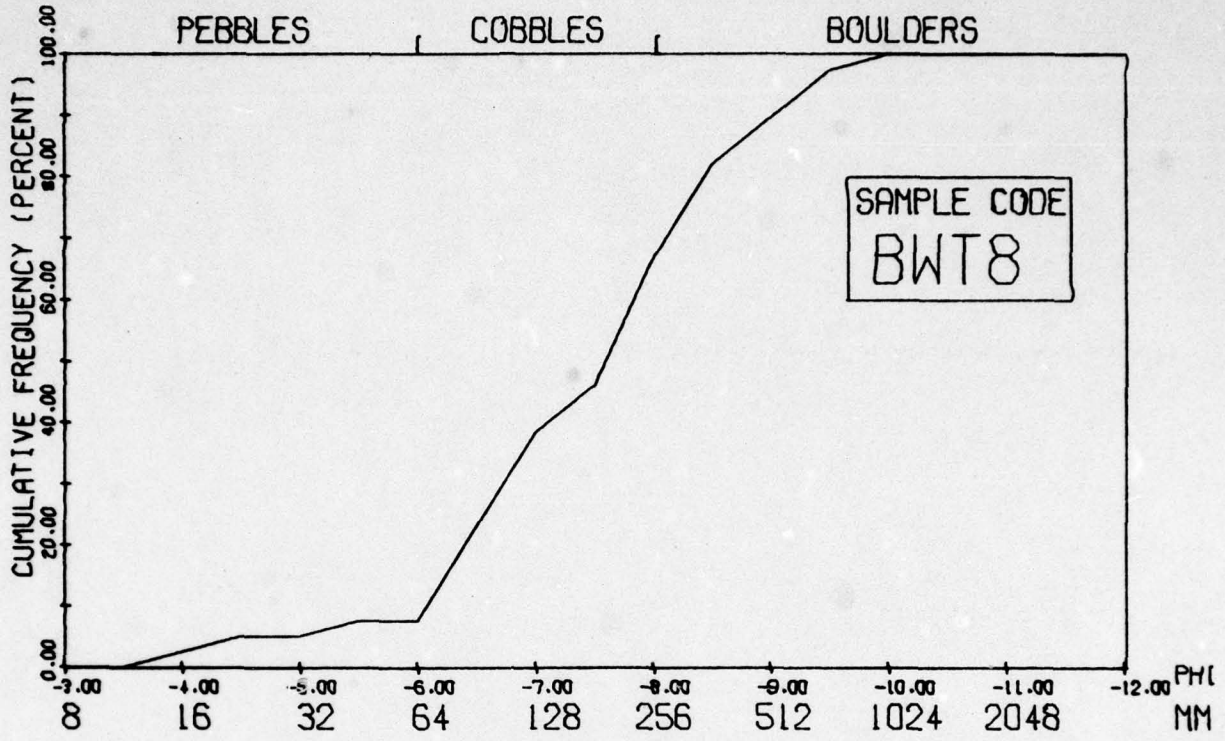
PEBBLES
COBBLES
BOULDERS
CUMULATIVE FREQUENCY (PERCENT)
0.00
20.00
40.00
60.00
80.00
100.00
SAMPLE CODE
BWT8
-3.00
-4.00
-5.00
-6.00
-7.00
-8.00
-9.00
-10.00
-11.00
-12.00
PHI
8
16
32
64
128
256
512
1024
2048
MM

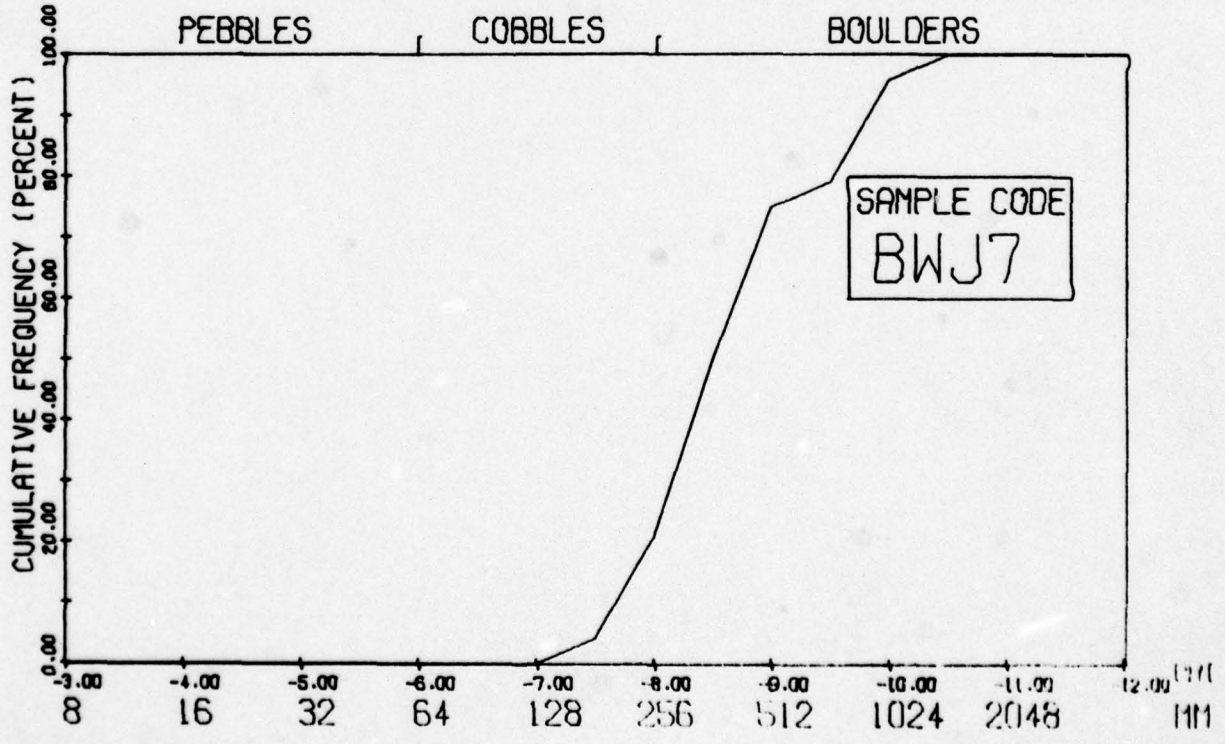
PEBBLES
COBBLES
BOULDERS
CUMULATIVE FREQUENCY (PERCENT)
0.00
20.00
40.00
60.00
80.00
100.00
SAMPLE CODE
BWJ7
-3.00
-4.00
-5.00
-6.00
-7.00
-8.00
-9.00
-10.00
-11.00
-12.00
PHI
8
16
32
64
128
256
512
1024
2048
MM

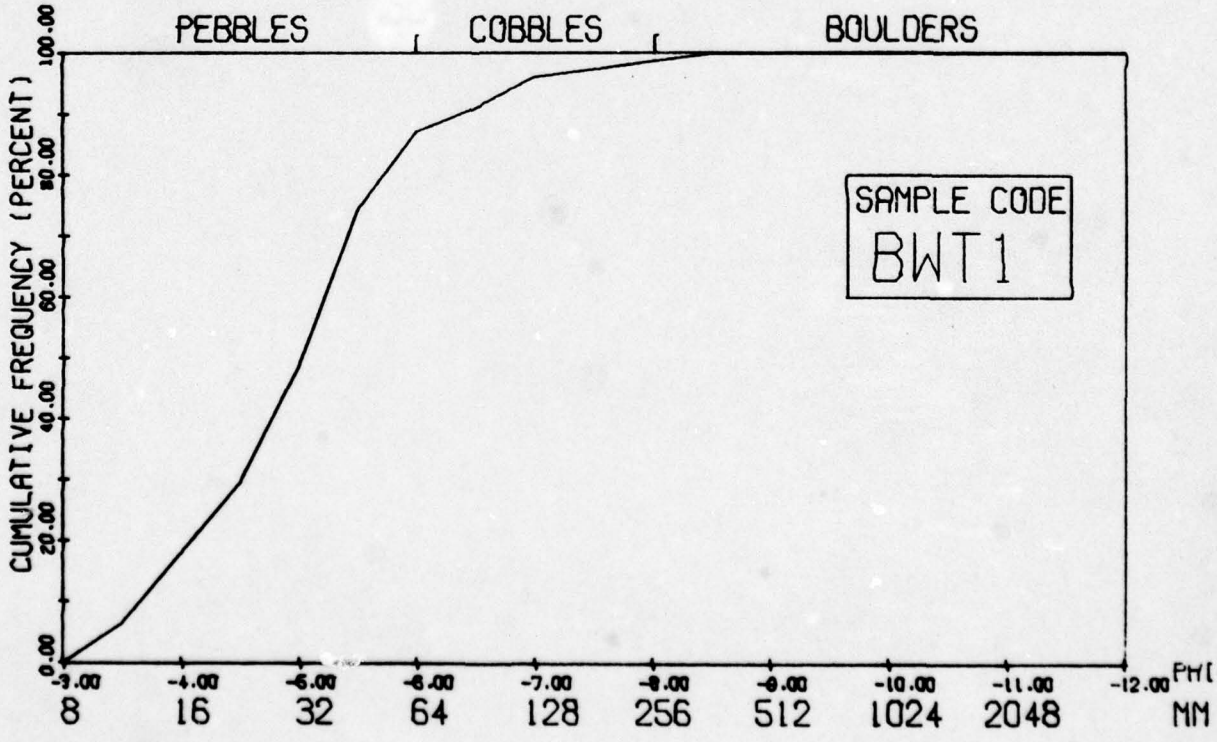
PEBBLES
COBBLES
BOULDERS
CUMULATIVE FREQUENCY (PERCENT)
100.00
80.00
60.00
40.00
20.00
0.00
SAMPLE CODE
BWT1
-3.00
-4.00
-5.00
-6.00
-7.00
-8.00
-9.00
-10.00
-11.00
-12.00
PHI
8
16
32
64
128
256
512
1024
2048
MM

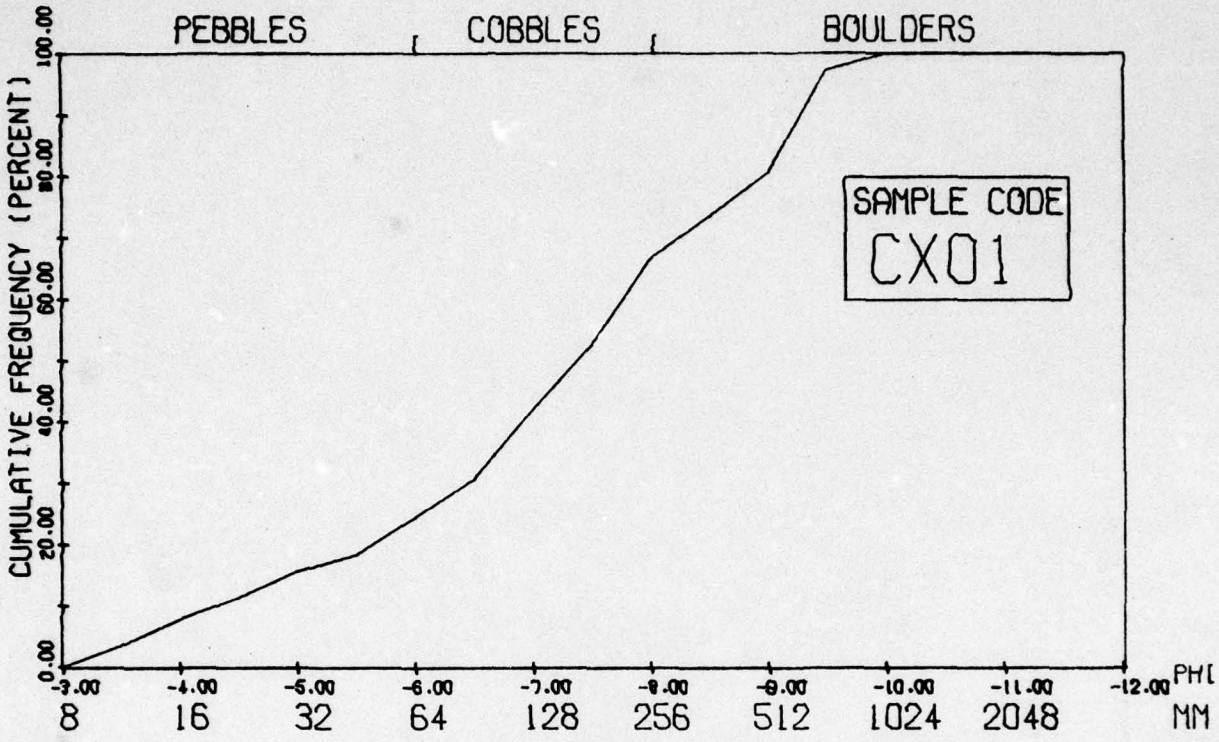
PEBBLES
COBBLES
BOULDERS
CUMULATIVE FREQUENCY (PERCENT)
100.00
80.00
60.00
40.00
20.00
0.00
SAMPLE CODE
CX01
-3.00
-4.00
-5.00
-6.00
-7.00
-8.00
-9.00
-10.00
-11.00
-12.00
PHI
8
16
32
64
128
256
512
1024
2048
MM

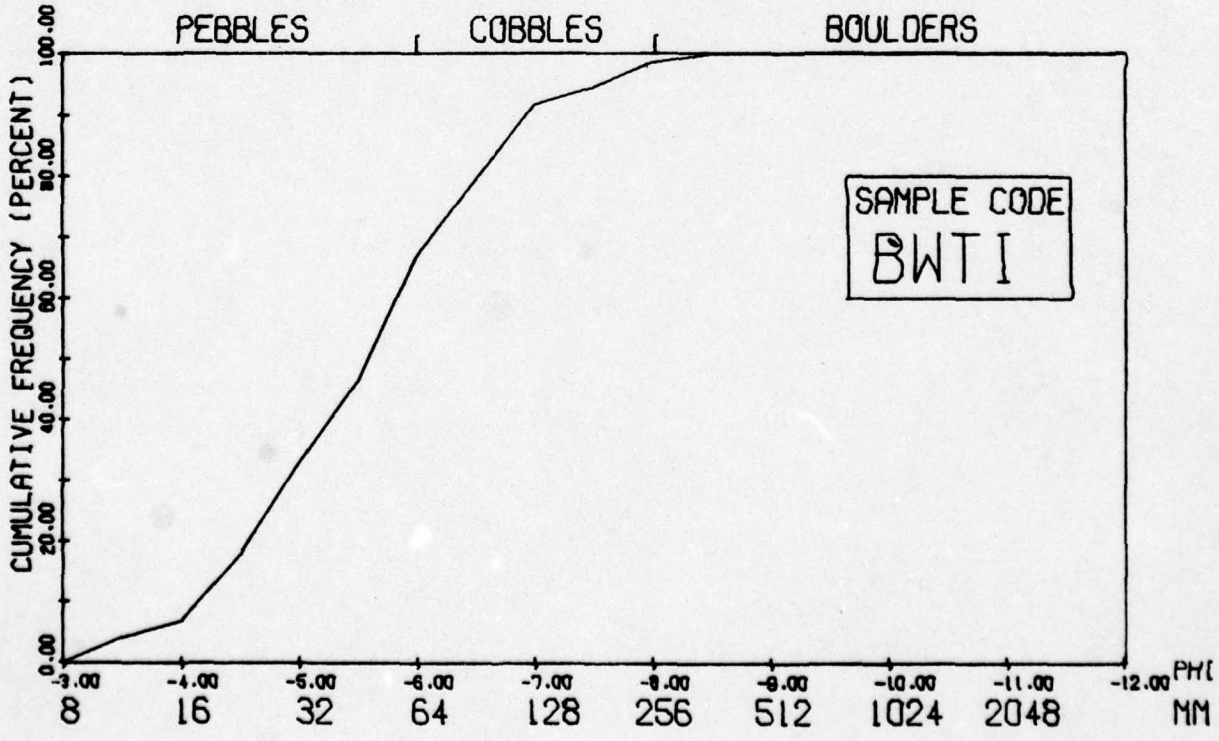
PEBBLES
COBBLES
BOULDERS
CUMULATIVE FREQUENCY (PERCENT)
100.00
80.00
60.00
40.00
20.00
0.00
SAMPLE CODE
BWT1
-3.00
-4.00
-5.00
-6.00
-7.00
-8.00
-9.00
-10.00
-11.00
-12.00
PHI
8
16
32
64
128
256
512
1024
2048
MM

| Sample Code | Maximum Category (mm) | Minimum Category (mm) | Mode (mm) | Median (mm) | Mean (mm) | Variance ($mm^2$) | Standard Deviation | Skewness | Kurtosis |
|---|---|---|---|---|---|---|---|---|---|
| CX01 | 889.0 | 9.5 | 632.0 | 152.9 | 251.8 | 56111.5 | 236.9 | 0.99 | -0.19 |
| CX02 | 889.0 | 76.0 | 632.0 | 458.1 | 450.0 | 60162.6 | 245.2 | 0.46 | -1.13 |
| CX03 | 889.0 | 13.4 | 453.0 | 450.8 | 454.4 | 86045.7 | 293.3 | 0.25 | -1.05 |
| CX04 | 1778.0 | 13.4 | 889.0 | 216.6 | 391.0 | 139462.5 | 373.4 | 1.44 | 2.32 |
| CX05 | 453.0 | 9.5 | 107.0 | 107.9 | 142.2 | 11440.8 | 106.9 | 1.04 | 0.79 |
| CX06 | 453.0 | 9.5 | 214.0 | 107.1 | 134.7 | 11029.5 | 105.0 | 1.34 | 1.97 |
| CX07 | 303.0 | 9.5 | 107.0 | 105.8 | 118.3 | 8906.3 | 94.3 | 0.79 | -0.63 |
| CXQ3 | 303.0 | 9.5 | 38.0 | 39.0 | 74.4 | 5925.8 | 76.9 | 1.54 | 1.70 |

Table G-40 Particle Size Statistics for Coxcomb Samples.

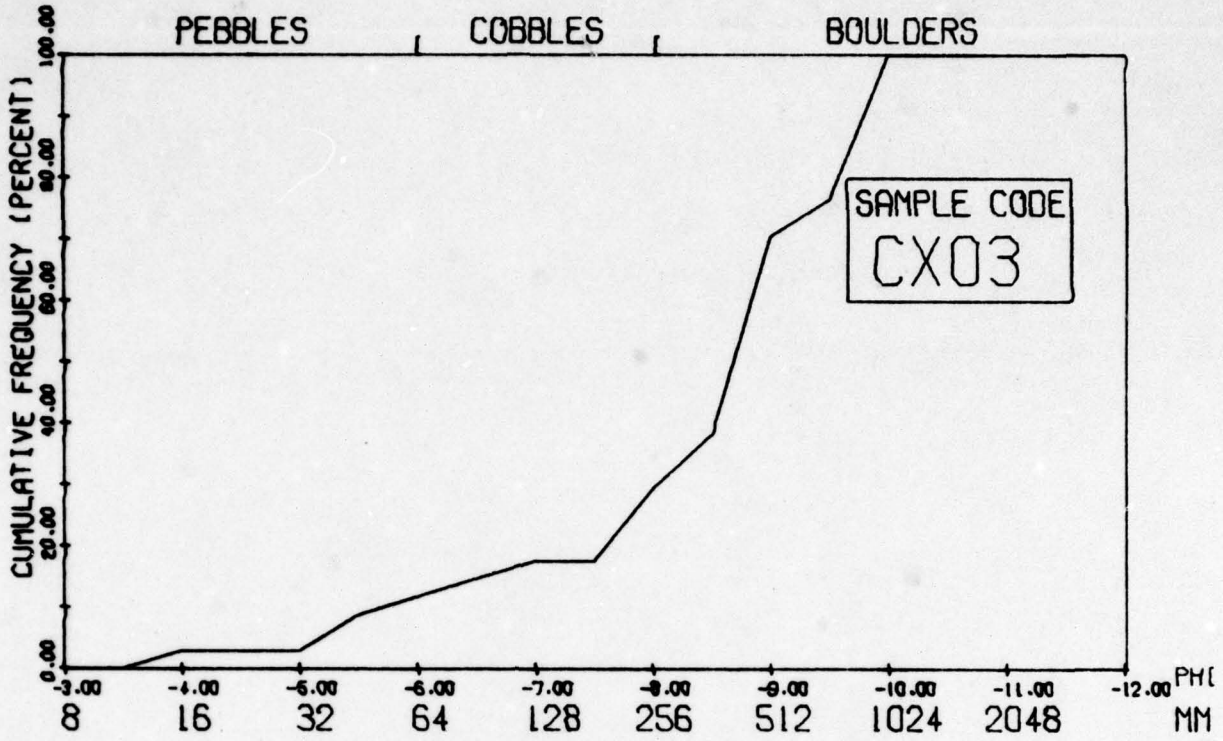
PEBBLES
COBBLES
BOULDERS
CUMULATIVE FREQUENCY (PERCENT)
100.00
80.00
60.00
40.00
20.00
0.00
SAMPLE CODE
CX03
-3.00
-4.00
-5.00
-6.00
-7.00
-8.00
-9.00
-10.00
-11.00
-12.00
PHI
8
16
32
64
128
256
512
1024
2048
MM

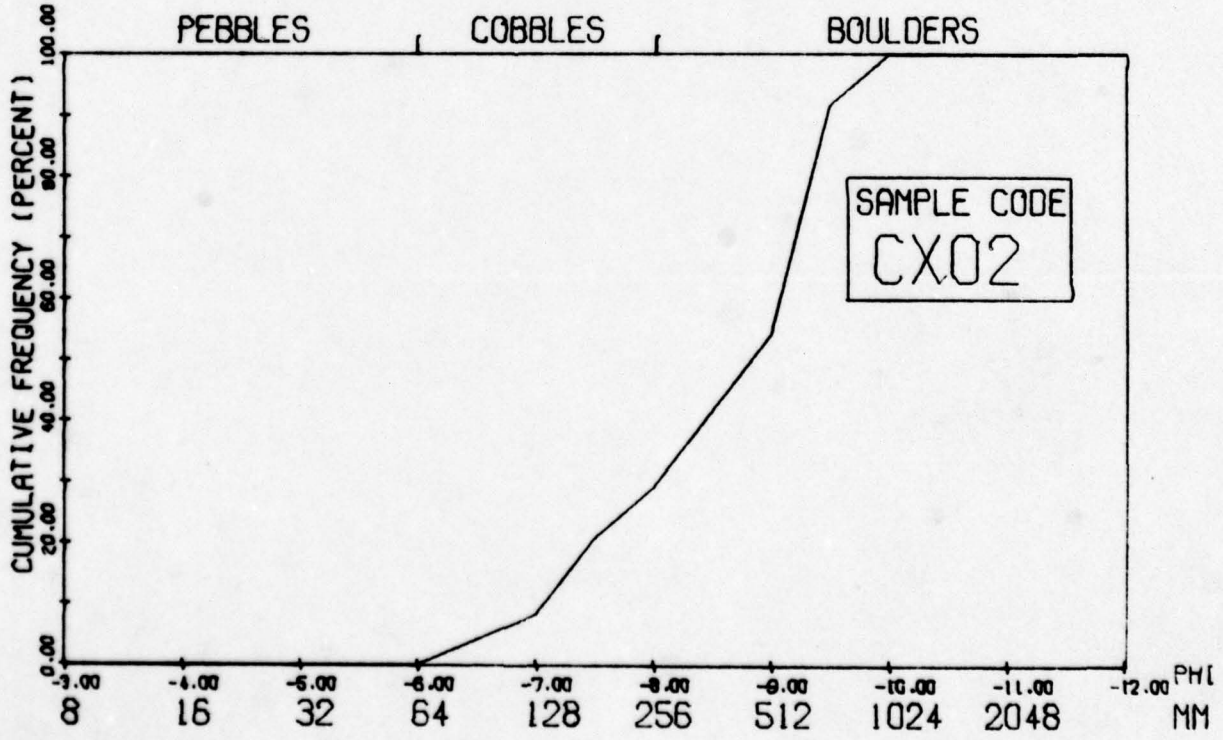
PEBBLES
COBBLES
BOULDERS
CUMULATIVE FREQUENCY (PERCENT)
100.00
80.00
60.00
40.00
20.00
0.00
SAMPLE CODE
CX02
-3.00
-4.00
-5.00
-6.00
-7.00
-8.00
-9.00
-10.00
-11.00
-12.00
PHI
8
16
32
64
128
256
512
1024
2048
MM

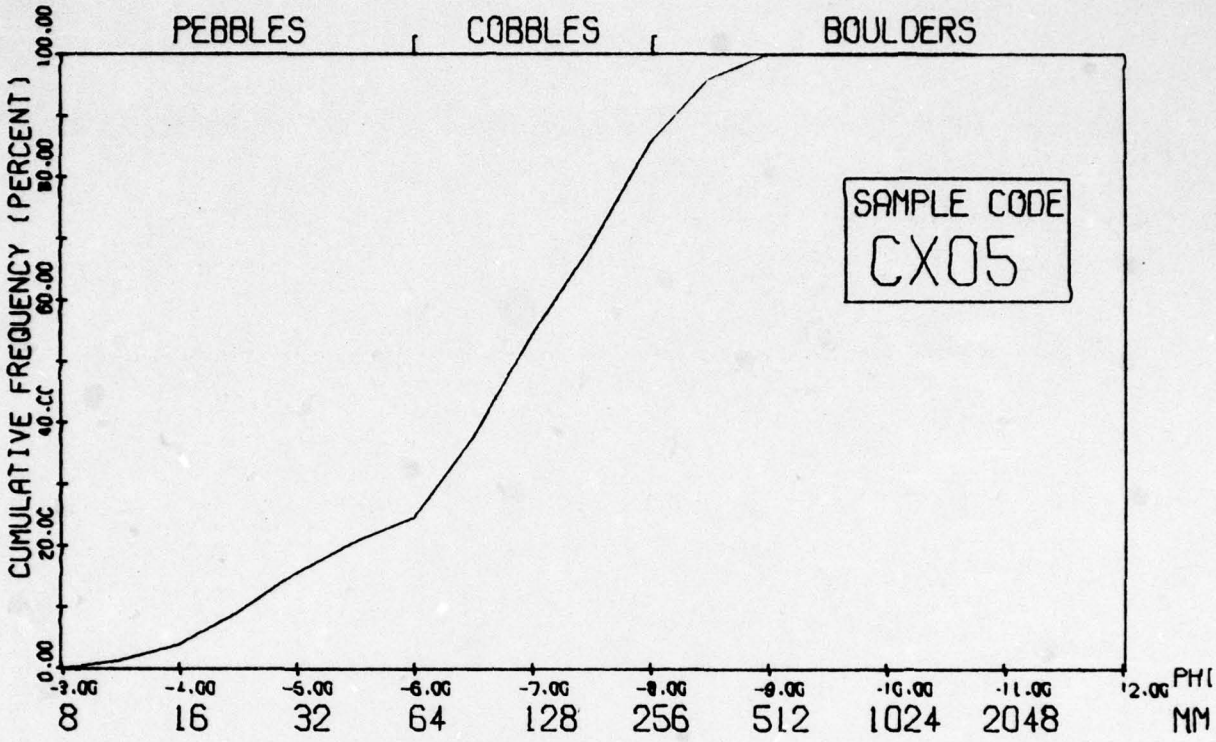
PEBBLES
COBBLES
BOULDERS
CUMULATIVE FREQUENCY (PERCENT)
100.00
80.00
60.00
40.00
20.00
0.00
SAMPLE CODE
CX05
-3.00
-4.00
-5.00
-6.00
-7.00
-8.00
-9.00
-10.00
-11.00
-12.00
PHI
8
16
32
64
128
256
512
1024
2048
MM

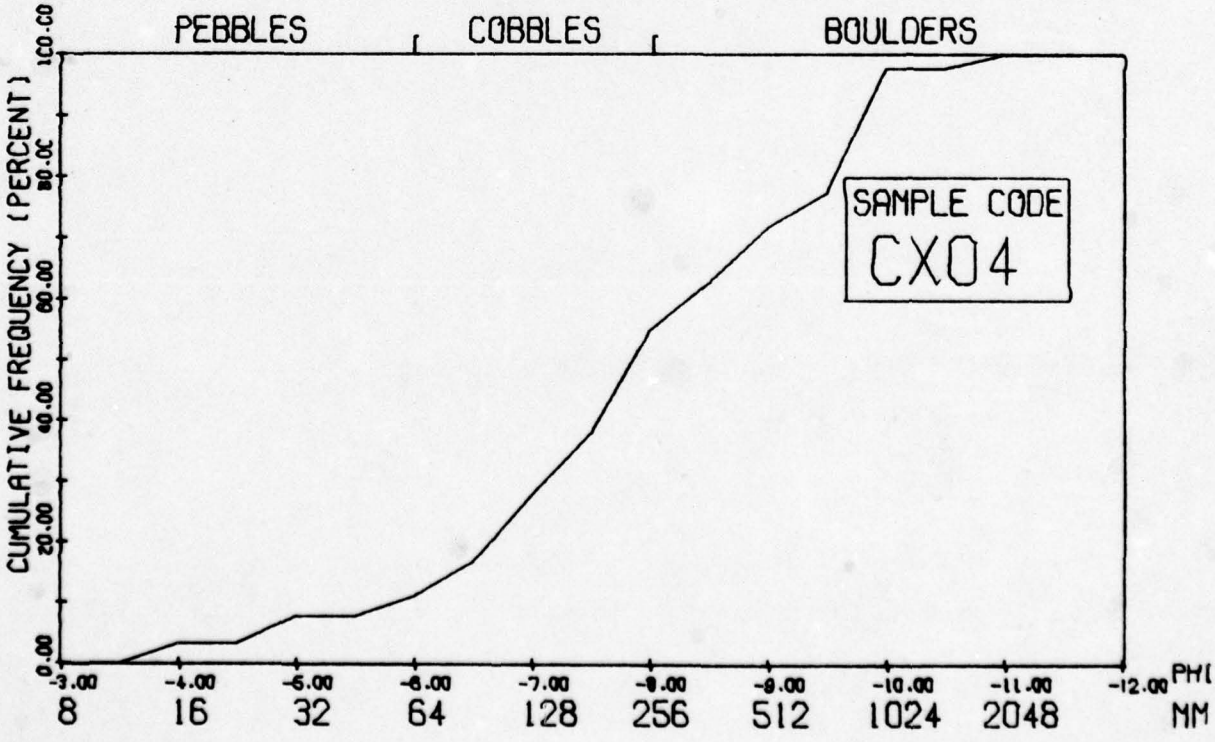
PEBBLES
COBBLES
BOULDERS
CUMULATIVE FREQUENCY (PERCENT)
100.00
80.00
60.00
40.00
20.00
0.00
SAMPLE CODE
CX04
-3.00
-4.00
-5.00
-6.00
-7.00
-8.00
-9.00
-10.00
-11.00
-12.00
PHI
8
16
32
64
128
256
512
1024
2048
MM

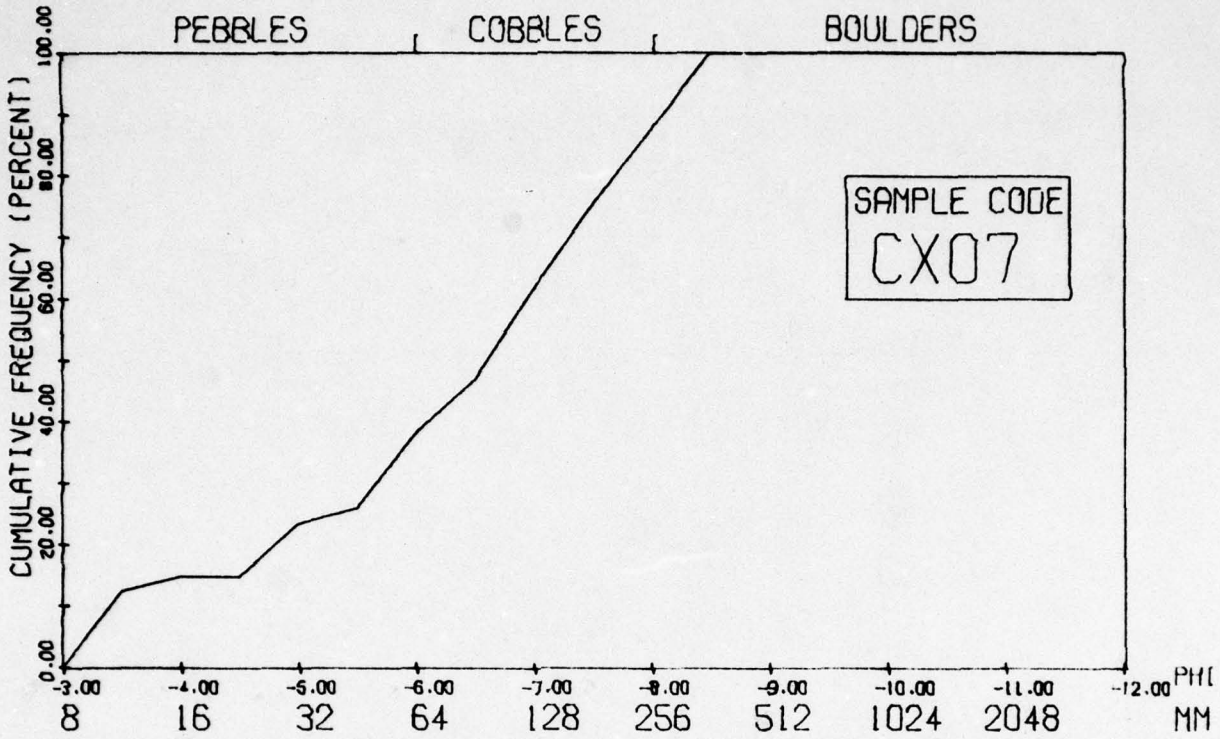
PEBBLES
COBBLES
BOULDERS
CUMULATIVE FREQUENCY (PERCENT)
0.00
20.00
40.00
60.00
80.00
100.00
SAMPLE CODE
CX07
-3.00
-4.00
-5.00
-6.00
-7.00
-8.00
-9.00
-10.00
-11.00
-12.00
PHI
8
16
32
64
128
256
512
1024
2048
MM

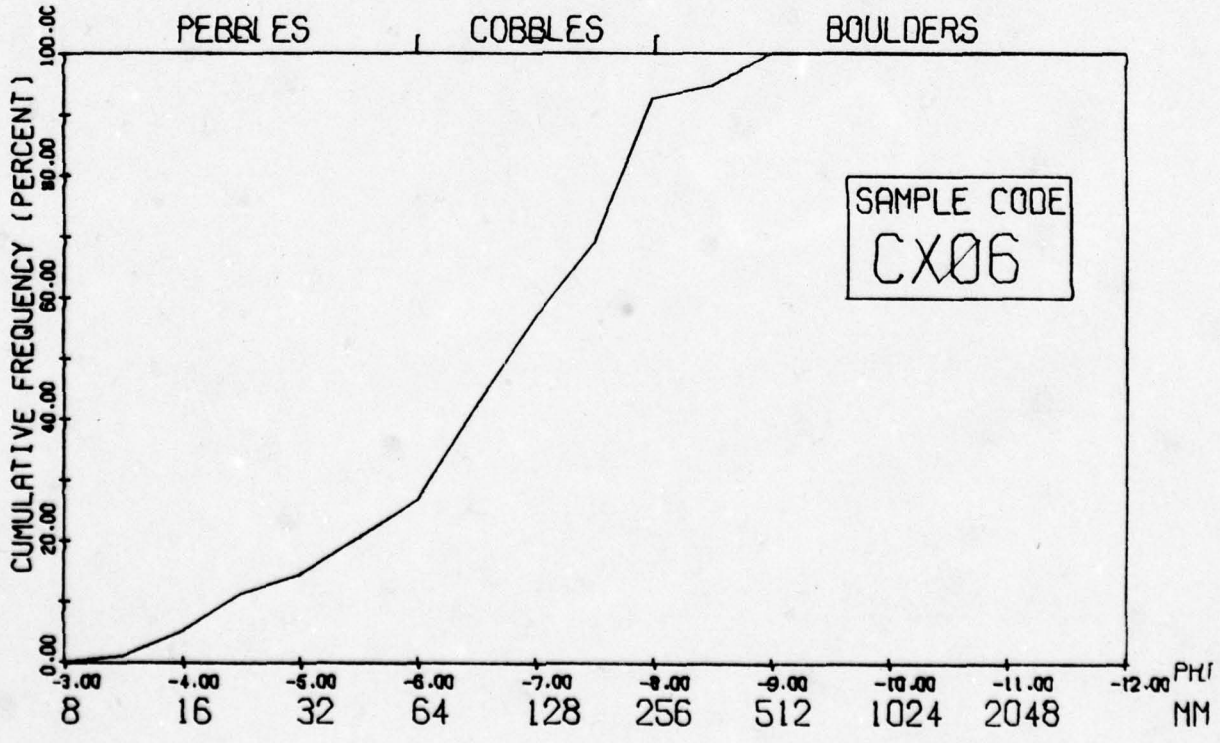
PEBBLES
COBBLES
BOULDERS
CUMULATIVE FREQUENCY (PERCENT)
0.00
20.00
40.00
60.00
80.00
100.00
SAMPLE CODE
CX06
-3.00
-4.00
-5.00
-6.00
-7.00
-8.00
-9.00
-10.00
-11.00
-12.00
PHI
8
16
32
64
128
256
512
1024
2048
MM

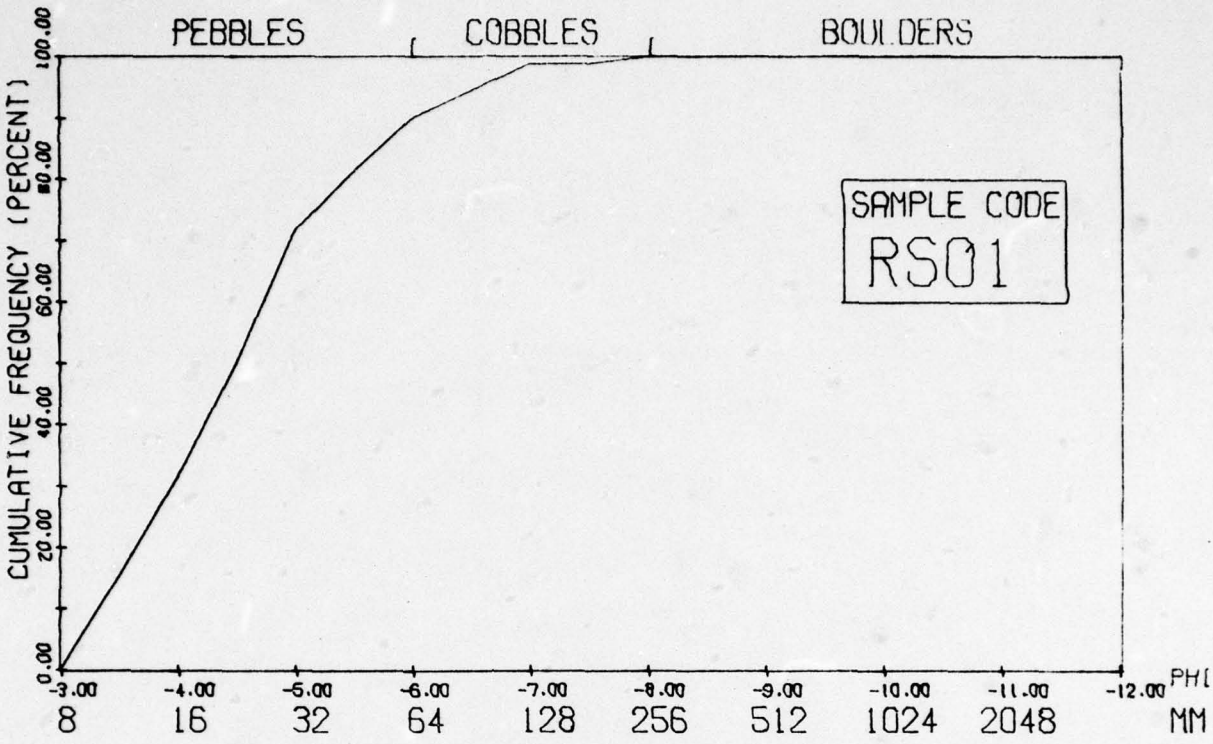
PEBBLES
COBBLES
BOULDERS
CUMULATIVE FREQUENCY (PERCENT)
100.00
80.00
60.00
40.00
20.00
0.00
SAMPLE CODE
RS01
-3.00
-4.00
-5.00
-6.00
-7.00
-8.00
-9.00
-10.00
-11.00
-12.00
PHI
8
16
32
64
128
256
512
1024
2048
MM

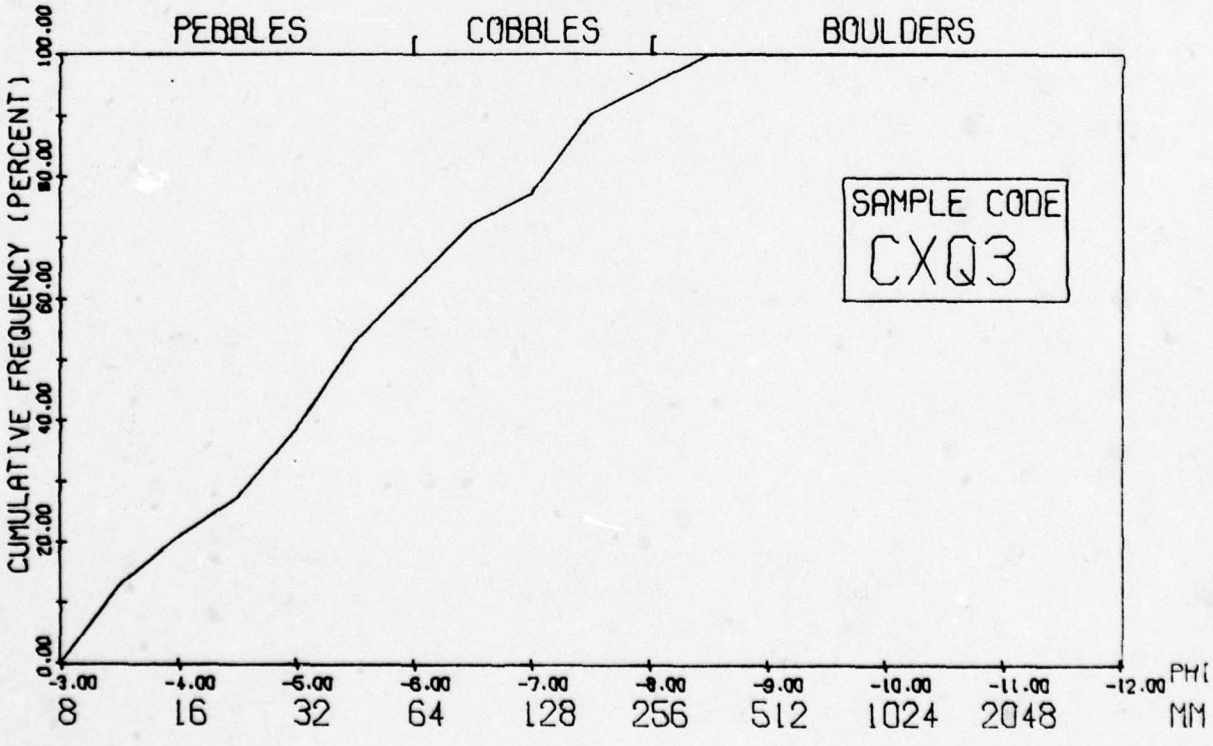
PEBBLES
COBBLES
BOULDERS
CUMULATIVE FREQUENCY (PERCENT)
100.00
80.00
60.00
40.00
20.00
0.00
SAMPLE CODE
CXQ3
-3.00
-4.00
-5.00
-6.00
-7.00
-8.00
-9.00
-10.00
-11.00
-12.00
PHI
8
16
32
64
128
256
512
1024
2048
MM

| Sample Code | Maximum Category (mm) | Minimum Category (mm) | Mode (mm) | Median (mm) | Mean (mm) | Variance | Standard Deviation | Skewness | Kurtosis |
|---|---|---|---|---|---|---|---|---|---|
| RS01 | 214.0 | 9.5 | 26.8 | 20.9 | 31.6 | 914.7 | 30.2 | 3.16 | 13.69 |
| RS02 | 107.0 | 9.5 | 19.0 | 20.2 | 27.4 | 336.2 | 18.3 | 1.86 | 4.07 |
| RS03 | 214.0 | 9.5 | 26.8 | 36.2 | 44.9 | 1353.6 | 39.1 | 2.34 | 6.49 |
| RS04 | 214.0 | 9.5 | 19.0 | 18.4 | 31.0 | 1548.7 | 39.3 | 3.36 | 11.69 |
| RS05 | 453.0 | 9.5 | 9.5 | 25.5 | 52.8 | 8602.6 | 92.7 | 3.42 | 11.08 |
| RS06 | 303.0 | 9.5 | 19.0 | 36.1 | 51.3 | 2608.4 | 51.0 | 1.98 | 4.46 |
| RS07 | 632.0 | 9.5 | 9.5 | 37.9 | 72.5 | 10236.5 | 101.1 | 3.52 | 15.16 |

Table G-45 Particle Size Statistics for Riverside Samples.

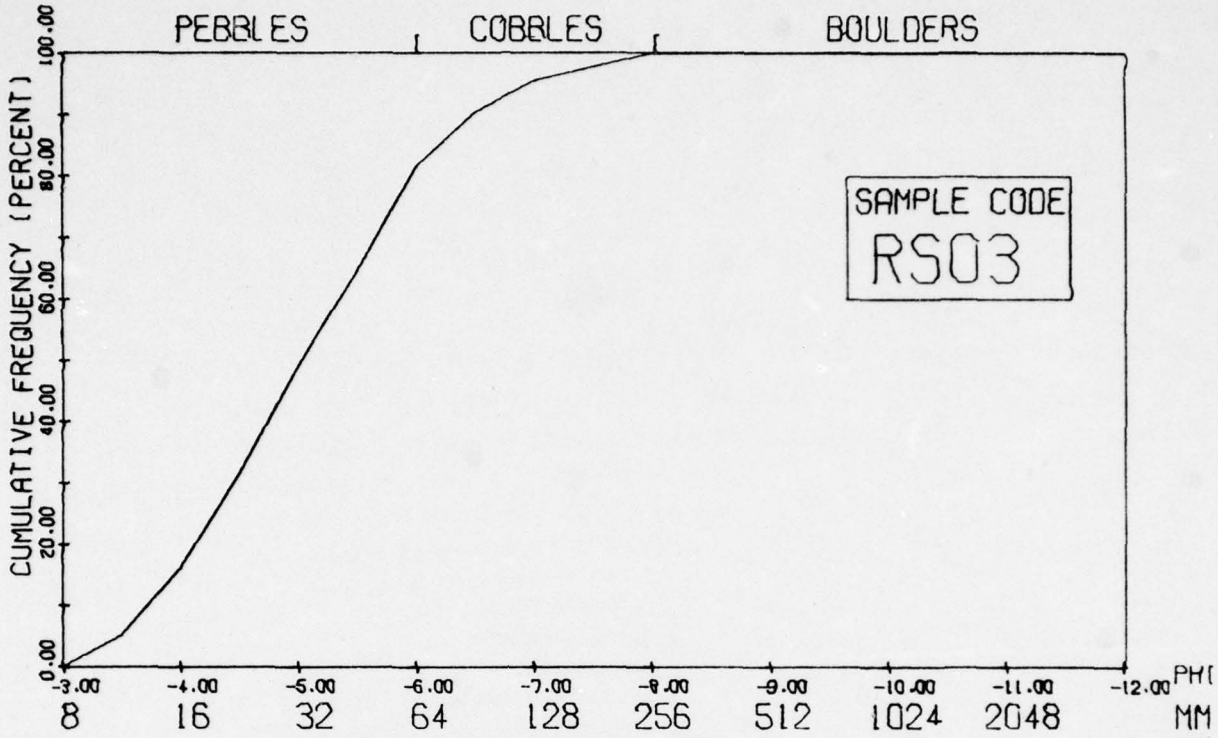
PEBBLES
COBBLES
BOULDERS
CUMULATIVE FREQUENCY (PERCENT)
0.00
20.00
40.00
60.00
80.00
100.00
SAMPLE CODE
RS03
-3.00
-4.00
-5.00
-6.00
-7.00
-8.00
-9.00
-10.00
-11.00
-12.00
PHI
8
16
32
64
128
256
512
1024
2048
MM

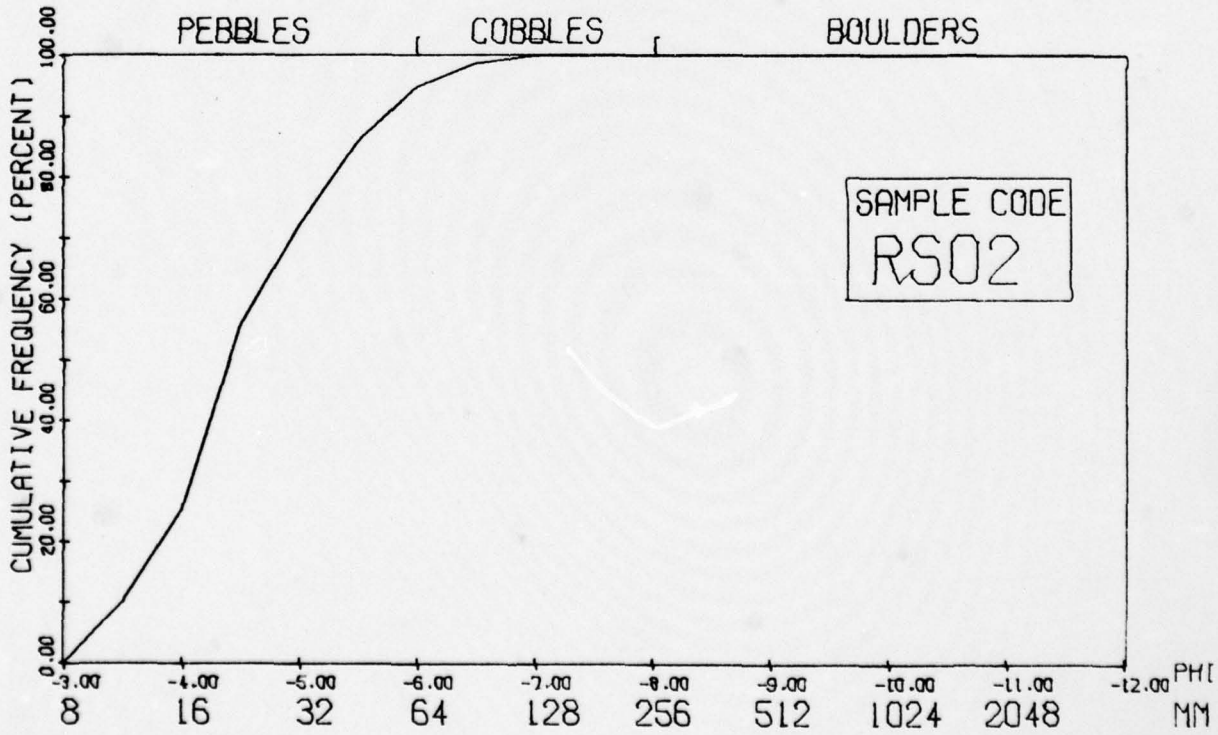
PEBBLES
COBBLES
BOULDERS
CUMULATIVE FREQUENCY (PERCENT)
0.00
20.00
40.00
60.00
80.00
100.00
SAMPLE CODE
RS02
-3.00
-4.00
-5.00
-6.00
-7.00
-8.00
-9.00
-10.00
-11.00
-12.00
PHI
8
16
32
64
128
256
512
1024
2048
MM

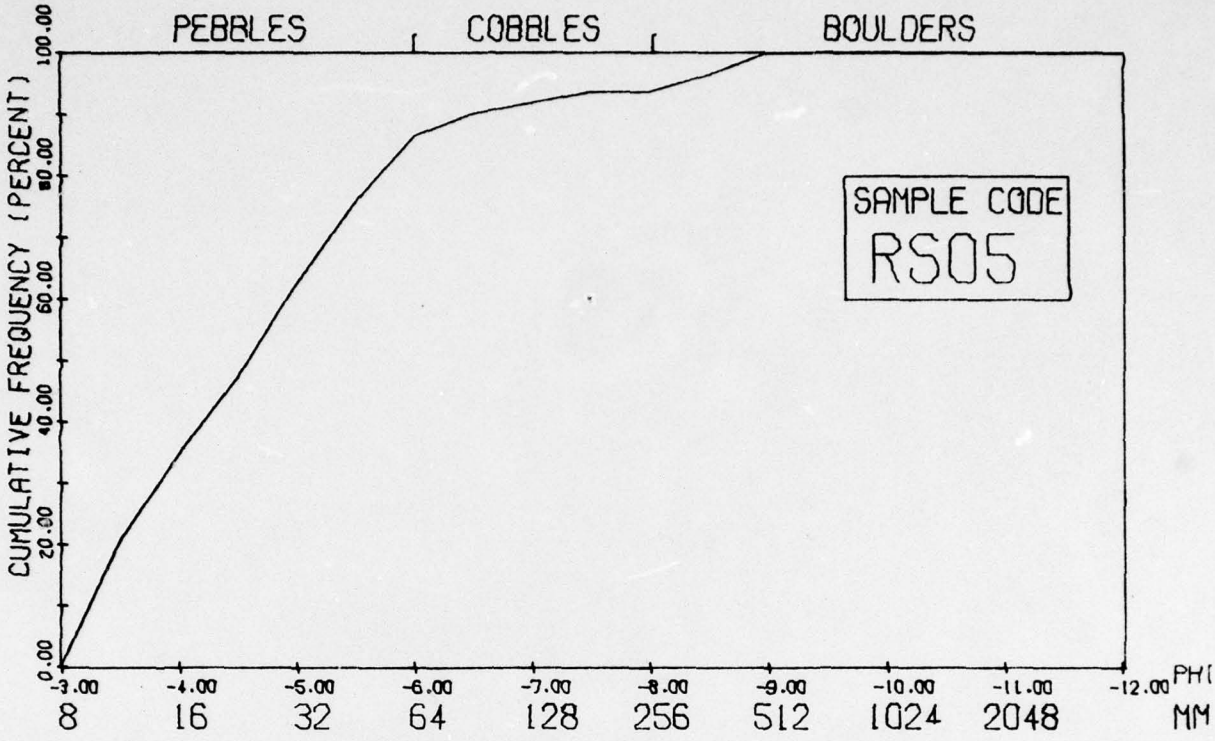
PEBBLES
COBBLES
BOULDERS
CUMULATIVE FREQUENCY (PERCENT)
0.00
20.00
40.00
60.00
80.00
100.00
SAMPLE CODE
RS05
-3.00
-4.00
-5.00
-6.00
-7.00
-8.00
-9.00
-10.00
-11.00
-12.00
PHI
8
16
32
64
128
256
512
1024
2048
MM

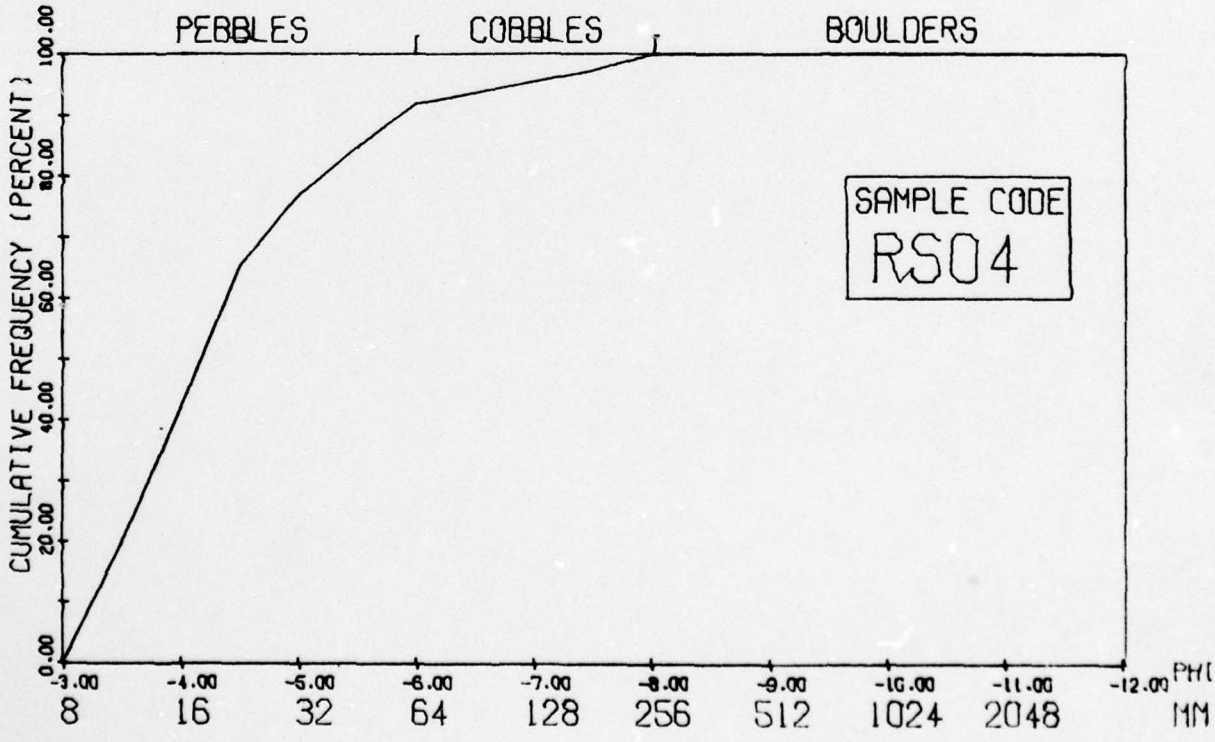
PEBBLES
COBBLES
BOULDERS
CUMULATIVE FREQUENCY (PERCENT)
0.00
20.00
40.00
60.00
80.00
100.00
SAMPLE CODE
RS04
-3.00
-4.00
-5.00
-6.00
-7.00
-8.00
-9.00
-10.00
-11.00
-12.00
PHI
8
16
32
64
128
256
512
1024
2048
MM

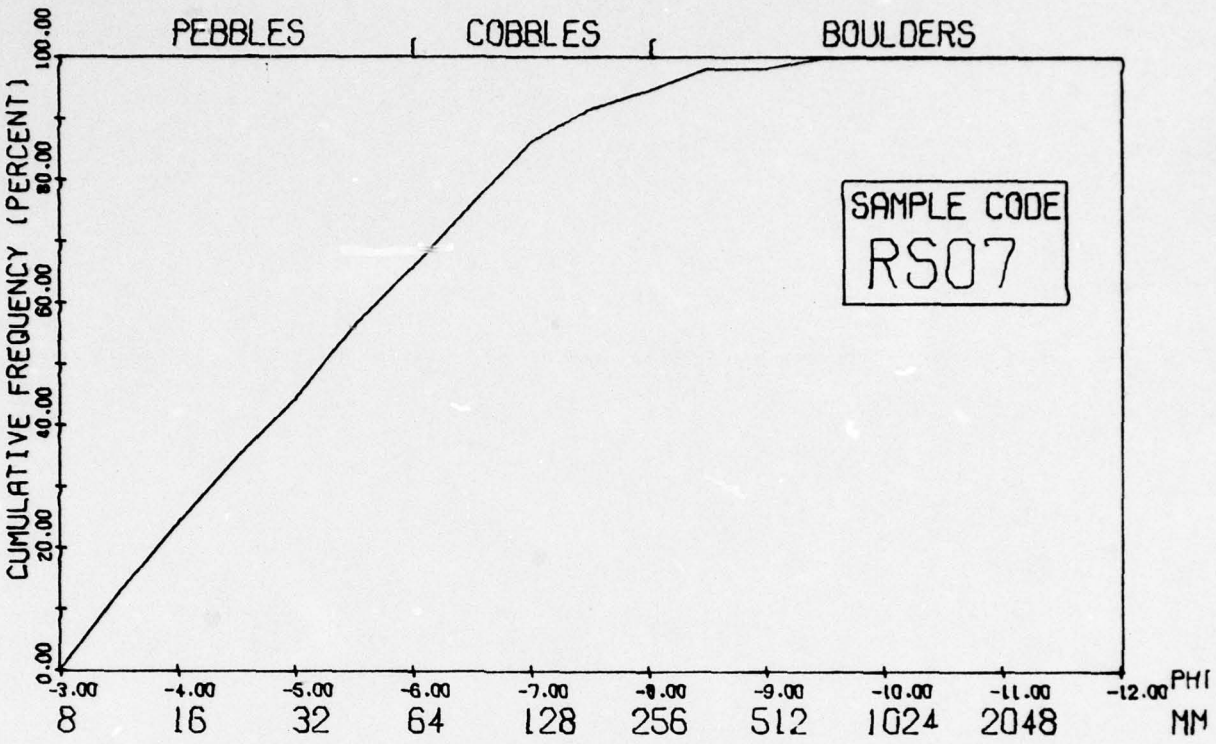
PEBBLES
COBBLES
BOULDERS
CUMULATIVE FREQUENCY (PERCENT)
0.00
20.00
40.00
60.00
80.00
100.00
SAMPLE CODE
RS07
-3.00
-4.00
-5.00
-6.00
-7.00
-8.00
-9.00
-10.00
-11.00
-12.00
PHI
8
16
32
64
128
256
512
1024
2048
MM

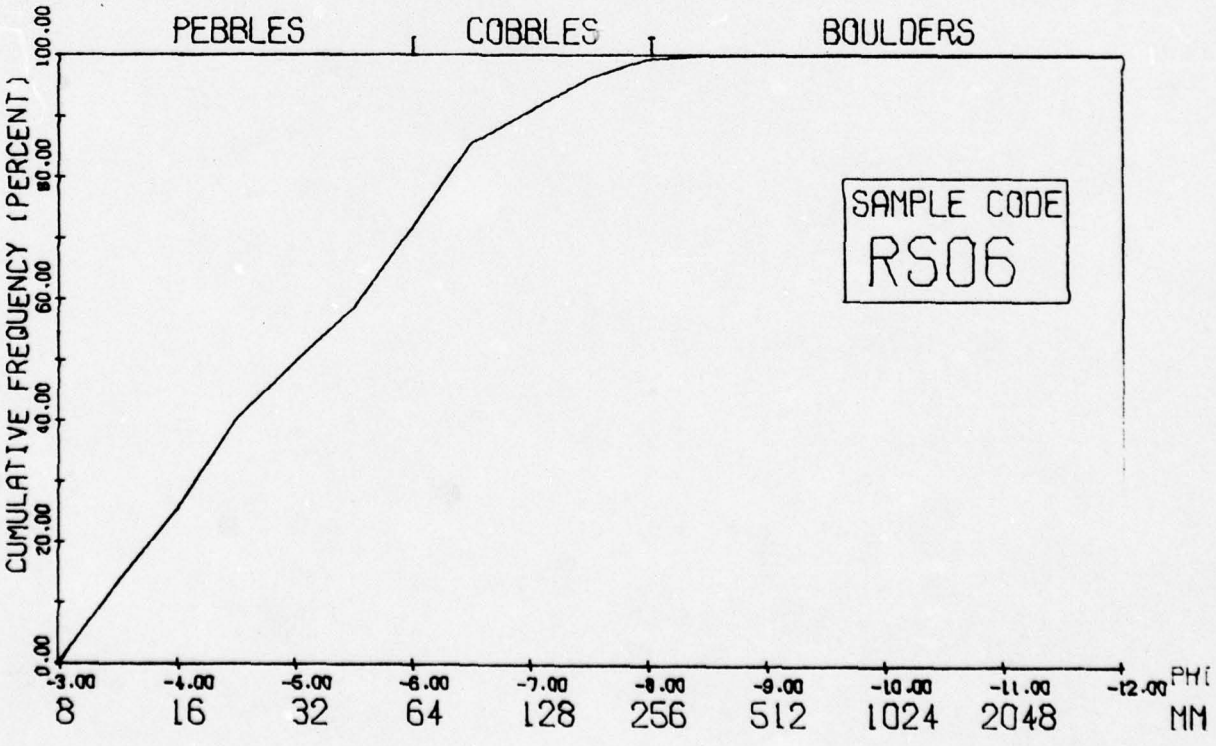
PEBBLES
COBBLES
BOULDERS
CUMULATIVE FREQUENCY (PERCENT)
0.00
20.00
40.00
60.00
80.00
100.00
SAMPLE CODE
RS06
-3.00
-4.00
-5.00
-6.00
-7.00
-8.00
-9.00
-10.00
-11.00
-12.00
PHI
8
16
32
64
128
256
512
1024
2048
MM

| Sample Code | Maximum Category (mm) | Minimum Category (mm) | Mode (mm) | Median (mm) | Mean (mm) | Variance | Standard Deviation | Skewness | Kurtosis |
|---|---|---|---|---|---|---|---|---|---|
| PR01 | 1252.0 | 26.8 | 214.0 | 214.6 | 312.8 | 96988.8 | 311.4 | 1.97 | 3.02 |
| PR02 | 632.0 | 9.5 | 214.0 | 152.2 | 173.5 | 21429.4 | 146.3 | 0.86 | 0.45 |
| PR03 | 889.0 | 13.4 | 214.0 | 154.4 | 232.9 | 38302.2 | 195.7 | 1.47 | 1.80 |
| PR04 | 303.0 | 9.5 | 19.0 | 19.8 | 56.1 | 5420.5 | 73.6 | 1.83 | 2.26 |
| AG01 | 38.0 | 9.5 | 13.4 | 13.9 | 15.3 | 28.6 | 5.3 | 2.27 | 6.74 |
| AG02 | 26.8 | 9.5 | 9.5 | 11.5 | 12.3 | 13.1 | 3.6 | 1.57 | 2.87 |

Table G-49 Particle Size Statistics for Painted Rock and Aguila Samples.

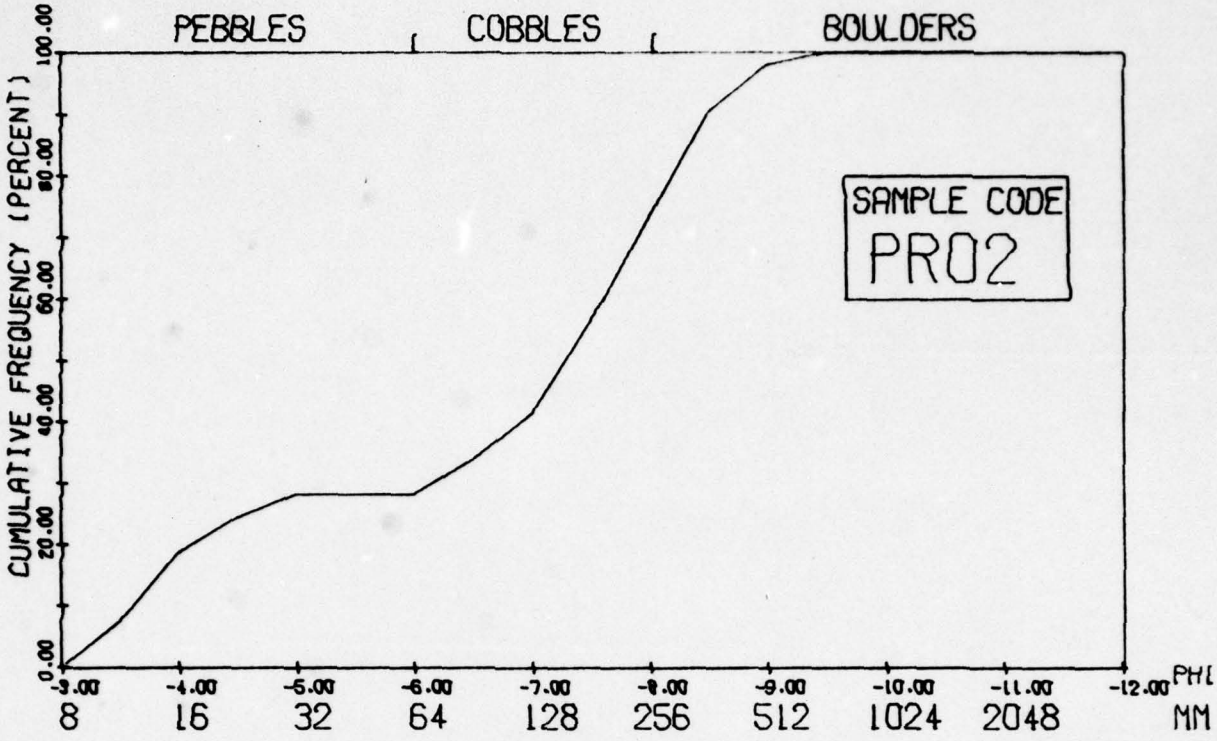
PEBBLES
COBBLES
BOULDERS
CUMULATIVE FREQUENCY (PERCENT)
0.00
20.00
40.00
60.00
80.00
100.00
SAMPLE CODE
PR02
-3.00
-4.00
-5.00
-6.00
-7.00
-8.00
-9.00
-10.00
-11.00
-12.00
PHI
8
16
32
64
128
256
512
1024
2048
MM

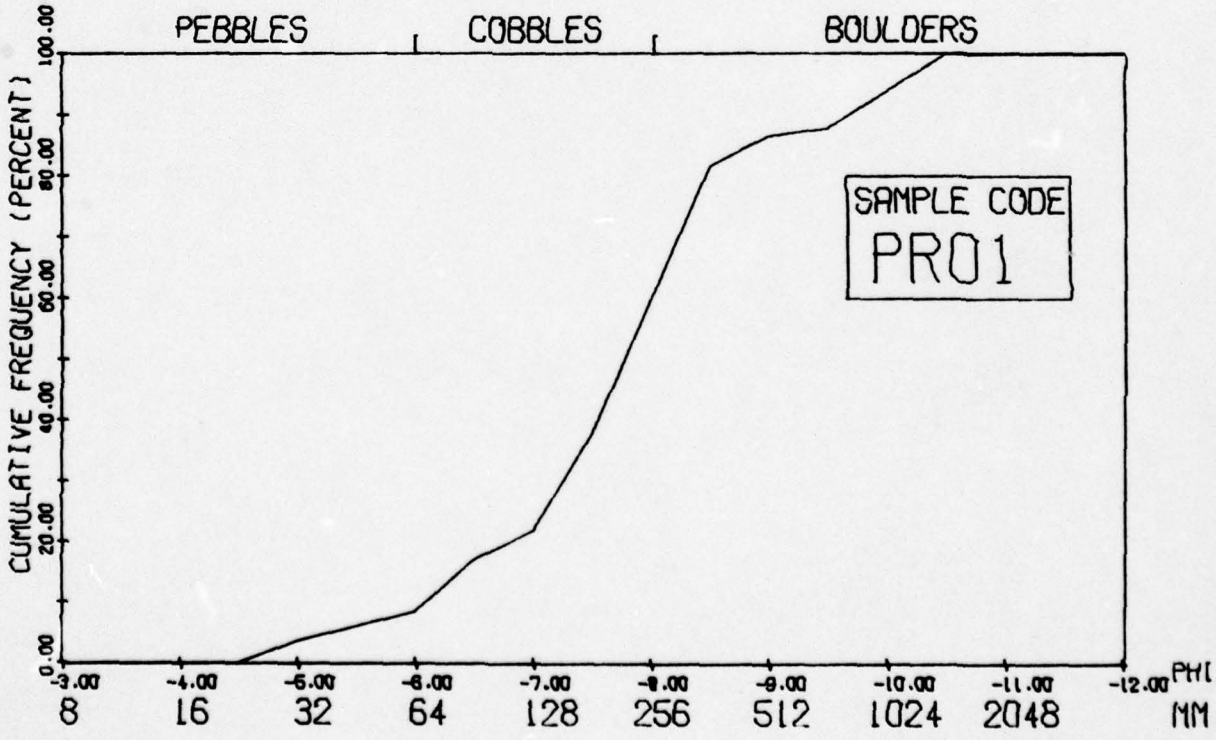
PEBBLES
COBBLES
BOULDERS
CUMULATIVE FREQUENCY (PERCENT)
0.00
20.00
40.00
60.00
80.00
100.00
SAMPLE CODE
PR01
-3.00
-4.00
-5.00
-6.00
-7.00
-8.00
-9.00
-10.00
-11.00
-12.00
PHI
8
16
32
64
128
256
512
1024
2048
MM

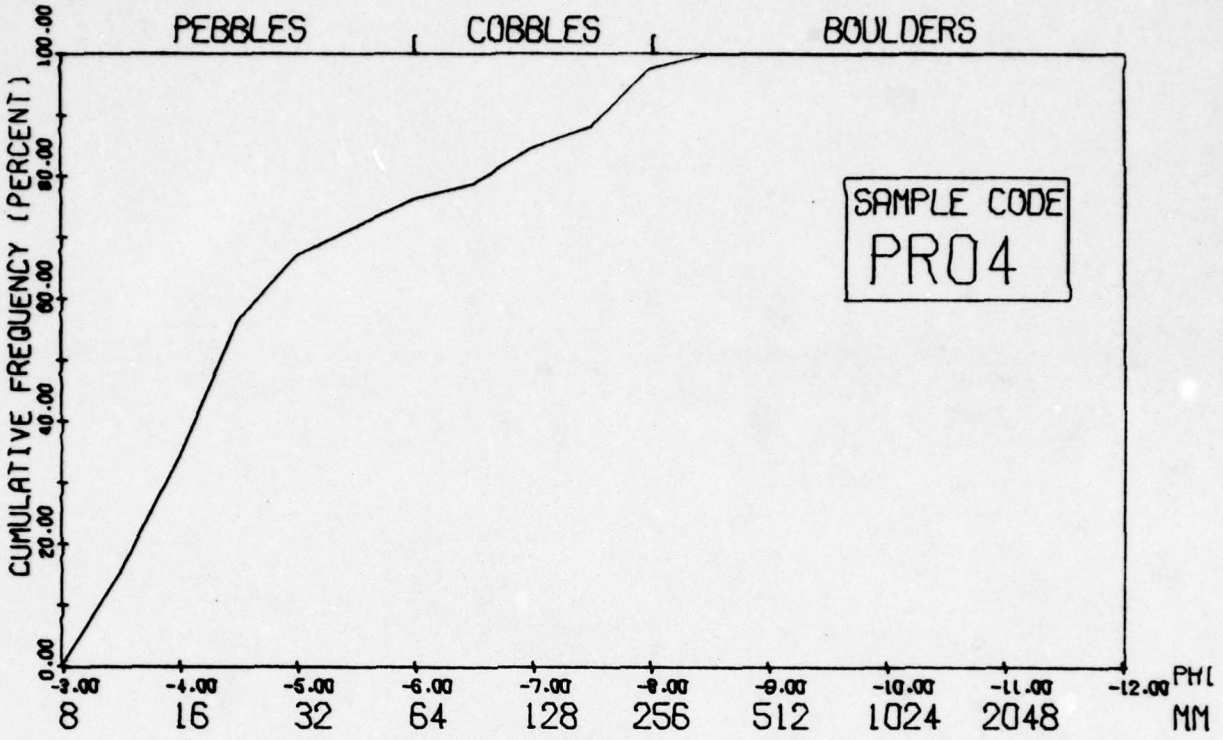
PEBBLES
COBBLES
BOULDERS
CUMULATIVE FREQUENCY (PERCENT)
0.00
20.00
40.00
60.00
80.00
100.00
SAMPLE CODE
PR04
-3.00
-4.00
-5.00
-6.00
-7.00
-8.00
-9.00
-10.00
-11.00
-12.00
PHI
8
16
32
64
128
256
512
1024
2048
MM

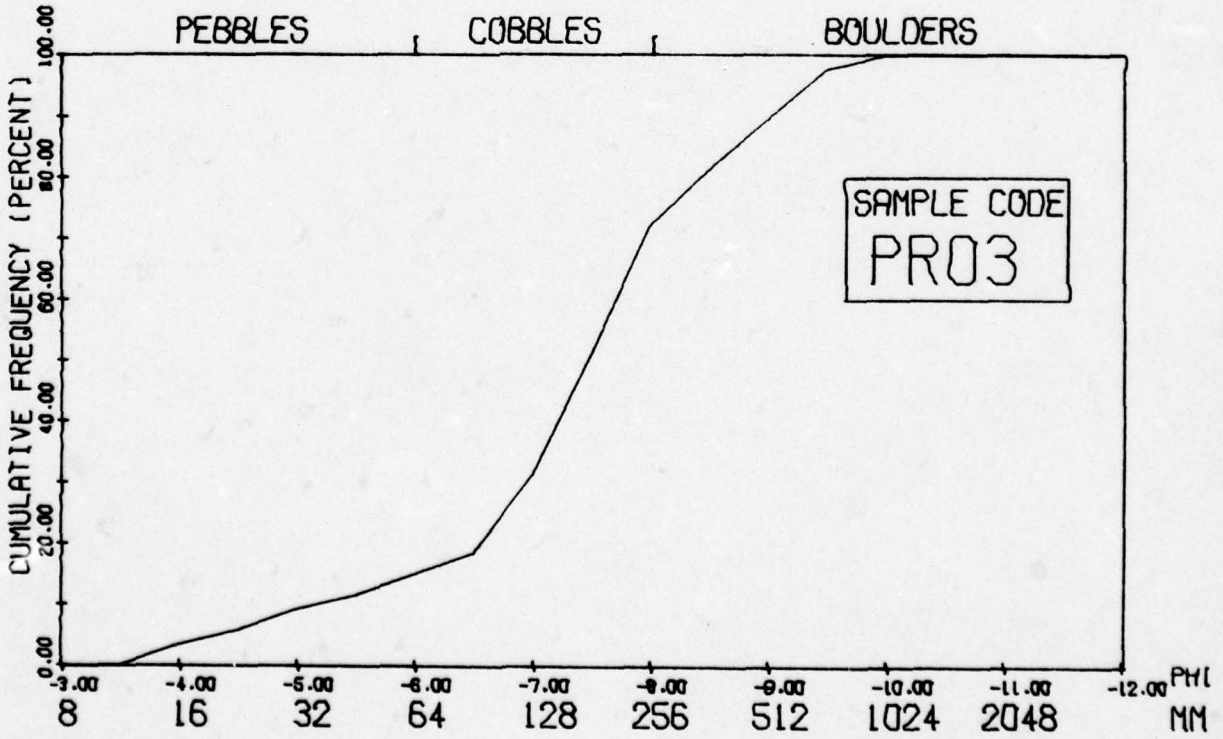
PEBBLES
COBBLES
BOULDERS
CUMULATIVE FREQUENCY (PERCENT)
0.00
20.00
40.00
60.00
80.00
100.00
SAMPLE CODE
PR03
-3.00
-4.00
-5.00
-6.00
-7.00
-8.00
-9.00
-10.00
-11.00
-12.00
PHI
8
16
32
64
128
256
512
1024
2048
MM

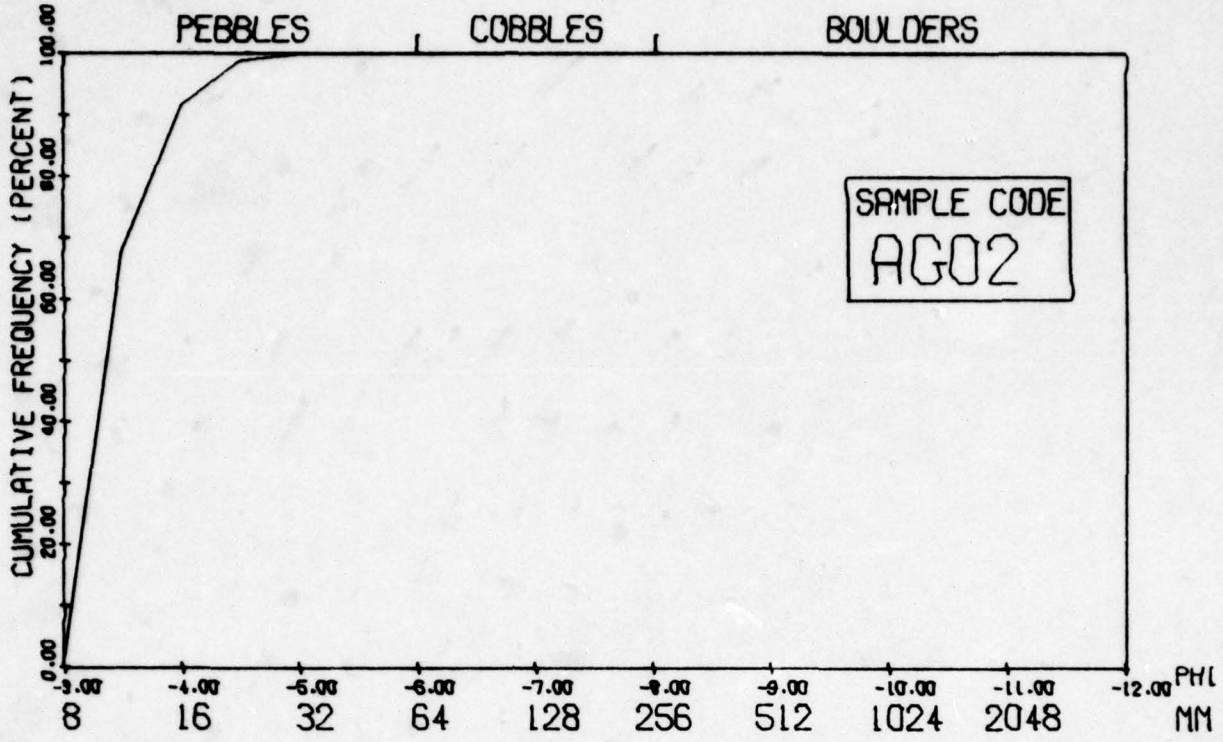
PEBBLES
COBBLES
BOULDERS
CUMULATIVE FREQUENCY (PERCENT)
100.00
80.00
60.00
40.00
20.00
0.00
SAMPLE CODE
AG02
-3.00
-4.00
-5.00
-6.00
-7.00
-8.00
-9.00
-10.00
-11.00
-12.00
PHI
8
16
32
64
128
256
512
1024
2048
MM

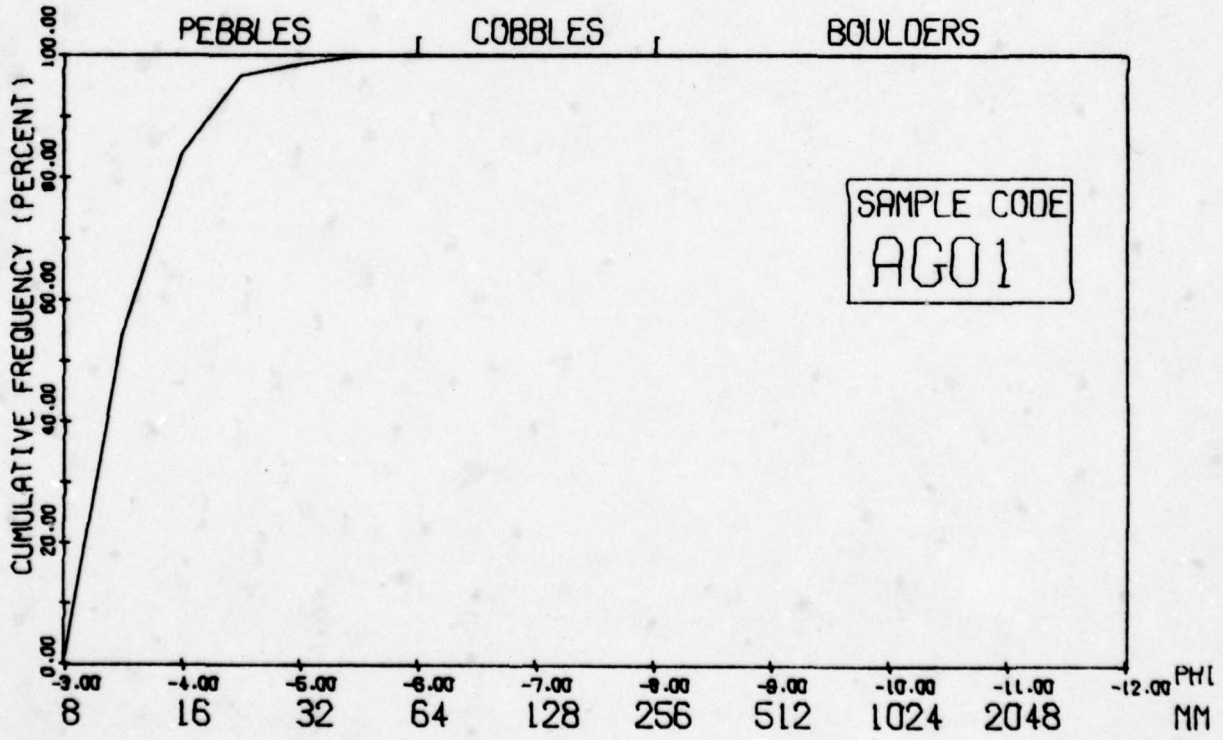
PEBBLES
COBBLES
BOULDERS
CUMULATIVE FREQUENCY (PERCENT)
100.00
80.00
60.00
40.00
20.00
0.00
SAMPLE CODE
AG01
-3.00
-4.00
-5.00
-6.00
-7.00
-8.00
-9.00
-10.00
-11.00
-12.00
PHI
8
16
32
64
128
256
512
1024
2048
MM

| Sample Code | Maximum Category (mm) | Minimum Category (mm) | Mode (mm) | Median (mm) | Mean (mm) | Variance | Standard Deviation | Skewness | Kurtosis |
|---|---|---|---|---|---|---|---|---|---|
| TT05 | 152.0 | 9.5 | 9.5 | 14.6 | 26.9 | 910.7 | 30.1 | 2.69 | 7.33 |
| TT11 | 1252.0 | 9.5 | 9.5 | 28.1 | 142.6 | 73263.2 | 270.6 | 2.86 | 7.70 |
| TT17 | 1778.0 | 9.5 | 19.0 | 77.4 | 260.7 | 160012.2 | 400.0 | 2.26 | 4.53 |
| TT20 | 1252.0 | 9.5 | 107.0 | 55.8 | 137.7 | 44420.8 | 210.7 | 3.35 | 13.0 |
| TT23 | 1252.0 | 9.5 | 632.0 | 152.0 | 319.9 | 121739.7 | 348.9 | 1.05 | 0.00 |
| TT25 | 1778.0 | 9.5 | 632.0 | 213.0 | 364.4 | 174271.6 | 417.4 | 1.49 | 1.92 |
| TT27 | 1778.0 | 9.5 | 632.0 | 304.4 | 428.0 | 145592.1 | 381.5 | 1.03 | 0.87 |
| TT30 | 889.0 | 9.5 | 107.0 | 108.3 | 210.4 | 49230.0 | 221.8 | 1.22 | 0.48 |
| TT34 | 453.0 | 9.5 | 76.0 | 53.6 | 72.5 | 5905.8 | 76.8 | 2.68 | 10.14 |

Table G-53 Particle Size Statistics for Tall Tale Samples.

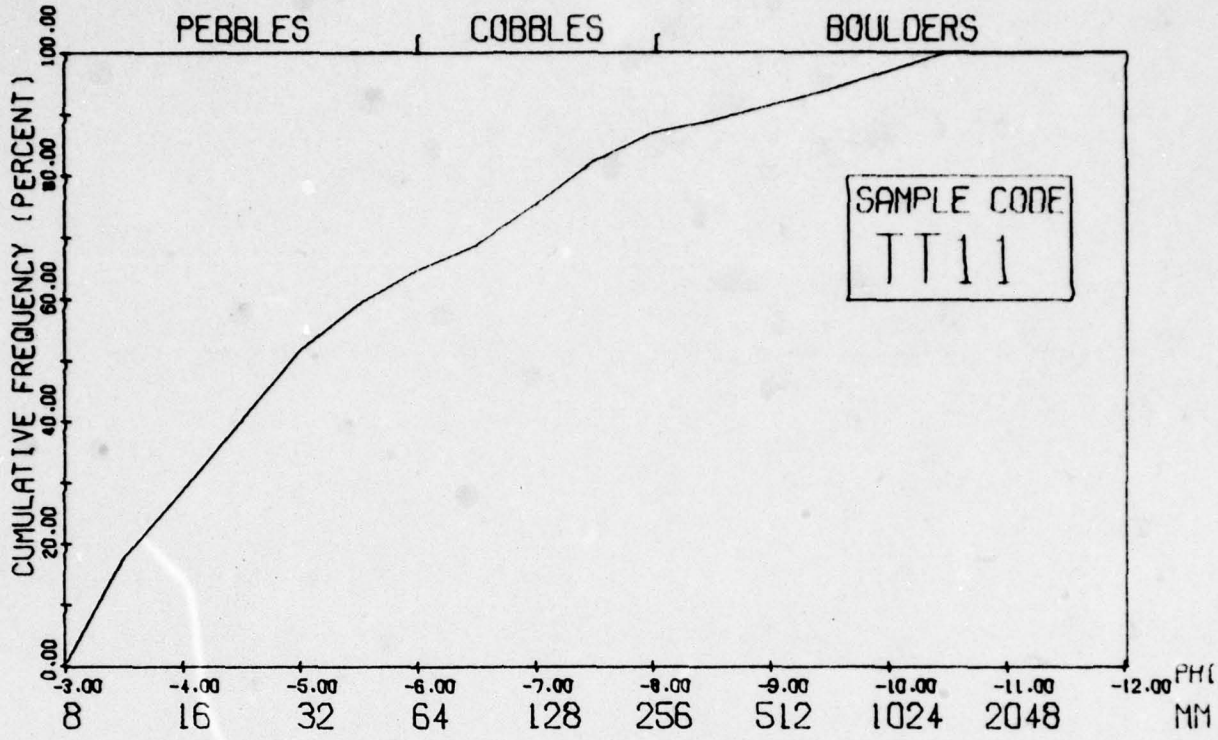
PEBBLES
COBBLES
BOULDERS
CUMULATIVE FREQUENCY (PERCENT)
100.00
80.00
60.00
40.00
20.00
0.00
SAMPLE CODE
TT11
-3.00
-4.00
-5.00
-6.00
-7.00
-8.00
-9.00
-10.00
-11.00
-12.00
PHI
8
16
32
64
128
256
512
1024
2048
MM

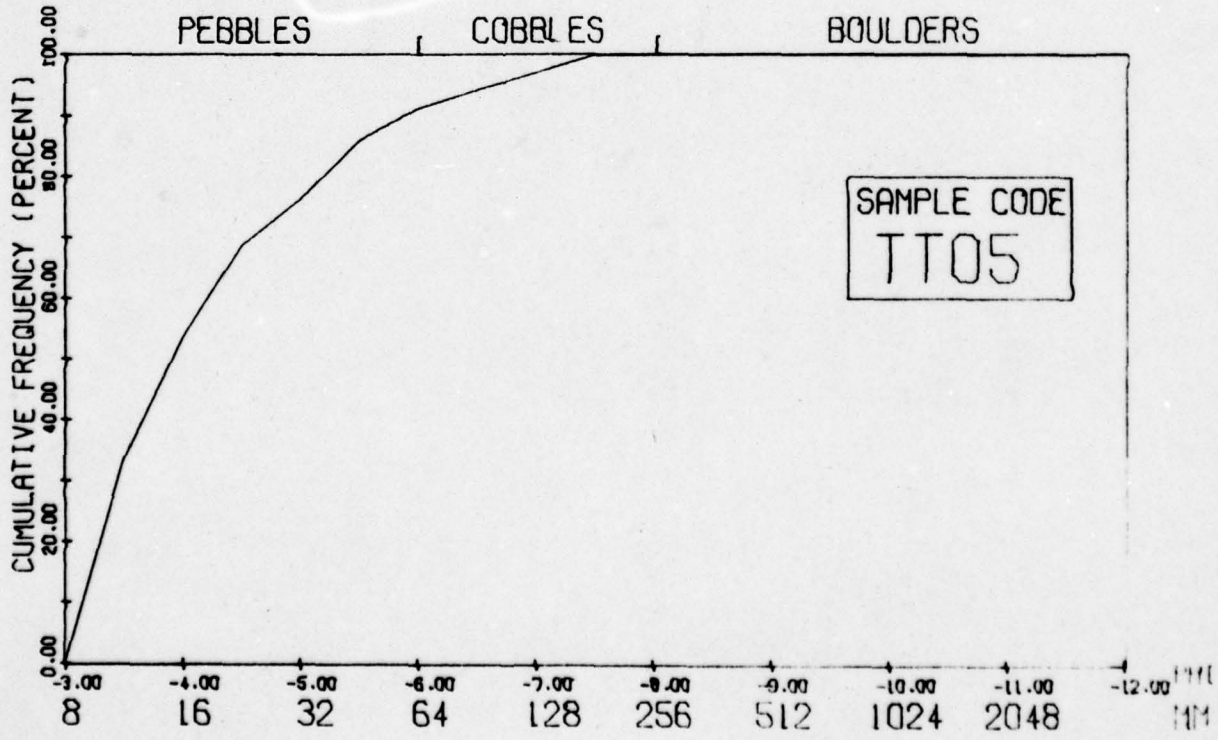
PEBBLES
COBBLES
BOULDERS
CUMULATIVE FREQUENCY (PERCENT)
100.00
80.00
60.00
40.00
20.00
0.00
SAMPLE CODE
TT05
-3.00
-4.00
-5.00
-6.00
-7.00
-8.00
-9.00
-10.00
-11.00
-12.00
8
16
32
64
128
256
512
1024
2048
MM

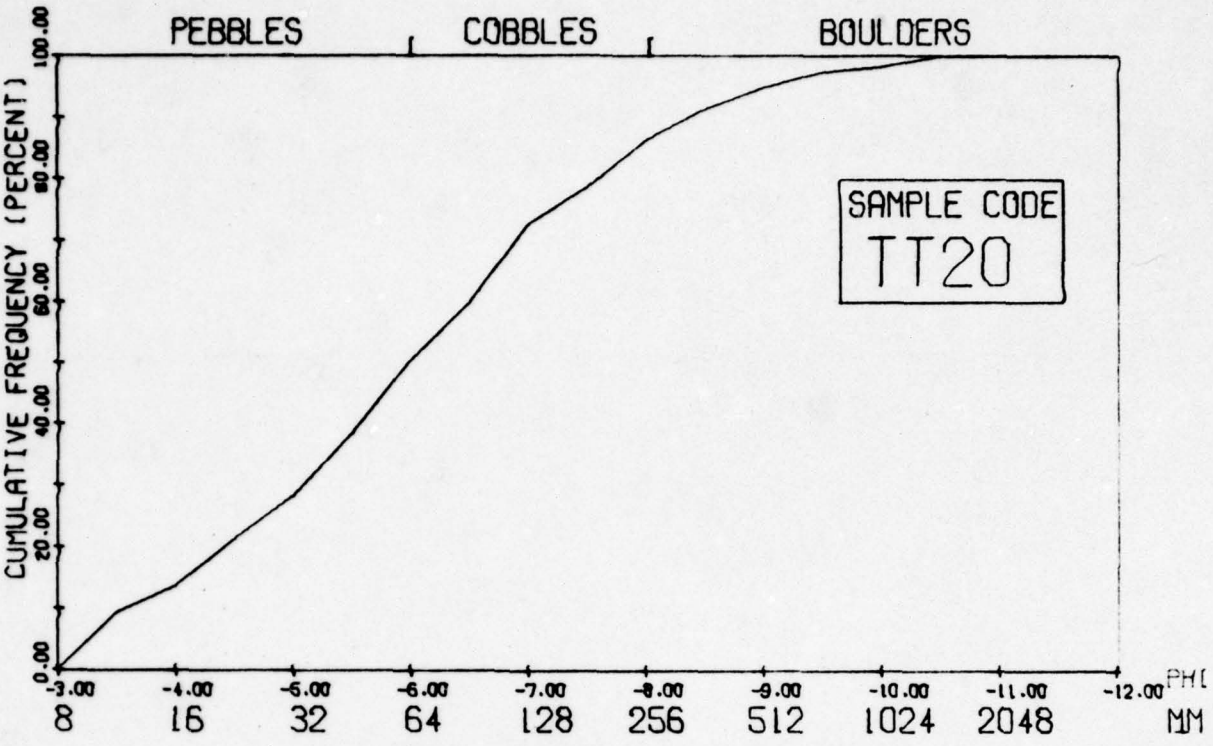
PEBBLES
COBBLES
BOULDERS
CUMULATIVE FREQUENCY (PERCENT)
100.00
80.00
60.00
40.00
20.00
0.00
SAMPLE CODE
TT20
-3.00
-4.00
-5.00
-6.00
-7.00
-8.00
-9.00
-10.00
-11.00
-12.00
PHI
8
16
32
64
128
256
512
1024
2048
MM

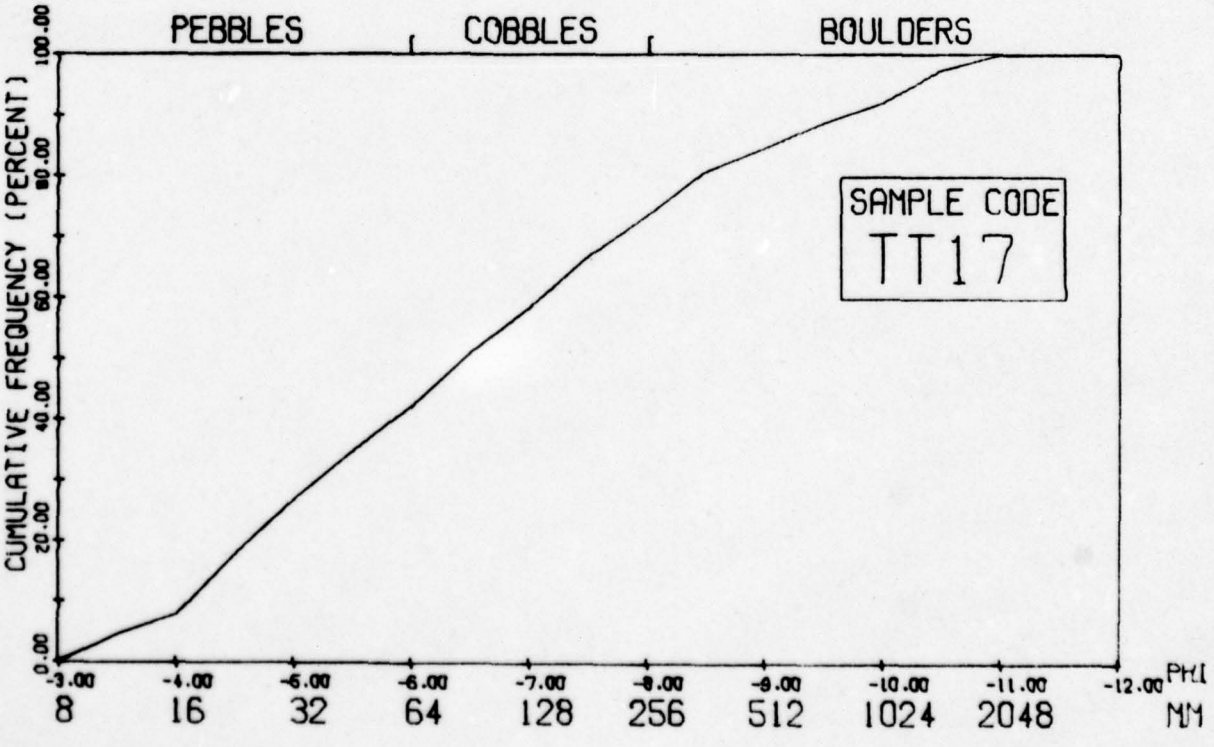
PEBBLES
COBBLES
BOULDERS
CUMULATIVE FREQUENCY (PERCENT)
100.00
80.00
60.00
40.00
20.00
0.00
SAMPLE CODE
TT17
-3.00
-4.00
-5.00
-6.00
-7.00
-8.00
-9.00
-10.00
-11.00
-12.00
PHI
8
16
32
64
128
256
512
1024
2048
MM

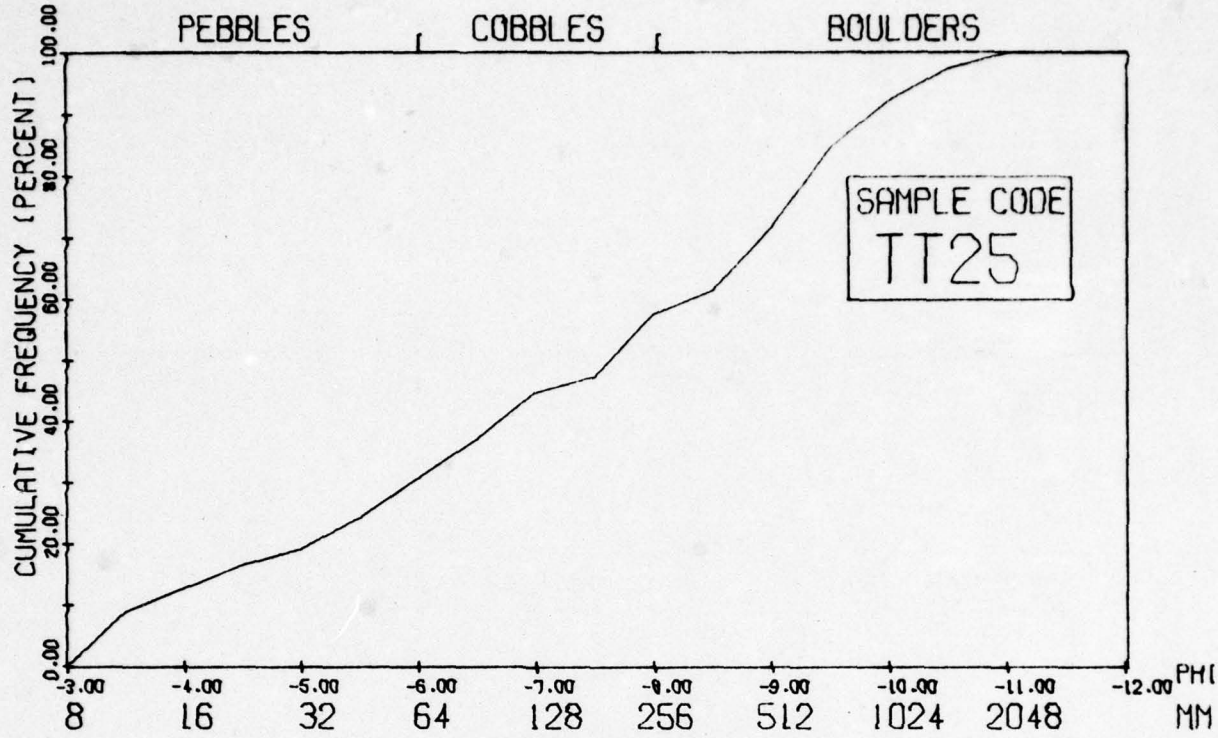
PEBBLES
COBBLES
BOULDERS
CUMULATIVE FREQUENCY (PERCENT)
0.00
20.00
40.00
60.00
80.00
100.00
SAMPLE CODE
TT25
-3.00
-4.00
-5.00
-6.00
-7.00
-8.00
-9.00
-10.00
-11.00
-12.00
PHI
8
16
32
64
128
256
512
1024
2048
MM

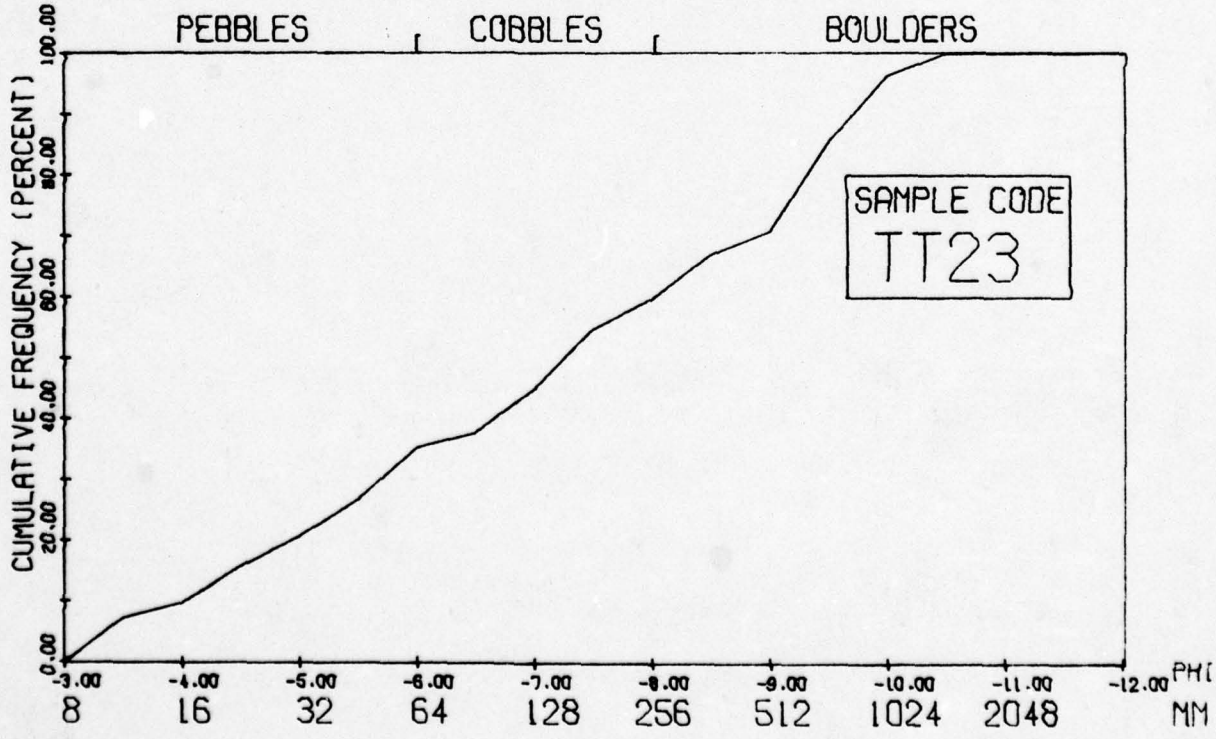
PEBBLES
COBBLES
BOULDERS
CUMULATIVE FREQUENCY (PERCENT)
0.00
20.00
40.00
60.00
80.00
100.00
SAMPLE CODE
TT23
-3.00
-4.00
-5.00
-6.00
-7.00
-8.00
-9.00
-10.00
-11.00
-12.00
PHI
8
16
32
64
128
256
512
1024
2048
MM

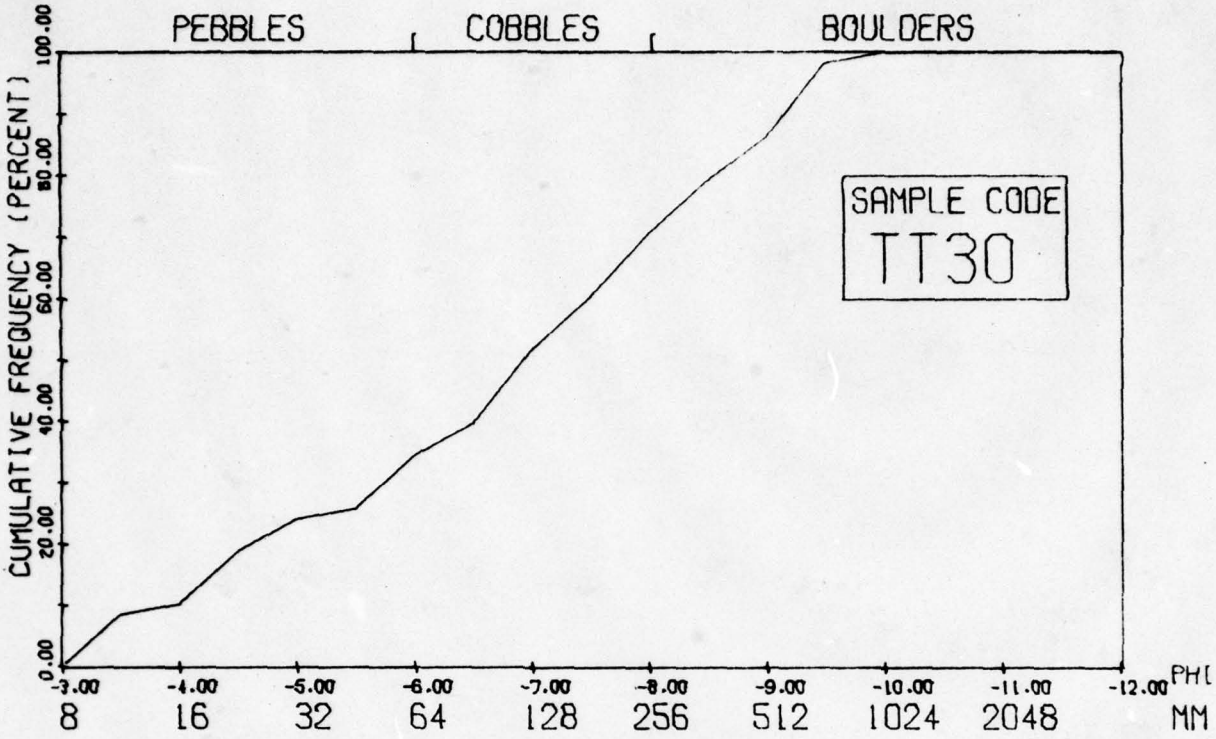
PEBBLES
COBBLES
BOULDERS
CUMULATIVE FREQUENCY (PERCENT)
0.00
20.00
40.00
60.00
80.00
100.00
SAMPLE CODE
TT30
-3.00
-4.00
-5.00
-6.00
-7.00
-8.00
-9.00
-10.00
-11.00
-12.00
PHI
8
16
32
64
128
256
512
1024
2048
MM

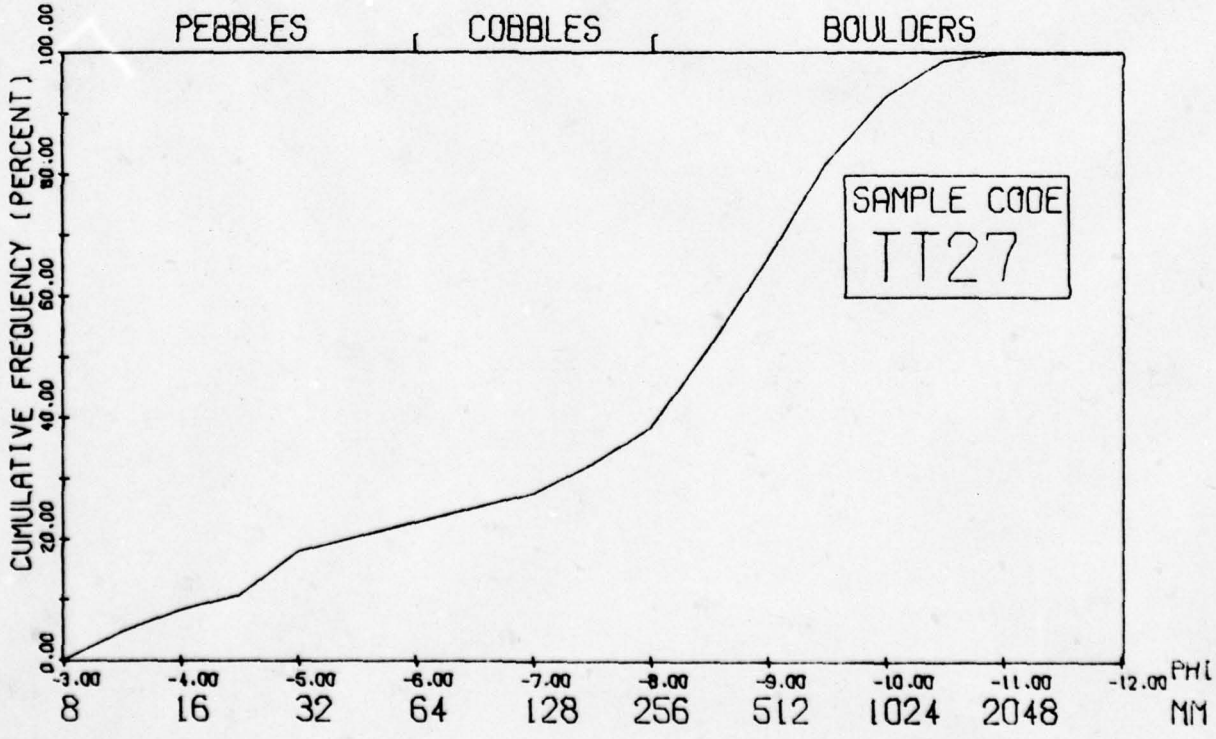
PEBBLES
COBBLES
BOULDERS
CUMULATIVE FREQUENCY (PERCENT)
0.00
20.00
40.00
60.00
80.00
100.00
SAMPLE CODE
TT27
-3.00
-4.00
-5.00
-6.00
-7.00
-8.00
-9.00
-10.00
-11.00
-12.00
PHI
8
16
32
64
128
256
512
1024
2048
MM

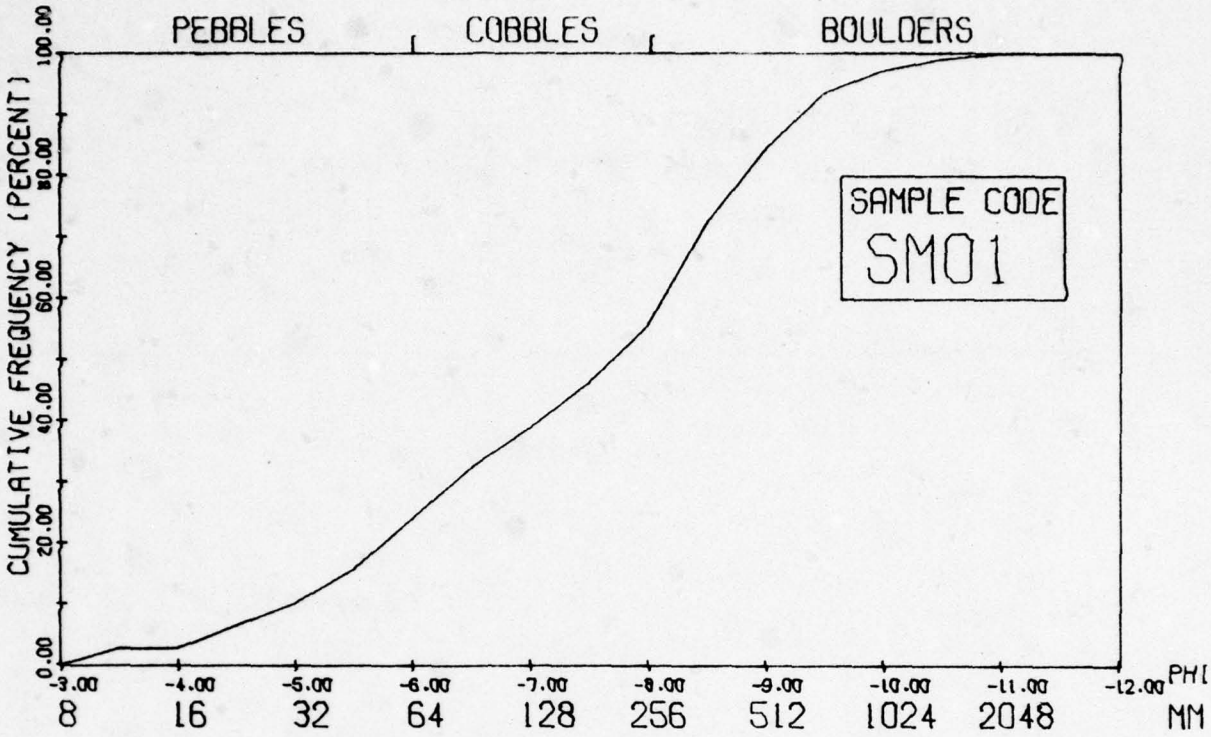
PEBBLES
COBBLES
BOULDERS
CUMULATIVE FREQUENCY (PERCENT)
0.00
20.00
40.00
60.00
80.00
100.00
SAMPLE CODE
SM01
-3.00
-4.00
-5.00
-6.00
-7.00
-8.00
-9.00
-10.00
-11.00
-12.00
PHI
8
16
32
64
128
256
512
1024
2048
MM

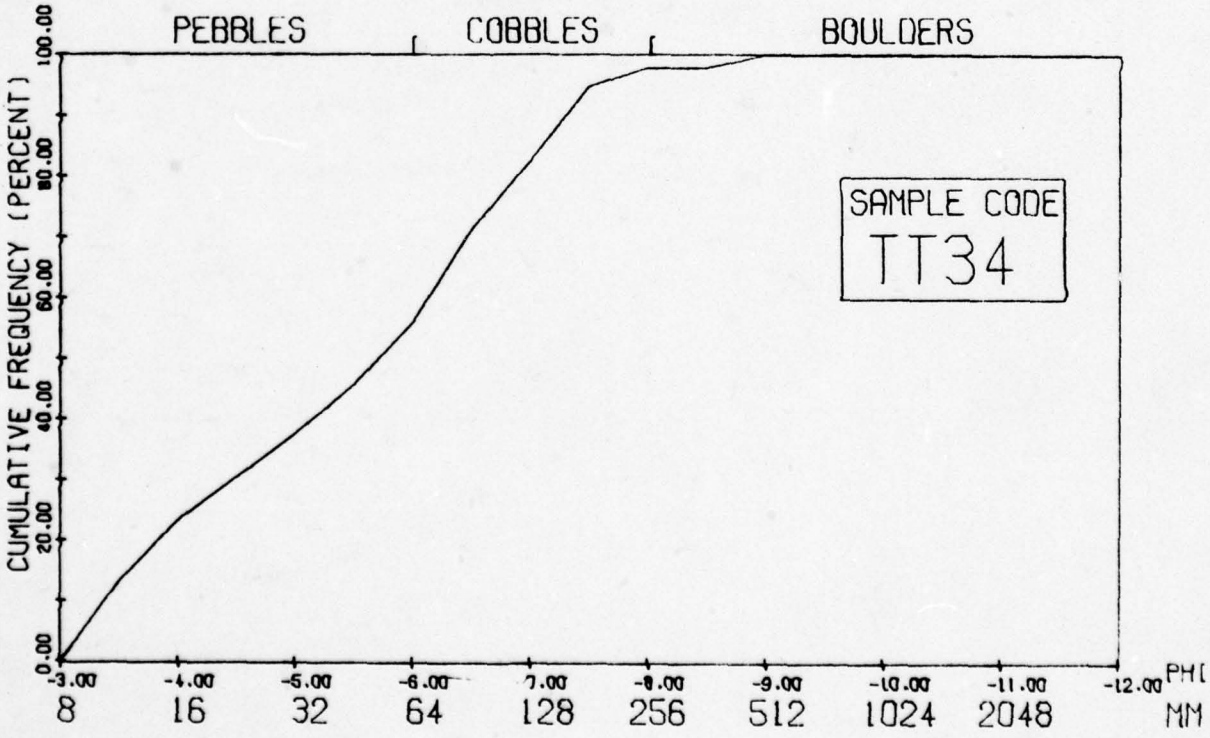
PEBBLES
COBBLES
BOULDERS
CUMULATIVE FREQUENCY (PERCENT)
0.00
20.00
40.00
60.00
80.00
100.00
SAMPLE CODE
TT34
-3.00
-4.00
-5.00
-6.00
7.00
-8.00
-9.00
-10.00
-11.00
-12.00
PHI
8
16
32
64
128
256
512
1024
2048
MM

| Sample Code | Maximum Category (mm) | Minimum Category (mm) | Mode (mm) | Median (mm) | Mean (mm) | Variance | Standard Deviation | Skewness | Kurtosis |
|---|---|---|---|---|---|---|---|---|---|
| SM01 | 1778.0 | 9.5 | 303.0 | 213.2 | 289.0 | 89384.1 | 298.9 | 2.04 | 5.78 |
| SM02 | 1252.0 | 9.5 | 107.0 | 105.3 | 153.7 | 40014.5 | 200.0 | 3.00 | 11.8 |
| SM05 | 632.0 | 9.5 | 214.0 | 75.2 | 111.2 | 13336.4 | 115.4 | 2.10 | 5.56 |
| SM06 | 214.0 | 9.5 | 13.4 | 28.5 | 53.1 | 2663.7 | 51.6 | 1.38 | 1.01 |
| SM07 | 303.0 | 9.5 | 9.5 | 26.0 | 53.2 | 3808.9 | 61.7 | 1.92 | 3.42 |
| SM08 | 303.0 | 9.5 | 9.5 | 25.2 | 38.3 | 2104.7 | 45.8 | 3.36 | 14.27 |
| SM09 | 214.0 | 9.5 | 9.5 | 19.3 | 34.2 | 1322.5 | 36.3 | 2.62 | 8.44 |
| SM11 | 76.0 | 9.5 | 9.5 | 18.3 | 23.7 | 273.1 | 16.5 | 1.29 | 0.73 |
| SM12 | 54.0 | 9.5 | 26.8 | 19.2 | 21.0 | 105.4 | 10.2 | 1.00 | 0.99 |
| SM13 | 76.0 | 9.5 | 19.0 | 17.9 | 21.6 | 212.0 | 14.5 | 2.09 | 4.68 |
| SM14 | 38.0 | 9.5 | 9.5 | 10.6 | 13.1 | 51.4 | 7.1 | 2.49 | 5.55 |
| SM16 | 107.0 | 9.5 | 9.5 | 18.2 | 26.4 | 464.6 | 21.5 | 1.68 | 2.38 |
| SM17 | 26.8 | 9.5 | 9.5 | 10.8 | 11.8 | 13.1 | 3.6 | 1.89 | 3.89 |
| SMI7 | 26.8 | 9.5 | 9.5 | 11.9 | 12.8 | 18.9 | 4.3 | 1.79 | 3.13 |
| SM18 | 26.8 | 9.5 | 9.5 | 10.8 | 12.0 | 15.5 | 3.9 | 1.91 | 3.75 |
| SM19 | 38.8 | 9.5 | 9.5 | 13.4 | 15.0 | 37.2 | 6.1 | 1.52 | 2.78 |
| SMI9 | 76.0 | 9.5 | 13.4 | 18.6 | 23.7 | 239.7 | 15.4 | 1.41 | 1.57 |
| SM20 | 26.8 | 9.5 | 9.5 | 11.3 | 12.5 | 16.6 | 4.0 | 1.57 | 2.36 |
| SM21 | 38.0 | 9.5 | 9.5 | 10.9 | 12.2 | 18.4 | 4.2 | 2.42 | 8.86 |

Table G-59 Particle Size Statistics for Stoval-Mohawk Samples

| Sample Code | Maximum Category (mm) | Minimum Category (mm) | Mode (mm) | Median (mm) | Mean (mm) | Variance | Standard Deviation | Skewness | Kurtosis |
|---|---|---|---|---|---|---|---|---|---|
| SM22 | 26.8 | 9.5 | 9.5 | 10.8 | 11.5 | 9.5 | 3.1 | 2.09 | 5.80 |
| SMB2 | 19.0 | 9.5 | 9.5 | 10.8 | 11.7 | 10.7 | 3.2 | 1.27 | 0.36 |
| SM24 | 38.0 | 9.5 | 9.5 | 11.5 | 13.0 | 23.6 | 4.8 | 2.02 | 5.82 |
| SM25 | 214.0 | 9.5 | 26.8 | 25.3 | 34.5 | 153.6 | 39.1 | 3.31 | 11.33 |
| SM26 | 152.0 | 9.5 | 26.8 | 25.5 | 31.1 | 668.8 | 25.8 | 2.05 | 5.04 |
| SM27 | 889.0 | 9.5 | 76.0 | 77.2 | 173.4 | 39613.5 | 199.0 | 1.57 | 1.67 |
| SM28 | 1252.0 | 9.5 | 632.0 | 213.5 | 313.8 | 80363.9 | 283.4 | 1.10 | 0.95 |
| SM29 | 453.0 | 9.5 | 76.0 | 75.0 | 104.6 | 10312.4 | 101.5 | 1.53 | 2.30 |
| SM30 | 303.0 | 9.5 | 54.0 | 55.0 | 76.4 | 3411.8 | 58.4 | 1.44 | 2.26 |
| SM31 | 214.0 | 9.5 | 13.4 | 28.3 | 50.1 | 2372.5 | 48.7 | 1.72 | 2.56 |
| SM32 | 303 | 9.5 | 54.0 | 39.0 | 60.7 | 3408.7 | 58.3 | 1.82 | 3.21 |
| SM33 | 453 | 9.5 | 38.0 | 39.2 | 78.6 | 8613.6 | 92.8 | 1.94 | 3.14 |
| SM34 | 38.0 | 9.5 | 9.5 | 10.8 | 12.5 | 25.7 | 5.0 | 2.20 | 5.09 |
| SM3D | 54.0 | 9.5 | 9.5 | 12.1 | 14.9 | 66.3 | 8.1 | 2.22 | 5.70 |
| SM35 | 453.0 | 9.5 | 76.0 | 55.7 | 94.1 | 7732.9 | 87.9 | 1.51 | 2.27 |
| SM36 | 632.0 | 9.5 | 76.0 | 107.6 | 178.3 | 31729.8 | 178.1 | 1.33 | 0.81 |
| SM37 | 632.0 | 9.5 | 107.0 | 105.5 | 138.7 | 18602.2 | 136.3 | 1.68 | 2.93 |
| SM38 | 38.0 | 9.5 | 9.5 | 12.4 | 14.1 | 31.5 | 5.6 | 1.36 | 1.84 |

Table G-60 Particle Size Statistics for Stoval-Mohawk Samples.

| Sample Code | Maximum Category (mm) | Minimum Category (mm) | Mode (mm) | Median (mm) | Mean (mm) | Variance | Standard Deviation | Skewness | Kurtosis |
|---|---|---|---|---|---|---|---|---|---|
| SM39 | 38.0 | 9.5 | 9.5 | 11.6 | 13.7 | 35.7 | 5.9 | 1.87 | 3.75 |
| SM40 | 453.0 | 9.5 | 76.0 | 52.6 | 73.0 | 5324.3 | 72.9 | 2.35 | 7.75 |
| SM41 | 214.0 | 9.5 | 19.0 | 27.5 | 39.6 | 1254.1 | 35.4 | 2.32 | 7.10 |
| SM42 | 214.0 | 9.5 | 13.4 | 25.2 | 38.2 | 1469.9 | 38.3 | 2.24 | 5.34 |
| SM43 | 214.0 | 9.5 | 38.0 | 39.5 | 54.7 | 1673.5 | 40.9 | 1.91 | 4.71 |
| SM44 | 152.0 | 9.5 | 26.8 | 27.7 | 38.6 | 1051.3 | 32.4 | 1.87 | 3.83 |
| SM45 | 107.0 | 9.5 | 26.8 | 25.9 | 29.2 | 349.9 | 18.7 | 1.59 | 2.83 |
| SM46 | 76.0 | 9.5 | 9.5 | 19.7 | 25.8 | 296.4 | 17.2 | 1.26 | 1.01 |
| SM47 | 107.0 | 9.5 | 19.0 | 25.0 | 31.7 | 480.5 | 21.9 | 1.19 | 0.74 |
| SM48 | 76.0 | 9.5 | 9.5 | 19.7 | 24.7 | 287.0 | 16.9 | 1.47 | 1.77 |
| SM49 | 54.0 | 9.5 | 9.5 | 17.5 | 20.6 | 169.3 | 13.0 | 1.42 | 1.20 |

Table G-61 Particle Size Statistics for Stoval-Mohawk Samples.

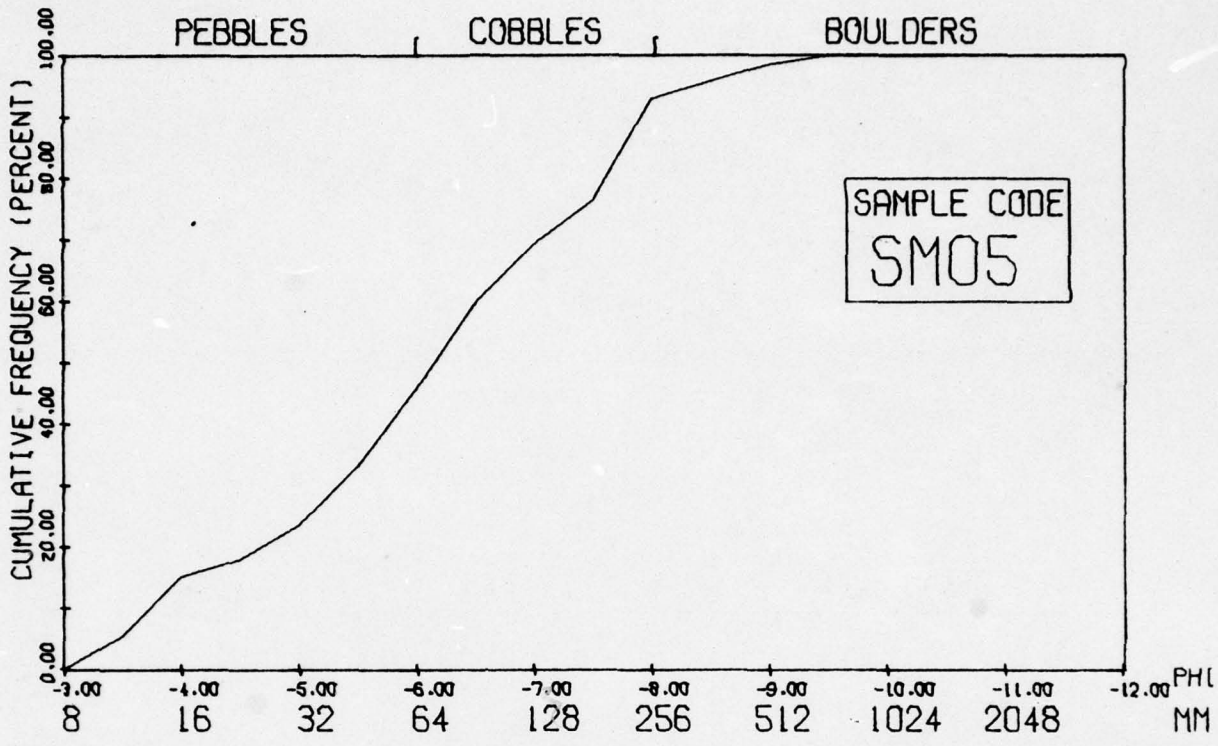
PEBBLES
COBBLES
BOULDERS
CUMULATIVE FREQUENCY (PERCENT)
100.00
80.00
60.00
40.00
20.00
0.00
SAMPLE CODE
SM05
-3.00
-4.00
-5.00
-6.00
-7.00
-8.00
-9.00
-10.00
-11.00
-12.00
PHI
8
16
32
64
128
256
512
1024
2048
MM

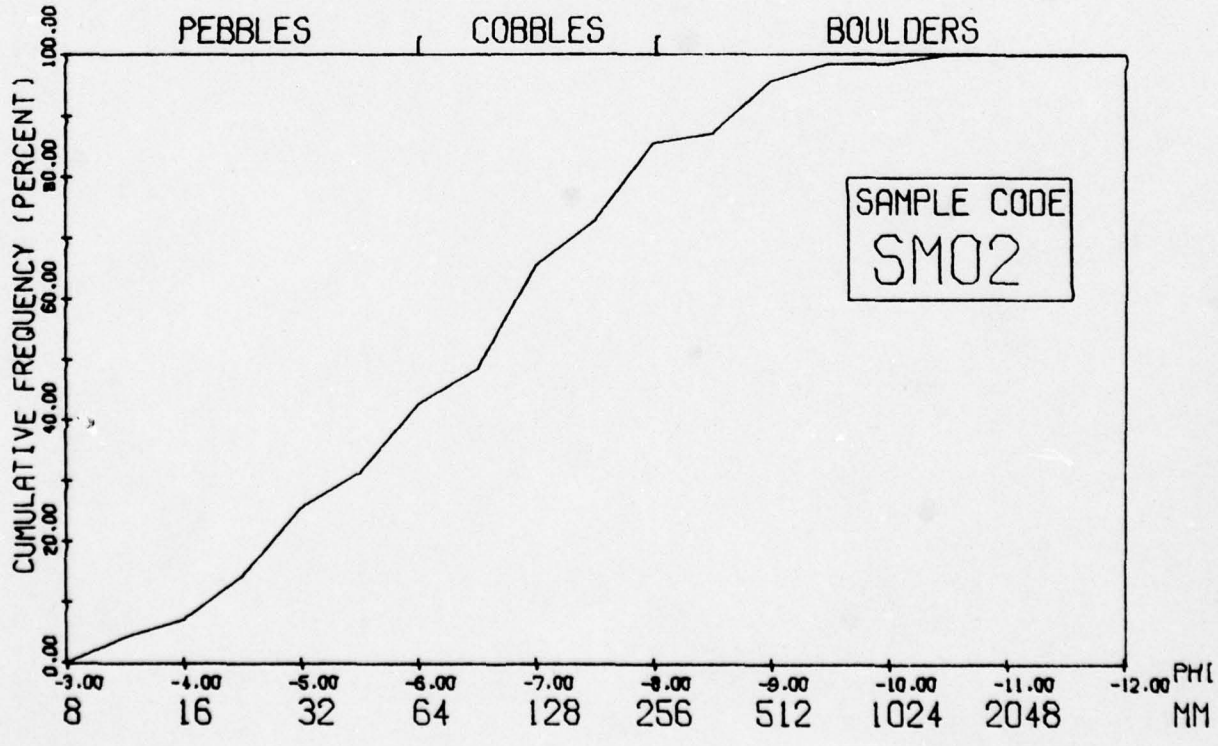
PEBBLES
COBBLES
BOULDERS
CUMULATIVE FREQUENCY (PERCENT)
100.00
80.00
60.00
40.00
20.00
0.00
SAMPLE CODE
SM02
-3.00
-4.00
-5.00
-6.00
-7.00
-8.00
-9.00
-10.00
-11.00
-12.00
PHI
8
16
32
64
128
256
512
1024
2048
MM

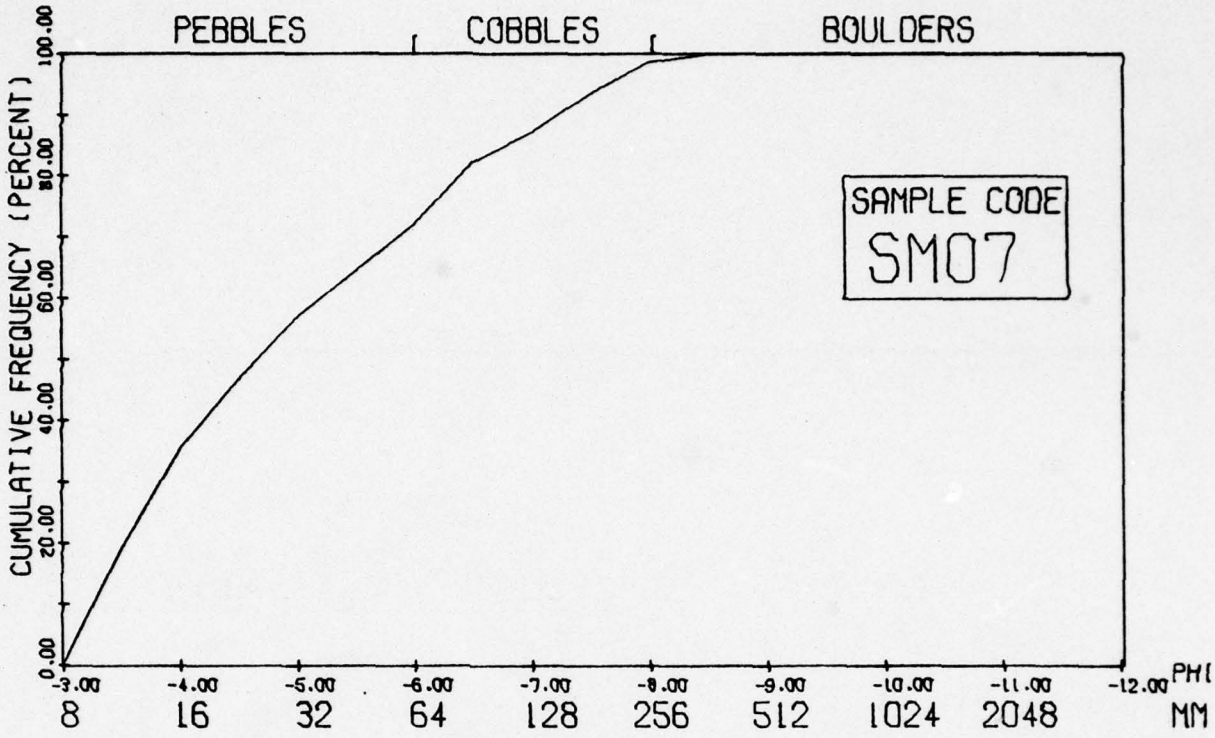
PEBBLES
COBBLES
BOULDERS
CUMULATIVE FREQUENCY (PERCENT)
0.00
20.00
40.00
60.00
80.00
100.00
SAMPLE CODE
SM07
-3.00
-4.00
-5.00
-6.00
-7.00
-8.00
-9.00
-10.00
-11.00
-12.00
PHI
8
16
32
64
128
256
512
1024
2048
MM

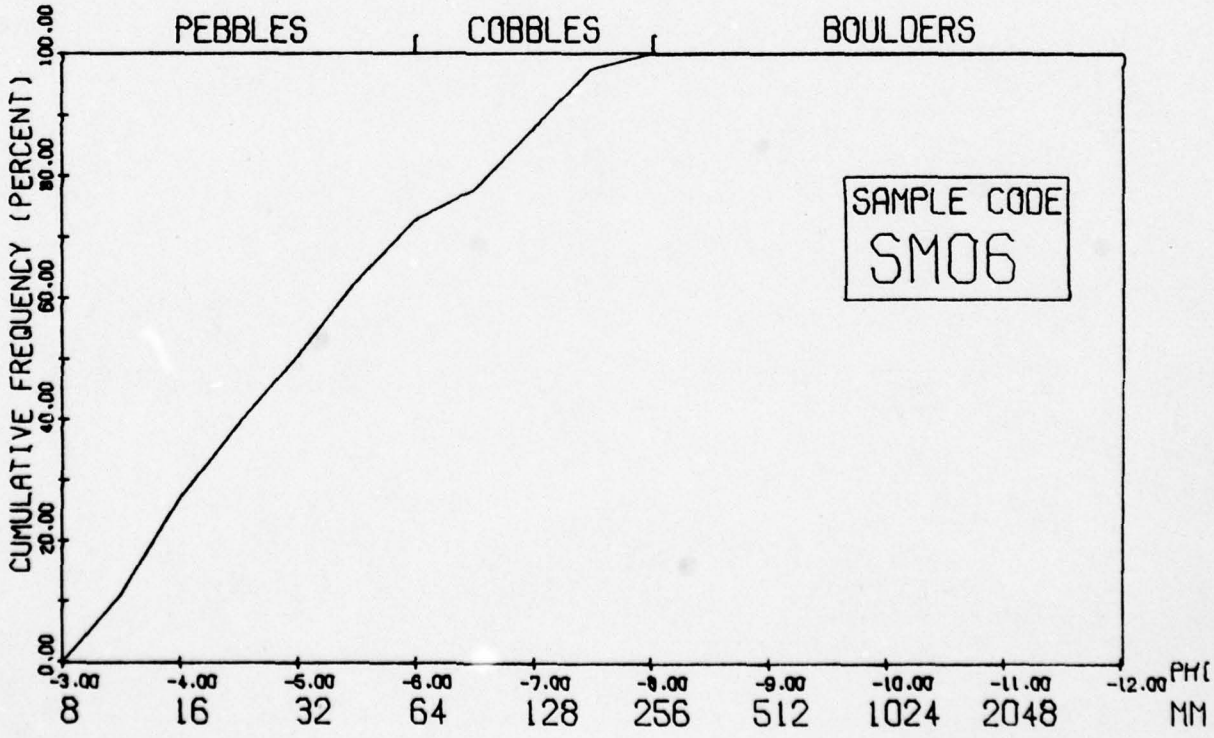
PEBBLES
COBBLES
BOULDERS
CUMULATIVE FREQUENCY (PERCENT)
0.00
20.00
40.00
60.00
80.00
100.00
SAMPLE CODE
SM06
-3.00
-4.00
-5.00
-6.00
-7.00
-8.00
-9.00
-10.00
-11.00
-12.00
PHI
8
16
32
64
128
256
512
1024
2048
MM

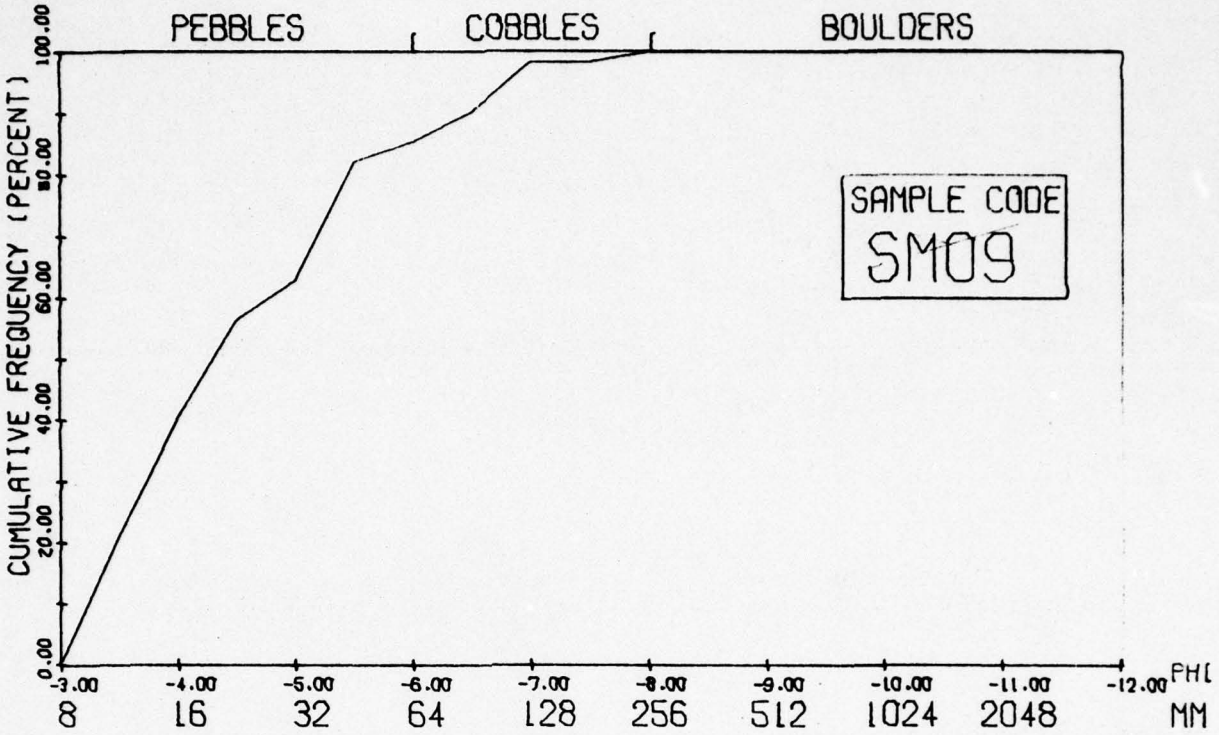
PEBBLES
COBBLES
BOULDERS
CUMULATIVE FREQUENCY (PERCENT)
0.00
20.00
40.00
60.00
80.00
100.00
SAMPLE CODE
SM09
-3.00
-4.00
-5.00
-6.00
-7.00
-8.00
-9.00
-10.00
-11.00
-12.00
PHI
8
16
32
64
128
256
512
1024
2048
MM

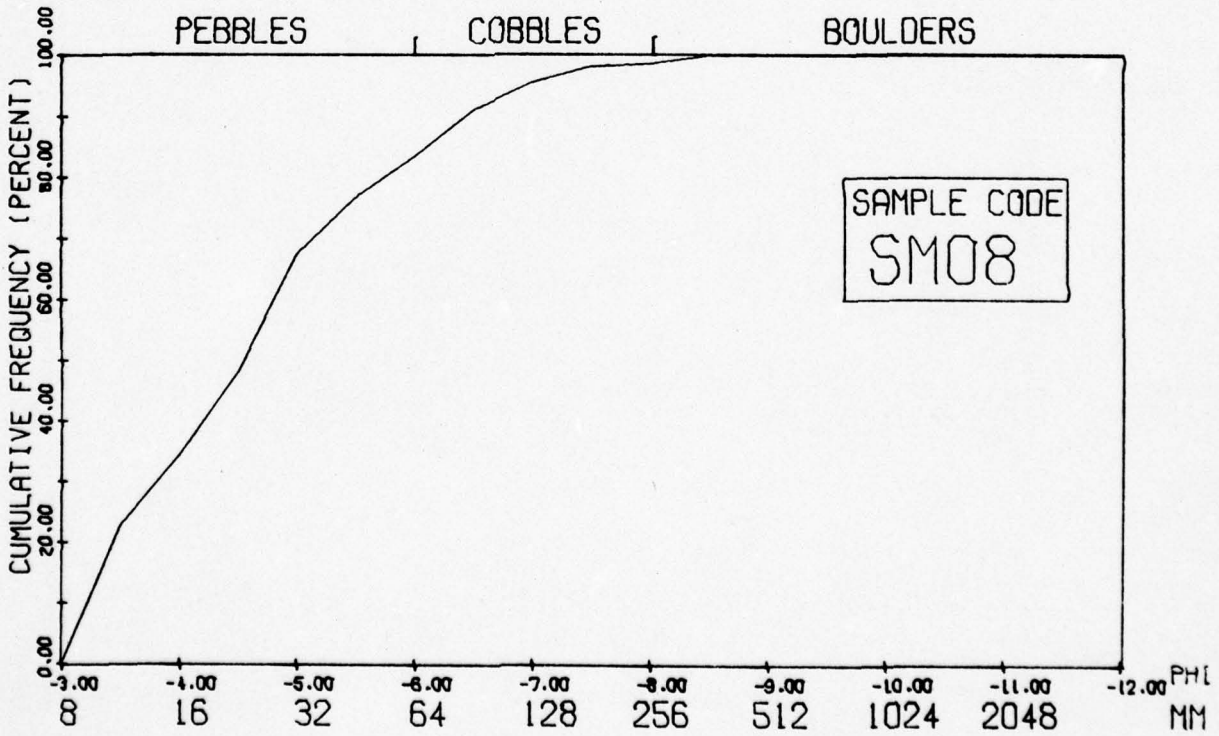
PEBBLES
COBBLES
BOULDERS
CUMULATIVE FREQUENCY (PERCENT)
0.00
20.00
40.00
60.00
80.00
100.00
SAMPLE CODE
SM08
-3.00
-4.00
-5.00
-6.00
-7.00
-8.00
-9.00
-10.00
-11.00
-12.00
PHI
8
16
32
64
128
256
512
1024
2048
MM

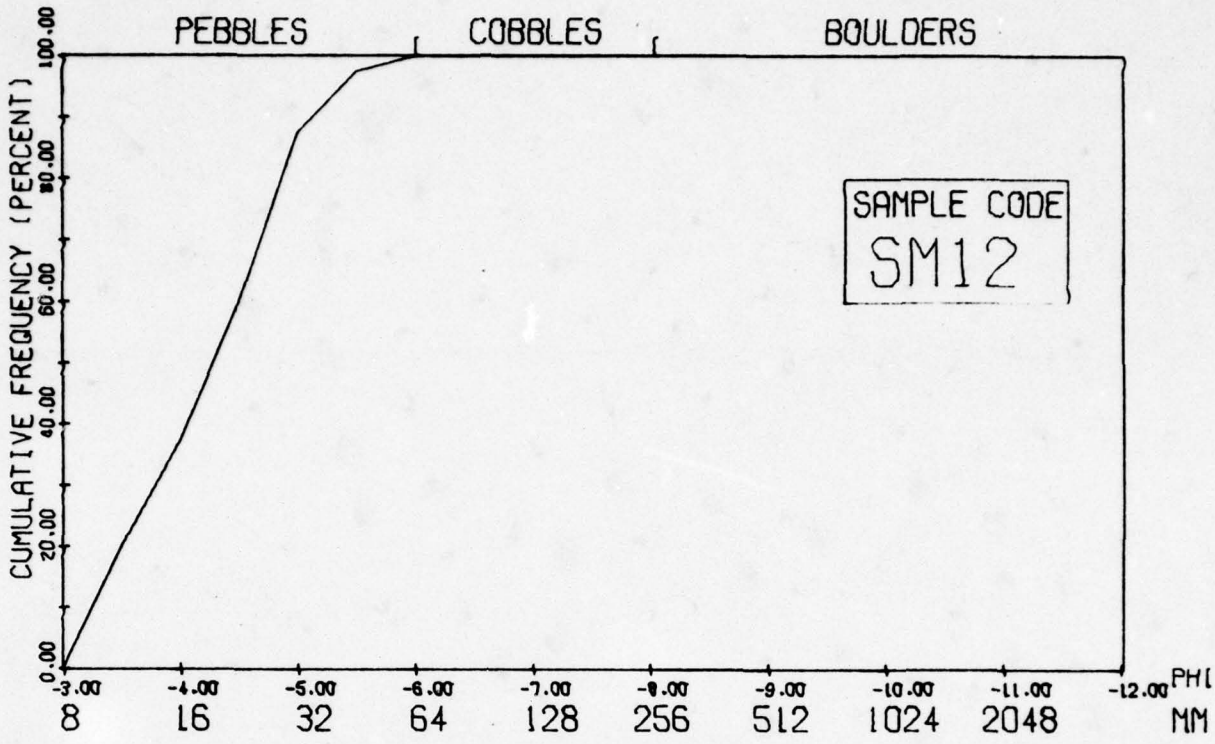
PEBBLES
COBBLES
BOULDERS
SAMPLE CODE
SM12
CUMULATIVE FREQUENCY (PERCENT)
100.00
80.00
60.00
40.00
20.00
0.00
-3.00
-4.00
-5.00
-6.00
-7.00
-8.00
-9.00
-10.00
-11.00
-12.00
PHI
8
16
32
64
128
256
512
1024
2048
MM

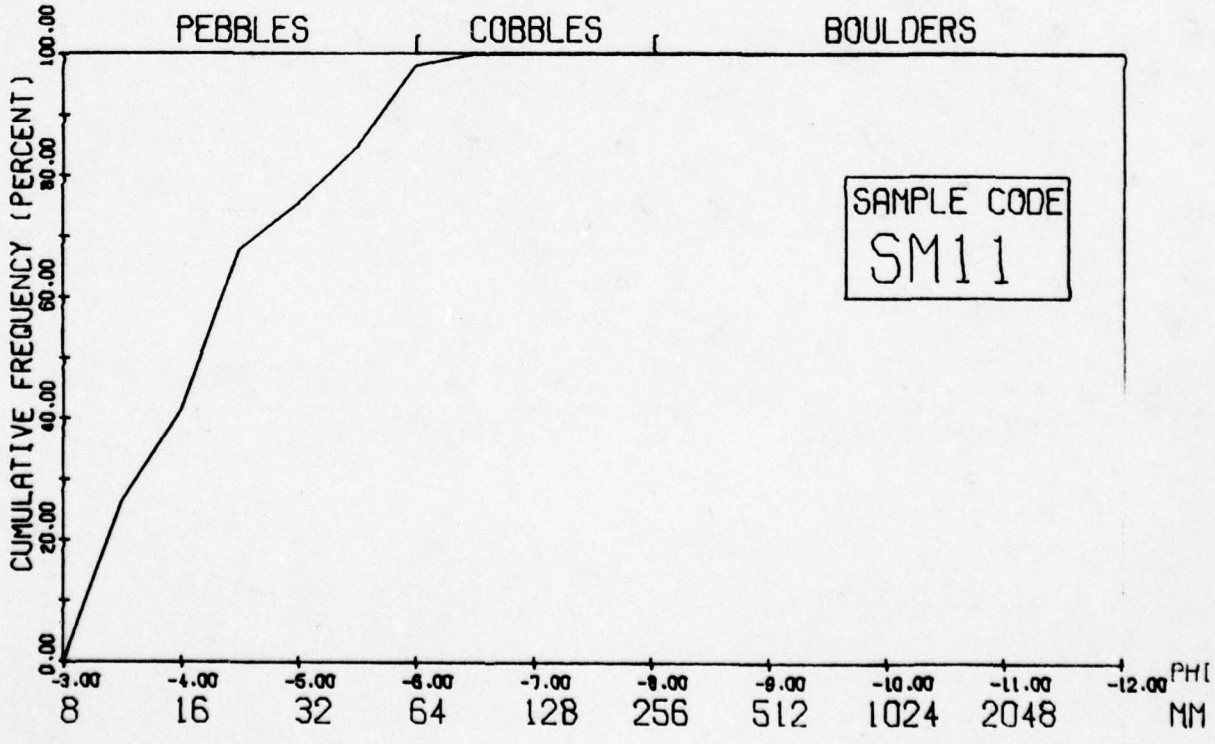
PEBBLES
COBBLES
BOULDERS
SAMPLE CODE
SM11
CUMULATIVE FREQUENCY (PERCENT)
100.00
80.00
60.00
40.00
20.00
0.00
-3.00
-4.00
-5.00
-6.00
-7.00
-8.00
-9.00
-10.00
-11.00
-12.00
PHI
8
16
32
64
128
256
512
1024
2048
MM

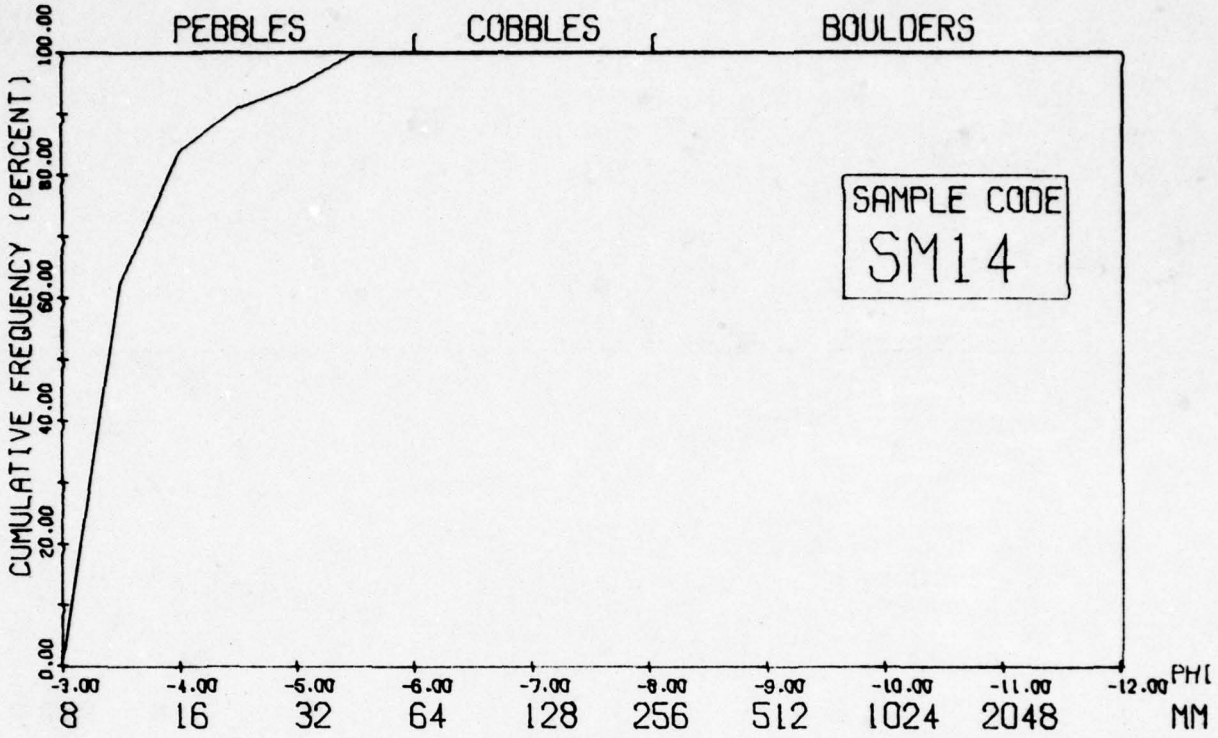
PEBBLES
COBBLES
BOULDERS
CUMULATIVE FREQUENCY (PERCENT)
100.00
80.00
60.00
40.00
20.00
0.00
SAMPLE CODE
SM14
-3.00
-4.00
-5.00
-6.00
-7.00
-8.00
-9.00
-10.00
-11.00
-12.00
PHI
8
16
32
64
128
256
512
1024
2048
MM

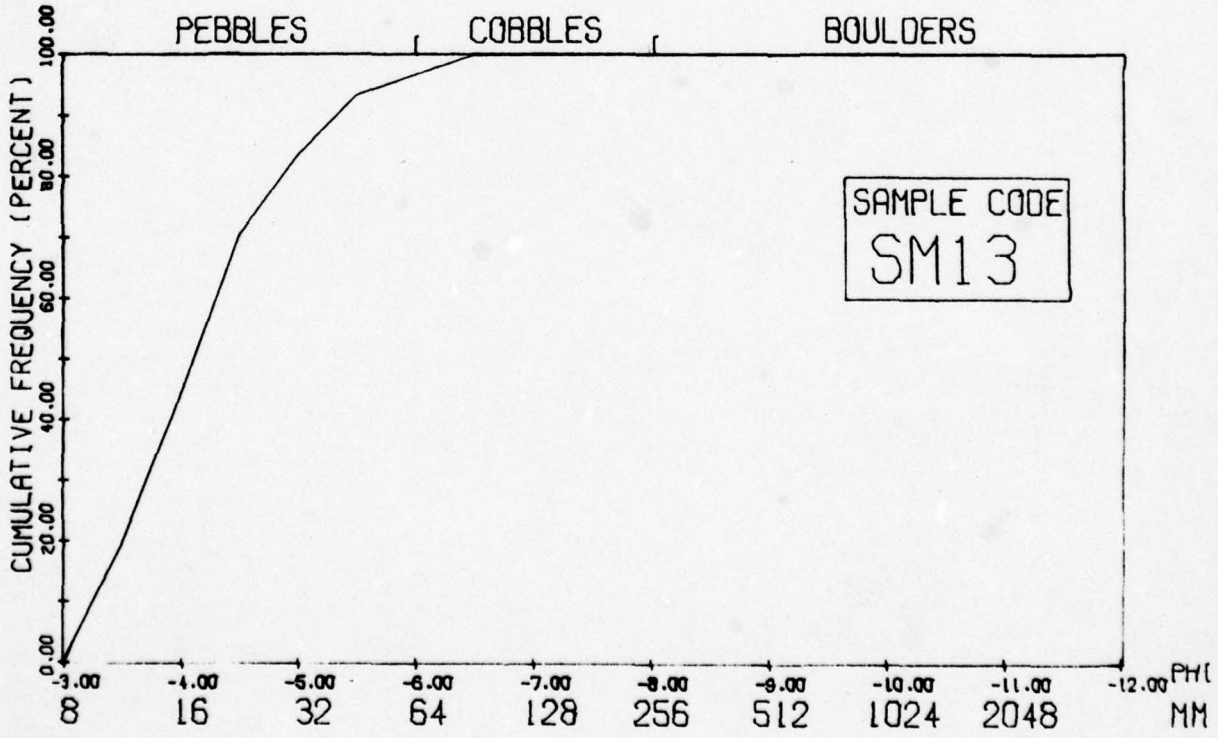
PEBBLES
COBBLES
BOULDERS
CUMULATIVE FREQUENCY (PERCENT)
100.00
80.00
60.00
40.00
20.00
0.00
SAMPLE CODE
SM13
-3.00
-4.00
-5.00
-6.00
-7.00
-8.00
-9.00
-10.00
-11.00
-12.00
PHI
8
16
32
64
128
256
512
1024
2048
MM

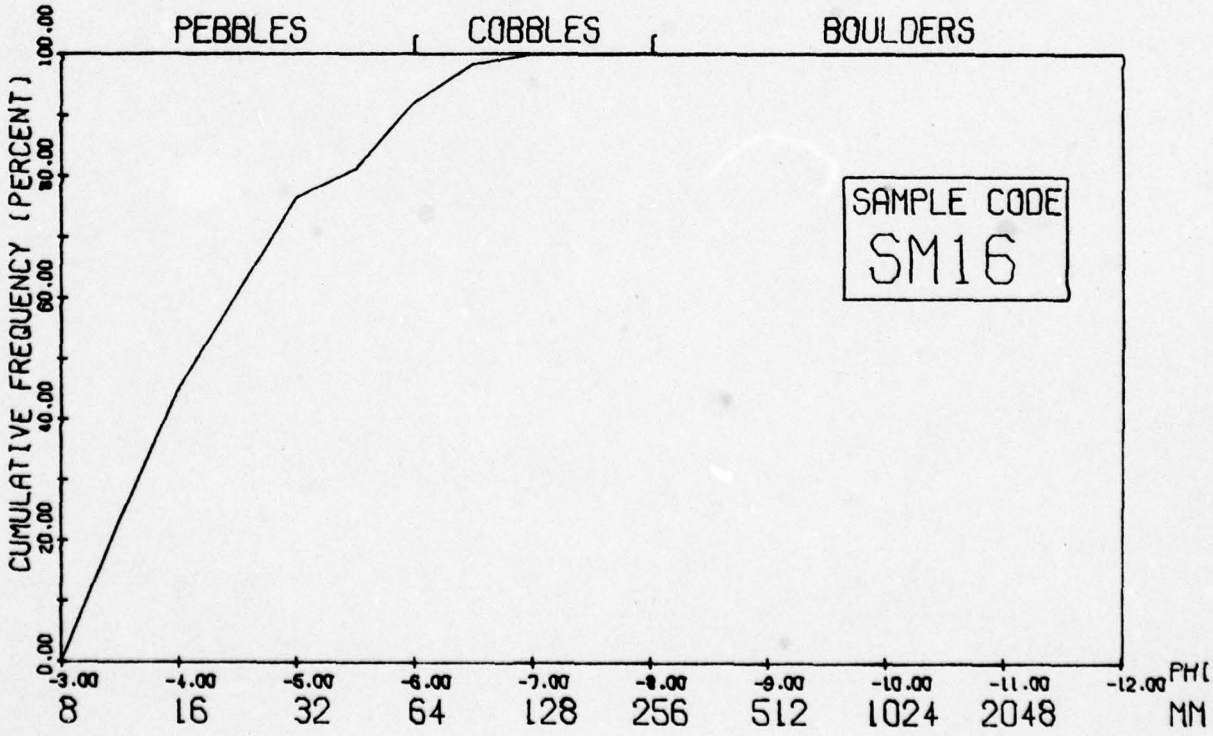
PEBBLES
COBBLES
BOULDERS
CUMULATIVE FREQUENCY (PERCENT)
0.00
20.00
40.00
60.00
80.00
100.00
SAMPLE CODE
SM16
-3.00
-4.00
-5.00
-6.00
-7.00
-8.00
-9.00
-10.00
-11.00
-12.00
PHI
8
16
32
64
128
256
512
1024
2048
MM

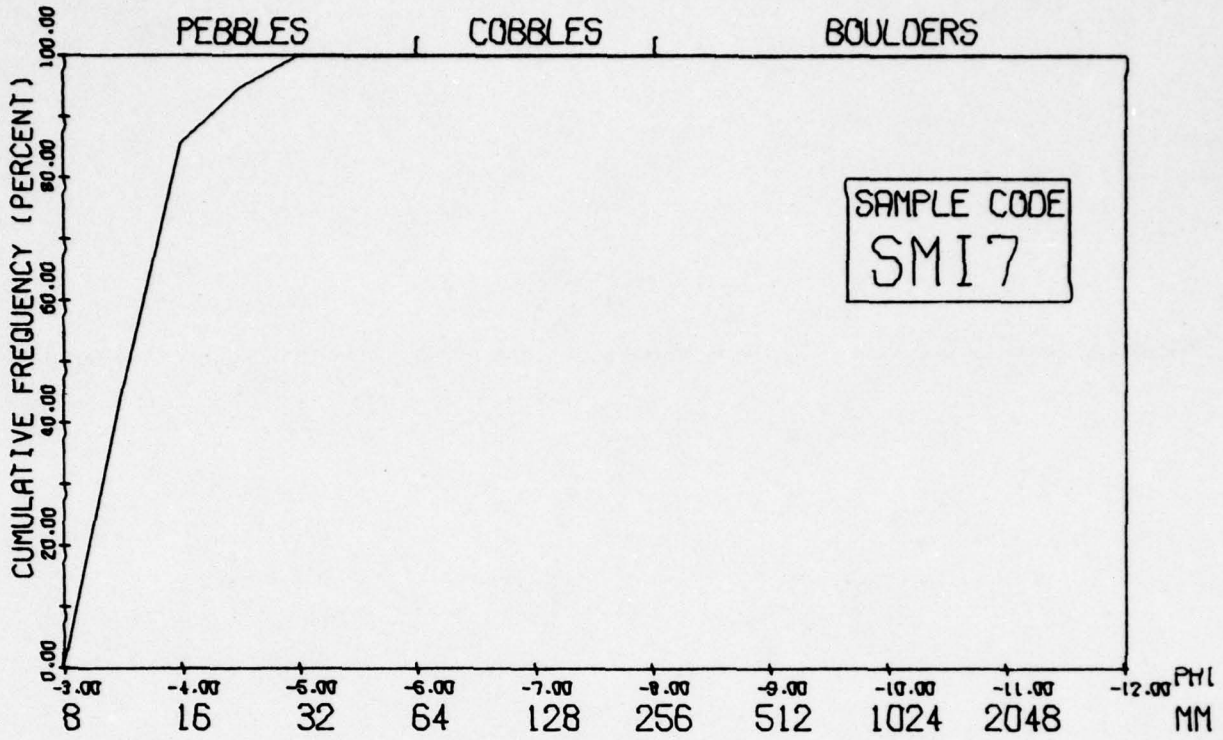
PEBBLES
COBBLES
BOULDERS
CUMULATIVE FREQUENCY (PERCENT)
100.00
80.00
60.00
40.00
20.00
0.00
SAMPLE CODE
SM17
-3.00
-4.00
-5.00
-6.00
-7.00
-8.00
-9.00
-10.00
-11.00
-12.00
PHI
8
16
32
64
128
256
512
1024
2048
MM

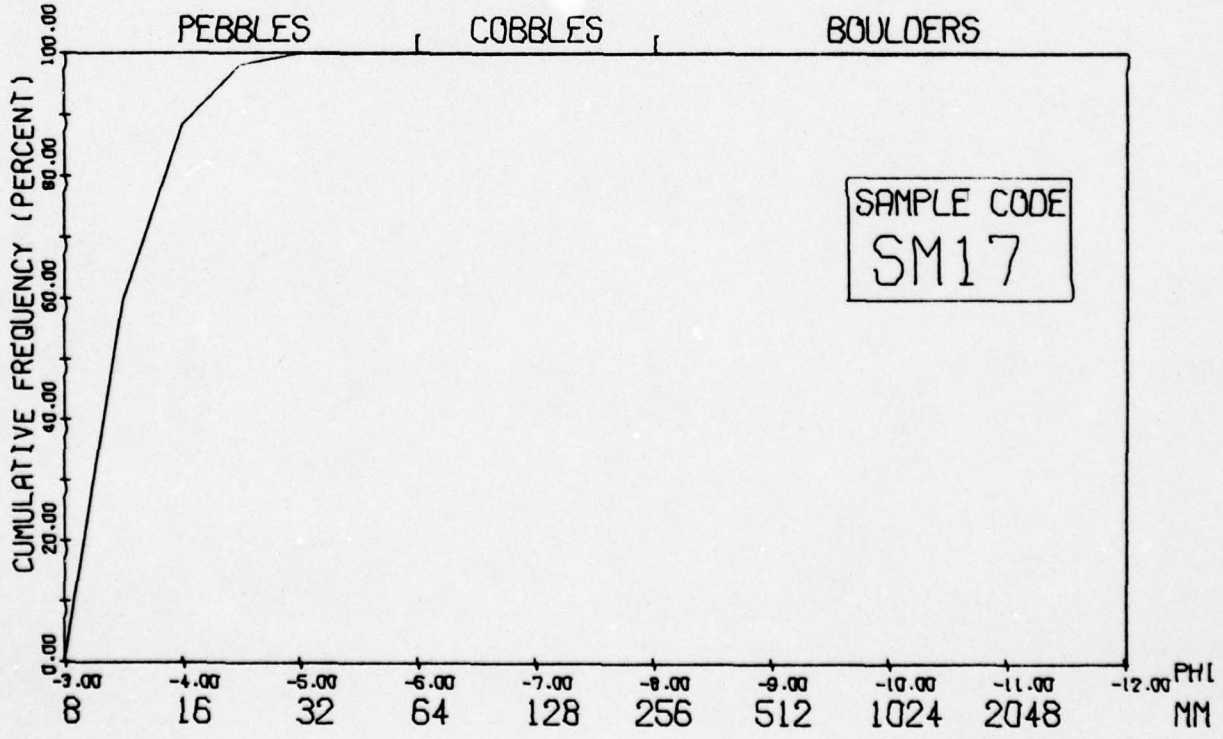
PEBBLES
COBBLES
BOULDERS
CUMULATIVE FREQUENCY (PERCENT)
100.00
80.00
60.00
40.00
20.00
0.00
SAMPLE CODE
SM17
-3.00
-4.00
-5.00
-6.00
-7.00
-8.00
-9.00
-10.00
-11.00
-12.00
PHI
8
16
32
64
128
256
512
1024
2048
MM

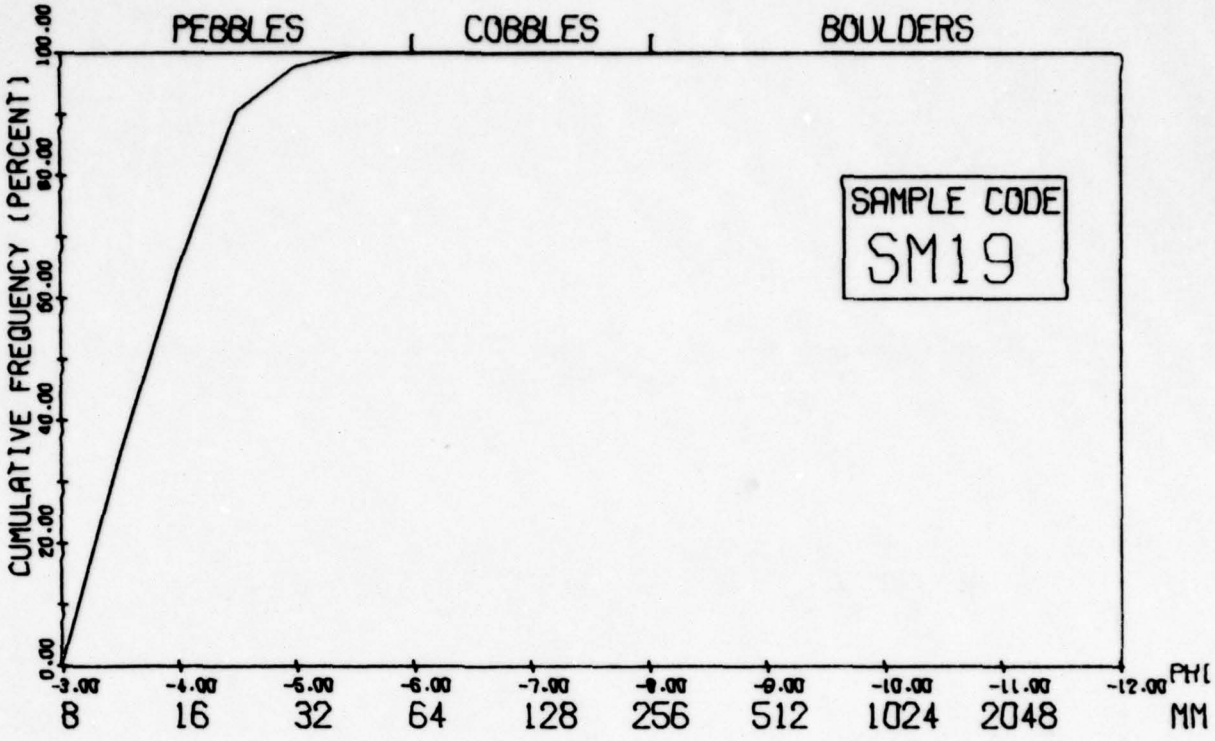
PEBBLES
COBBLES
BOULDERS
CUMULATIVE FREQUENCY (PERCENT)
100.00
80.00
60.00
40.00
20.00
0.00
SAMPLE CODE
SM19
-3.00
-4.00
-5.00
-6.00
-7.00
-8.00
-9.00
-10.00
-11.00
-12.00
PHI
8
16
32
64
128
256
512
1024
2048
MM

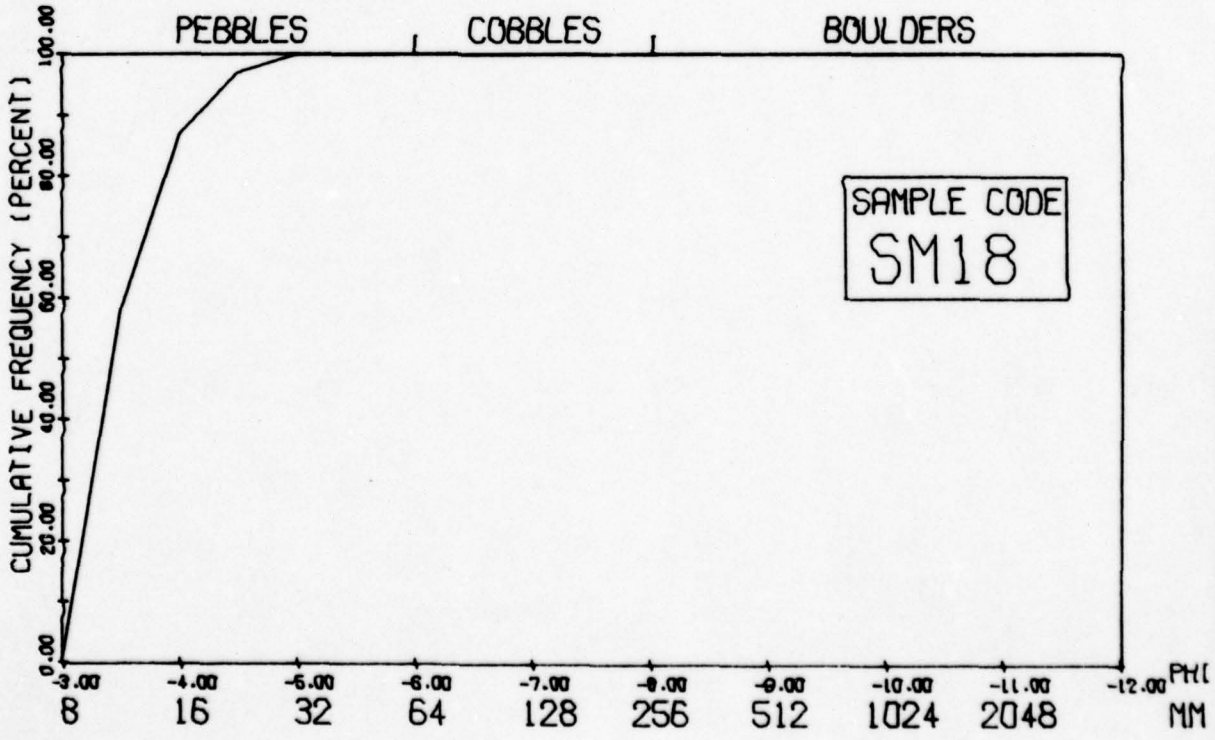
PEBBLES
COBBLES
BOULDERS
CUMULATIVE FREQUENCY (PERCENT)
100.00
80.00
60.00
40.00
20.00
0.00
SAMPLE CODE
SM18
-3.00
-4.00
-5.00
-6.00
-7.00
-8.00
-9.00
-10.00
-11.00
-12.00
PHI
8
16
32
64
128
256
512
1024
2048
MM

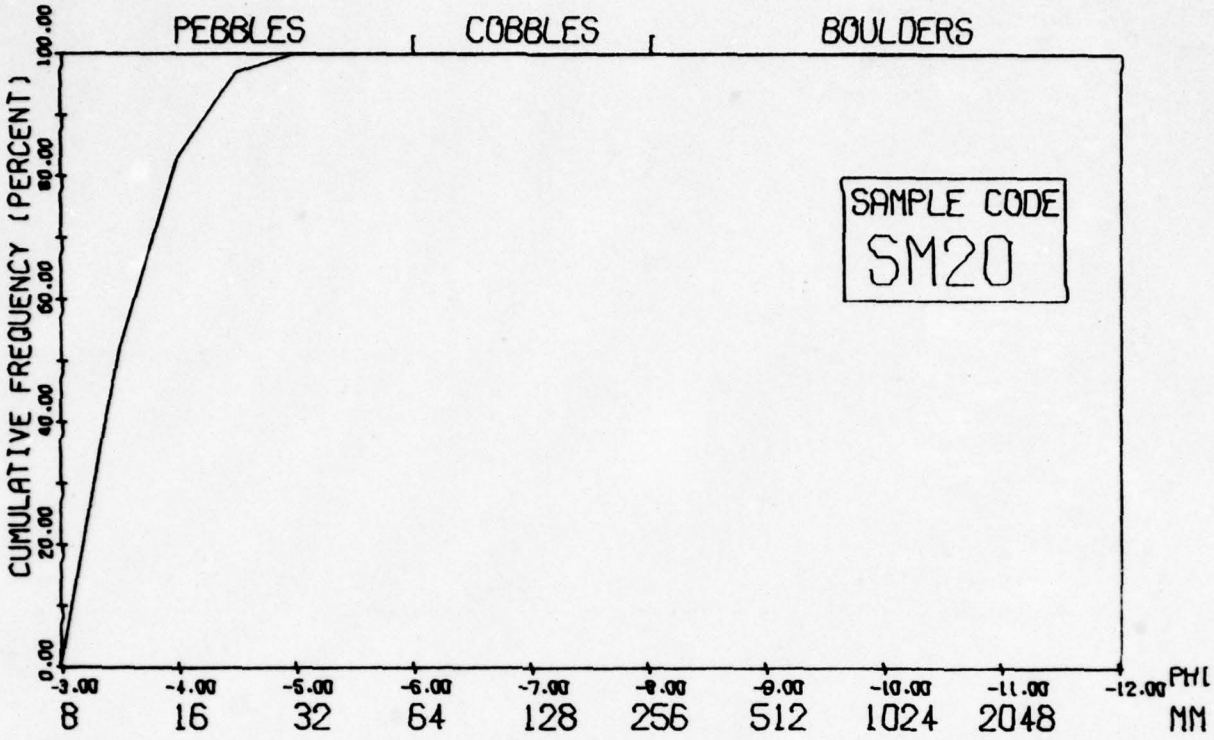
PEBBLES
COBBLES
BOULDERS
CUMULATIVE FREQUENCY (PERCENT)
0.00
20.00
40.00
60.00
80.00
100.00
SAMPLE CODE
SM20
-3.00
-4.00
-5.00
-6.00
-7.00
-8.00
-9.00
-10.00
-11.00
-12.00
PHI
8
16
32
64
128
256
512
1024
2048
MM

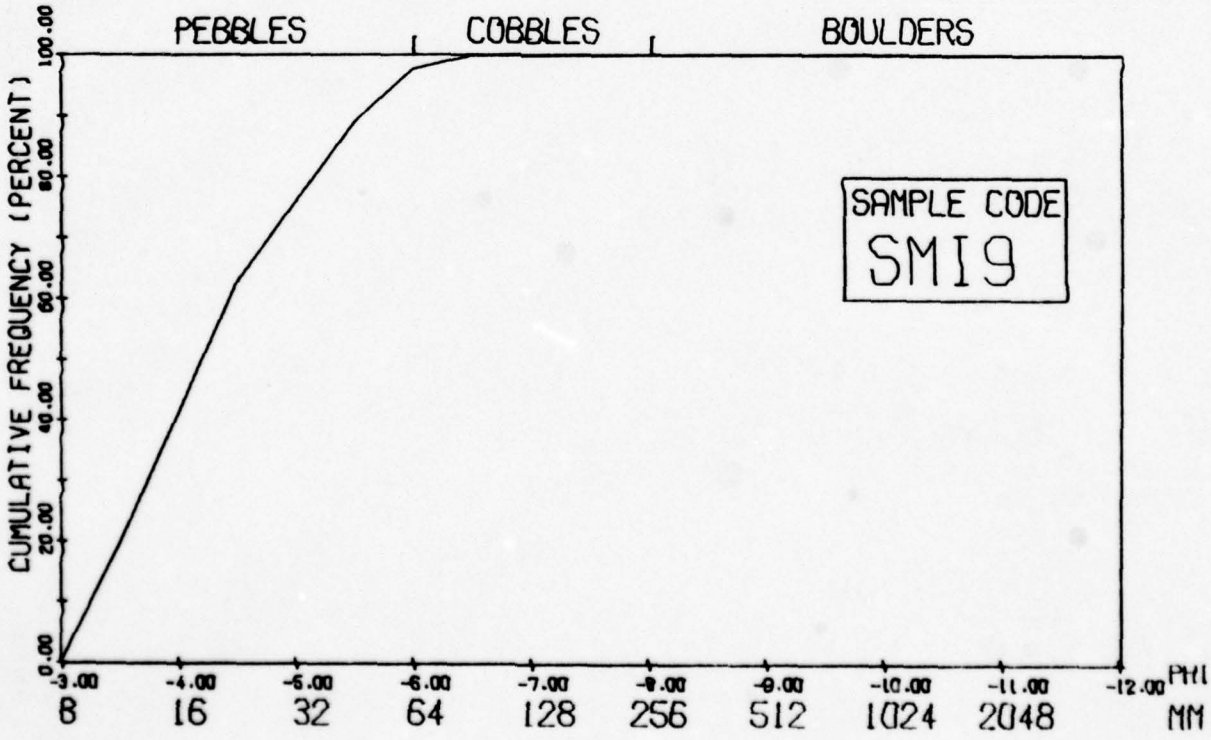
PEBBLES
COBBLES
BOULDERS
CUMULATIVE FREQUENCY (PERCENT)
0.00
20.00
40.00
60.00
80.00
100.00
SAMPLE CODE
SMI9
-3.00
-4.00
-5.00
-6.00
-7.00
-8.00
-9.00
-10.00
-11.00
-12.00
PHI
8
16
32
64
128
256
512
1024
2048
MM

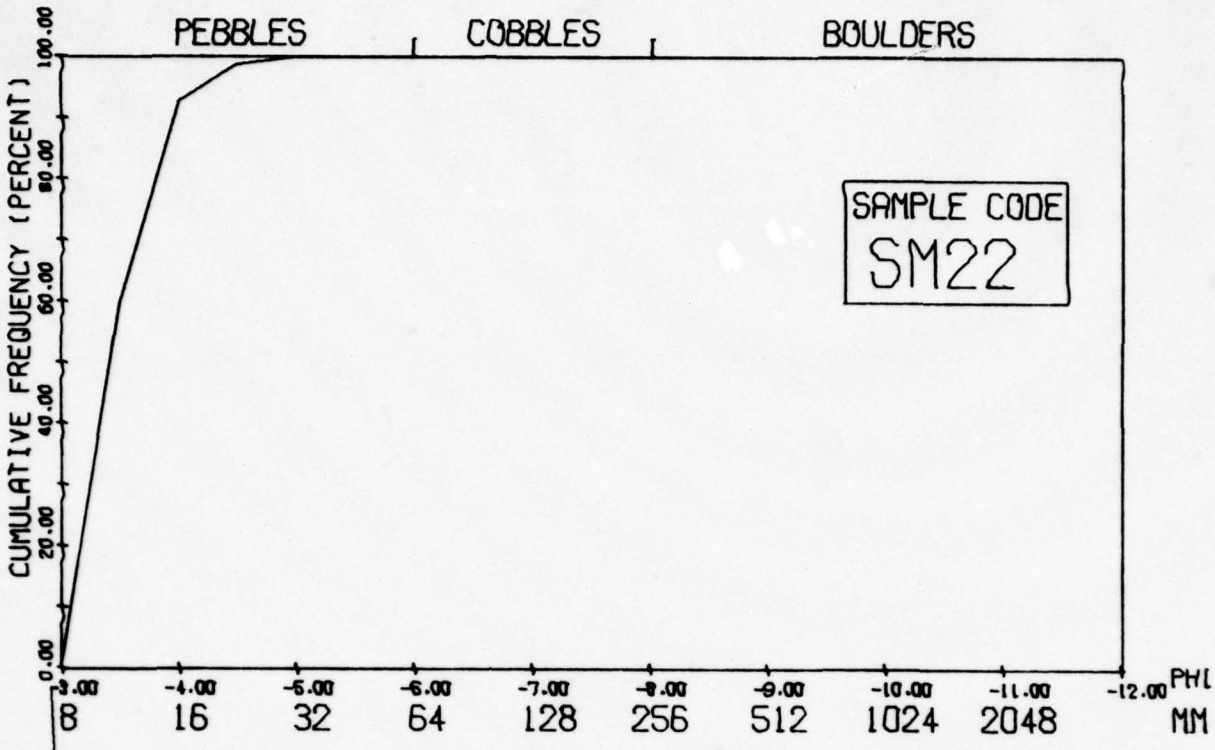
PEBBLES
COBBLES
BOULDERS
CUMULATIVE FREQUENCY (PERCENT)
100.00
80.00
60.00
40.00
20.00
0.00
SAMPLE CODE
SM22
-3.00
-4.00
-5.00
-6.00
-7.00
-8.00
-9.00
-10.00
-11.00
-12.00
PHI
8
16
32
64
128
256
512
1024
2048
MM

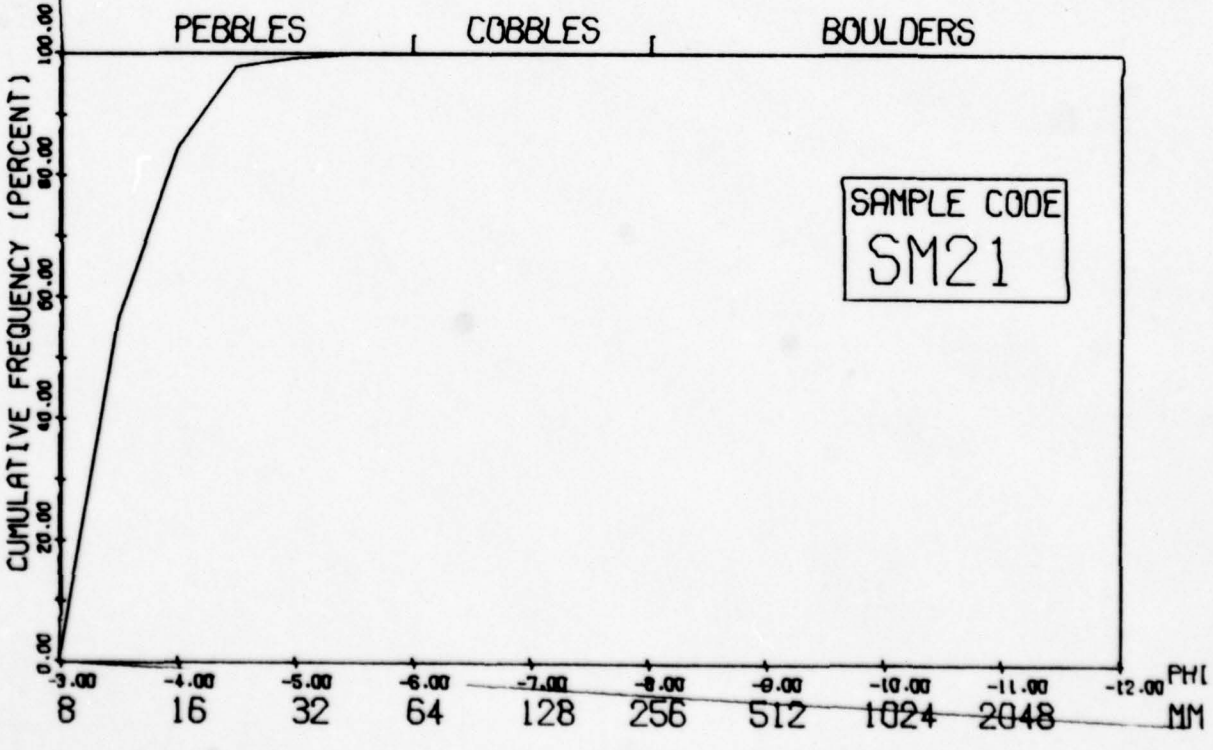
PEBBLES
COBBLES
BOULDERS
CUMULATIVE FREQUENCY (PERCENT)
100.00
80.00
60.00
40.00
20.00
0.00
SAMPLE CODE
SM21
-3.00
-4.00
-5.00
-6.00
-7.00
-8.00
-9.00
-10.00
-11.00
-12.00
PHI
8
16
32
64
128
256
512
1024
2048
MM

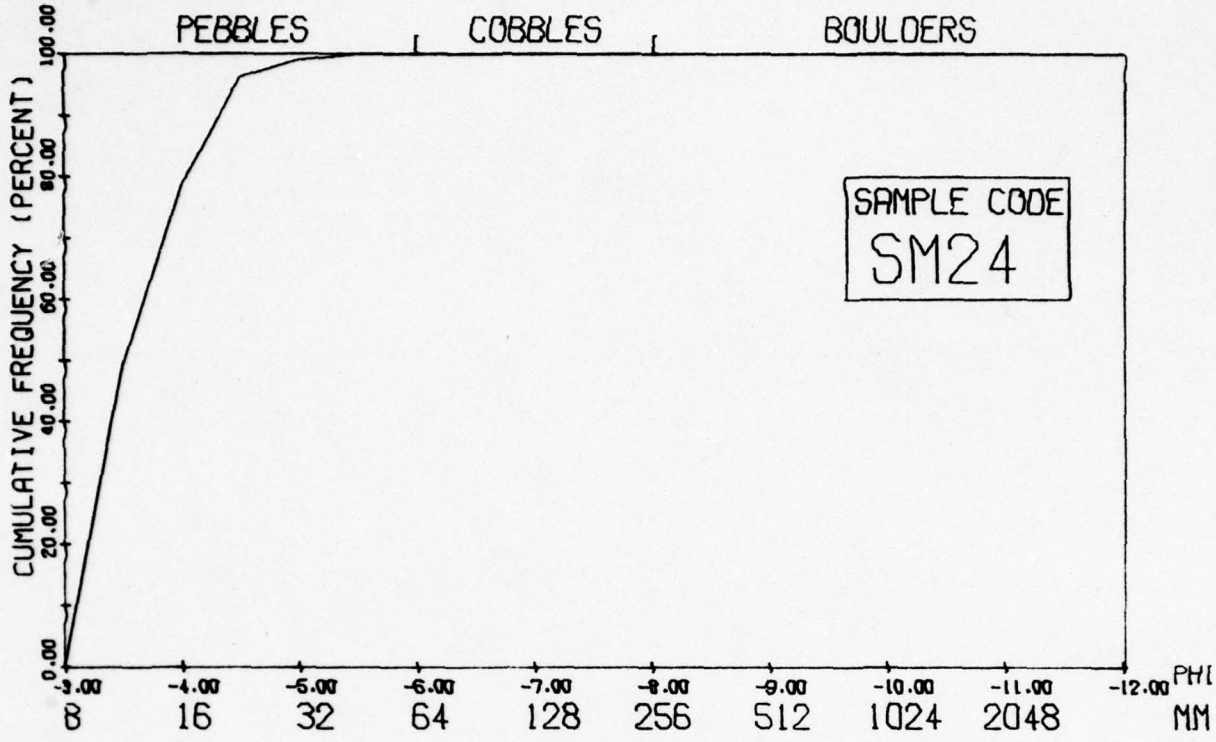
PEBBLES
COBBLES
BOULDERS
CUMULATIVE FREQUENCY (PERCENT)
100.00
80.00
60.00
40.00
20.00
0.00
SAMPLE CODE
SM24
-3.00
-4.00
-5.00
-6.00
-7.00
-8.00
-9.00
-10.00
-11.00
-12.00
PHI
8
16
32
64
128
256
512
1024
2048
MM

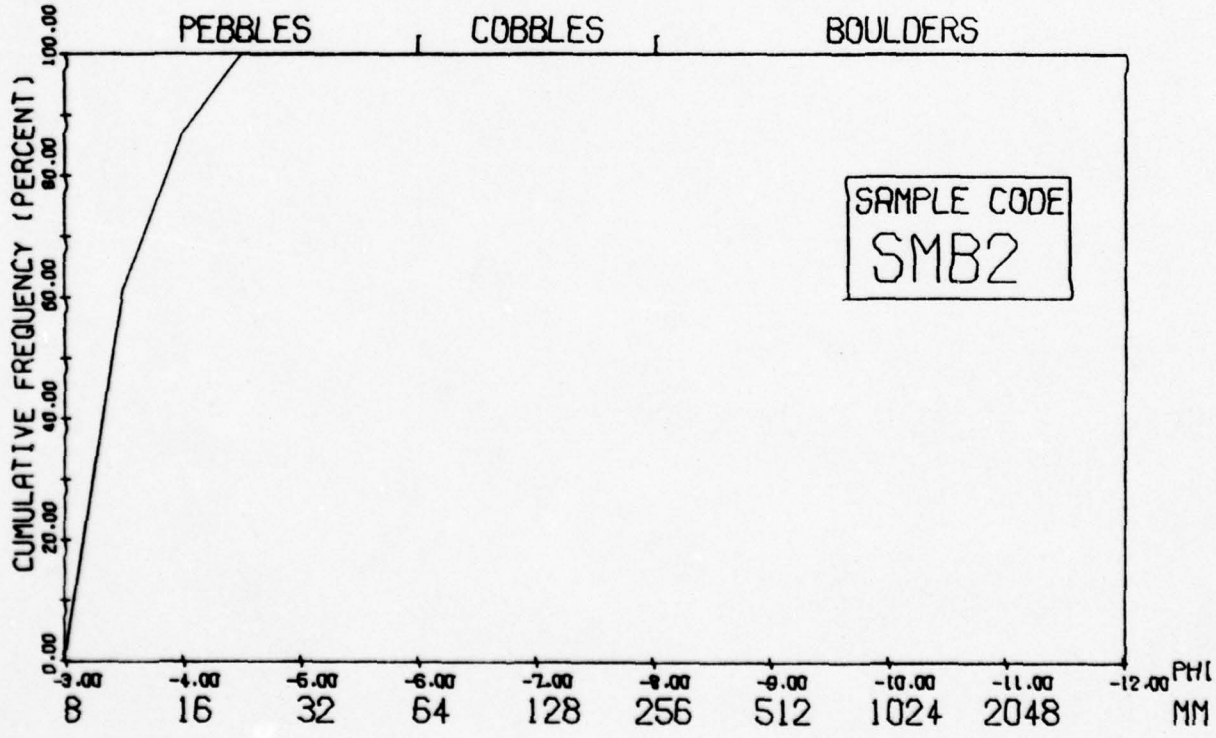
PEBBLES
COBBLES
BOULDERS
CUMULATIVE FREQUENCY (PERCENT)
100.00
80.00
60.00
40.00
20.00
0.00
SAMPLE CODE
SMB2
-3.00
-4.00
-5.00
-6.00
-7.00
-8.00
-9.00
-10.00
-11.00
-12.00
PHI
8
16
32
64
128
256
512
1024
2048
MM

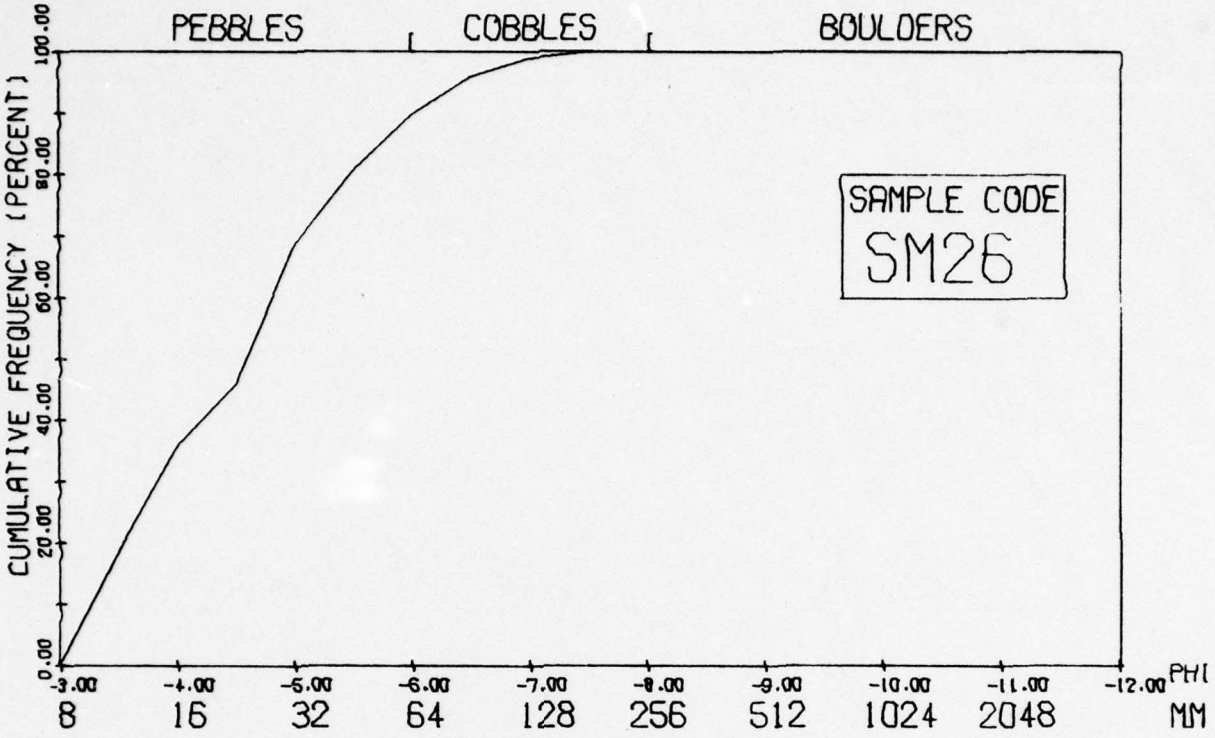
PEBBLES
COBBLES
BOULDERS
CUMULATIVE FREQUENCY (PERCENT)
100.00
80.00
60.00
40.00
20.00
0.00
SAMPLE CODE
SM26
-3.00
-4.00
-5.00
-6.00
-7.00
-8.00
-9.00
-10.00
-11.00
-12.00
PHI
8
16
32
64
128
256
512
1024
2048
MM

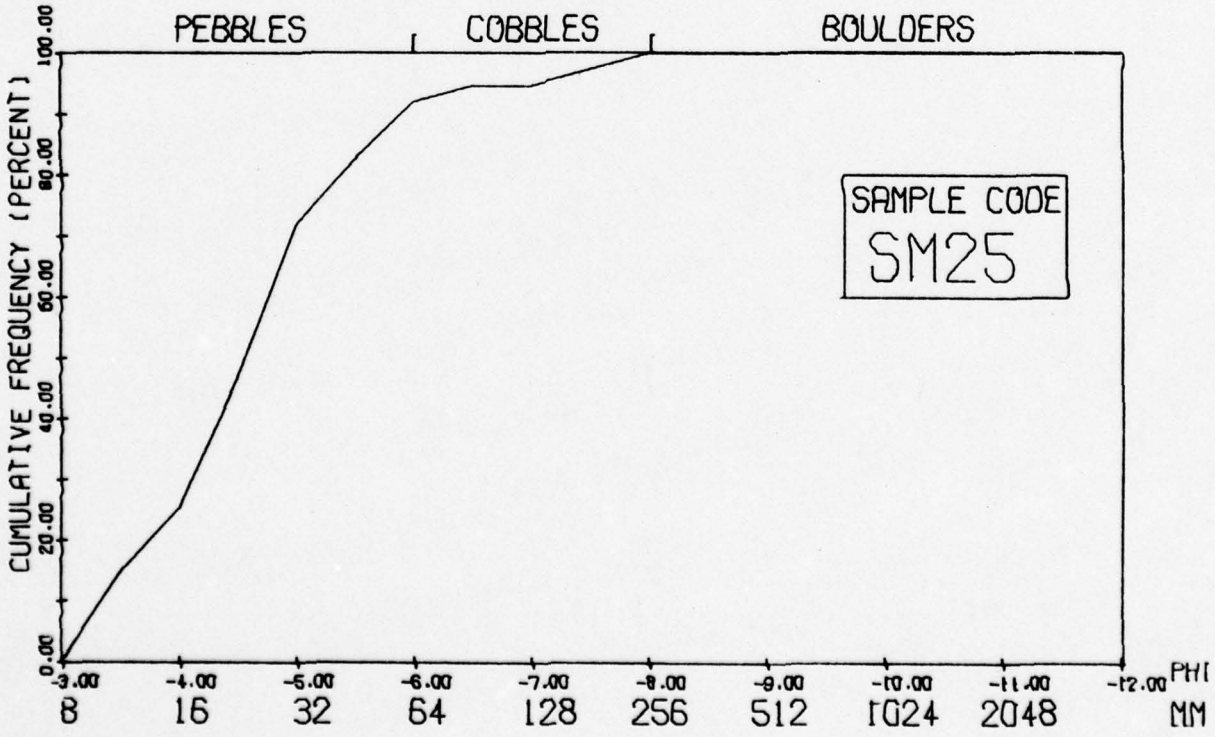
PEBBLES
COBBLES
BOULDERS
CUMULATIVE FREQUENCY (PERCENT)
100.00
80.00
60.00
40.00
20.00
0.00
SAMPLE CODE
SM25
-3.00
-4.00
-5.00
-6.00
-7.00
-8.00
-9.00
-10.00
-11.00
-12.00
PHI
8
16
32
64
128
256
512
1024
2048
MM

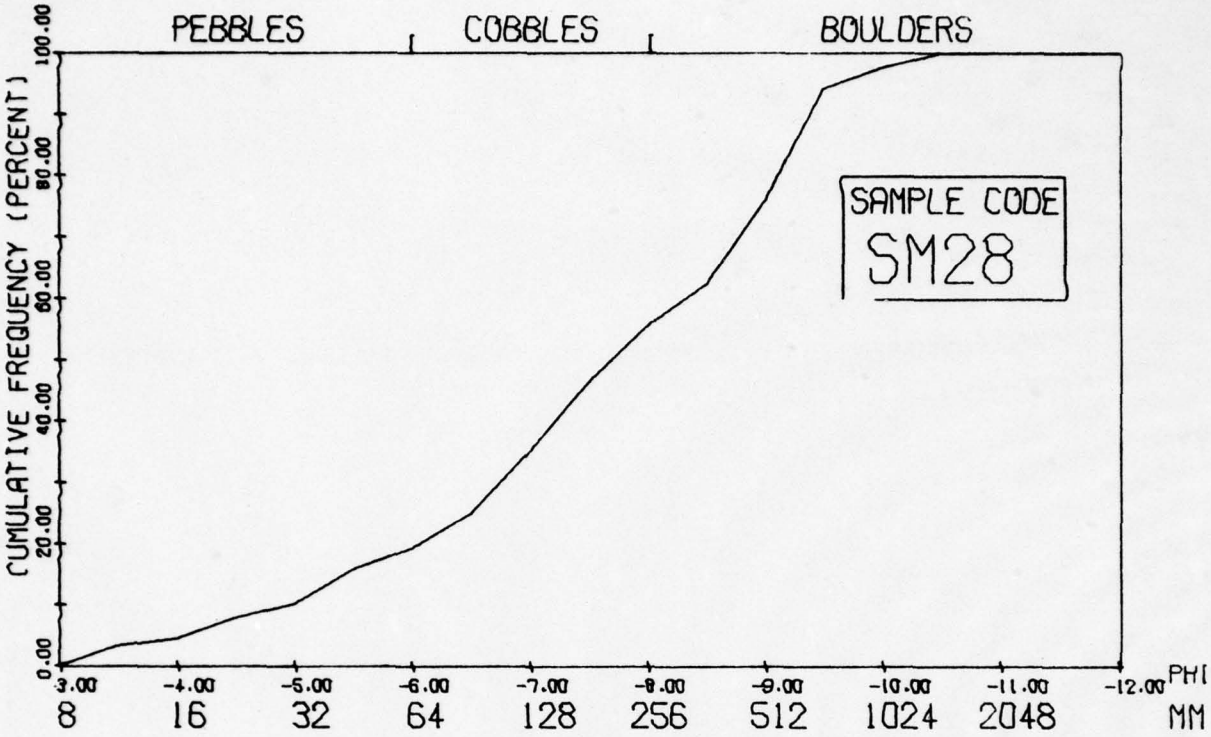
PEBBLES
COBBLES
BOULDERS
CUMULATIVE FREQUENCY (PERCENT)
0.00
20.00
40.00
60.00
80.00
100.00
SAMPLE CODE
SM28
-3.00
-4.00
-5.00
-6.00
-7.00
-8.00
-9.00
-10.00
-11.00
-12.00
PHI
8
16
32
64
128
256
512
1024
2048
MM

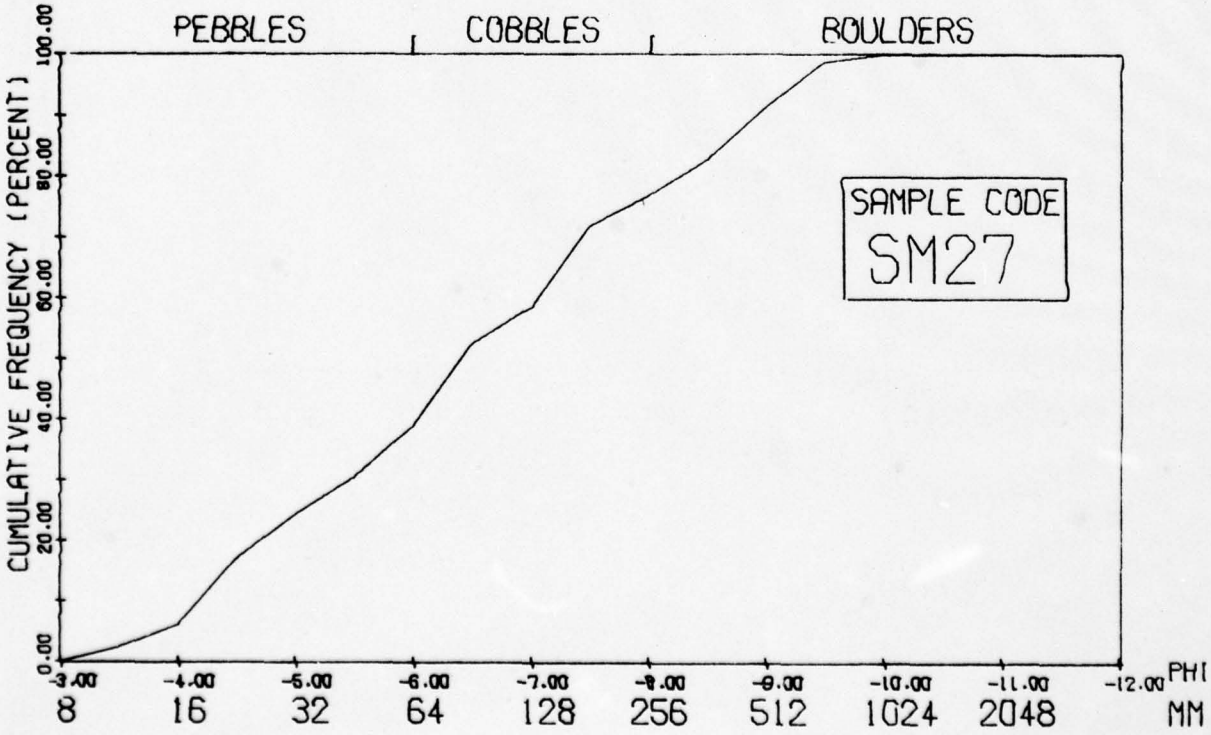
PEBBLES
COBBLES
BOULDERS
CUMULATIVE FREQUENCY (PERCENT)
0.00
20.00
40.00
60.00
80.00
100.00
SAMPLE CODE
SM27
-3.00
-4.00
-5.00
-6.00
-7.00
-8.00
-9.00
-10.00
-11.00
-12.00
PHI
8
16
32
64
128
256
512
1024
2048
MM

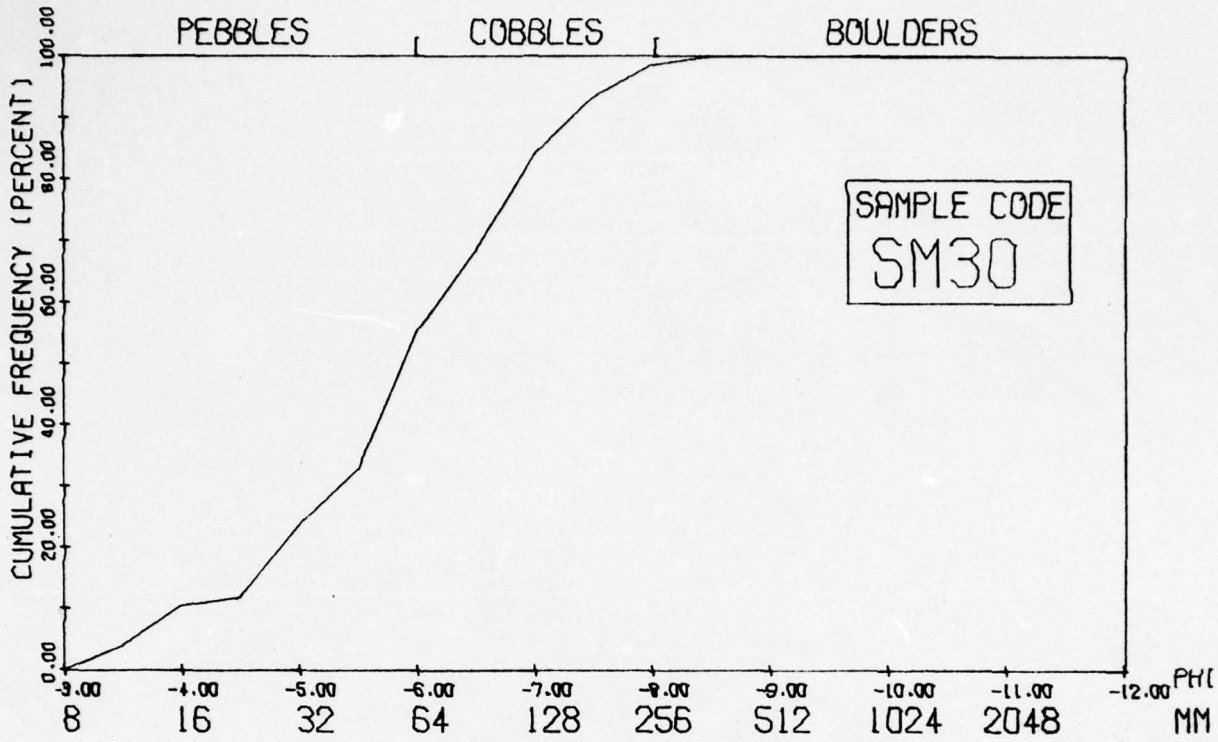
PEBBLES
COBBLES
BOULDERS
CUMULATIVE FREQUENCY (PERCENT)
100.00
80.00
60.00
40.00
20.00
0.00
SAMPLE CODE
SM30
-3.00
-4.00
-5.00
-6.00
-7.00
-8.00
-9.00
-10.00
-11.00
-12.00
PHI
8
16
32
64
128
256
512
1024
2048
MM

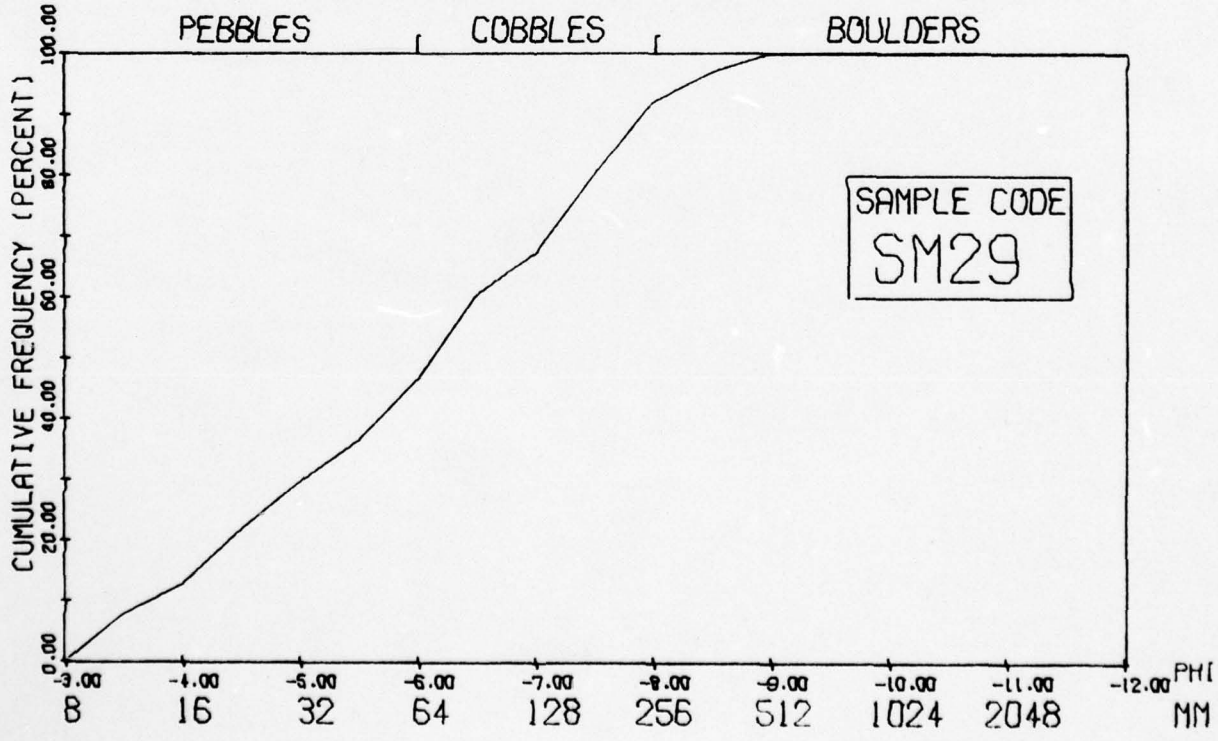
PEBBLES
COBBLES
BOULDERS
CUMULATIVE FREQUENCY (PERCENT)
100.00
80.00
60.00
40.00
20.00
0.00
SAMPLE CODE
SM29
-3.00
-4.00
-5.00
-6.00
-7.00
-8.00
-9.00
-10.00
-11.00
-12.00
PHI
8
16
32
64
128
256
512
1024
2048
MM

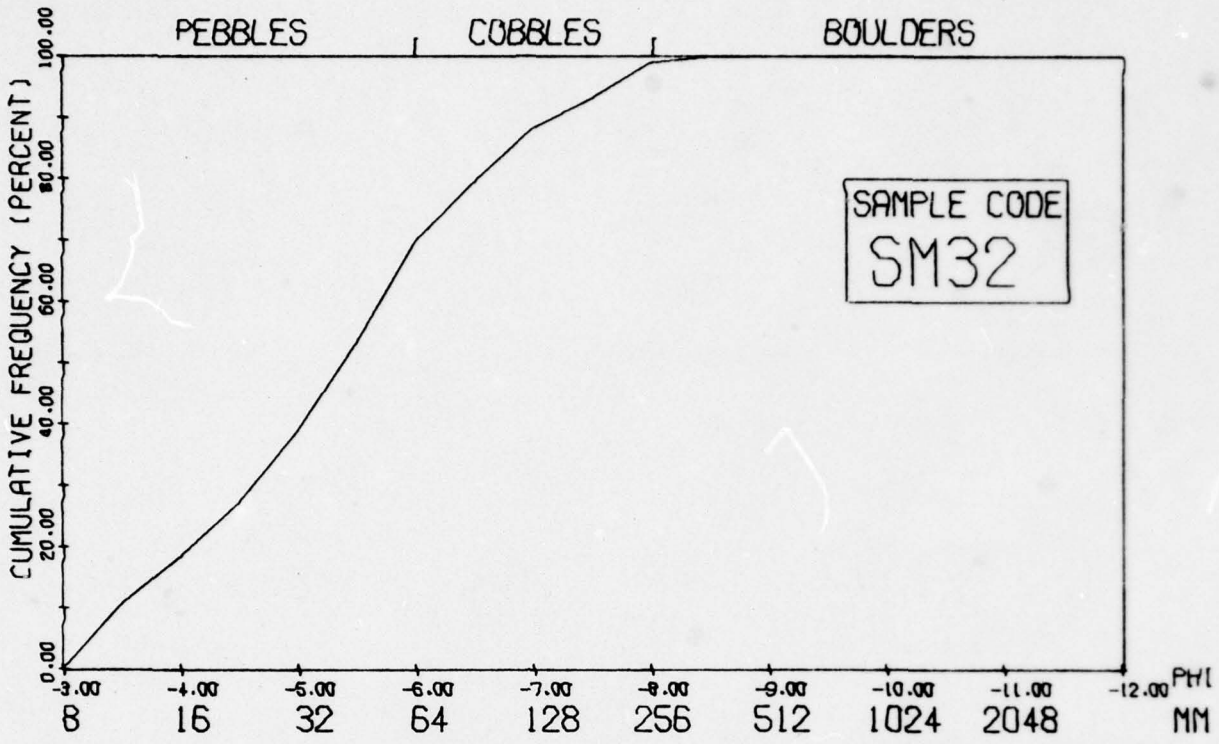
PEBBLES
COBBLES
BOULDERS
CUMULATIVE FREQUENCY (PERCENT)
0.00
20.00
40.00
60.00
80.00
100.00
SAMPLE CODE
SM32
-3.00
-4.00
-5.00
-6.00
-7.00
-8.00
-9.00
-10.00
-11.00
-12.00
PHI
8
16
32
64
128
256
512
1024
2048
MM

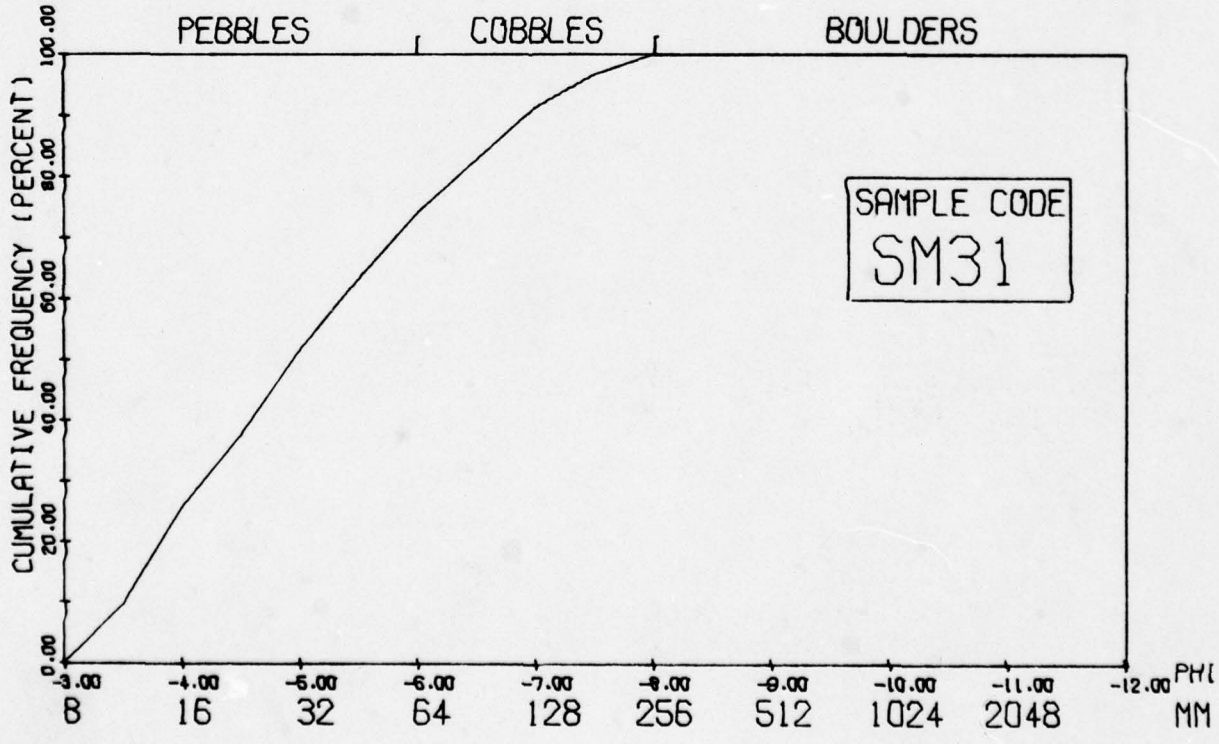
PEBBLES
COBBLES
BOULDERS
CUMULATIVE FREQUENCY (PERCENT)
0.00
20.00
40.00
60.00
80.00
100.00
SAMPLE CODE
SM31
-3.00
-4.00
-5.00
-6.00
-7.00
-8.00
-9.00
-10.00
-11.00
-12.00
PHI
8
16
32
64
128
256
512
1024
2048
MM

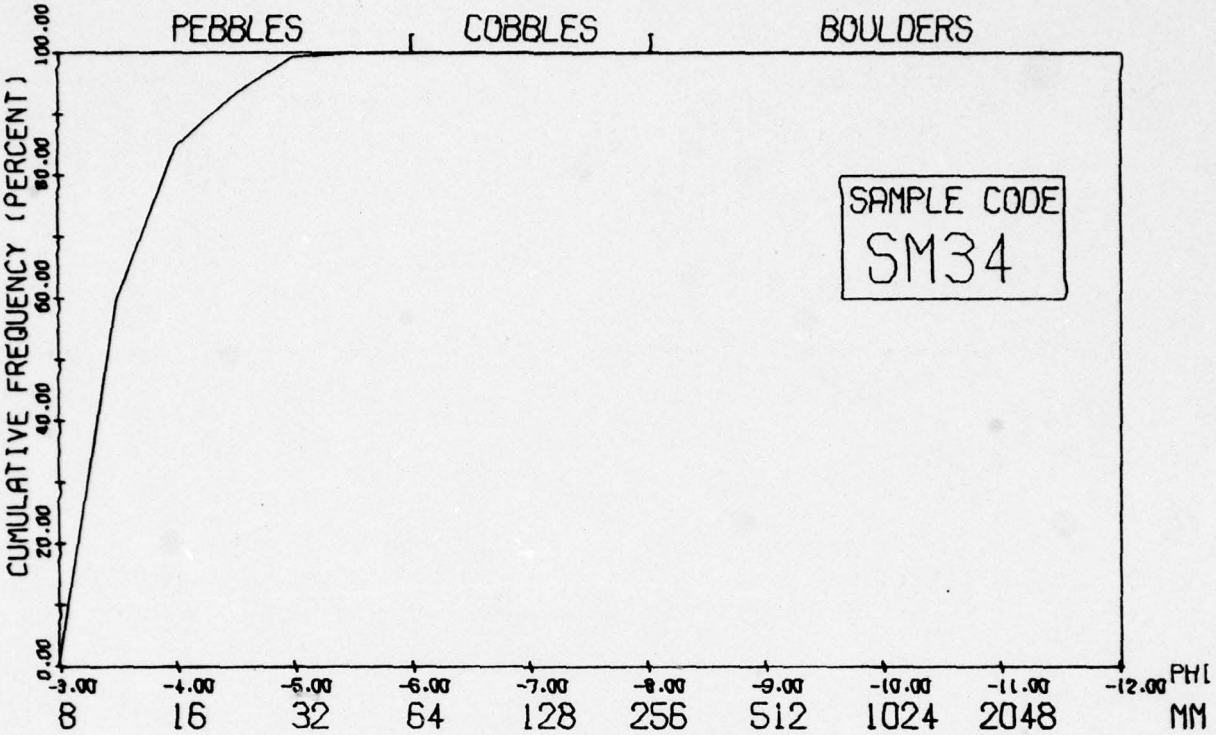
PEBBLES
COBBLES
BOULDERS
CUMULATIVE FREQUENCY (PERCENT)
100.00
80.00
60.00
40.00
20.00
0.00
SAMPLE CODE
SM34
-3.00
-4.00
-5.00
-6.00
-7.00
-8.00
-9.00
-10.00
-11.00
-12.00
PHI
8
16
32
64
128
256
512
1024
2048
MM

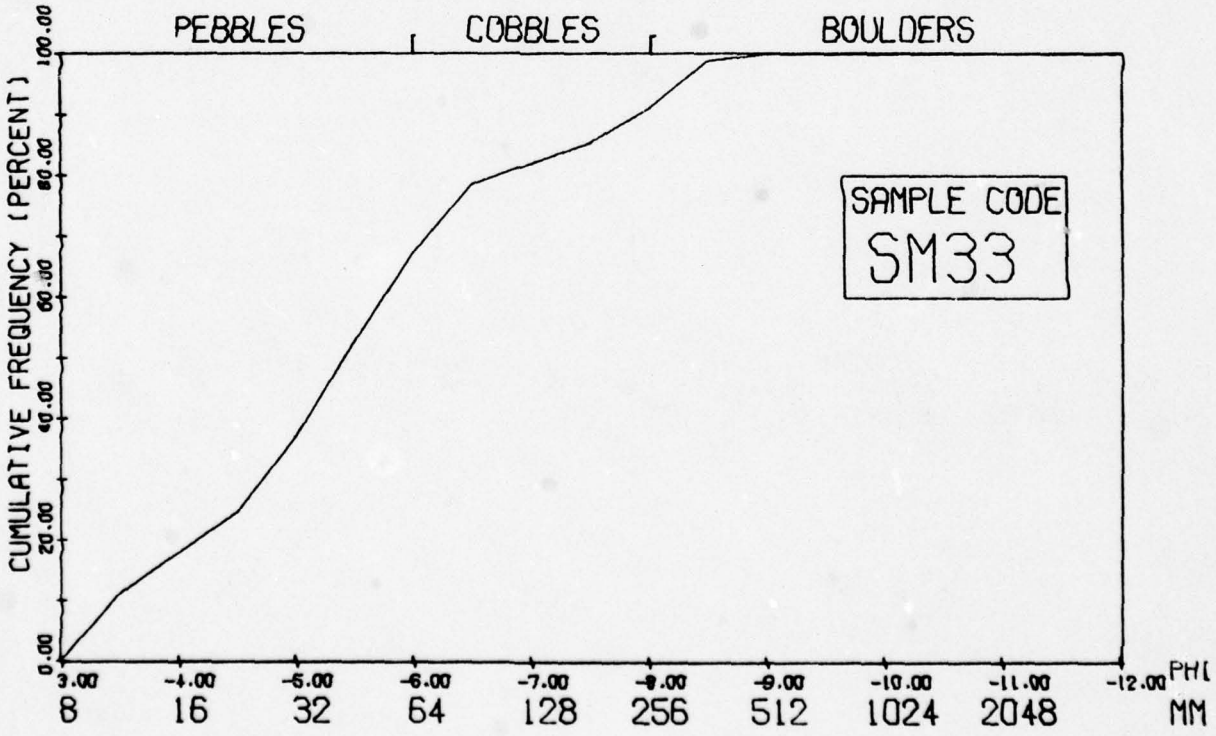
PEBBLES
COBBLES
BOULDERS
CUMULATIVE FREQUENCY (PERCENT)
100.00
80.00
60.00
40.00
20.00
0.00
SAMPLE CODE
SM33
-3.00
-4.00
-5.00
-6.00
-7.00
-8.00
-9.00
-10.00
-11.00
-12.00
PHI
8
16
32
64
128
256
512
1024
2048
MM

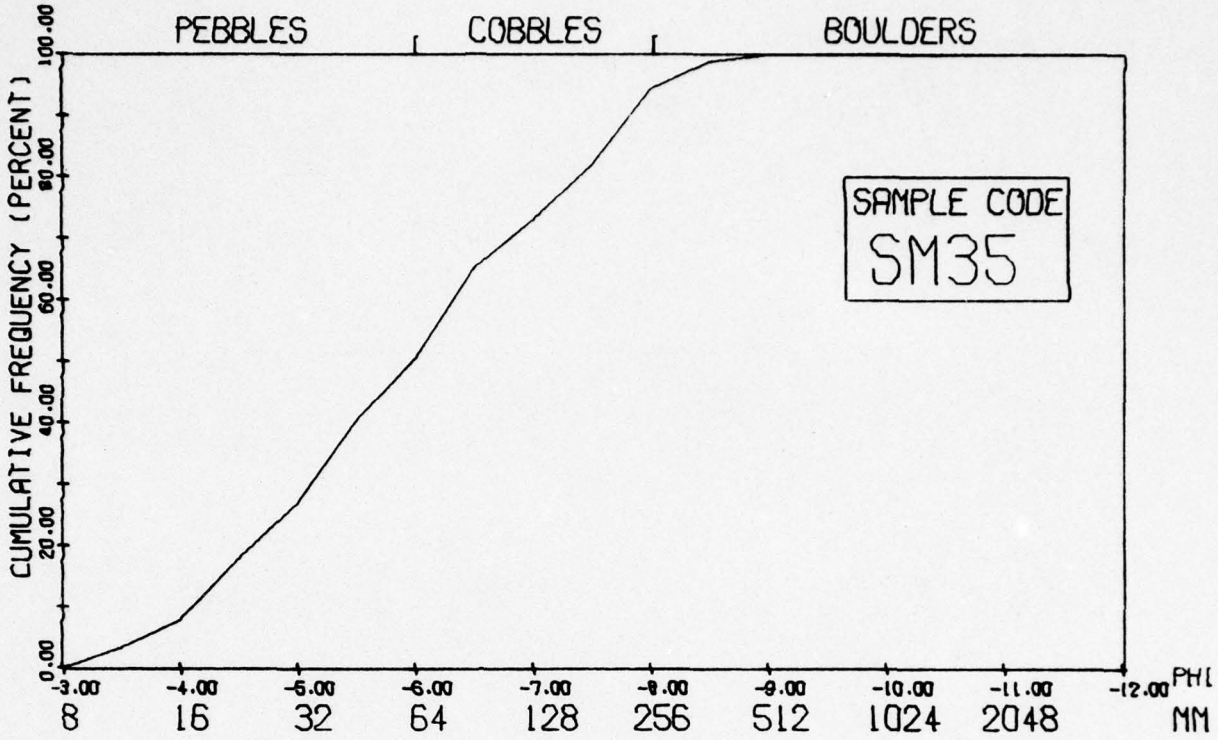
PEBBLES
COBBLES
BOULDERS
CUMULATIVE FREQUENCY (PERCENT)
100.00
80.00
60.00
40.00
20.00
0.00
SAMPLE CODE
SM35
-3.00
-4.00
-5.00
-6.00
-7.00
-8.00
-9.00
-10.00
-11.00
-12.00
PHI
8
16
32
64
128
256
512
1024
2048
MM

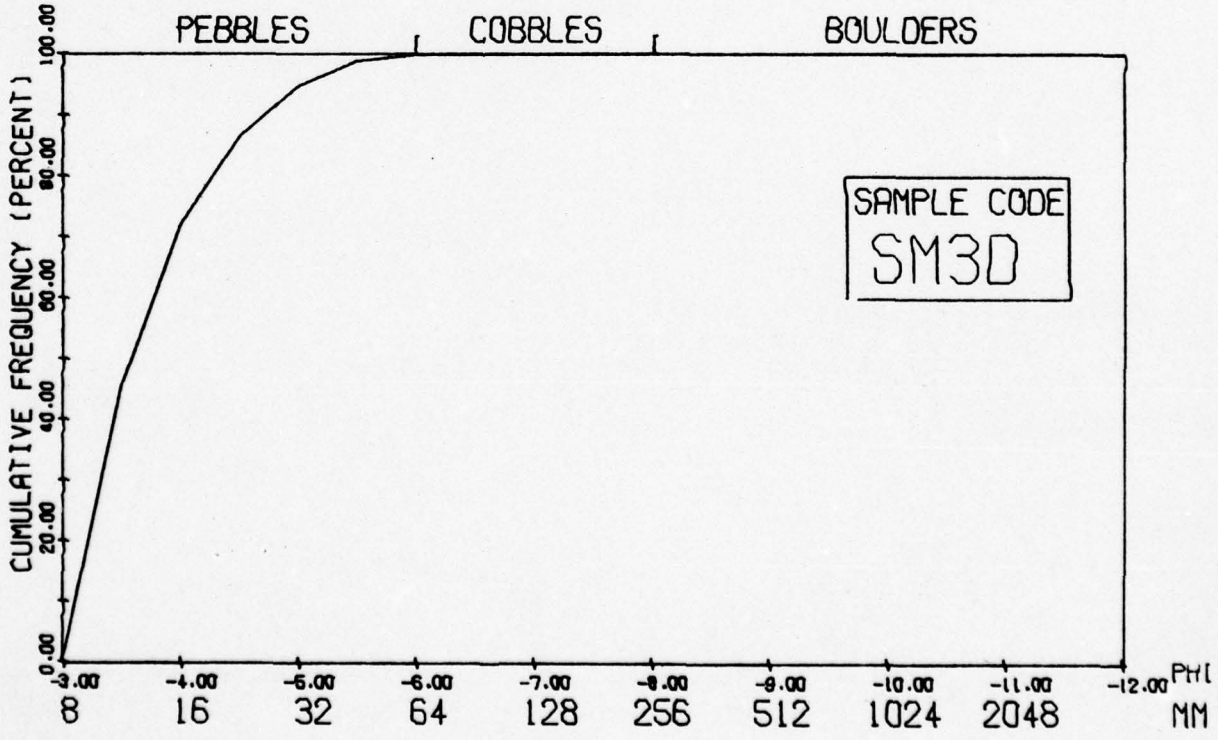
PEBBLES
COBBLES
BOULDERS
CUMULATIVE FREQUENCY (PERCENT)
100.00
80.00
60.00
40.00
20.00
0.00
SAMPLE CODE
SM3D
-3.00
-4.00
-5.00
-6.00
-7.00
-8.00
-9.00
-10.00
-11.00
-12.00
PHI
8
16
32
64
128
256
512
1024
2048
MM

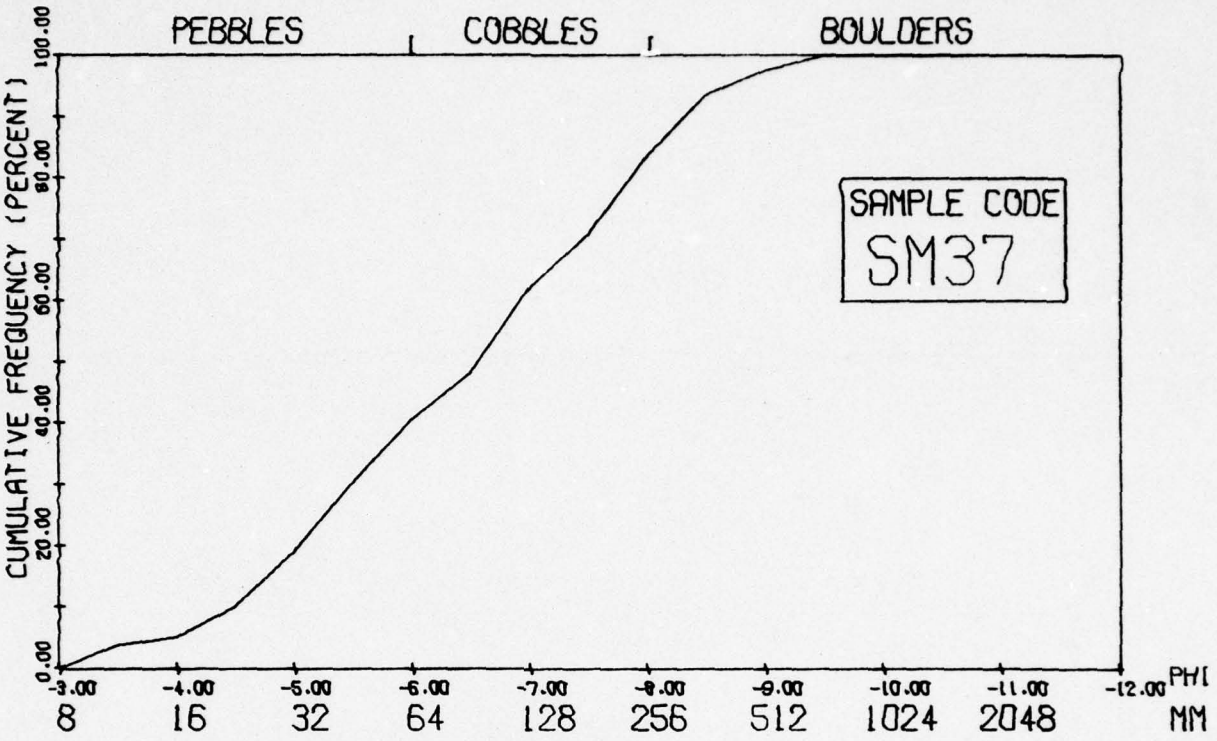
PEBBLES
COBBLES
BOULDERS
CUMULATIVE FREQUENCY (PERCENT)
0.00
20.00
40.00
60.00
80.00
100.00
SAMPLE CODE
SM37
-3.00
-4.00
-5.00
-6.00
-7.00
-8.00
-9.00
-10.00
-11.00
-12.00
PHI
8
16
32
64
128
256
512
1024
2048
MM

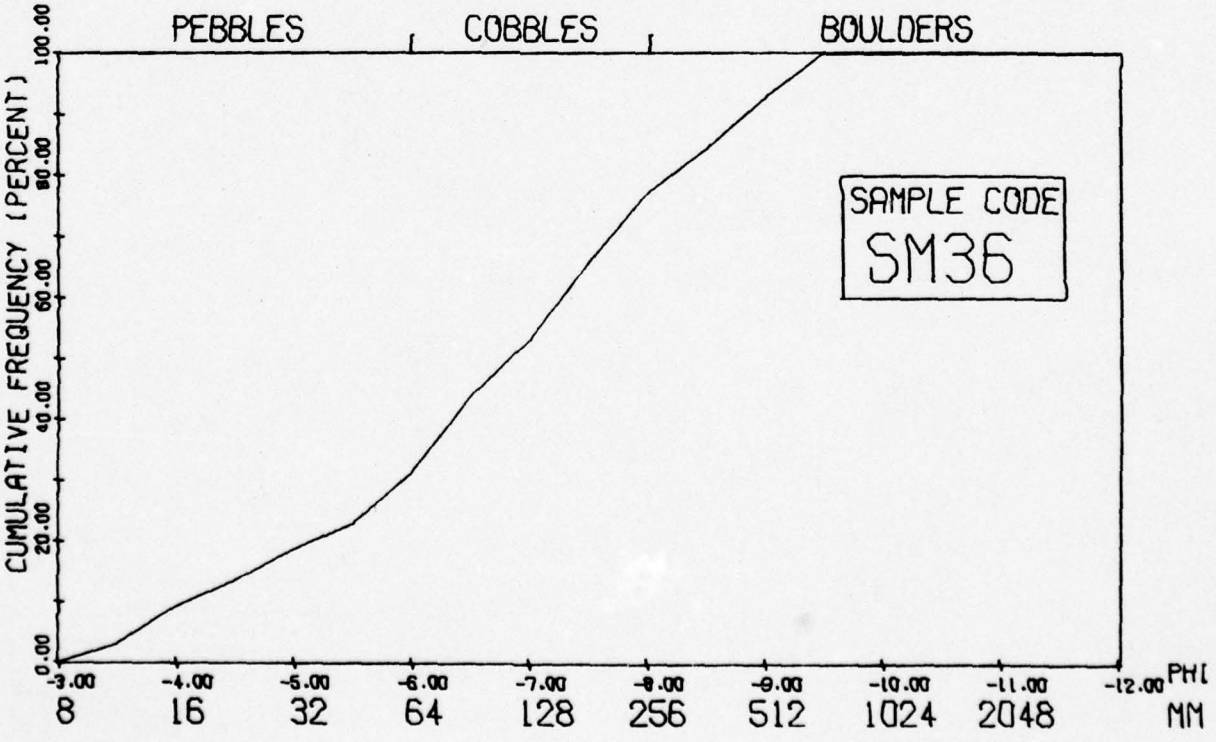
PEBBLES
COBBLES
BOULDERS
CUMULATIVE FREQUENCY (PERCENT)
0.00
20.00
40.00
60.00
80.00
100.00
SAMPLE CODE
SM36
-3.00
-4.00
-5.00
-6.00
-7.00
-8.00
-9.00
-10.00
-11.00
-12.00
PHI
8
16
32
64
128
256
512
1024
2048
MM

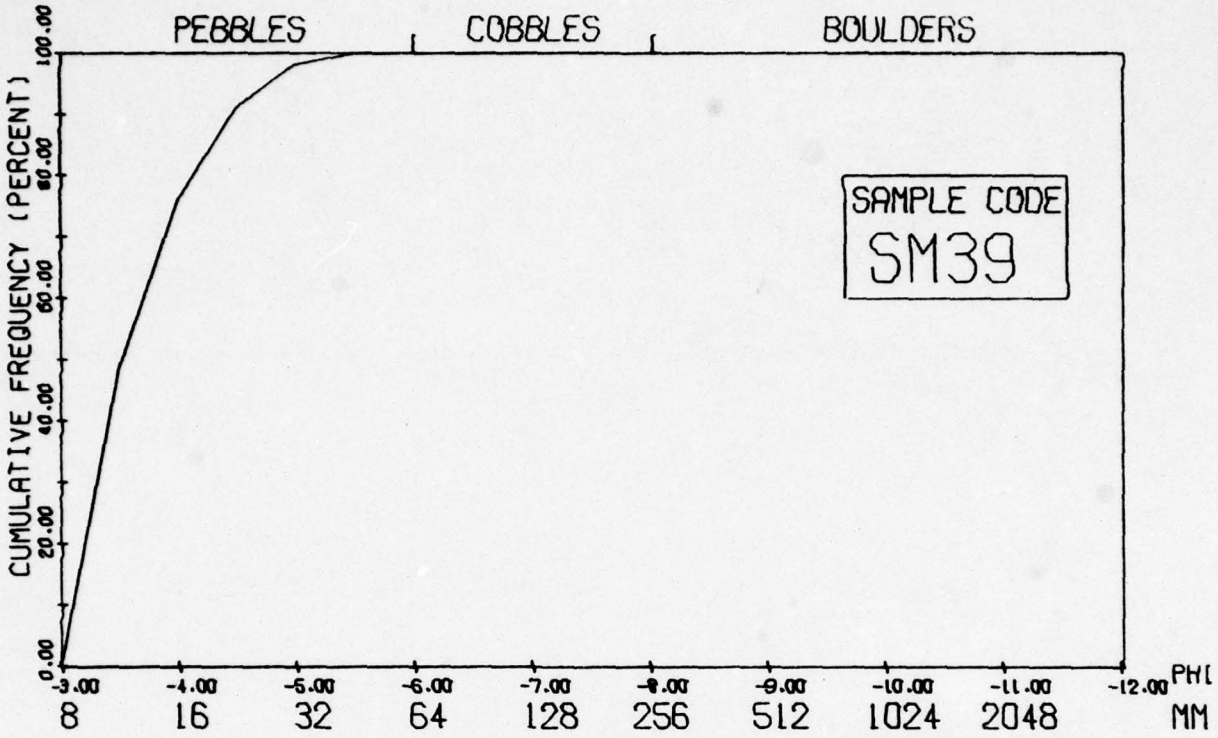
PEBBLES
COBBLES
BOULDERS
CUMULATIVE FREQUENCY (PERCENT)
0.00
20.00
40.00
60.00
80.00
100.00
SAMPLE CODE
SM39
-3.00
-4.00
-5.00
-6.00
-7.00
-8.00
-9.00
-10.00
-11.00
-12.00
PHI
8
16
32
64
128
256
512
1024
2048
MM

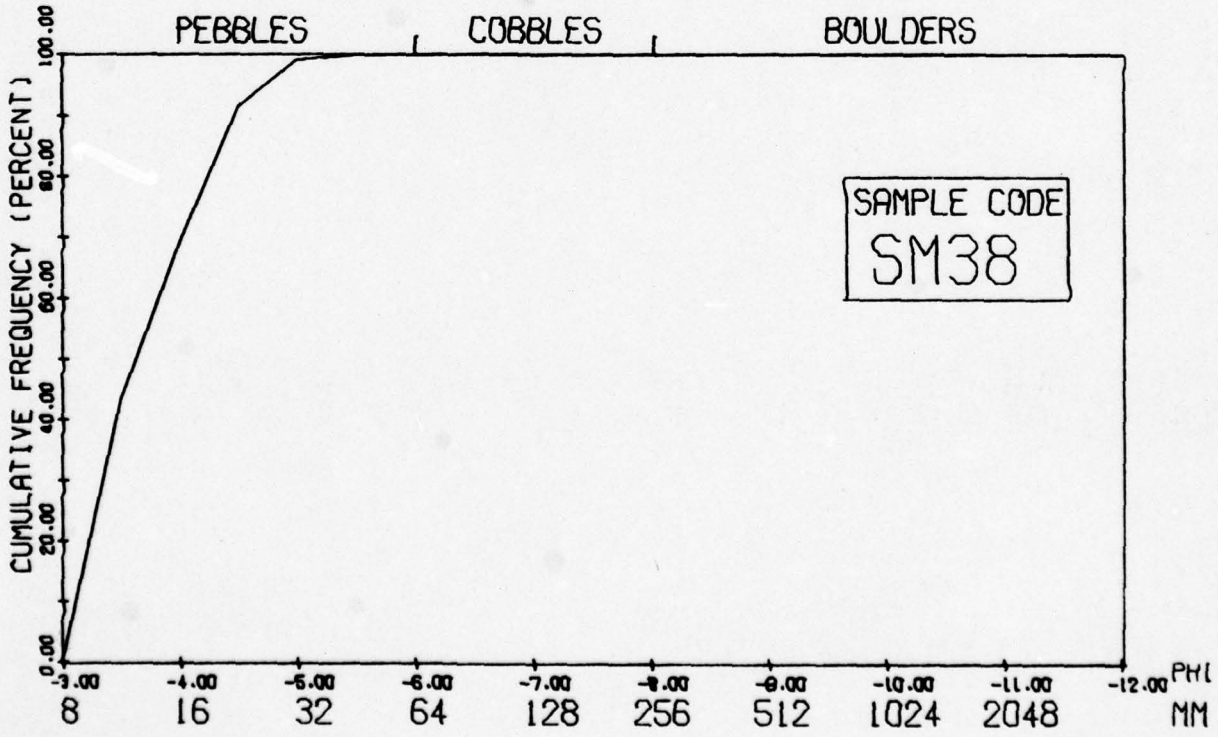
PEBBLES
COBBLES
BOULDERS
CUMULATIVE FREQUENCY (PERCENT)
0.00
20.00
40.00
60.00
80.00
100.00
SAMPLE CODE
SM38
-3.00
-4.00
-5.00
-6.00
-7.00
-8.00
-9.00
-10.00
-11.00
-12.00
PHI
8
16
32
64
128
256
512
1024
2048
MM

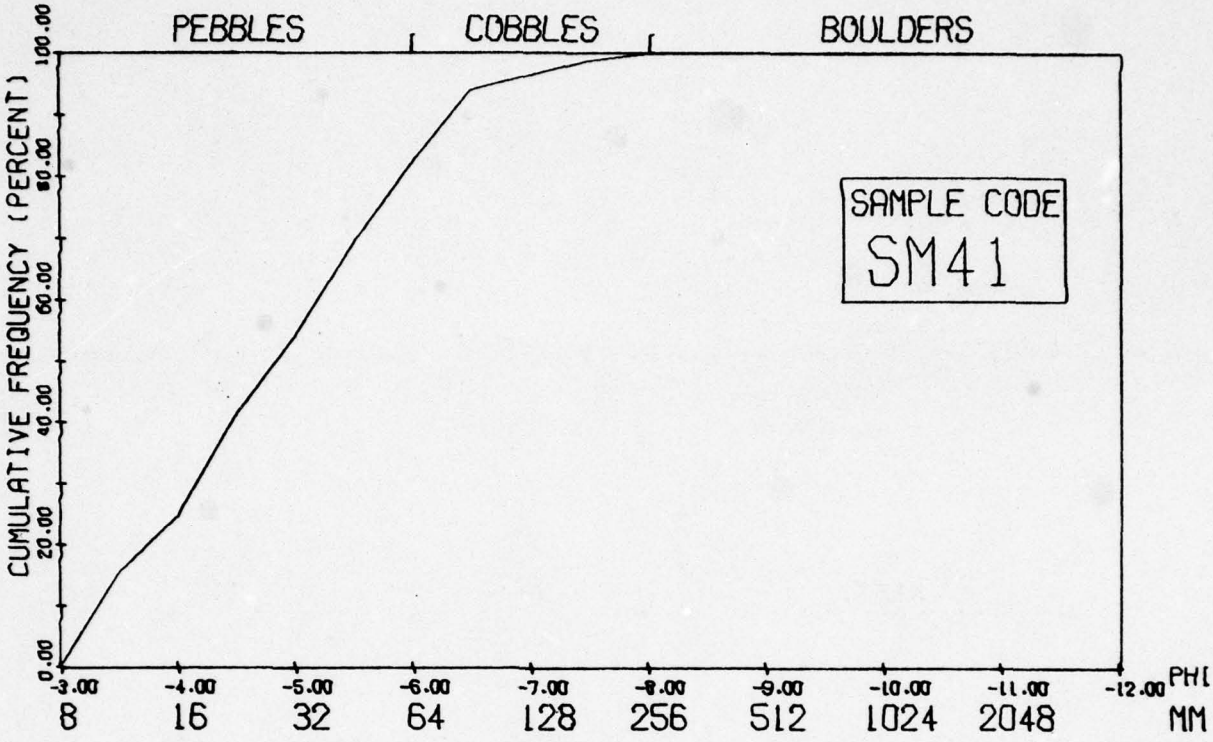
PEBBLES
COBBLES
BOULDERS
CUMULATIVE FREQUENCY (PERCENT)
0.00
20.00
40.00
60.00
80.00
100.00
SAMPLE CODE
SM41
-3.00
-4.00
-5.00
-6.00
-7.00
-8.00
-9.00
-10.00
-11.00
-12.00
PHI
8
16
32
64
128
256
512
1024
2048
MM

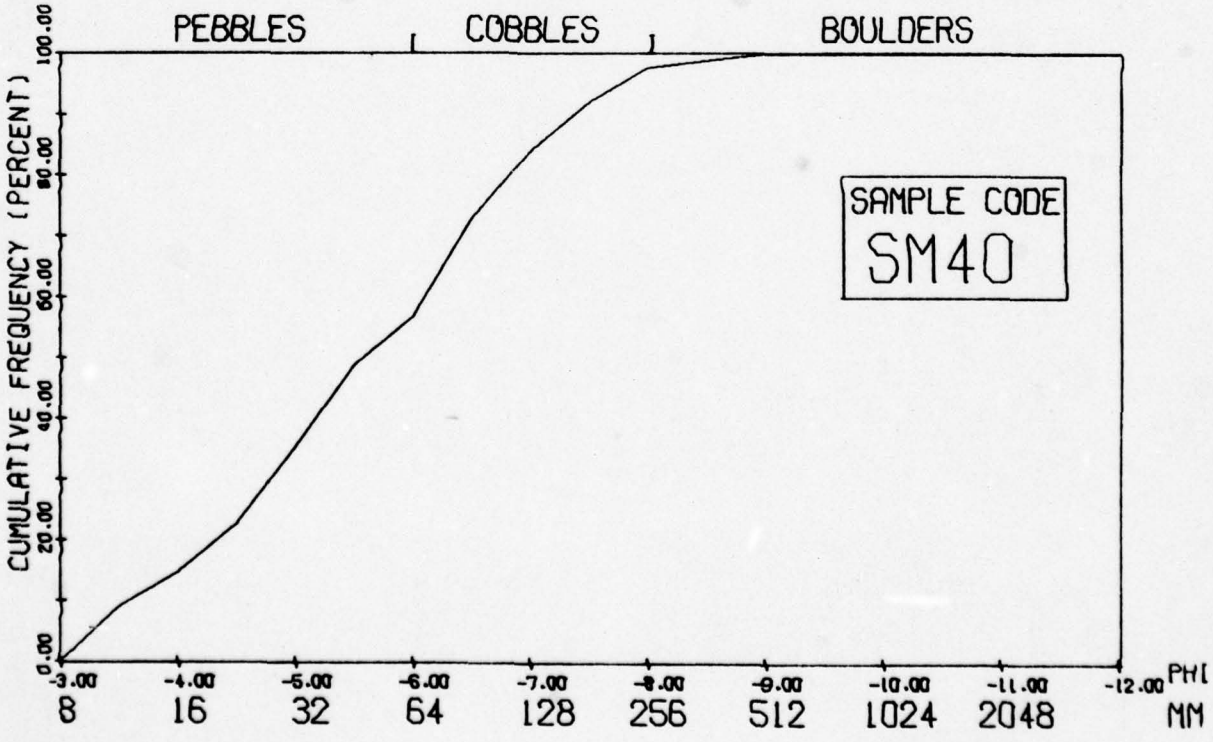
PEBBLES
COBBLES
BOULDERS
CUMULATIVE FREQUENCY (PERCENT)
0.00
20.00
40.00
60.00
80.00
100.00
SAMPLE CODE
SM40
-3.00
-4.00
-5.00
-6.00
-7.00
-8.00
-9.00
-10.00
-11.00
-12.00
PHI
8
16
32
64
128
256
512
1024
2048
MM

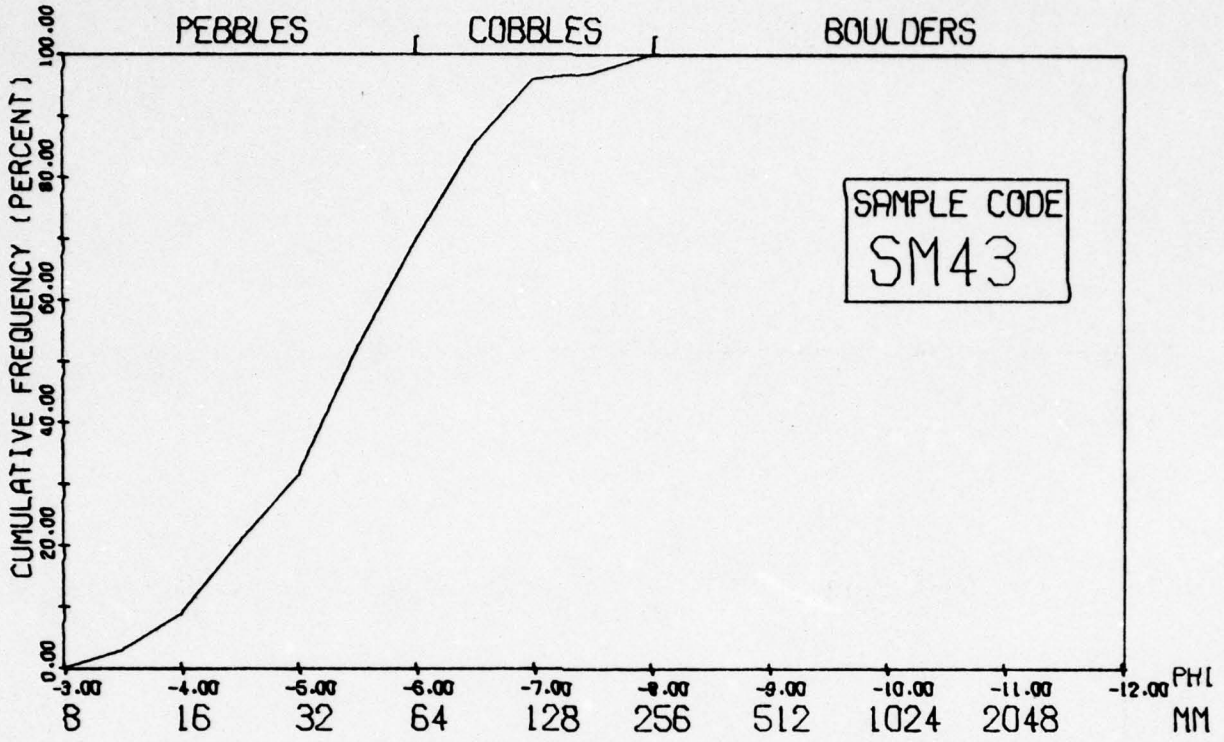
PEBBLES
COBBLES
BOULDERS
CUMULATIVE FREQUENCY (PERCENT)
100.00
80.00
60.00
40.00
20.00
0.00
SAMPLE CODE
SM43
-3.00
-4.00
-5.00
-6.00
-7.00
-8.00
-9.00
-10.00
-11.00
-12.00
PHI
8
16
32
64
128
256
512
1024
2048
MM

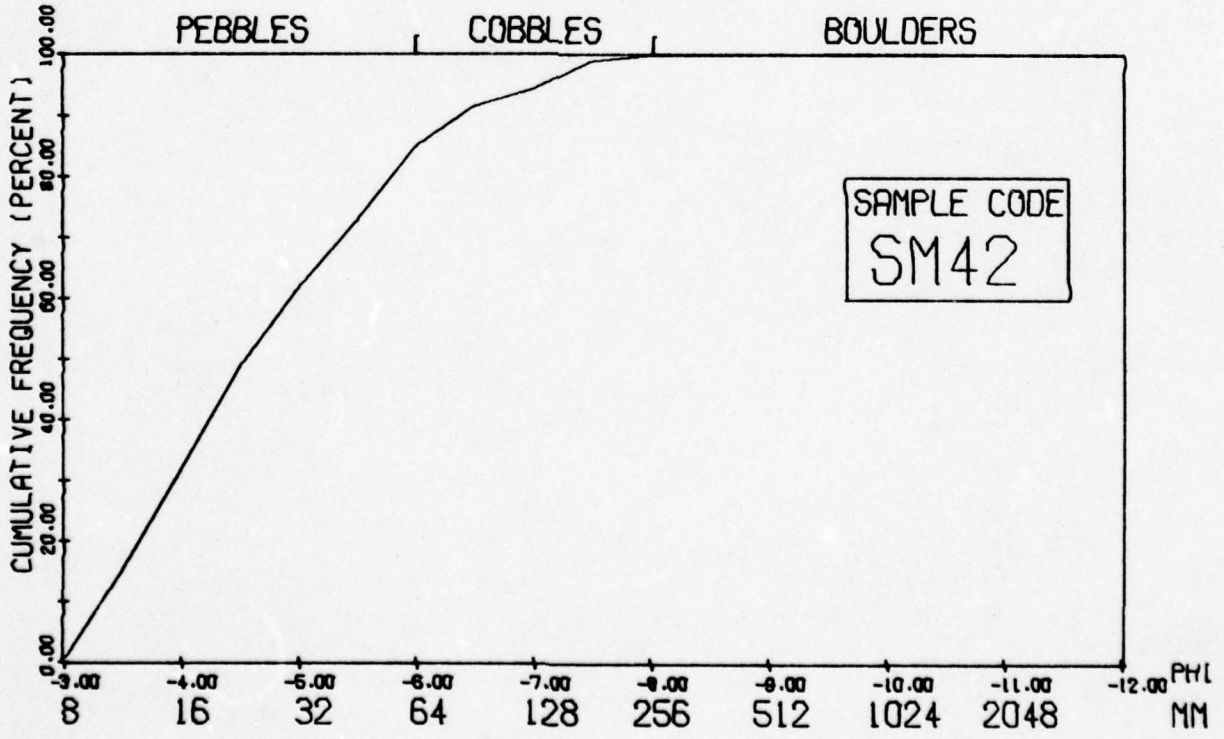
PEBBLES
COBBLES
BOULDERS
CUMULATIVE FREQUENCY (PERCENT)
100.00
80.00
60.00
40.00
20.00
0.00
SAMPLE CODE
SM42
-3.00
-4.00
-5.00
-6.00
-7.00
-8.00
-9.00
-10.00
-11.00
-12.00
PHI
8
16
32
64
128
256
512
1024
2048
MM

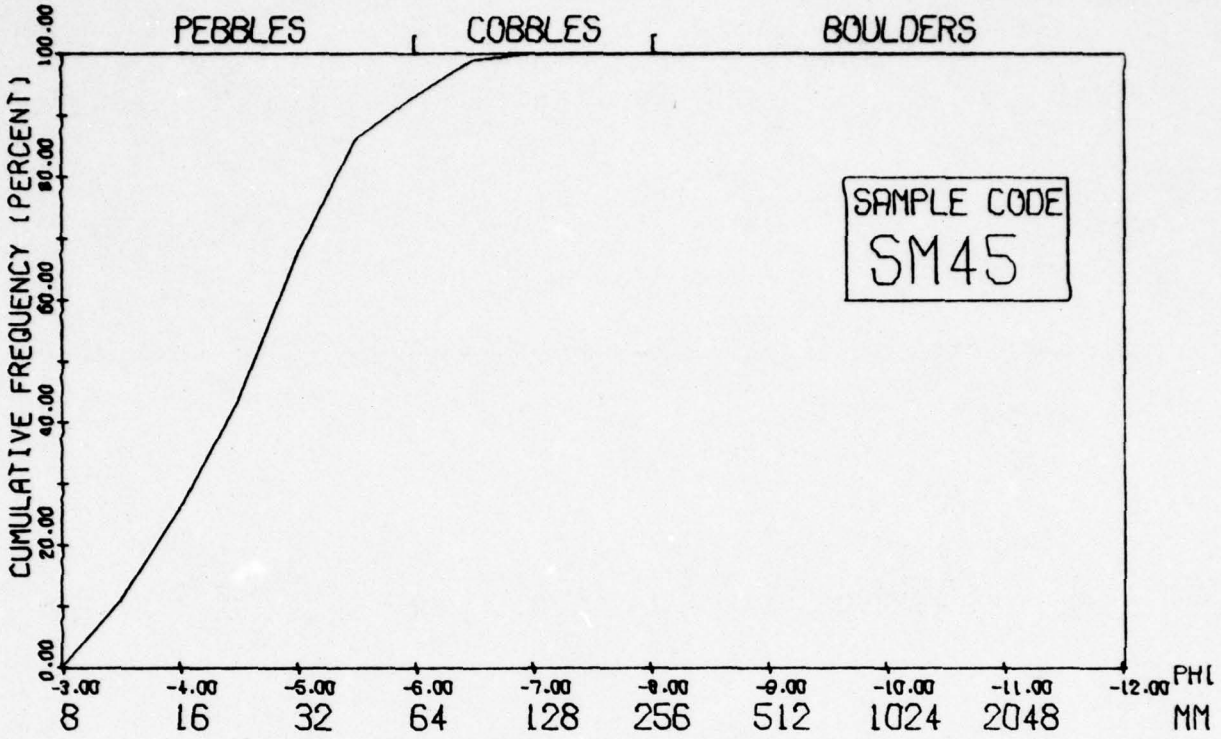
PEBBLES
COBBLES
BOULDERS
CUMULATIVE FREQUENCY (PERCENT)
100.00
80.00
60.00
40.00
20.00
0.00
SAMPLE CODE
SM45
-3.00
-4.00
-5.00
-6.00
-7.00
-8.00
-9.00
-10.00
-11.00
-12.00
PHI
8
16
32
64
128
256
512
1024
2048
MM

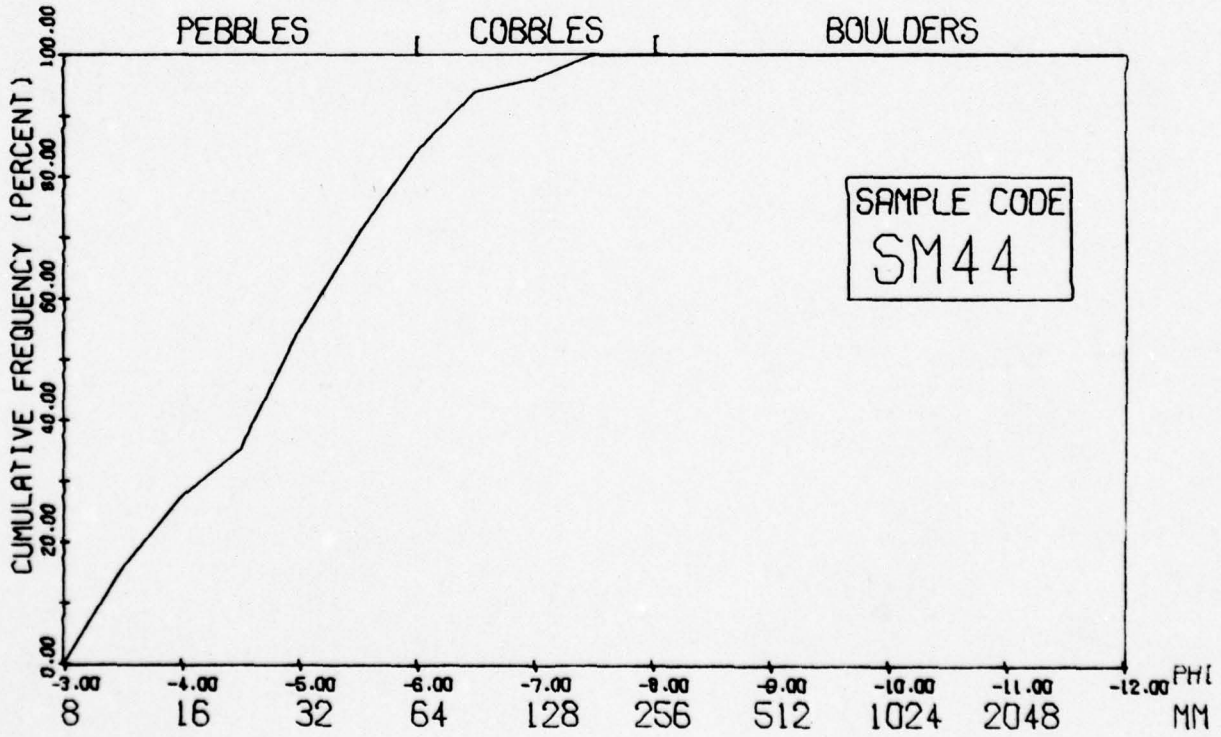
PEBBLES
COBBLES
BOULDERS
CUMULATIVE FREQUENCY (PERCENT)
100.00
80.00
60.00
40.00
20.00
0.00
SAMPLE CODE
SM44
-3.00
-4.00
-5.00
-6.00
-7.00
-8.00
-9.00
-10.00
-11.00
-12.00
PHI
8
16
32
64
128
256
512
1024
2048
MM

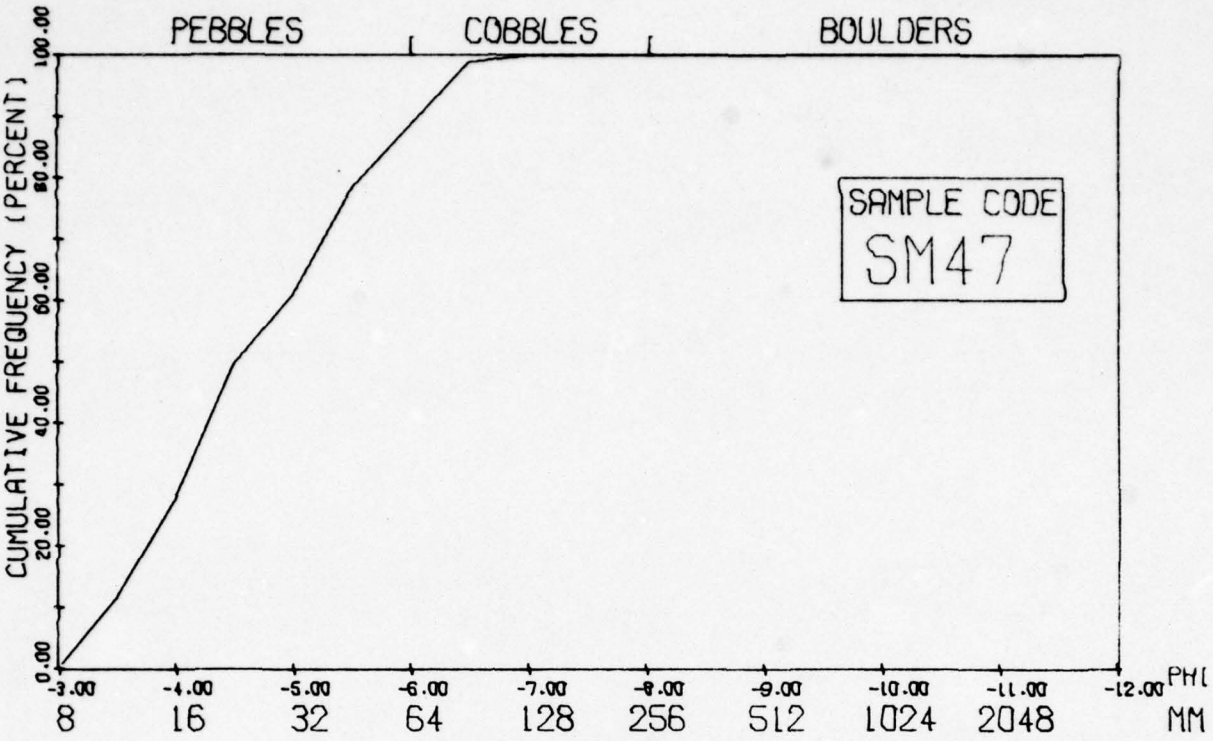
PEBBLES
COBBLES
BOULDERS
CUMULATIVE FREQUENCY (PERCENT)
0.00
20.00
40.00
60.00
80.00
100.00
SAMPLE CODE
SM47
-3.00
-4.00
-5.00
-6.00
-7.00
-8.00
-9.00
-10.00
-11.00
-12.00
PHI
8
16
32
64
128
256
512
1024
2048
MM

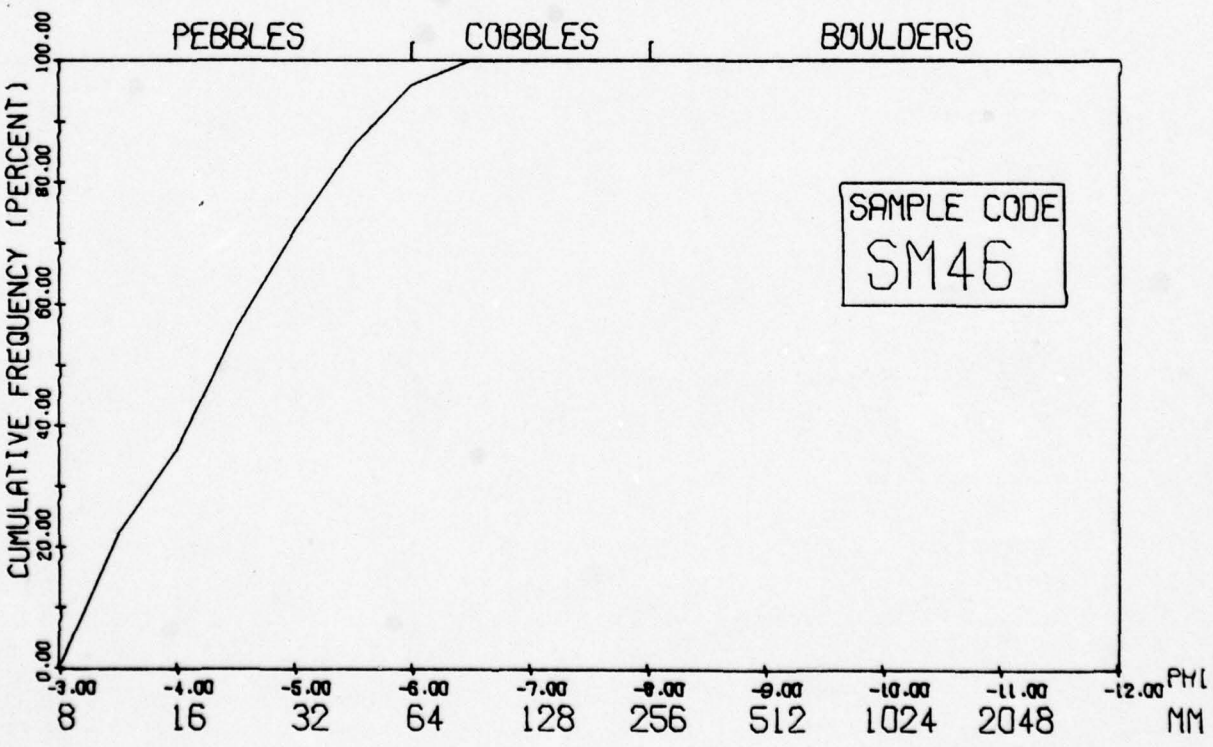
PEBBLES
COBBLES
BOULDERS
CUMULATIVE FREQUENCY (PERCENT)
0.00
20.00
40.00
60.00
80.00
100.00
SAMPLE CODE
SM46
-3.00
-4.00
-5.00
-6.00
-7.00
-8.00
-9.00
-10.00
-11.00
-12.00
PHI
8
16
32
64
128
256
512
1024
2048
MM

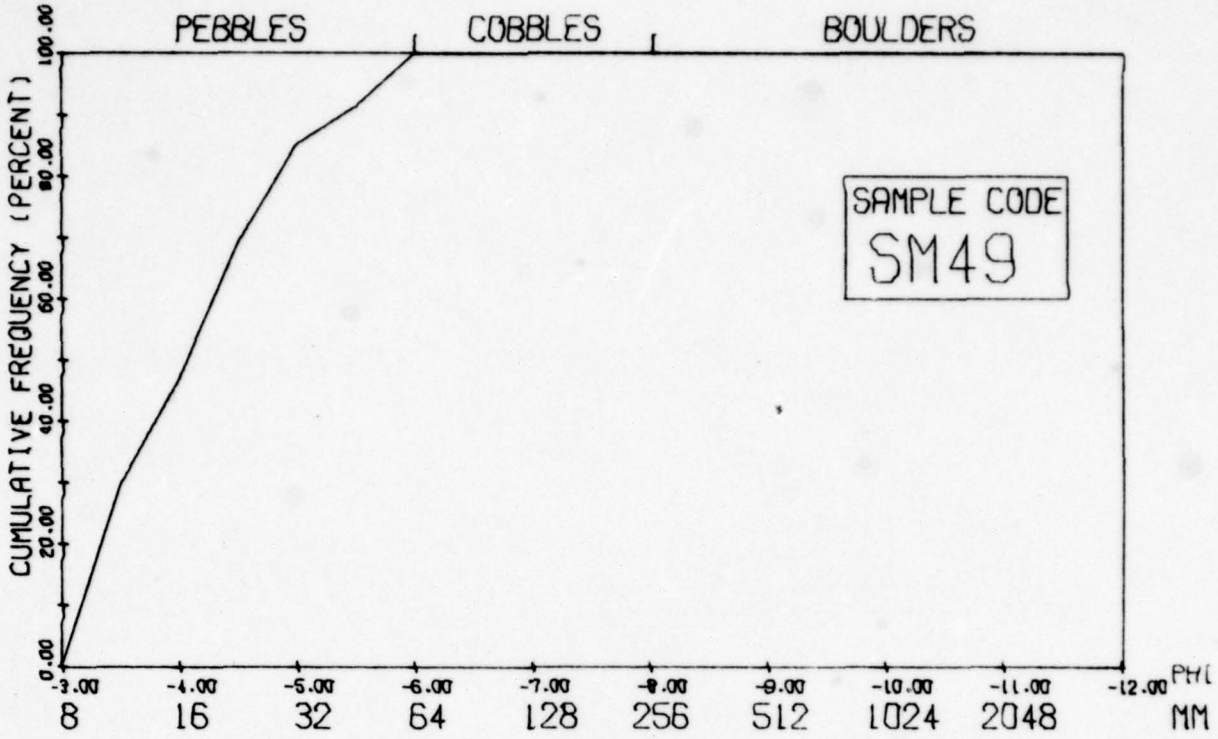
PEBBLES
COBBLES
BOULDERS
CUMULATIVE FREQUENCY (PERCENT)
100.00
80.00
60.00
40.00
20.00
0.00
SAMPLE CODE
SM49
-3.00
-4.00
-5.00
-6.00
-7.00
-8.00
-9.00
-10.00
-11.00
-12.00
PHI
8
16
32
64
128
256
512
1024
2048
MM

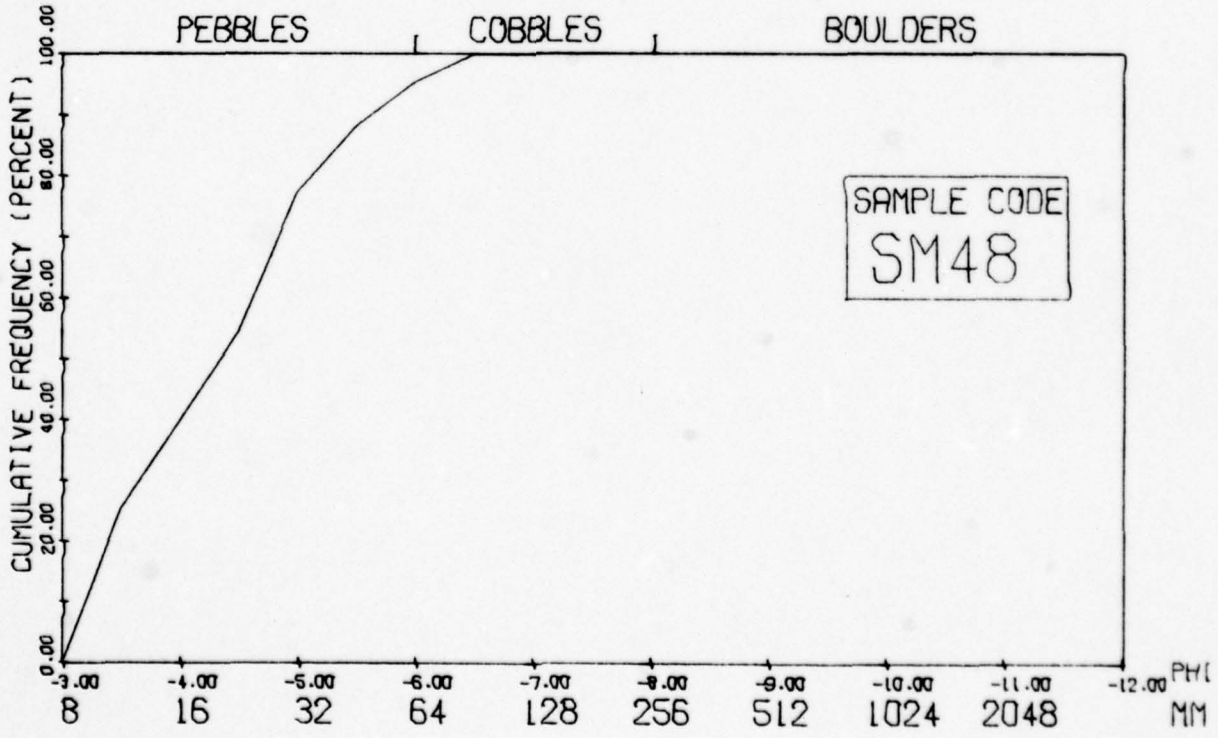
PEBBLES
COBBLES
BOULDERS
CUMULATIVE FREQUENCY (PERCENT)
100.00
80.00
60.00
40.00
20.00
0.00
SAMPLE CODE
SM48
-3.00
-4.00
-5.00
-6.00
-7.00
-8.00
-9.00
-10.00
-11.00
-12.00
PHI
8
16
32
64
128
256
512
1024
2048
MM

| Sample Code | Sample Size | Sample Code | Sample Size | Sample Code | Sample Size |
|---|---|---|---|---|---|
| BB01 | 84 | BW05 | 86 | BWJ5 | 27 |
| BB02 | 72 | BW06 | 117 | BWJ6 | 19 |
| BB03 | 69 | BW07 | 97 | BWJ7 | 24 |
| BB04 | 66 | BW08 | 98 | BWT8 | 39 |
| BB05 | 81 | BW09 | 51 | BWT1 | 92 |
| BB06 | 89 | BWXA | 31 | BWT1 | 73 |
| BB07 | 91 | BWXB | 49 | CX01 | 114 |
| BB08 | 76 | BW12 | 30 | CX02 | 24 |
| LHBJ | 70 | BW15 | 44 | CX03 | 34 |
| LH02 | 77 | BW16 | 63 | CX04 | 89 |
| LH03 | 42 | BW17 | 81 | CX05 | 77 |
| LH04 | 54 | BW18 | 97 | CX06 | 97 |
| LH09 | 53 | BW19 | 97 | CX07 | 81 |
| LH10 | 82 | BW20 | 51 | CXQ3 | 62 |
| LH11 | 61 | BW2X | 28 | RS01 | 92 |
| LH12 | 56 | BW22 | 102 | RS02 | 79 |
| LH13 | 49 | BW30 | 91 | RS03 | 136 |
| LH14 | 52 | BW31 | 112 | RS04 | 112 |
| LH15 | 42 | BW32 | 101 | RS05 | 112 |
| LHQ2 | 44 | BW33 | 81 | RS06 | 189 |
| LHQ3 | 72 | BWJ1 | 41 | RS07 | 167 |
| BW01 | 147 | BWJ2 | 31 | PR01 | 82 |
| BW02 | 122 | BWJ3 | 30 | PR02 | 53 |
| BW03 | 145 | BWJ4 | 24 | PR03 | 86 |

Table G-86 Sample Sizes for Gravel.

| Sample Code | Sample Size | Sample Code | Sample Size | Sample Code | Sample Size |
|---|---|---|---|---|---|
| PR04 | 85 | SM17 | 112 | SM38 | 131 |
| AG01 | 113 | SMI7 | 133 | SM39 | 113 |
| AG02 | 174 | SM18 | 139 | SM40 | 88 |
| TT05 | 173 | SM19 | 137 | SM41 | 85 |
| TT11 | 199 | SMI9 | 46 | SM42 | 107 |
| TT17 | 241 | SM20 | 175 | SM42 | 102 |
| TT20 | 117 | SM21 | 143 | SM44 | 51 |
| TT23 | 82 | SM22 | 82 | SM45 | 101 |
| TT25 | 78 | SMB2 | 62 | SM46 | 50 |
| TT27 | 83 | SM24 | 108 | SM47 | 87 |
| TT30 | 58 | SM25 | 75 | SM48 | 110 |
| TT24 | 98 | SM26 | 98 | SM49 | 81 |
| SM01 | 108 | SM27 | 82 | | |
| SM02 | 70 | SM28 | 88 | | |
| SM05 | 72 | SM29 | 101 | | |
| SM06 | 81 | SM30 | 76 | | |
| SM07 | 79 | SM31 | 93 | | |
| SM08 | 224 | SM32 | 103 | | |
| SM09 | 62 | SM33 | 89 | | |
| SM11 | 53 | SM34 | 164 | | |
| SM12 | 40 | SM3D | 97 | | |
| SM13 | 61 | SM35 | 89 | | |
| SM14 | 56 | SM36 | 96 | | |
| SM16 | 64 | SM37 | 79 | | |

Table G-87 Sample Sizes for Gravel.

PROGRAM FRQPLT LISTING

```
      PROGRAM FRQPLT(INPUT,OUTPUT,PLOT,TAPE5=INPUT,TAPE6=OUTPUT,TAPE99=PLOT)
      DIMENSION CUMFRT(19)
      DIMENSION X(21)
      DIMENSION Y(19)
      DIMENSION CUMFRQ(21)
      DIMENSION RELFRQ(19)
      DIMENSION CUMFRK(21)
      DIMENSION XI(19)
      DIMENSION PT(35)
      INTEGER BXFACT,BCUMFT
      DATA PT/35*(1H*)/
      TEST=1
      CALL INITIAL(0,99,.1,0,0)
      CALL PLTCHK(0)
      CALL SETFACT (6.5/10.5,9.5/14.0)
      DO 300 K=1,45
      READ(5,53) NSYMBL
      WRITE(6,14) NSYMBL
   14 FORMAT(" ",4(/),15X,A4,T60,"HISTOGRAM",T96,"CUMULATIVE PERCENT",/)
      WRITE(6,11)
   11 FORMAT(" ",2X,"CODE",7X,"PHI",5X,"COUNT",3X,"FREQ",5X,"CUM FREQ",/)
      YSUM=0
      DO 100 I=1,19
      READ (5,10) TITL,X(I),Y(I)
      YSUM=YSUM+Y(I)
      IF (I .EQ. 1) X(I)= -3.0
      IF (I .GT. 1) X(I)=X(I-1) -0.5
      CUMFRQ(I)=0
  100 CONTINUE
      DO 200 J=1,19
      RELFRQ(J)=100*Y(J)/YSUM
      IF (J .EQ. 1) CUMFRQ(J)=CUMFRQ(J)+RELFRQ(J)
      IF (J .GT. 1) CUMFRQ(J)=CUMFRQ(J-1)+RELFRQ(J)
  200 CONTINUE
      DO 240 J=1,19
      IF (J .EQ. 1) GO TO 240
      CUMFRT(J)=CUMFRQ(J-1)
  240 CONTINUE
      CUMFRT(1)=0.0
      DO 250 J=1,19
      WRITE(6,33)NSYMBL, X(J),Y(J),RELFRW(J),CUMFRT(J)
   33 FORMAT (" ",2X,A4,5X,F6.1,4X,F6.2,2X,F6.3,5X,F7.3, T50,"I")
      IF (Y(J) .GT 35) BXFACT=35
      IF (Y(J) .LE. 35) BXFACT=Y(J)
      BCUMFT=(CUMFRT(J)*0.01*30)
      WRITE(6,83)(PT(L),L=1,BXFACT
   83 FORMAT ("+",T51,35(A1))
      WRITE(6,84)
   84 FORMAT("+",T85,"I",T90,"I")
      WRITE(6,85)(PT(L),L=1,BCUMFT
   85 FORMAT("+",T91,35(A1))
      WRITE(6,87)
   87 FORMAT("+",T120,"I")
      CUMFRK(J)=CUMFRT(20-J)
```

```
250 CONTINUE
    TOT=0
    SUM=0
    DO 152 I=1,19
    IF(I .EQ. 1) XI(I)=-3.5
    IF(I .GT. 1) XI(I)=XI(I-1)-0.5
    TOT=XI(I)*Y(I)
    SUM=SUM+TOT
152 CONTINUE
    XMEAN=SUM/YSUM
    SVAR2=0
    DO 153 I=1,19
    VAR2=((XI(I)*Y(I)) -XMEAN*Y(I))**2
    SVAR2=SVAR2+VAR2
153 CONTINUE
    ASVAR2=SVAR2/YSUM-1
    SD=SQRT(ASVAR2)
    WRITE(6,92) NSYMBL,AD,XMEAN
 92 FORMAT(" ",10X,"THE STANDARD DEVIATION FOR LOCATION",1X,A4,"  IS",
   +1X,F10.5,3X,"PHI : THE MEAN IS",F10.5," PHI")
    CALL SCALE (X, 9.5,19,1,19.0)
    CALL SCALE (CUMFRK,5.0,19,1,20.0)
    CALL AXIS(0.0,2.0,9H       ,-9,9.5,0.0,-3.0,-.95,9.5)
    CALL AXIS(0.0,2.0,30H                          ,
   +30,5.0,90.0,0.0,20.0,20.0)
    CALL PLOT(0.0,2.0,-3)
    W=CUMFRK(19)/20.00
    CALL PLOT(0.0,W,-3)
    CALL LINE(X,CUMFRK,19,1,0,L)
    CALL PLOT(0.0,-W,-3)
    CALL PLOT(0.0,0.0,-3)
    CALL PLOT(7.0,3.0,3)
    CALL PLOT(9.0,3.0,2)
    CALL PLOT(9.0,4.0,2)
    CALL PLOT(7.0,4.0,2)
    CALL PLOT(7.0,3.0,2)
    CALL SYMBOL(-.3,.75,.16,"CUMULATIVE FREQUENCY (PERCENT)",90.,30.)
    CALL CYMBOL(7.1,3.7,0.2,"SAMPLE CODE",0.0,11)
    CALL SYMBOL(7.25,3.13,0.40,NSYMBL,0.0,4)
    CALL SYMBOL(1.03,5.1,.2,"PEBBLES",0.0,7)
    CALL SYMBOL(3.12,5.0,.15,"I",0.0,1)
    CALL SYMBOL(3.66,5.1,.2,"COBBLES",0.0,7)
    CALL SYMBOL(5.25,5.0,.15,"I",0.0,1)
    CALL SYMBOL(6.84,5.1,.2,"BOULDERS",0.0,8)
    CALL PLOT(0.0,5.0,3)
    CALL PLOT( 9.5,5.0,2)
    CALL PLOT( 9.5,0.0,2)
    CALL SYMBOL(9.95,-.13,.15,"PHI",0.0,3)
    CALL SYMBOL(0.0,-.5,.2,"8",0.0,1)
    CALL SYMBOL(1.0,-.5,12,"16",0.0,2)
    CALL SYMBOL(2.1,-.5,.2,"32",0.0,2)
    CALL SYMBOL(3.13,-.5,12,"64",0.0,2)
    CALL SYMBOL(4.13,-.5,.2,"128",0.0,3)
    CALL SYMBOL(5.13,-.5,.2,"256",0.0,3)
    CALL SYMBOL(6.2,-.5,.2,"512",0.0,3)
    CALL SYMBOL(7.2,-.5,.2,"1024",0.0,4)
    CALL SYMBOL(8.25,-.5,.2,"2048",0.0,4)
```

```
      CALL SYMBOL(9.95,-.5,.2,"MM",0.0,2)
      CALL PLOT (0.0,0.0,3)
      IF (TEST .EQ. 1) GO TO 260
      GO TO 261
  260 CALL PLOT(0.0,5.0,-3)
      TEST=0
      GO TO 300
  261 CALL PLOT (14.0,-9.0,-3)
      TEST=1
  300 CONTINUE
   10 FORMAT (A4,1X,F6.1,1X,F3.0)
   13 FORMAT (" ",2X,A4,5X,F6.0,4x,F6.2,2X,F6.3,5X,F7.3)
   53 FORMAT(A4)
      CALL ENDPLT
      STOP
      END
```

# APPENDIX H

## MULTIVARIATE ANALYSIS: COMPUTER PROGRAMS

BY

LARRY MAYER

# APPENDIX H

## MULTIVARIATE ANALYSIS

Multivariate analysis is the quantitative study of problems that involve more than a single variable. One tool of multivariate analysis is correlation and regression. When one variable increases in value and a second variable increases or decreases uniformly with changes of the first variable, correlation is said to exist. A measure of how closely variables are correlated is called the correlation coefficient whose symbol is the letter "r". Where an increase of one variable is perfectly correlated with an increase of a second variable, the correlation coefficient would be +1.00. Where an increase of one variable is perfectly correlated with a decrease of a second variable, the correlation coefficient would be -1.00. Values of r, therefore, can vary between +1.00 through -1.00. The values of these two variables may be plotted on an x-y coordinate graph commonly called a scattergram. When these variables show good correlation (values near +1.00 or -1.00) the points tend to lie on a line called the regression line. The equation of the regression line, can be called the regression equation, which describes the estimated change of the second variable with a given change of the first variable. The difference between values estimated by the regression equation and the actual value is called a residual.

The Statistical Package for the Social Sciences (SPSS) was used (see Appendix G) to perform the multiple regression analysis (Nie and others, 1975, p. 320-367). SPSS uses the following formulas to calculate the above described statistics:

$$B = \frac{\Sigma(x-\bar{x})\ (y-\bar{y})}{\Sigma(x-\bar{x})^2} \qquad (1)$$

$$A = \bar{y} - B\bar{X} \qquad (2)$$

Where A, B are part of the regression equation,

$$Y^1 = A + BX \tag{3}$$

$Y^1$ is the expected value of the dependent variable and y is the actual value of the dependent variable.

$$\text{Residuals} = y - y^1 \tag{4}$$

r is calculated by the Pearson product moment equation,

$$r = \frac{N \Sigma XY - (\Sigma X)(\Sigma Y)}{N \Sigma X^2 - (\Sigma X)^2 \quad N \Sigma X^2 - (\Sigma Y)^2} \tag{5}$$

The significance of the regression coefficient is evaluated by SPSS using the F ratio

$$F = \frac{\Sigma(y^1 - \bar{y}) / 1}{\Sigma(y - y^1) / (N-2)} \tag{6}$$

SPSS provides the significance level of the F ratio routinely. The confidence level is simply 1-significance leve. In univariate analysis, the F ratio is used to test whether more variation occurs between categories than within categories. In multivariate analysis, the F ratio is used to determine whether correlation between variables may be due to sampling fluctuation or measurement error. When the significance of the F ratio is low (e.g., 0.001), it is unlikely that the sample was drawn from a population where the multiple correlation coefficient equals zero.

The SPSS subprograms used for regression and multiple regression are SCATTERGRAM and REGRESSION. Subprogram SCATTERGRAM performs bivariate regressions and outputs a scatter diagram (see Figure H-5).

The format of the input data is provided by the user. The control cards for executing SCATTERGRAM are:

```
Column 1          16
  RUN NAME        REGRESSION ANALYSIS
  VARIABLE LIST   V1 TO V7
  INPUT FORMAT    FIXED (A2,3X,A2,2X,F5.2,5X,F5.3,5X,F4.0,5X,F5.0)
  INPUT MEDIUM    CARD
  N OF CASES      UNKNOWN
  RECODE          V1("LH"=1) ("TT"=2) ("BB"=3)
  DO REPEAT       X1=V23 TO V27/
                  X2=V3 TO V7/
  COMPUTE         X1-LN(X2)
  END REPEAT
  VAR LABELS      V1 WATERSHED CODE/
                  V2 SAMPLE LOCATION/
                  V3 DISTANCE/
                  V4 SLOPE/
                  V5 MEAN PARTICLE SIZE/
                  V6 STANDARD DEVIATION/
                  V7 MAXIMUM PARTICLE SIZE/
                  V23 NATURAL LOG OF DISTANCE/
                  V24 NATURAL LOG OF SLOPE/
                  V25 NATURAL LOG OF MEAN SIZE/
```

V26 NATURAL LOG OF STANDARD DEVIATION/

V27 NATURAL LOG OF MAXIMUM SIZE/

VALUE LABELS V1 (1) LH (2) TT (3) BB

SCATTERGRAM V5 WITH V3 TO V4/V25 WITH V23 TO V24/

STATISTICS ALL

READ INPUT DATA

Data-files HERE

These control cards tell SPSS SCATTERGRAM:

1. The computer run is called Regression Analysis.

2. The variables inputted consist of V1, V2, V3, V4, V5, V6, V7.

3. The format of the data input is:

| VARIABLE | COLUMNS | FORMAT |
|---|---|---|
| V1 | 1-2 | A2 |
| V2 | 6-7 | A2 |
| V3 | 10-14 | F5.2 |
| V4 | 20-24 | F5.3 |
| V5 | 30-33 | F4.0 |
| V6 | 40-43 | F4.0 |
| V7 | 49-53 | F5.0 |

4. The data will be input from punched cards.

5. The number of cases is unknown.

6. Variable 1 (V1) will have 3 labels.

7-10. Calculate V23-V27 from V3-V7

11-22. The labels of the 12 variables are as described.

23. V1 is given numeric labels for testing when needed.

24. Produces a scatter diagram for V5-V3, V5-V4, V25-V23, V25-V24.

14. All statistical options are to be calculated

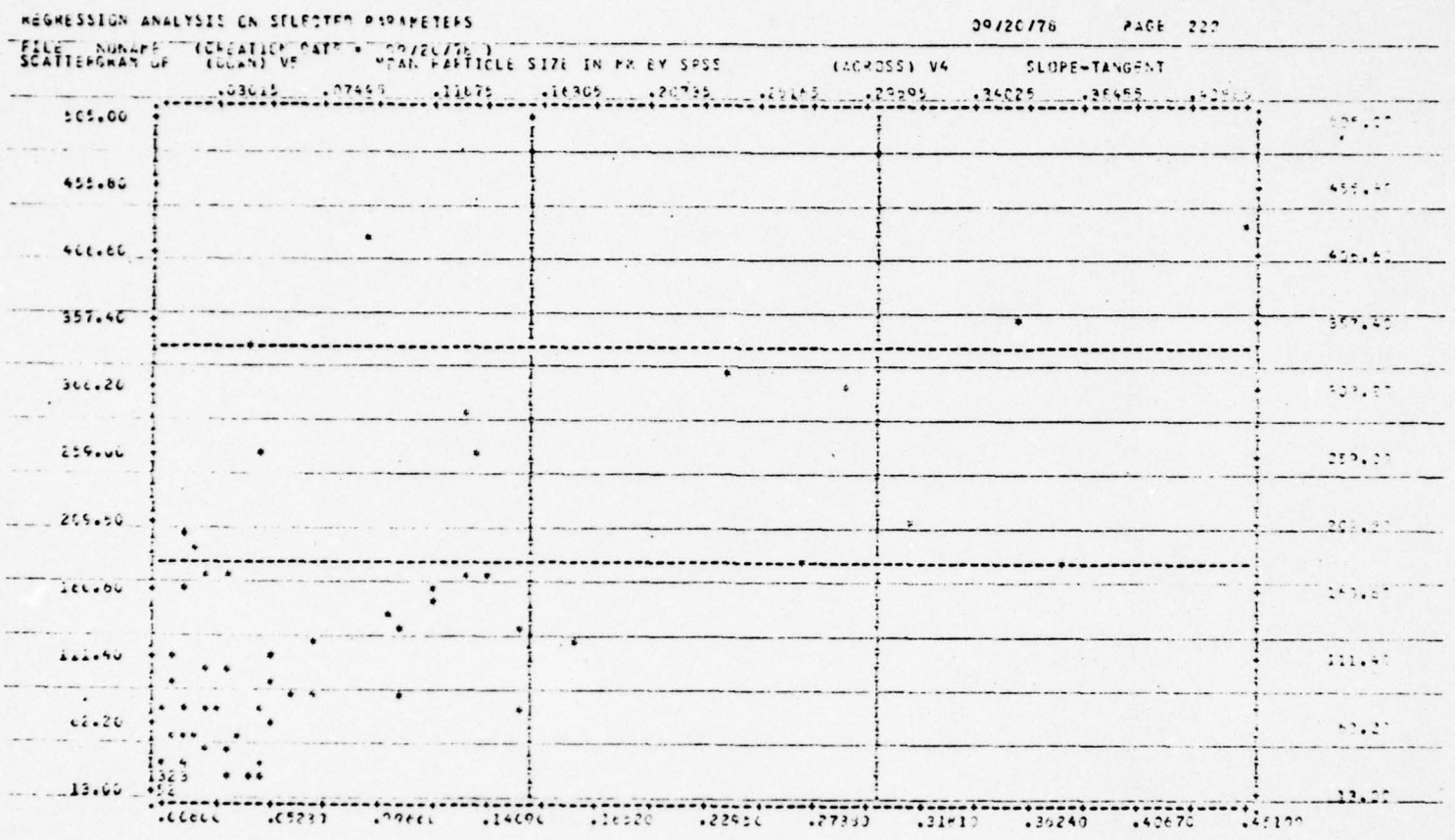


Figure H-5 Sample output of subprogram SCATTERGRAM

In order to use subprogram REGRESSION, the SCATTERGRAM card (24) may be replaced with:

| Column 1 | 16 |
|---|---|
| REGRESSION | VARIABLES = V3 TO V7 /REGRESSION = V5 WITH V3 TO V4 |

Both can be executed in a single run by placing the REGRESSION card after the data. The data-file for regression analysis is defined by the select card which precedes the REGRESSION card.

```
*SELECT IF (V1 EQ 3)
```

This card informs SPSS that the operation is to be performed on the watershed with value lable of 3 (control card 23).

The results of regression analysis is presented in Table H-7 through Table H-18. The data in even numbered tables are taken from SPSS REGRESSION while the odd numbered tables are derived from SPSS SCATTERGRAM.

| Variable | (V3) Distance | | (V4) Slope | | (V23) ln Distance | | (V24) ln Slope | |
|---|---|---|---|---|---|---|---|---|
| | r | Significance | r | Significance | r | Significance | r | Significance |
| Mean Particle Size (V5) | -.23 | .264 | .82 | .001 | -.29 | .208 | .81 | .002 |
| Maximum Particle Size (V7) | -.39 | .130 | .70 | .012 | -.43 | .108 | .67 | .017 |
| Sorting-Standard Deviation (V6) | -.32 | .183 | .71 | .011 | -.35 | .163 | .69 | .013 |
| ln Mean Particle Size (V25) | | | | | -.12 | .368 | .79 | .003 |
| ln Maximum Particle Size (V27) | | | | | -.30 | .196 | .62 | .028 |
| ln Sorting-Standard Deviation (V26) | | | | | -.25 | .243 | .70 | .012 |

Table H-7 Correlation Coefficients and Significance of Lost Home Bivariate Regressions.

| Multiple Regression Equation | F | Significance | Multiple-r |
|---|---|---|---|
| V5 = 2680.3(V4) + 7.3(V3) - 77.8 | 7.80 | 0.017 | 0.83 |
| V6 = 5474.4(V4) - 6.3(V3) - 152.9 | 3.59 | 0.085 | 0.71 |
| V7 = 25701.9(V4) - 99.6(V3) - 553.2 | 3.62 | 0.083 | 0.71 |
| V25 = 2.1(V24) + 0.4(V23) + 10.3 | 7.08 | 0.021 | 0.81 |
| V26 = 2.8(V24) + 0.1(V23) + 12.3 | 3.33 | 0.096 | 0.70 |
| V27 = 2.4(V24) - 0.2(V23) + 13.4 | 2.22 | 0.179 | 0.62 |

Table H-8 Regression Equations for Lost Home Samples, with F, Significance and Multiple Correlation Coefficient.

| Variable | (V3) Distance | | (V4) Slope | | (V23) ln Distance | | (V24) ln Slope | |
|---|---|---|---|---|---|---|---|---|
| | r | Significance | r | Significance | r | Significance | r | Significance |
| Mean Particle Size (V5) | -.31 | .207 | .86 | .002 | -.03 | .466 | .84 | .002 |
| Maximum Particle Size (V7) | -.04 | .460 | .58 | .052 | .05 | .450 | .72 | .015 |
| Sorting-Standard Deviation (V6) | -.06 | .440 | .61 | .041 | .20 | .302 | .67 | .024 |
| ln Mean Particle Size (V25) | | | | | -.08 | .418 | .87 | .001 |
| ln Maximum Particle Size (V27) | | | | | .21 | .293 | .64 | .032 |
| ln Sorting-Standard Deviation (V26) | | | | | .08 | .423 | .73 | .012 |

Table H-9 Correlation Coefficients and Significance of Tall Tale Bivariate Regressions.

| Multiple Regression Equation | F | Significance | Multiple-r |
|---|---|---|---|
| V5= 1143.2(V4) + 207.8(V3) - 128.9 | 14.68 | 0.005 | .91 |
| V6= 1031.9(V4) + 298.2(V3) - 103.7 | 3.84 | 0.084 | .75 |
| V7 = 4167.4(V4) + 1244.2(V3) - 321.4 | 3.27 | 0.109 | .72 |
| V25 = 1.3(V24) + 0.5(V3) + 7.9 | 26.09 | 0.001 | .95 |
| V26 = 1.3(V24) + 0.6(V3) + 8.1 | 10.26 | 0.012 | .88 |
| V27 = 1.1(V24) + 0.5(V3) + 9.3 | 7.39 | 0.024 | .84 |

Table H-10 Regression Equations for Tall Tale Samples, with F, Significance and Multiple Correlation Coefficient.

| Variable | (V3) Distance | | (V4) Slope | | (V23) ln Distance | | (V24) ln Slope | |
|---|---|---|---|---|---|---|---|---|
| | r | Significance | r | Significance | r | Significance | r | Significance |
| Mean Particle Size (V5) | -.91 | .015 | .95 | .007 | -.87 | .029 | .96 | .004 |
| Maximum Particle Size (V7) | -.80 | .052 | .80 | .052 | -.72 | .086 | .91 | .016 |
| Sorting-Standard Deviation (V6) | -.86 | .030 | .89 | .022 | -.79 | .057 | .95 | .006 |
| ln Mean Particle Size (V25) | | | | | -.85 | .031 | .97 | .003 |
| ln Maximum Particle Size (V27) | | | | | -.70 | .093 | .90 | .019 |
| ln Sorting-Standard Deviation (V26) | | | | | -.78 | .061 | .95 | .006 |

Table H-11 Correlation Coefficients and Significance of Bumble Bee Bivariate Regressions.

| Multiple Regression Equation | F | Significance | Multiple-r |
|---|---|---|---|
| V5 = 1419.9(V4) + 697.6(V3) - 558.0 | 31.56 | 0.031 | .98 |
| V6 = 1081.8(V4) + 503.3(V3) - 376.8 | 4.92 | 0.169 | .91 |
| V7 = -638.2(V3) + 904.2 | 5.39 | 0.103 | .80 |
| V25 = 0.7(V24) + 0.3(V23) + 6.3 | 23.77 | 0.040 | .98 |
| V26 = 0.9(V24) + 0.8(V23) + 6.9 | 94.67 | 0.010 | .99 |
| V27 = 0.8(V24) + 0.8(V23) + 8.2 | 11.89 | 0.078 | .96 |

Table H-12 Regression Equations for Bumble Bee Samples, with F, Significance and Multiple Correlation Coefficient.

| Variable | (V3) Distance | | (V4) Slope | | (V23) ln Distance | | (V24) ln Slope | |
|---|---|---|---|---|---|---|---|---|
| | r | Significance | r | Significance | r | Significance | r | Significance |
| Mean Particle Size (V5) | -.95 | .000 | .95 | .000 | -.98 | .000 | .99 | .000 |
| Maximum Particle Size (V7) | -.88 | .001 | .98 | .000 | -.95 | .000 | .94 | .000 |
| Sorting-Standard Deviation (V6) | -.93 | .000 | .97 | .000 | -.97 | .000 | .98 | .000 |
| ln Mean Particle Size (V25) | | | | | -.92 | .000 | .89 | .001 |
| ln Maximum Particle Size (V27) | | | | | -.92 | .000 | .90 | .000 |
| ln Sorting-Standard Deviation (V26) | | | | | -.91 | .000 | .89 | .001 |

Table H-13 Correlation Coeffecients and Significance of Boulder Wash (I) Bivariate Regressions.

| Multiple Regression Equation | F | Significance | Multiple-r |
|---|---|---|---|
| V5 = 1600.8(V4) - 57.7(V3) + 363.5 | 127.84 | .000 | .99 |
| V6 = 2254.8(V4) - 47.9(V3) + 298.8 | 117.62 | .000 | .98 |
| V7 = 17729.3(V4) - 108.9(V3) + 722.8 | 107.59 | .000 | .99 |
| V25 = -2.1(V23) - 0.8(V24) + 7.4 | 16.89 | .003 | .92 |
| V26 = -2.1(V23) + 7.6 | 35.91 | .001 | .91 |
| V27 = -2.2(V23) + 9.4 | 40.54 | .000 | .92 |

Table H-14 Regression Equations for Boulder Wash (I) Samples, with F, Significance and Multiple Correlation Coefficient.

| Variable | (V3) Distance | | (V4) Slope | | (V23) ln Distance | | (V24) ln Slope | |
|---|---|---|---|---|---|---|---|---|
| | r | Significance | r | Significance | r | Significance | r | Significance |
| Mean Particle Size (V5) | -.65 | 0.006 | .93 | .000 | -.68 | .004 | .94 | .000 |
| Maximum Particle Size (V7) | -.65 | .006 | .96 | .000 | -.69 | .003 | .96 | .000 |
| Sorting-Standard Deviation (V6) | -.67 | .005 | .94 | .000 | -.69 | .003 | .95 | .000 |
| ln Mean Particle Size (V25) | | | | | -.75 | .001 | .93 | .000 |
| ln Maximum Particle Size (V27) | | | | | -.95 | .001 | .89 | .000 |
| ln Sorting-Standard Deviation (V26) | | | | | -.74 | .001 | .88 | .000 |

Table H-15 Correlation Coefficients and Significance of Stoval-Mohawk (I) Bivariate Regressions.

| Multiple Regression Equations | F | Significance | Multiple-r |
|---|---|---|---|
| V5 = 1543.4(V4) - 3.4(V3) + 33.6 | 40.78 | .000 | .94 |
| V6 = 1647.7(V4) - 4.5(V3) + 36.3 | 48.57 | .000 | .95 |
| V7 = 10439.9(V4) - 21.1(V3) + 155.7 | 63.21 | .000 | .96 |
| V25 = 0.9(V24) + 7.4 | 78.16 | .000 | .93 |
| V26 = 1.0(V24) - .1(V23) + 7.7 | 19.33 | .000 | .88 |
| V27 = 1.0(V24) - .1(V23) + 9.6 | 21.58 | .000 | .89 |

Table H-16 Regression Equations for Stoval-Mohawk (I) Samples, with F, Significance, and Multiple Correlation Coefficients.

| Variable | (V3) Distance | | (V4) Slope | | (V23) ln Distance | | (V24) ln Slope | |
|---|---|---|---|---|---|---|---|---|
| | r | Significance | r | Significance | r | Significance | r | Significance |
| Mean Particle Size (V5) | -.63 | .001 | .97 | .000 | -.78 | .000 | .93 | .000 |
| Maximum Particle Size (V7) | -.69 | .000 | .91 | .000 | -.82 | .000 | .92 | .000 |
| Sorting-Standard Deviation (V6) | -.67 | .001 | .94 | .000 | -.82 | .000 | .94 | .000 |
| ln Mean Particle Size (V25) | | | | | -.95 | .000 | .93 | .000 |
| ln Maximum Particle Size (V27) | | | | | -.94 | .000 | .86 | .000 |
| ln Sorting-Standard Deviation (V26) | | | | | -.96 | .000 | .88 | .000 |

Table H-17 Correlation Coefficients and Significance of Stoval-Mohawk (II) Bivariate Regressions.

| Multiple Regression Equations | F | Significance | Multiple-r |
|---|---|---|---|
| V5 = 931.8(V4) - 6.7(V3) + 52.5 | 273.08 | .000 | .98 |
| V6 = 836.9(V4) - 8.4(V3) + 55,8 | 164.56 | .000 | .98 |
| V7 = 3370.7(V4) - 42.2(V3) + 292.2 | 95.45 | .000 | .96 |
| V25 = .4(V24) - .6(V23) + 5.8 | 129.55 | .000 | .97 |
| V26 = .2(V24) - 1.0(V23) + 5.4 | 110.14 | .000 | .96 |
| V27 = .2(V24) - 1.0(V23) + 6.8 | 69.00 | .000 | .94 |

Table H-18 Regression Equations for Stoval-Mohawk (II) Samples, with F, Significance and Multiple Correlation Coefficients.

APPENDIX I

# THE ALLUVIAL FAN ENVIRONMENT

BY

WILLIAM B. BULL

# The alluvial-fan environment

by William B. Bull

## I Introduction

Alluvial fans are distinct terrestrial landforms that have been studied intensively, especially during the last two decades. It is the purpose of this review to summarize the present state of knowledge about alluvial fans. The section about the depositional environment discusses some recent work about the hydraulics of streamflow on a small alluvial fan, describes the great diversity of depositional environments that are characteristic of fans, and summarizes the stratigraphy of fans as a distinct sedimentary environment. Mathematical description of alluvial fans and the factors affecting fan area and slope are the subject of a section about fan morphology. Then, some new ideas are presented about the tectonic environment of alluvial fans. An attempt is made to explain why alluvial fans occur adjacent to some mountain fronts, whereas pediments are the typical landform adjacent to other mountains. The tectonic environment is but one of many aspects of fans that are important to man.

An alluvial fan is a deposit whose surface forms a segment of a cone that radiates downslope from the point where the stream leaves the source area. The coalescing of many fans forms a depositional piedmont that commonly is called a bajada (Blackwelder, 1931). Each fan is derived from a source area with a drainage net that transports the erosional products of the source area to the fan apex in a single trunk stream. The plan view of the cone-shaped deposit is often fan-shaped, and the contours bow downslope. Overall radial profiles are concave and cross-fan profiles are convex. Those authors using the term 'alluvial cone' generally are referring to small cones steeper than 20°, which are formed both by fluvial deposition and gravitational processes more typical of talus and debris cones.

In trying to distinguish an alluvial fan from a pediment in the field, it is useful to remember that alluvial fans are formed in a depositional environment and that pediments are formed in an erosional environment. Many pedimented areas have a large number of streams and rills that drain to the piedmont, but an alluvial-fan piedmont has fewer streams, each acting as a major conduit for water and sediment that is transported to the fanhead. Bedrock knobs rarely protrude through the alluvium of fans but are typical of pedimented terrains, where a veneer of alluvium and colluvium mantles bevelled

bedrock. No one criterion should be used to define an alluvial fan. Some pediments approximate a segment of a cone (Hadley, 1967, Figure 2) and many alluvial fans are not fan-shaped because they are restricted by adjacent larger fans. Surell (1841) may have been the first to discuss alluvial fans, and Haast (1864, 1879) and Thompson (1873) outlined the deposition of fans on the Canterbury Plain in New Zealand. In his detailed account of the Upper Indus basin Drew (1873) first used the term 'alluvial fan' (Dana, 1880; Cotton, 1948). Dutton (1880), Gilbert (1875; 1877; 1890), Geikie (1886), Miller (1883), McGee (1891), Davis (1905), Baker (1911), Eckis (1928), Longwell (1930), and Twenhofel (1932) and most subsequent workers have continued to use the term 'alluvial fan' in the same general context as defined above. An alluvial piedmont that lacks the form of several coalescing alluvial fans is best called an 'alluvial slope' (Hawley and Wilson, 1965, 8).

The above aspects of alluvial fans are easy to recognize by viewing the landform from the ground, from a mountain or aeroplane; or through the use of topographic maps and aerial photographs. A more difficult characteristic to determine is the minimum thickness of deposits needed to class part of a piedmont as an alluvial fan. Doehring (1970) has indicated that the minimum thickness of an alluvial fan is 15.3 m. Fans vary greatly in size (Spearing, 1974) from less than 10 m in length to more than 20 km. Thus it is not possible to assign some minimum value of thickness (such as 10 m) as being definitive of alluvial fans. Three metres of deposits would be substantial for a small fan that is only 30 m from apex to toe. The same thickness on a piedmont that is 20 km long would be best interpreted as a pediment mantle that could be easily removed by streams, thus exposing the bedrock. As a general guideline, fans may be distinguished from pediments as being landforms where the thickness of deposits is more than 1/100 the length of the landform. Many large fans are thicker than 300 m. Information about the thickness of alluvial fans may be obtained from stream-channels incised into the fan, from water wells or other boreholes, and by geophysical techniques.

Some characteristics of alluvial fans are shown in Figures 1 and 2. The individual nature of the component fans of the piedmont is readily apparent. A marked downfan change in the size of the debris deposited on a fan can be seen in Figure 1c. At the mountain front, the largest boulders have an intermediate diameter of 350 cm, but the maximum size decreases to only 15 cm at the toe of the fan. Downfan variation of particle size may also be affected by temporary channel entrenchment, which causes deposition to occur in different areas along a given radial line (Buwalda, 1951). Several variations of mean particle size along a given contour, such as occur on the fans of the eastern Sinai peninsula, can be ascribed to large variations in flood competence.

Alluvial fans have greatly diverse sizes, slopes, types of deposits, and source-area characteristics. They are most widespread in the drier parts of the world (Blissenbach, 1954; Suslov, 1961; Anstey, 1965; 1966), but occur also in humid regions (Butzer, 1965; Lustig, 1974) such as Japan (Sato, 1960; Murata, 1931a; 1931b; 1966; Yazawa *et al.*, 1971), in the Himalayan Mountains

**Figure 1** Alluvial fans northeast of Sheep Mountain, Arizona.
**a** Small, steep alluvial fan that coalesces with a much larger fan in the foreground.

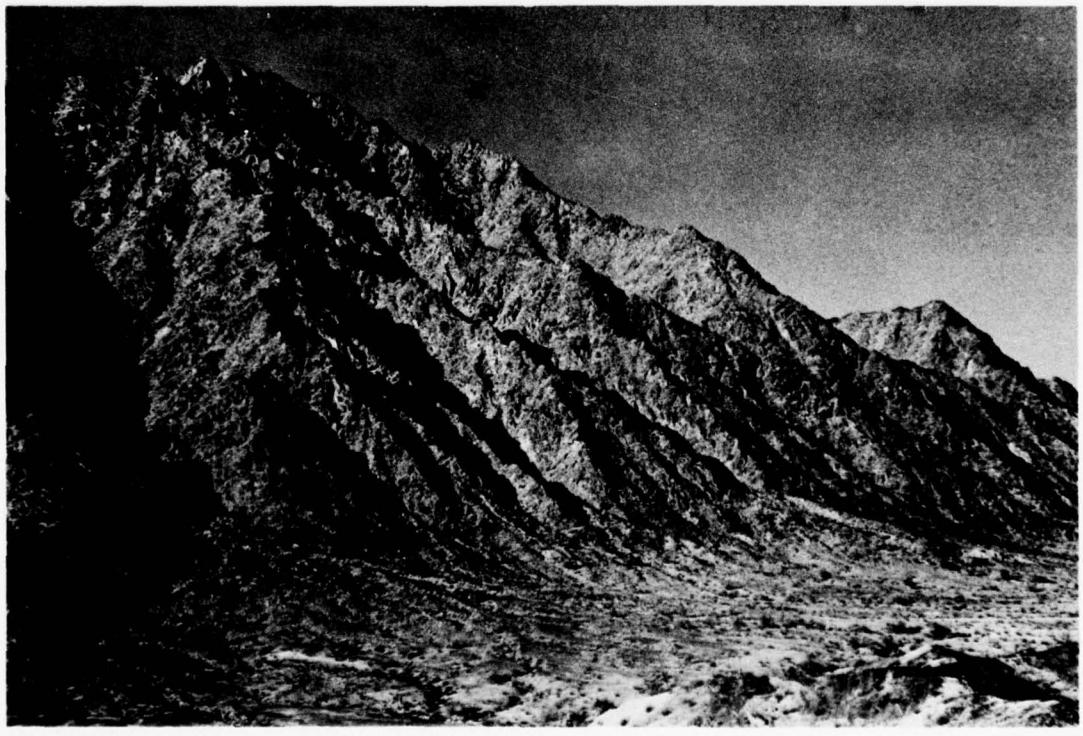

**b** Small alluvial fans that have been deposited at the base of an eroded fault scarp.

**c** Small fan that has a visible decrease in the size of the surficial material in the downfan direction. See text for discussion about decrease in maximum particle size.

(Drew, 1873; Gansser, 1964; Leopold *et al.*, 1964; Hurelbrink and Fehrenbacher, 1970), Canada (Winder, 1965), in Arctic regions (Anderson and Hussey, 1962; Rapp, 1962; Hoppe and Ekman, 1964; Legget *et al.*, 1966; Smith, 1972), in the tropics (Bond, 1949; Thomas, 1974, 129–30, 171, 276; Pain, 1973; Knight *et al.*, 1973), and in coastal areas (Cotton, 1918; Arnold, 1962).

The alluvial fans that are accumulating in various parts of the world have several characteristics in common. They occur in areas of decreased confinement of streamflow. Generally, they form as a result of base-level fall of the depositional area relative to the source area. Erosional base-level falls tend to result in temporary thin fans, and tectonic base-level falls tend to result in prolonged accumulation of thick fans. Deposition occurs as a result of the stream being unable to transport its load through the reach where the fan accumulates, either because of the decrease of confinement of streamflow, or because of changes in the sediment load being supplied to the stream from the hillslopes of the source area. An example of the latter cause would be changes in climate that increase sediment yields, and thus result in accelerated fan deposition.

Throughout this review, alluvial fans will be treated as parts of erosional–depositional systems. Sediment eroded from rocks within a mountainous source area is transported to a valley where it is deposited as another increment on the cone-shaped body of deposits. The stream is the connecting link between the erosional and depositional parts of the system, and is a dominant influence on the fan morphology. Changes in stream-channel slope, depth and width

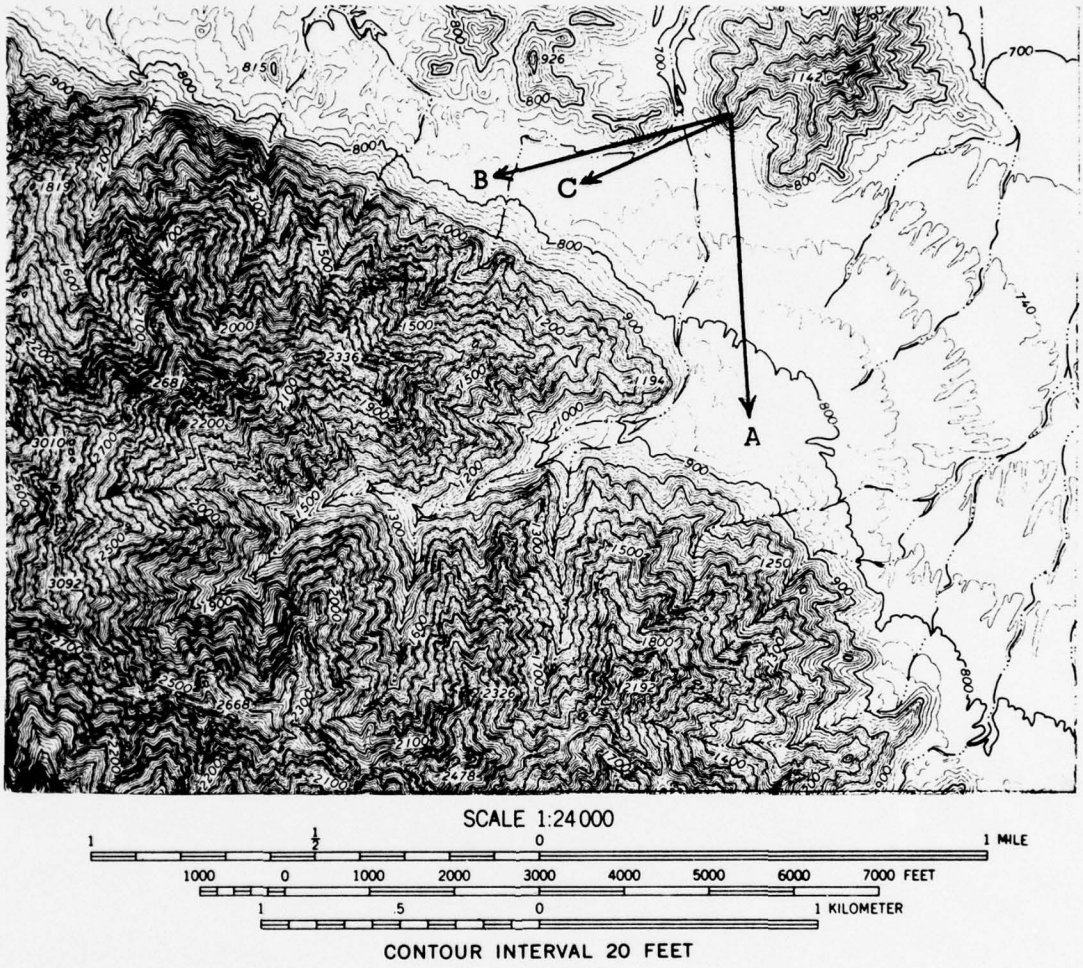


**Figure 2** Topographic map of the alluvial fans and their source areas northeast of Sheep Mountain in southwestern Arizona. The arrows and letters refer to the directions from which the photographs in Figures 1a, b, c were taken. From the United States Geological Survey Wellton Hills topographic quadrangle.

affect the slope, and loci and mode of deposition. Such changes may be caused by changes in discharge, of sediment and water, mode of transport, or by tectonic events.

Several conceptual frameworks have been used in studies of alluvial fans. Davis (1905) and his students regarded fans as indicative of conditions of youth in the cycle of erosion—'fan development is temporary, a mere incident in the geographic cycle' (Eckis, 1928, 247). Hack (1965) and Denny (1965; 1967) have used alluvial fans as examples to support the dynamic equilibrium (steady state) model. In their view, fans are disequilibrium landforms while they are growing, but increase in fan area will result in a balance between the amounts of sediment delivered to and eroded from a fan. Lustig (1965) and Bull (1976) have contended that it is highly unlikely that fans ever attain a steady state. A fan is an endpoint of an erosional–depositional system. Although streamflow processes, channel morphologies and area interrelations of adjacent alluvial

fans (Hooke, 1968) may tend towards steady states, a fan is a depositional landform that increases in volume. Overall degradation may exceed aggradation if the sediment yield of the erosional part of the system is reduced, or should the rate of accumulation of deposits be decreased in any other way. If erosion predominates, most of the surfaces of a fan are best considered as erosional slopes that are underlain by alluvium. For a fleeting instant of geological time the overall rates of fan deposition and erosion may be equal, but this instant should not be regarded as an attainment of steady state. Steady state not only implies time-independent landforms but also implies that, once achieved, steady-state conditions will persist as long as the independent variables of the system remain unchanged. Those who are interested in fans as growing landforms that are related to the erosional parts of their open systems may prefer to use the conceptual framework of allometric change (Bull, 1975a) where landscape elements are considered to be changing at different rates, and adjustment to relative rates of change is emphasized.

## II The depositional environment

### 1 *Streamflow hydrology on alluvial fans*

In 1909 Chamberlain and Salisbury introduced the unsubstantiated idea that fan deposition results from an abrupt change of stream gradient. Repetition of this false generalization, particularly in textbooks, has continued to the present despite contrary arguments and evidence published by Bull (1964a), Melton (1965), Denny (1965) and Hooke (1972).

The slopes of the upper parts of most alluvial fans are about the same as the stream-channel gradients immediately upstream from the fan apexes. Therefore alluvial-fan deposition is not caused by an abrupt decrease in stream-channel gradient. Deposition is caused by changes in the hydraulic geometry of flow after the stream leaves the confines of the trunk stream-channel (Bull, 1964a, 17). The trunk stream-channel may end at or upslope from the mountain front, or it may emerge from a reach entrenched into the fanhead at what has been termed the 'intersection point' (Hooke, 1967; Wasson, 1974; 1975). The stream discharge ($Q$) is equal to the product of the mean width ($w$), depth ($d$) and velocity of flow ($v$).

$$Q = wdv \tag{1}$$

A stream or debris flow spreads out when it reaches the end of a stream-channel on a fan. The increase in width is accompanied by concurrent decreases in depth and velocity, which are the primary causes of deposition of sediment. Discharge also may decrease when flowing over permeable surficial deposits, thereby tending to increase sediment concentration and cause deposition.

The proportion of an alluvial fan that is flooded by a low recurrence-interval flow varies with the size of the source and fan areas. Large flows may cover less than 5 per cent of fans that are larger than 100 km$^2$, particularly in arid regions. Flows of similar recurrence interval may cover more than 20 per cent

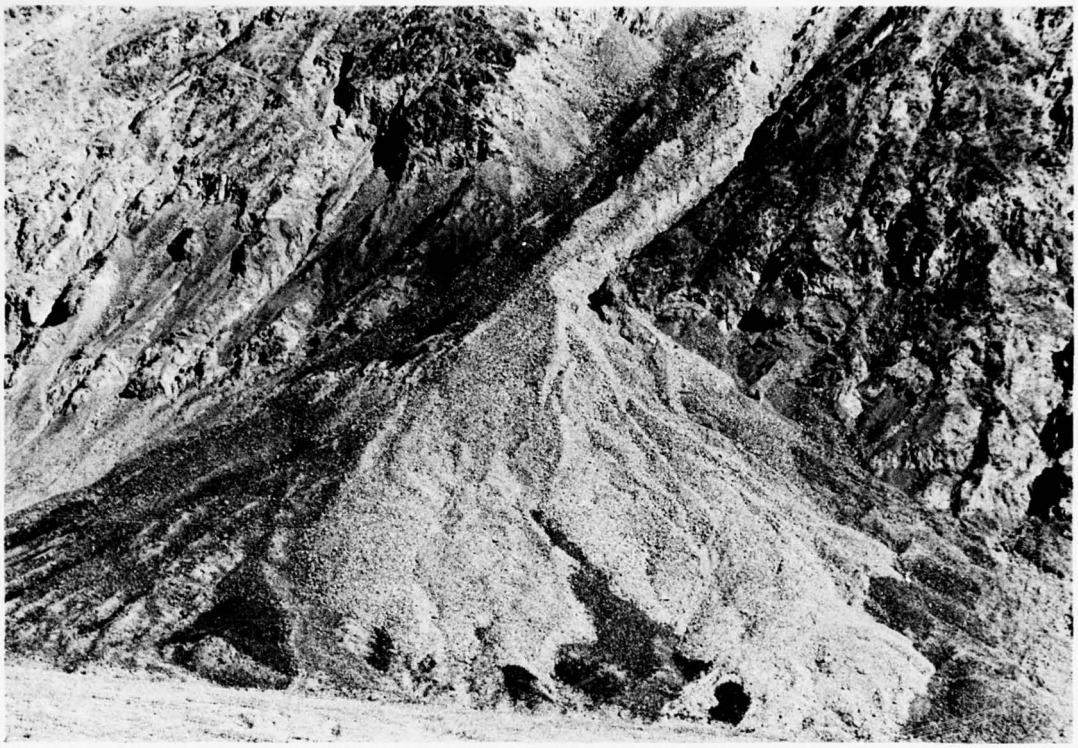

**Figure 3** *Different ages of debris flows on a fan of about 0.04 km²; east of the Copper* Canyon fan, Death Valley, California. Note the fault scarp cutting the fan deposits to the left of the centre debris flow.

of fans that are smaller than 1 km². An example is shown in Figure 3. The parts of the fan that have not received fresh deposits for several thousand years have been darkened by desert varnish. Two large debris flows cover much of the centre and right sides of the fan. The centre flow has been darkened slightly by desert varnish. The right-side flow has no varnishing of the surface materials, and has better preserved surficial flow features. The younger flow has also been the site of some smaller subsequent water flows. The two major flows that are chiefly responsible for the two depositional areas probably have a recurrence interval in excess of 1000 years. Along the edges of the Sinai Peninsula, fan areas are small compared to their source areas because the ocean removes part of the sediment deposited on the fans. A given flood event will inundate a larger proportion of the Sinai fans than similar-size fans that have been deposited in an alluvial basin.

Few measurements have been made of water and sediment discharge on alluvial fans. Difficulties in making such measurements include:

1 the infrequency and short duration of streamflows,
2 the presence of boulders in transport, or creating irregularities in stream-channels,
3 the difficulties inherent in measuring sheetflow, and flow in shallow rills, and

4 the large width for which streamflow should be measured in a short period of time.

A detailed study of streamflow on an alluvial fan that is part of a discontinuous stream system in southern Arizona has been made by Packard (1974). The stream system studied by Packard had the advantage of small size, and nearly all the sediment transported was sand-size and finer material. The Dead Mesquite fan (Figure 4) is 700 m long and has maximum width of 270 m. The 8.6 km² drainage basin upstream from the fan is underlain by sandy gravel with an extensive valley fill of clayey sediments. The maximum discharge measured in the fifth-order stream-channel upstream from the fan apex was 3.5 m³.

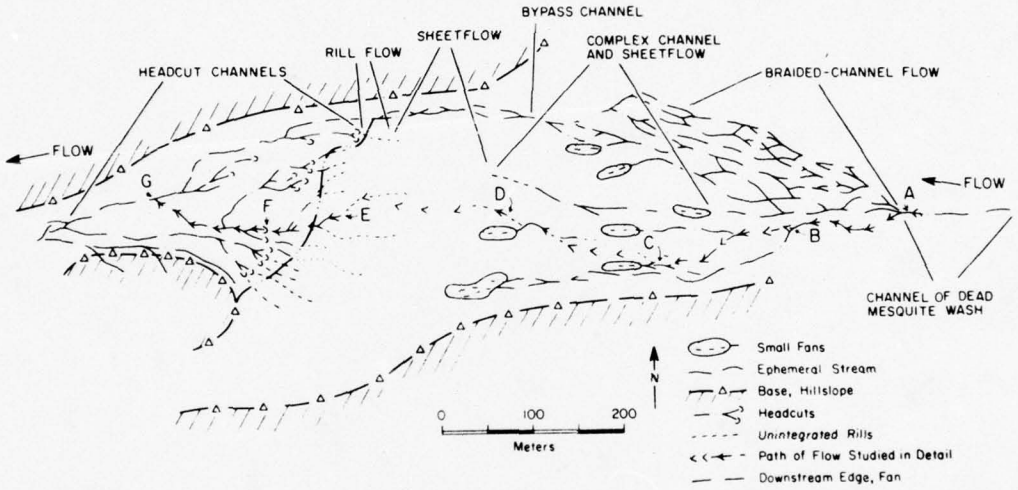


**Figure 4** Map of the Dead Mesquite alluvial fan, southern Arizona. After *Packard, 1974, Figure 25*

After streamflow leaves the trunk stream-channel, the flow on the Dead Mesquite fan consists of the following progression (Packard, 1974): flow in braided channels, complex channel flow and sheetflow, sheetflow, and rillflow that enters headcut channels at the toe of the fan. A bypass channel along the north side of the fan receives water from several tributaries as well as flow from the main channel. All the streamflow upstream and downstream from the fan is in entrenched channels. The above types of streamflow on the fan were measured along a single selected path of flow indicated by the arrows in Figure 4. In the fanhead area, flow is along wide shallow braided channels with a mean slope of 0.0053 (the trunk channel slope is 0.0042). The depth of the channels decreases downfan until at point C the channel ends (which would be the intersection point of Hooke, 1967). A miniature fan of coarse-grained sand occurs immediately downstream from the end of the channel along the path of flow studied in detail. Other similar miniature fans are common in the fanhead area, and each occurs where flow in shallow channels changes to sheetflow. The change to a surface where all the streamflow occurs

as sheetflow is accompanied by a marked increase in slope. Sheetflow surface slopes (points C–E) average 0.009. Local scour within the sheetflow reach has made several narrow incised channels into which part of the sheetflow is collected, only to spread out again at the end of the channel. These discontinuous channels are small-scale analogues of the large discontinuous stream.

The toe of the fan is characterized by the collection of water from sheetflow into rillflow. The rills are broad swales that are hardly noticeable, except during times of flow. Sheetflow may occupy much of the toe of the fan, but the flow velocities are much greater along the rills than between the rills. The rills end in headcuts that abruptly channelize all the sheetflow, and which represent an erosional modification at, and downslope from, the toe of the fan. The mean slope along the rills is 0.0102 and along the headcut channels it is 0.0116.

As is the case for most alluvial fans in arid regions, the area of modern streamflow is also the area of maximum density of vegetation. A mean annual precipitation of about 250 mm supports only a widely scattered growth of bushes on the hillslopes adjacent to the fan, but flow durations as long as 5 hours may occur on the fan. Small trees are the dominant type of vegetation in the area of braided-channel flow on the fanhead, but shrubs and grass are the most important vegetative cover in the sheetflow part of the fan (Packard, 1974). In the headcut channels downstream from the fan, practically no vegetation grows between the stream channels.

Important self-enhancing feedback mechanisms operate between the vegetation and streamflow. Prolonged sheetflow allows abundant water to soak into the clayey soil to support shrubs, grass and trees. The vegetation tends to disperse flow and maintain the sheetflow mode of streamflow. Slow flow velocities on the vegetated part of the fan promote deposition. Near the toe of the fan, flow becomes channelized once again, in part because of a decrease in sediment concentration. The formation of headcut channels is part of an opposite feedback mechanism that decreases infiltration and vegetation between the channels, thereby tending to enhance further erosion of channels.

Packard made hydraulic measurements of two 2.4 $m^3 s^{-1}$ flows on the alluvial fan. His observations are summarized in Figure 5. The graphs of bed slope and flow velocity change with the types of streamflow on the fan. The fanhead, characterized by braided channels, has a variable bed slope and a flow velocity that decreases downfan. Flow velocities are minimal on the sheetflood part of the fan despite the marked increase in bed slope downslope from the fanhead area. Low velocities in the sheetflood area are the result of the high hydraulic roughness due to decreased depth of flow and increased vegetative density. An increase in depths of flow in the channelized reach below the toe of the fan results in increased velocities. The graph showing flow depths and width–depth ratios in Figure 5 shows the marked change in mode of flow and an increase of two orders of magnitude in the width–depth ratio on the sheetflood part of a fan.

Packard collected scour and backfill data at nine stations along the channels

in the upper and middle parts of the fan. The data are for a variety of flows ranging from low- to high-stage. The scour-cord data indicates that low- and intermediate-stage flows cause net deposition along the channels, and that high-stage flows cause net scour of the channels on the fan.

The hydraulics of the fan studied by Packard are similar to those of larger alluvial fans. Most large alluvial fans do not have headcuts near the toe of the fan, chiefly because streamflow on most large fans occupies only a small part of the fan; whereas the Dead Mesquite fan is largely covered by sheetflow during times of major runoff. The presence of clayey deposits also favours the formation of headcuts. Large fans composed chiefly of sand and silt commonly have rills downslope from the area of promminent sheetflow, which indicates that deposition in an area of slow-moving sheetflow decreases sediment concentration so that a threshold is crossed and incipient erosion of channels can begin on the lower parts of fine-grained fans during certain large flow events.

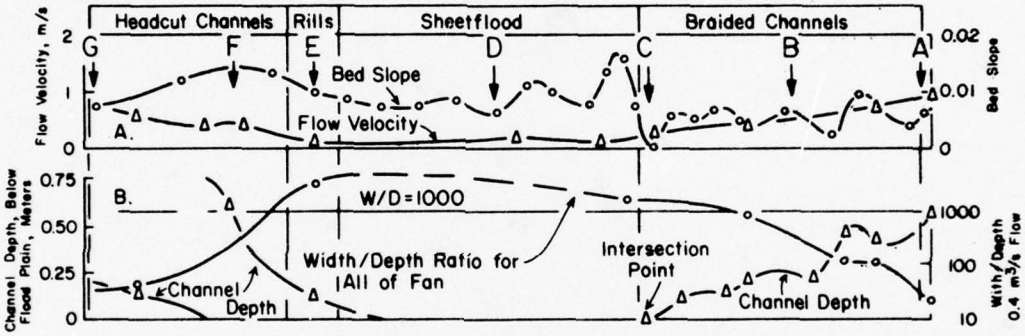


**Figure 5** Summary of hydraulic data for the Dead Mesquite fan. *After Packard, 1974, Figure 26*

**a** Graphs of bed slope and flow velocity. The letters A–G refer to the locations on Figure 4.
**b** Graphs of channel depth and width–depth ratio.

Fans that are much larger than the Dead Mesquite fan will have a greater range of discharges during the course of accumulation of fan deposits. The hydraulic model outlined by Packard's study of the Dead Mesquite fan should be regarded as suggestive of the processes that occur locally for time spans of a few years or decades on large fans. The longer-term hydraulic processes on large fans include marked shifts in the area of deposition along radial lines—shifts that are in part the result of depositional and fan-gradient contrasts in areas of braided streamflow and sheetflow. The irregularities created by hydraulic variations such as those described by Packard result in local variations in surficial topography of alluvial fans.

During the accumulation of an alluvial fan, stream-channel shifts may occur both across the fan and along the radial lines of the fan. Lateral migration of the area of deposition across the fan occurs when deposition has raised the fan surface sufficiently to favour shifting of the stream to an adjacent lower part of the fan. Minor shifts in stream-channel position near the fan apex may cause large changes in channel position on the downslope parts of the fan

**Figure 6** Braided stream deposits of Furnace Creek Wash, Death Valley, California. **a** Bar-and-channel topography in area of present-day streamflow.

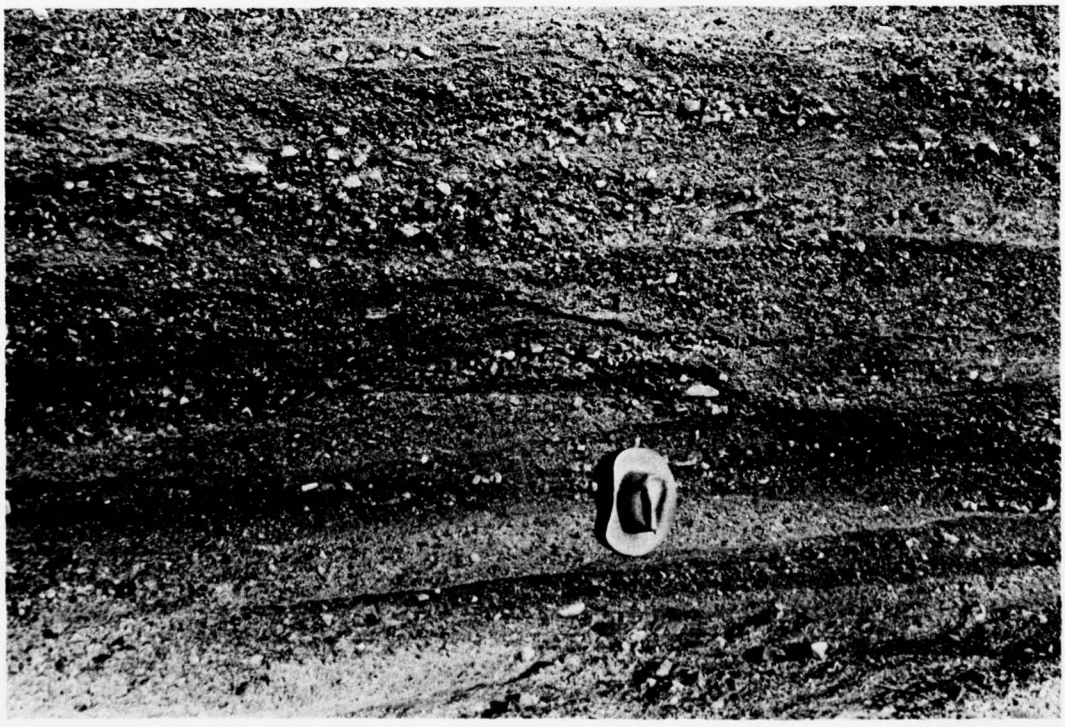

**b** Overlapping lenses of braided-stream deposits in an exposure normal to the direction of streamflow.

**c** Sequence of beds deposited by braided streams, *in exposure parallel to the direction of* streamflow.

(Denny, 1967). These changes in the area of fan deposition along the radiating streamflow lines from the fan apex are largely responsible for the fan-shaped plan view of the resulting deposit.

Migration of the depositional area along a given radial line occurs as a result of entrenchment or backfilling of the stream-channel extending from the source area. Fanhead trenches commonly extend half the length of a fan. Some streams are permanently entrenched, and may have channel bottoms that are as much as 50 m below a fan surface with an old soil profile. Other fanhead trenches appear to be temporary, being less that 15 m below a fan surface having no visible soil profile; and having been entrenched and backfilled one or more times before the present channel down-cutting.

Stream-channel entrenchment tends to mask trends in downfan particle-size distribution by providing a channel to transport streamflows to the downslope parts of fans that previously did not receive the coarsest part of the sediment load (Buwalda, 1951). Decrease in the maximum and the mean particle sizes on alluvial fans has been noted by many workers (Blissenback, 1952; 1954; Beaty, 1963; Drewes, 1963; Bull, 1964a; Ruhe, 1964; Bluck, 1964; and Hooke, 1967).

2 *Alluvial-fan deposits*

Alluvial fans have greatly differing lithologies. Some fans consist of organic silt (Leggett *et al.*, 1966, 21). Others consist largely of pebble- to boulder-size

material with minimal amounts of sand and silt (Hooke, 1967, 456). More than one mode of deposition occurs on most fans, and the proportions of different types of deposits may vary both vertically and downslope from the fan apex. The runoff that is supplied to the main stream-channel leading to a fan may be the result of rainfall or snowmelt runoff from all or part of a given basin. Thus differences in runoff characteristics, source, and amount of sediment load, mode of transport, and other factors vary greatly and are reflected in the individual beds preserved in the fan.

*a Water-laid deposits*: Two types of water-laid deposits can be found in most alluvial fans, and a third type occurs on fans with certain source-area conditions. Most of the water-laid sediments consist of sheets of sand, silt and gravel deposited by a network of braided distributary channels. The second type of sediment consists of fillings of stream-channels that were entrenched temporarily into the fan. The third type is sieve deposits (Hooke, 1967, 453–6), which are formed when the surficial fan material is so coarse and permeable that most discharges infiltrate the fan before reaching the toe.

Sheets of sediments are deposited by surges of sediment-laden water that spread out from the end of the stream channel on a fan. Depths of water generally are 0.1–0.5 m, and shallow distributary channels rapidly fill with sediments and then shift a short distance. The resulting deposit is commonly a sheet-like deposit of sand and gravel traversed by shallow channels, which repeatedly divide and rejoin.

Water-laid sediments commonly consist of gravel, sand and silt that contains little visible clay. Clayey sand may be the typical deposit on fans derived from source areas underlain by shale, mudstone and other clay-rich rocks. Waterlaid deposits may be well sorted and may be cross-bedded, laminated or massive. The characteristics of sediments deposited by braided streams are described in detail by Doeglas (1962).

Low bars and anastomosing channels characteristic of water-laid sheets of sediments on fans are shown in Figure 6. Deposition of low bars results in the lensing nature of most braided-stream deposits, which is readily apparent in exposures of fan deposits normal to the direction of flow (see Figure 6b).

Deposits that backfill stream-channels temporarily entrenched into a fan generally are coarser-grained and more poorly sorted than adjacent sheets of water-laid sediments that were deposited by braided distributary channels. Bedding of the channel-fill sediments may not be as well defined as for the sheet-like deposits. The thickness of individual beds ranges from less than 1 cm to more than 2 m, but bed thicknesses of 5 cm to 1 m are the most common.

If the source area supplies little sand, silt and clay to the fan, deposits may be sufficiently permeable to allow water from a flood discharge to infiltrate entirely before reaching the toe of the fan. Lobes of gravel deposited where the flow infiltrates decrease the local slope, which also tends to promote deposition. Hooke (1967, 453–6) has studied these lobate gravel deposits and has named them 'sieve deposits'. He stated that because 'water passes through

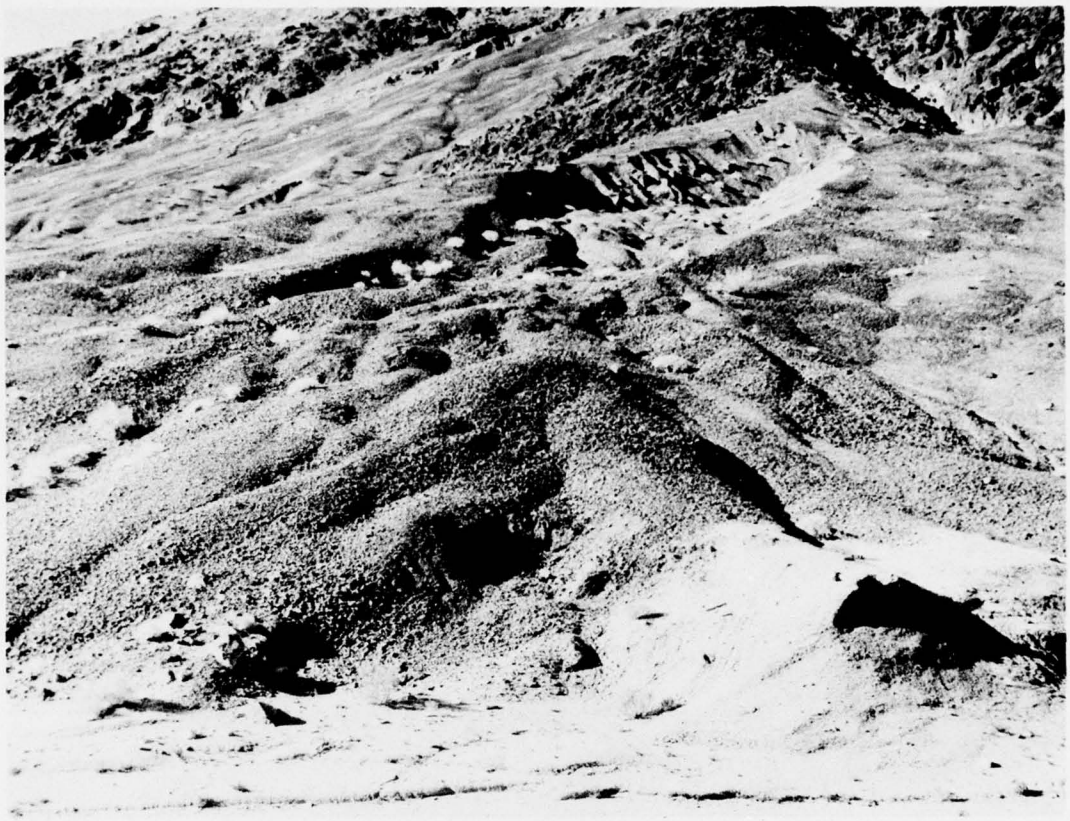

**Figure 7** Alluvial fan formed by sieve deposition, Eureka Valley, California. **a** Hummocky topography formed by sieve-deposit lobes. The slope is 16° along the medial radial line, and is 20° in the area of older and smoother fan surface to the right of the fanhead trench.

**b** Unvarnished sieve-deposit lobes in the fanhead trench shown in Figure 7a.

rather than over such deposits, they act as strainers or sieves by permitting the water to pass while holding back the coarse material in transport'. Sieve deposits are much less common than other types of water-laid alluvial-fan deposits, but are among the most distinctive. Sieve deposits on a small, steeply sloping fan are shown in Figure 7. Most of the surficial dolomitic gravel has been darkened slightly by desert varnish, thereby making the most recently deposited sieve lobes more obvious by their lighter tone. Each lobe may have a different particle-size distribution.

Unique source-area conditions are responsible for fans composed of sieve deposits. Source areas for sieve deposits are underlain by rocks such as jointed quartzite, and the clasts supplied to the fans are characteristically sub-angular blocks instead of well-rounded gravel. The excellent sorting of sieve deposits results in massive beds and poorly defined contacts between beds.

For additional information about processes on fans the reader is referred to Blackwelder (1954), Beaumont and Oberlander (1971), Karcz (1972), Cooke and Warren (1973) and Picard and High (1973).

*b Debris-flow deposits*: Water flows can selectively deposit part of their sediment load as a result of decrease in velocity or depth of flow. When a flow incorporates sufficient sediment, sediment entrainment becomes irreversible and the flow behaves more like a plastic mass (a Bingham substance according to Johnson, 1970, 496) than a Newtonian fluid. Debris flows have a high density and viscosity compared to streamflows (Fisher, 1971). Because of these traits debris-flow deposits are poorly sorted, are deposited as levees adjacent to stream-channels, and have lobate tongues with well-defined margins extending from sheet-like deposits on the fan surfaces. Debris flows are capable of transporting boulders weighing many tons. Factors that promote debris flows are abundant water (usually intense rainfall) over short periods of time at regular intervals, steep slopes having insufficient vegetative cover to prevent rapid erosion, and a source material that provides a readily available and abundant source of detritus and a matrix of mud. Viscous debris flows are most common near fan apexes (Hooke, 1967, 452; Crowell, 1954). Since the publication of Blackwelder's important paper (1928), publications about debris flows have treated theoretical, experimental and field aspects: Sharp (1942), Woolley (1946), Jahns, (1949), Sharp and Nobles (1953), Bagnold (1954; 1956), Kesseli and Beaty (1959), Rapp (1962), Bull (1962b; 1964a), Beaty (1963; 1968; 1974), Winder (1965), Hooke (1967), Pashaly (1967), Lindsay (1968), Landim and Frakes (1968), Oliferov (1970), Johnson (1970), Johnson and Rahn (1970), Fisher (1971), Morton and Campbell (1974), Price (1974), Campbell (1975), Pe and Piper (1975), Rodine and Johnson (1976).

Debris flows also occur on hillslopes (an erosional environment) (Conway, 1893; Rickmers, 1913), and in river valleys. However, debris flows are generally stored only temporarily in river valleys, because they are associated with terrains that produce rapid runoff, and are likely to be eroded by subsequent

water flows. Little erosion occurs on an actively aggrading alluvial fan; the fan environment is thus ideal for preservation of debris flows in the stratigraphic record.

The proportions of water-laid and debris-flow deposits vary greatly from fan to fan, and may change during the history of accumulation of a fan. Where source-area conditions are not conducive to the production of debris flows, the fan may consist entirely of water-laid sediments. Other fans consist mainly of debris flows (Schäfer and Schwab, 1975). Most fans whose source areas produce debris flows also have flood events that result in the deposition of water-laid deposits.

Part of a thick debris flow is shown in Figure 8a. Thick margins of lobate tongues of debris in the foreground indicate that the flow was highly viscous. the round protuberances further upslope are 1 to 3 m mud-covered boulders. The smooth surface of most of the flow is characteristic of fresh debris flows deposited on alluvial fans. Old debris flows commonly consist of surficial lobes and levees of cobbles and boulders, because rain splash has removed much of the matrix. Subsequent water flows may cut through the debris-flow deposits. The maximum thickness of the flow shown in Figure 8a is 1.3 to 2 m (Beaty, 1968, 18).

A mudflow is a type of debris flow that consists mainly of sand-size and finer sediment. Many workers use the term 'mudflow' in a genetic sense for *all types of debris flows, because a matrix of mud is the distinguishing feature* as contrasted with water flows (Blackwelder, 1928; Crandell, 1971).

The mudflow shown in Figure 8b consists of poorly sorted clayey sand. The viscosity of the flow was not great, as is indicated by the thin margins of the lobate tongue. The flow thickens rapidly inward from the margins and is 10 cm thick by the shovel. Although the flow contained virtually no material larger than 4 mm, the cobble train shown at the right side of the photograph was part of a lobate tongue of an earlier debris flow that transported larger particles. Polygonal desiccation cracks are characteristic of clay-rich mudflows that contain little gravel.

The bedding of debris-flow sequences is not usually well defined, but upon close examination, bedding planes between flows can be discerned in outcrops (see Figure 8c). Where interbedded with water-laid sediments, debris-flow beds are readily apparent.

The relative viscosities of debris flows can be obtained by study of the position and orientation of the the larger clasts. A low-viscosity debris flow will have graded bedding and a horizontal or imbricated orientation of the tabular gravel fragments. The more viscous flows have the larger clasts distributed uniformly throughout the flow (Figure 8c). The most viscous flows not only have uniform distribution of the larger clasts, but the tabular particles commonly have a vertical preferred orientation normal to the direction of flow.

Poor sorting is characteristic of debris flows. Many debris-flow deposits are so coarse grained that it is difficult to obtain a representative sample for determining the particle-size distribution of the material. As a result, few particle-

**Figure 8** Characteristics of debris flows.
**a** Debris flow on the Sparkplug Canyon fan, west side of the White Mountains, California.

size analyses have been made of debris flows (Crawford and Thackwell, 1931; Sharp and Nobles, 1953, 566). Bull (1964a) made 50 particle-size analyses of mudflows.

Logarithmic plots of the coarsest one-percentile versus median particle size may make patterns distinctive of depositional environments on fans (Bull, 1962b). Sinuous patterns indicate shallow ephemeral-stream environments. Rectilinear patterns indicate debris-flow environments.

3 *Stratigraphy of alluvial fans*

Two early workers who considered the stratigraphy of alluvial fans were Drew (1873) and Gilbert (1890). Some of the first workers to relate fans to adjacent deposits and Pleistocene chronology were Rickmers (1913), and Terra and Paterson (1939). Criteria for the recognition of alluvial-fan deposits in the stratigraphic record are discussed by Bull (1972a). Relations of fans to terraces have been discussed by Bull (1964b), Lustig (1965) and Pain and Pullar (1968).

The bedding of the deposits is one of the better methods of identifying the alluvial-fan environment in the stratigraphic record. Within a single outcrop

**b** Mudflow on the Santiago Creek fan, north side of the San Emigdio Mountains, California.

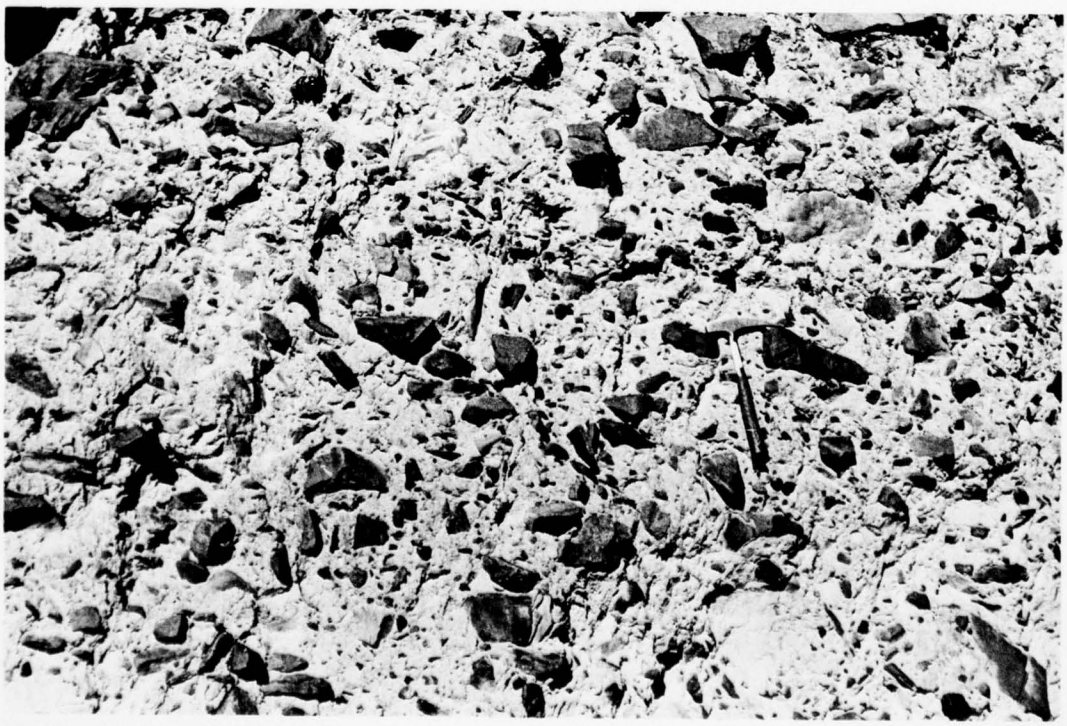

**c** Bedding of viscous debris flows, Johnson Canyon alluvial fan, Death Valley, California. The lower two-thirds of the photograph shows a single debris flow. Above the rock hammer is a band of finer gravel resulting from minor water flooding that reworked the top of the debris flow. The upper third of the photograph shows another debris flow that is coarser grained, and slightly lighter in colour.

**Figure 9** Bedding of the late Cenozoic alluvial-fan deposits, south side of the Catalina Mountains, Arizona.

a variety of strata can generally be observed, each bed representing hydraulic conditions for a flow event generated within the source area; which determined the thickness, particle size and distribution, particle orientation, and type of contact with the underlying bed. Even in fans composed entirely of water-laid sediments, differences in flow result in marked differences in the sedimentological characteristics of the beds. Bedding differences are even more striking in those fans composed of both water-laid and debris-flow deposits. The poorly sorted, massive beds of debris-flow deposits stand out in marked contrast to the beds of water-laid sediments.

Because most fan deposits were laid down as sheets, uniform thickness for a given bed is common in most outcrops, particularly for debris-flow deposits. Bed thickness of water-laid deposits is usually a function of the amount of relief between the bars and the braided stream-channels in the area at the time of deposition, and the degree of erosional modification by post-depositional flows.

An example of bedding variety is shown in Figure 9. The massive bed of uniform thickness above the hat consists of clayey gravel that was deposited as a viscous debris flow. Beneath the debris flow are beds of well-sorted water-laid sand. A 1 cm bed of water-laid clay immediately above the sands is typical of the waning phase of ephemeral water flooding on a fan, when the competence is sufficient to transport only silt and clay. Beds of poorly sorted, silty gravel occur above the debris-flow bed and beneath the water-laid beds. These

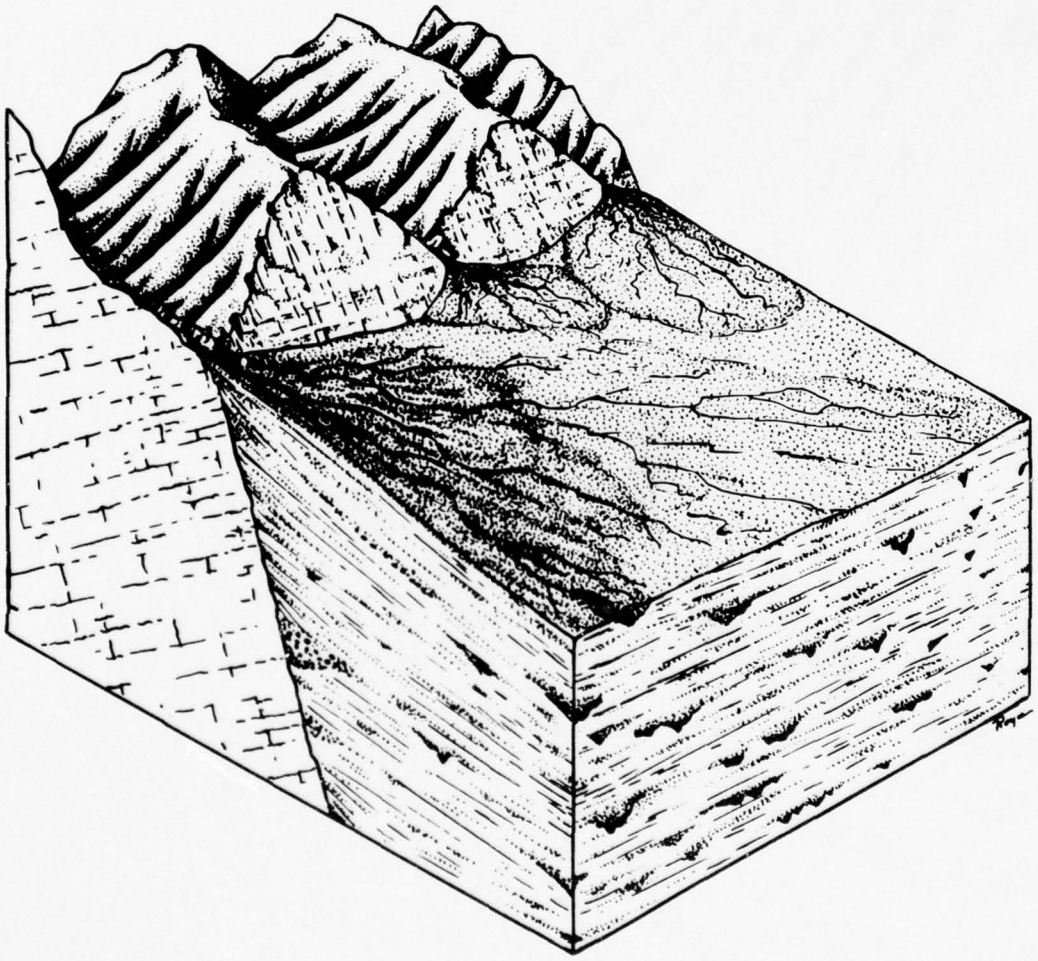

**Figure 10** A diagrammatic sketch showing the internal structure of a typical alluvial fan.

beds may be interpreted as low-viscosity debris-flow deposits, or as poorly sorted water-laid deposits.

The sheets and tongues of water-laid and debris-flow deposits of alluvial fans are generally 5–20 times as long as they are wide. The lengths of the sheets range from a few tens of metres to many kilometres. Exposures are not usually available to indicate the extent of the larger sheets comprising fans.

Although local variations of flow direction on a given fan may exceed 30° (Bull, 1972b, Figure 52), the lack of meandering channels on most fans results

AD-A069 729 ARIZONA UNIV TUCSON DEPT OF GEOSCIENCES F/G 8/7
ORIGIN AND DISTRIBUTION OF GRAVEL IN STREAM SYSTEM OF ARID REGI--ETC(U)
DEC 78 R GERSON, W B BULL, L H FLEISCHHAUER F49620-77-C-0115
UNCLASSIFIED AFOSR-TR-79-0681 NL

3 OF 3
AD
A069729

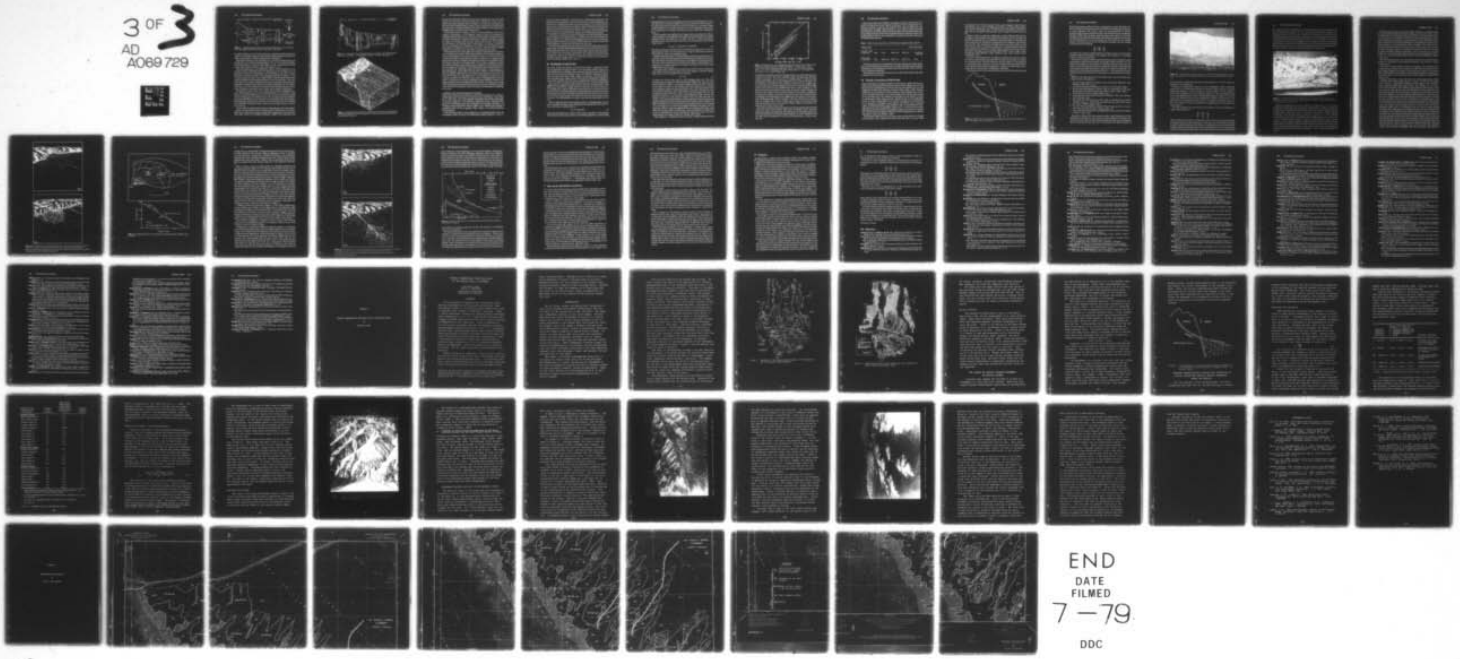

END
DATE
FILMED
7-79
DDC

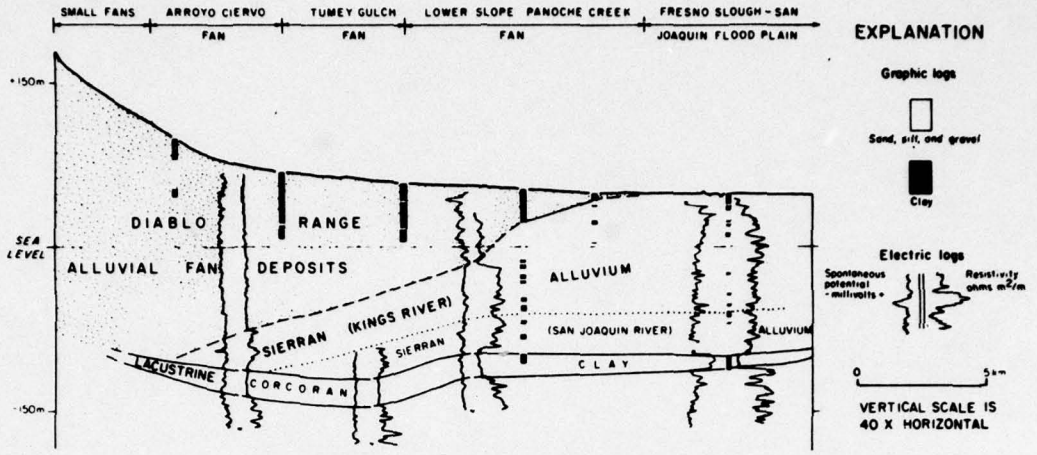


**Figure 11** Longitudinal section of fan deposits that are thickest adjacent to the mountain front. *After Magleby and Klein (1965, Plate 5).* (*From Figure 13. Bull 1972a*)

in a high consistency of current flow directions. Statistical studies by Howard (1966, 152) and Nilsen (1969, 50) indicate that a high consistency of flow directions is characteristic of ancient alluvial-fan environments.

Depositional hiatuses in fan deposition are commonly represented by soil profiles that have formed during periods of $10^3$–$10^6$ years while deposition occurred elsewhere on the fan. Soil profiles on fans are discussed by Ruhe (1964), Bull (1964b), Hawley (1965) and Lattman (1973).

The overall geometry of an alluvial fan reflects the accumulation of vast numbers of beds of differing extent and thickness, and the changes in loci of deposition caused by entrenchment and backfilling of the trunk stream-channel. The typical situation is shown diagrammatically in Figure 10. The area portrayed is one where recent uplift along a boundary fault has induced rapid accumulation of fan deposits adjacent to the mountain front. The truncated ends of the ridges extending out from the mountains form triangular-shaped facets similar to those shown in the right side of Figure 1b. The surface of the fan is not entrenched and is traversed by braided distributary streams, some of which are associated with the most recent episode of deposition.

Considerable variety exists in the radial and cross-fan stratigraphic relations. Along radial sections of a fan, individual beds may be traced for long distances, and channel-fill deposits are rare. In contrast, the cross-fan sections reveal overlapping beds of limited extent that are interrupted by backfilled stream channels. Because some channels were entrenched only a short distance downslope from the fan apex and others were entrenched as far as the midfan area, backfilled channels are most common near the apex and rare near the toe of the fan.

The overall shape of alluvial fans may be wedge-shaped or lenticular. Figure 11 shows a wedge of deposits that is thickest near the mountains. In this area, uplift of the mountains occurred mainly before deposition of the Corcoran Lake Clay, which is only slightly deformed. Uplift of the mountains has

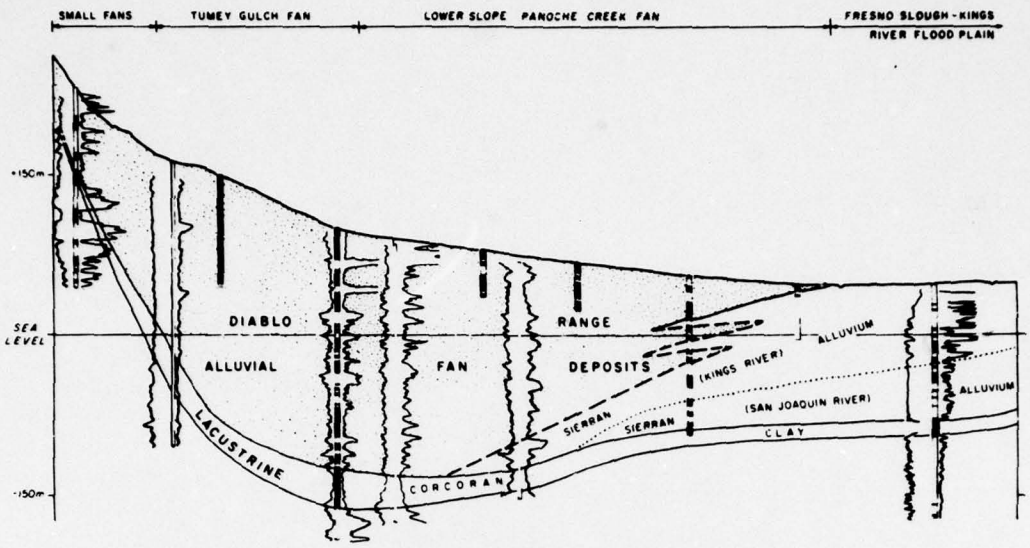


**Figure 12** Longitudinal section of fan deposits that are lenticular. *After Magleby and Klein (1965, Plate 4)*. See Figure 11 for explanation of symbols. *(From Bull, 1972a, Figure 14)*

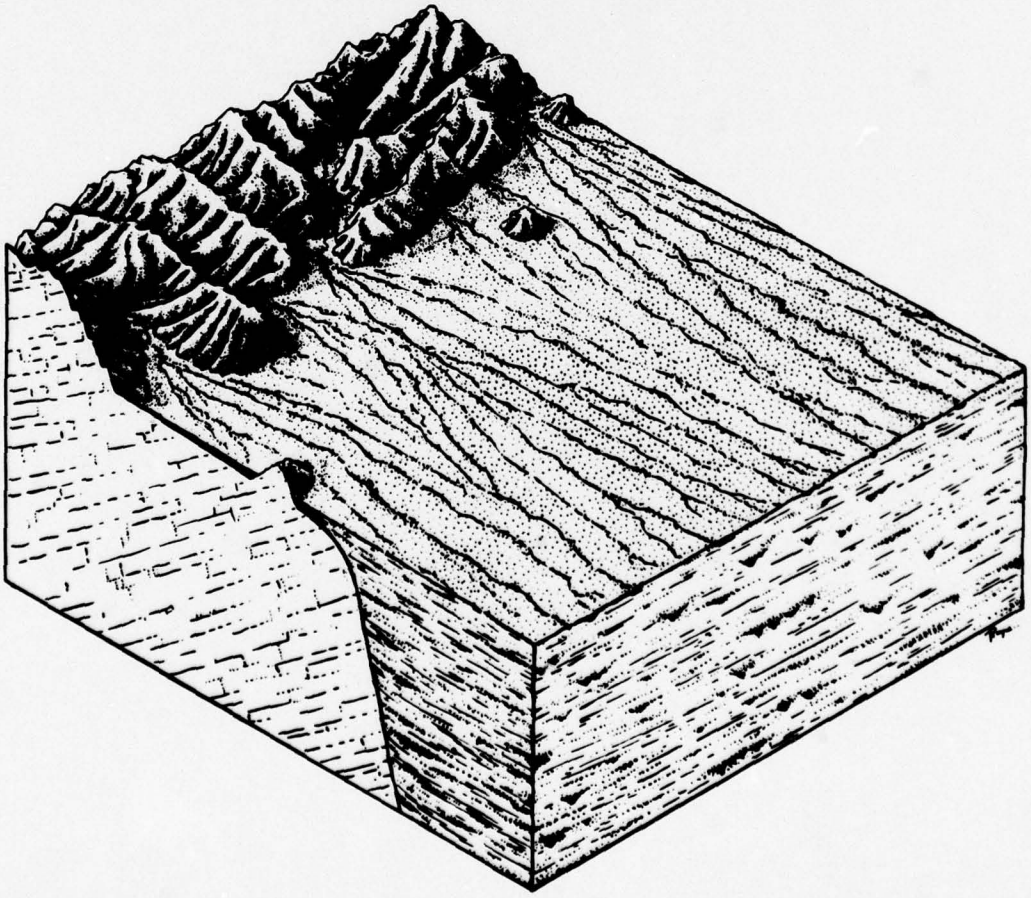

**Figure 13** Diagrammatic sketch showing a tectonically stable terrain with a single erosion surface that truncates the rocks of the mountains, the fault, and the alluvial fans that had been deposited in the basin.

increased the sediment yield of the source areas, and fans that were only 4 km long at the end of the lacustrine period have expanded to 35 km. A lens-shaped mass of fan deposits is shown in Figure 12. In this case, the Pleistocene lake clay has been folded along its western extent, along with an undetermined amount of the overlying fan deposits. The largest thickness of post-pluvial fan deposition have occurred in the midfan area.

The relations shown in Figures 11 and 12 reveal the influence of an active orogenic environment—an environment typical of thick accumulations of young fan deposits (Beaty, 1970). After the tectonic uplift of a mountain ceases, the stream will continue to downcut within the mountains, and will eventually cut below the altitude of the fan apex (Eckis, 1928, 237–8). The resulting entrenchment of the fanhead may be permanent if it removes the fanhead area as a potential area of deposition. The surface of a fan may lose much of its aspect of a segment of a cone after extensive erosion of the fan deposits upslope from the point where the stream intersects the fan surface.

Continued lack of tectonic uplift will change the depositional environment to an erosional environment where pedimentation is the main process operating on the landscape. The typical situation of those parts of the world with a basin-and-range structural setting is shown in Figure 13. A highly eroded mountain front has retreated from its original location at the buried fault scarp. Remnants of the former mountain mass now rise above a pediment mantle traversed by shallow stream-channels that transport new debris derived from the mountains, and rework the weathering products from the pedimented surface and alluvium. Downslope from the buried fault is a thick sequence of basin-fill deposits, whose upper part has been eroded so that the alluvium has an erosional surface that is an extension of the sediment. The beds of the basin fill continue for long distances in the downslope direction, but the exposure parallel to the mountain front reveals overlapping beds of limited extent interrupted by numerous backfilled stream-channels—features that suggest that the basin fill was deposited as alluvial fans. In this case, the change from a depositional to an erosional environment may have removed more than 100 m of surficial fan deposits, and has destroyed the depositional morphology of the fans.

### 4 *Relation of fans to adjacent depositional environments*

Alluvial-fan deposits are commonly in contact with adjacent fans or deposits of flood-plain and lacustrine environments (Hunt and Mabey, 1966; Vita-Finzi, 1969; Hunt, 1975). The deposits of individual alluvial fans interfinger in zones of coalescence. The distinctive lithologies between individual fans derived from differing source-area lithologies are discernible through use of lithology studies of gravel-size detritus (Miall, 1970), differing percentages of components such as clay or gypsum (Bull, 1964a), or by electric-log data from boreholes.

If the downslope edge of a fan is adjacent to a through-flowing stream, the fan deposits will be in contact with flood-plain deposits (Figures 11 and 12).

If the rate of fan deposition exceeds the rate of flood-plain deposition, the fans will tend to expand their area by encroachment over the flood-plain area until the rates of deposition of the two areas are equal. In the western Fresno County area, accelerating rates of sediment yield during the last 600 000 years (the age of the top of the lake clay (Janda, 1965, 131)) and the tendency towards equal rates of accumulation of the various types of basin-fill deposits have resulted in overlap of the fan deposit on the flood-plain deposits.

The tendency towards equal rates of deposition among coalescing alluvial fans and between fans and the playa in a closed basin has been described by Hooke (1968, 614–16). Hooke's model suggests that the areas of accumulation of fan and playa deposits are directly proportional to the volumes of materials being supplied to each fan and the playa per unit time.

In closed basins, pluvial lakes may have formed and inundated parts of the alluvial fans. Lake beds deposited during pluvial intervals form extensive blanket-like deposits that occur as layers in the sequence of fan deposits (Smith, 1968). Where the areal extent of a lake bed can be defined in the subsurface, the upslope extent of the lake beds will not only depict the location of the shoreline, but also the fan contour at that point in history of accumulation of the fan deposits (Miller *et al.*, 1971, 31).

## III Morphology of alluvial fans

The areas, slopes and deposits of alluvial fans record a tendency towards mutual adjustment among a complex set of controlling variables. These variables include the area, lithology, mean slope and vegetation cover of the source area; slope of the stream-channel, water and sediment discharge, climatic (Tricart, 1966) and tectonic (Bull, 1964b) environment; and the geometry of the mountain front, adjacent fans, and the basin of deposition. Changes in one or more variables will tend to cause a readjustment of the fan morphology.

The concentric contours and fan-shaped plan view of many alluvial fans suggests that the shape of the deposit can be expressed mathematically. If the gradient of a fan did not change, and if its contours were true circular arcs, it is configuration could be expressed by the equation for a circular cone. Few fans meet these requirements because the slope generally decreases downslope from the fan apex; and, for most fans, only parts of the contours are true circular arcs about a given point. The typical fan has both concave and convex curvature—the radial profiles are concave, and the cross-fan profiles are convex.

Troeh (1965) has derived an equation which, by changing signs, may be used to describe four basic types of landforms. His equation for the concave–convex curvature of alluvial fans is:

$$Z = P + SR + LR^2 \qquad (2)$$

where $Z$ is the altitude of any point on the surface of the fan. $P$ is the altitude of the theoretical fan apex, and may be located graphically by constructing

perpendiculars to two or more tangents to a contour that approximates a circle. The altitude of $P$ usually is higher than the true altitude of the fan apex. $S$ is a slope of the theoretical fan at $P$, and $L$ is half the rate of change of slope along a radial line. $R$ is a radial distance from $P$. The equation can be solved for a specific fan by making measurements along radial lines topographic maps.

Troeh's equation was applied to the Copper Canyon alluvial fan in Death Valley, California. Although this fan has segmented radial profiles, the change of slope between fan segments is not large. The fan is a fairly symmetrical segment of a cone whose contours make 180 arcs. The equation for the Copper Canyon fan is:

$$Z = 49\ \text{m} - (93/\text{km})R + (12/\text{km}^2)R^2 \qquad (3)$$

Discrepancies between estimated and true altitudes average only 2 to 3 m, less than a quarter of the 15 m contour interval—except for the extreme northwest side of the fan, which is anomalously steep.

Mathematical descriptions of individual fans using Troeh's general equation provide a means of describing variations of depositional landforms. Such equations also define anomalies of fan geometry and suggest the depositional processes that cause anomalies from the general fan shape as determined by the equation. An example would be the presence of steeper lateral slopes than medial slopes on most fans.

The area of a fan is influenced by many factors. One of the most important is the effect of the size of the source area of the deposits. A general relation (Bull, 1962a) can be expressed by the equation:

$$A_f = cA_d^n \qquad (4)$$

in which $A_f$ is the fan area, and $A_d$ is the drainage basin area. Fan area/drainage-basin area plots for widely spaced suites of fans in the western United States are shown in Figure 14. The plots roughly parallel each other and have a mean slope ($n$) about 0.9. The mean value of the exponent of 0.9 is similar to the exponent of the power function between source area and sediment yield as determined by Brune (1948). In Equation 4, fan area is serving as a proxy for sediment yield. However, Lustig (1965, 134) has pointed out that one should be careful not to use fan areas as a sole indicator of fan volumes. The relation between fan areas and fan volumes may vary from one basin to another, with small enclosed basins having small thick fans and large open basins having large thin fans. Furthermore, fan area/fan volume relations will differ if deposition is concentrated near the mountain front, or if it is spread out over a large area as a result of prolonged deposition downslope from the mountains. Hooke (1968) has suggested that an exponent of less than unity reflects lower mean slopes of large source areas as compared to small source areas, less likelihood of a storm covering the large source areas, and more opportunities for storage of alluvium in larger source areas.

The coefficient, $c$, of Equation 4 has more than a tenfold variation because

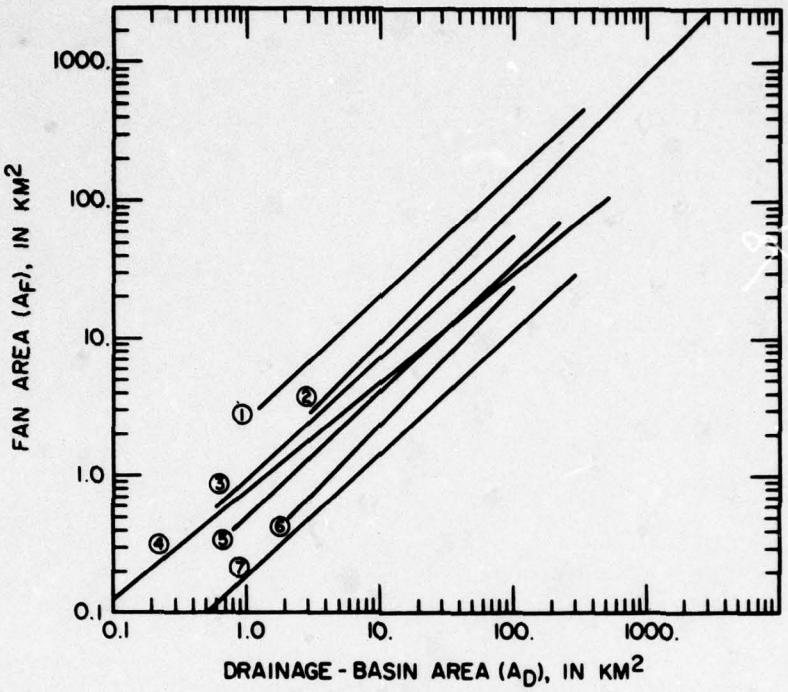


**Figure 14** Relations of fan area to drainage-basin area for groups of fans in California and Nevada. The equations and sources of data are as follows: (1, 2) $A_f = 2.1A_d^{0.91}$, $A_f = 0.96A_d^{0.98}$, least square revisions from *Bull (1962)*; (3) $A_f = 0.74A_d^{0.98}$ (*Hawley and Wilson, 1965*); (4) $A_f = 0.5A_d^{0.8}$, depositional parts of fans (*Denny, 1965*); (5, 6, 7) $A_f = 0.42A_d^{0.94}$, $A_f = 0.24A_d^{1.01}$, $A_f = 0.15A_d^{0.90}$ (Hooke, 1968).

of the effects of variables other than drainage-basin area which affect fan areas of different localities. The other variables include drainage-basin lithology, climate, mean slope, and the amount of available space in which fans can be deposited. Within a given basin of deposition, such as the San Joaquin Valley, California, fans derived from mudstone source areas are roughly twice as large as those derived from sandstone source areas of comparable size (Bull, 1962a). This is shown by the coefficients for lines 1 and 2 in Figure 14. The fans derived from the mudstone source areas are also the thickest and the differences in fan volume can be attributed largely to the greater erodibility of the mudstone and shale. Extremes in fan size that may be attributed largely to lithology can be illustrated by the coefficients of sets of fans in the San Joaquin and Deep Springs Valleys, California. The fans derived from mudstone areas are roughly twice the size of their source areas, but the fans derived from the quartzite source areas studied by Hooke (1968) are only about one-sixth the size of their source areas.

The effect of tectonic activity on the sizes of fans on opposite sides of Death Valley was noted by both Hooke (1968; 1972) and Denny (1965). Eastward tilting of the valley has caused the west-side fans to be extended, and the toes of the east-side fans to be buried by playa deposits. Tectonic tilting has been the chief cause of coefficients of 1.05 for the west-side and 0.15 for the east-side fans.

Many of the factors that influence the slopes of streams also influence the slopes of alluvial fans, but the relative importance of the variables may vary between localities. In general, fan slope decreases with increasing fan and drainage-basin size (Bull, 1962a; Beaumont, 1972). Hooke (1968) concluded from laboratory and field studies that fans produced by small discharges had steeper slopes than fans produced by large discharges and that fans constructed largely by debris flows or sieve deposition were steeper than fans constructed by other fluvial processes.

**Table 1** Effect of mode of deposition on alluvial-fan slope (*modified from Hooke, 1968, 626*)

| Steepest slopes | | | | | Most gentle slopes |
|---|---|---|---|---|---|
| Dominant mode of deposition | Sieve | Sieve | Debris flow | Water-laid | Fine grained water-laid |
| Other modes of deposition | None | Debris flow | Water-laid | Debris flow | None |

Steeper fan slopes also are associated with larger particle sizes. Bull (1964b, 95) concluded that fans derived from source areas with high rates of sediment production were both larger and steeper than fans from source areas with low rates of sediment production.

The importance of tectonic environments on alluvial-fan slopes is discussed in detail in the next section.

## IV Tectonic environment of alluvial fans

Thick alluvial fans are orogenic deposits, not only because uplift creates mountainous areas that provide debris and increased stream competence, but also because the loci of deposition on alluvial fans are controlled by the rate and magnitude of uplift of the adjacent mountains (Bull, 1964b; 1968). Optimal conditions for accumulation of thick sequences of fan deposits occur where the rate of uplift exceeds the rate of downcutting of the trunk stream-channel at the mountain front. The orogenic interpretation of fan deposits is useful in evaluating the thick sequences of fan deposits found in the stratigraphic record. A variety of discussions of the tectonic environment of alluvial fans are in the papers of Pumpelly (1905), Berkey and Morris (1927), Longwell (1930), Teilhard de Chardin (1933) and Beaty (1961). Initial deposition, faulting, erosion and renewed deposition of fans may be a common but unrecognized sequence of events because of insufficient exposures or burial by younger fans. Two of the better studies of this aspect of fan stratigraphy are by Berkey and Morris (1927) and Pashley (1966).

Small alluvial fans may occur in areas of non-tectonic base-level change, such as where a river or glacier has eroded the trunk valley at a more rapid

rate than have the tributary streams (Cotton, 1922; Suggate, 1963; Carryer, 1966; Ryder, 1971a; 1971b; McPherson and Hirst, 1972; Church and Ryder, 1972; Roed and Wasylyk, 1973). The first extensive description of fans (Drew, 1873) was in a paraglacial setting, rather than a setting of tectonic base-level fall.

Climate is also an important independent variable affecting alluvial fans. Changes in entrenchment of the trunk stream-channel and in the mode and loci of fan deposition that are ascribed to climatic changes are discussed by Lustig (1965, 183–6). Periods of accumulation of thin temporary alluvial fans may coincide with climatically controlled times of increased sediment yield of the source areas, or decreased competence of transportational processes across piedmonts of pediment or glacis origin. Temporary fans that may be ascribed to this origin occur in the study areas of Bond (1949), Czajka (1958), Mensching (1958), Mabbutt (1966), Williams (1970; 1973), Werner (1972) and Busche (1972).

In order to understand better the effects of uplift on alluvial-fan systems, one has to consider all processes that affect the altitude of a point on a stream at a mountain front—the local base-level tectonic uplift ($u$), fan deposition ($s$) and channel downcutting ($w$). The rate of uplift of the mountains relative to the adjacent basin, either by pulsatory or continuous uplift, largely determines the loci and thickness of alluvial-fan deposition.

The diagrammatic cross-section of Figure 15 shows the interrelations of local

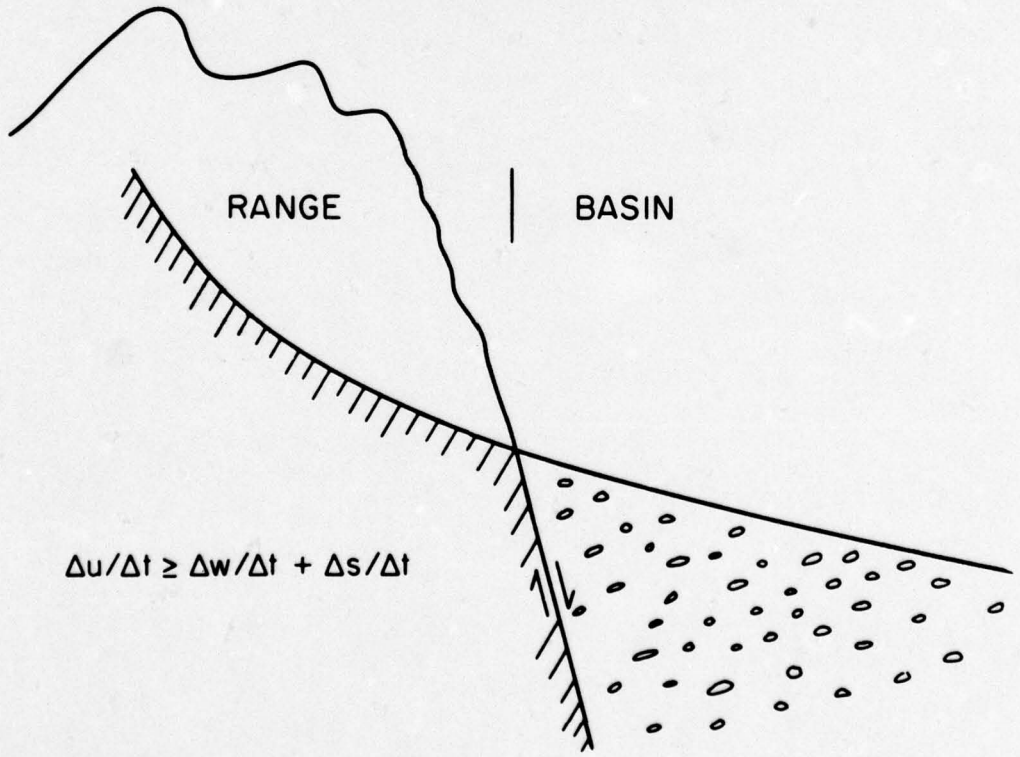


**Figure 15** Diagrammatic cross-section showing conditions that favour the accumulation of alluvial-fan deposits next to the mountains.

base-level processes conducive for the accumulation of thick alluvial-fan deposits. The base-level processes of either channel downcutting in the mountains or basin deposition will tend to cause the stream-channel to become entrenched into the apex of the alluvial fan, and thus shift the loci of deposition downfan. Uplift of the mountain range counteracts the tendency to entrench the fanhead. The uplift also allows both channel downcutting in the mountains and fan deposition next to the mountains, but only when the rate of uplift equals or exceeds the sums of the two base-level processes that are tending to cause fan-head trenching.

$$\frac{\Delta u}{\Delta t} \geqslant \frac{\Delta w}{\Delta t} + \frac{\Delta s}{\Delta t} \tag{5}$$

As long as the amounts of uplift equals or exceeds the sums of the amounts of downcutting and deposition, fan deposits will continue to accumulate adjacent to the mountain front.

Some of the rift valleys of the world provide ideal tectonic settings for rapid accumulation of alluvial-fan deposits. An example is shown in Figure 16. The alluvial fans along the eastern margin of the Sinai Peninsula are steep and consist of water-laid gravel that has an indissected surficial morphology and only minimal soil-profile development, indicative of rapid accumulation. The typical alluvial fan along this mountain front is not entrenched and the interrelations between the local base-level processes are those described by Equation 5.

Deposition of thick sequences of fan deposits have occurred during many orogenic periods. Examples are:

1 the fan deposits along the northwest coast of Scotland (Maycock, 1962; Williams, 1966; Steel, 1974);
2 the late Precambrian Kewenawan red beds of the Canadian shield;
3 the Devonian fan deposits of Norway that are associated with the post-Caledonian Svalbardian disturbance (Nilsen, 1968a; 1968b; 1969);
4 the Devonian of Arctic Canada (Miall, 1970);
5 the Pennsylvanian Fountain Formation of Colorado (Tieje, 1923; Hubert, 1960; Howard, 1966;
6 the Triassic Newark Group associated with the Appalachian revolution (Dunbar, 1949, 311–16; Krynine, 1950; Reinemund, 1955; Klein, 1962);
7 the Triasic of Wales (Bluck, 1965);
8 the early Tertiary fanglomerates of the Rocky Mountains that are associated with Laramide tectonism (Sharp, 1948); and
9 the late Tertiary deposition in the Ridge Basin area of southern California (Crowell, 1954; 1974).

Equation 5 requires that the minimum relative uplift associated with the alluvial-fan environment is more than the thickness of preserved deposits. The amount of stream-channel downcutting during a specified span of geological time is not known for most sites, but on the basis of the limited amount of

**Figure 16** Unentrenched alluvial fans along the east side of the Sinai Peninsula west of the Neviot. The rapid rate of accumulation of these fans can be described by Equation 5 of the text.

data presently available channel downcutting appears to at least equal the thickness of fan deposition.

Thickness of alluvial-fan deposits in the stratigraphic record commonly exceed 3000 m, and therefore represent evidence of large amounts of vertical differential uplift of ancestral mountain ranges relative to their adjacent basins. The conglomerate and sandstone adjacent to the San Gabriel fault scarp of the Ridge Basin area has a stratigraphic thickness of 8000 m (Crowell, 1954). The Newark Group in the Appalachian region exceeds 6000 m, and the Devonian fan deposits in Norway have a maximum thickness of 5000 m. Even the remnants of the Precambrian Torridonian fans of Scotland are 2400 m thick.

The interrelations of base-level processes conducive to the development of incised alluvial fans are

$$\frac{\Delta u}{\Delta t} < \frac{\Delta w}{\Delta t} > \frac{\Delta e}{\Delta t} \tag{6}$$

where $u$ and $w$ are the same as in Equation 5 and $e$ is the erosion of the alluvial-fan deposits adjacent to the mountains. In this case, the rate of long-term uplift is relatively less than indicated by Figure 15 and Equation 5. Since intermittent to slight uplift is continuing or has occurred sufficiently recently in the geological past, the fanhead morphology of these alluvial fans has not been destroyed

by erosion. The loci of deposition have permanently shifted downslope from the mountain front because the rate of stream-channel downcutting at the mountain front exceeds the rate of uplift at the mountain front. Thus, the fanhead area has been removed as a possible area of deposition and the degree of soil-profile development will provide clues as to the length of time since the fanhead area last received deposits. The complete and intense weathering profiles that are characteristic of the fanhead areas of many entrenched alluvial fans also indicate that the rate of erosion of the abandoned depositional surface has been less than the mean rate of soil-profile development.

**Figure 17** Entrenched alluvial fan of Hanuapah Canyon, Death Valley, California. The interrelations of the base-level processes that resulted in the fanhead trenching of this fan are described by Equation 6 of the text.

Fanhead trenching may also be temporary, lasting only $10^1$ to $10^4$ years compared to the permanent entrenchment discussed in relation to Equation 6. Fanhead trenching caused by climatic variations has been studied in detail by Bull (1964b) and Wasson (1975). Schumm (1973) points out that changes in climatic and tectonic factors need not be present to cause channel entrenchment, and that entrenchment and backfilling of stream systems may occur as complex response patterns. Weaver and Schumm (1974) demonstrated a case of complex response as applied to fanhead trenching of a physical model. The entrenchment of the fans of discontinuous ephemeral streams, such as the one discussed by Packard (1974), has been the topic of discussion of many workers including Schumm and Hadley (1957) and Cooke and Reeves (1976).

The Hanaupah Canyon fan in Death Valley, California, is a good example of a permanently enriched alluvial fan. Deposition occurred initially at the mountain front, then along the north side of the fan (the right side of Figure 17), and then in the central part of the fan but still further downslope. Only minor faulting has occurred at the mountain front, as is indicated by the few fault scarps that cut the fanhead. Although vertical differential uplift may be still occurring at the mountain front, the rate of uplift is lower than the rate of channel downcutting at the mountain front. These relative rates of local base-level processes conform to the format of Equation 6 and have resulted in modern deposition being concentrated at the toe, instead of at the head of the fan. A vertical aerial photograph of the fan has been published by Denny (1965, 34), and a geomorphic map of the fan has been published by Hooke (1972, 2079).

With decreasing tectonic activity, pediments become the typical landform and can be described by three additional equations (one of which is shown by Bull, 1973).

The slope of an alluvial fan is sensitive to changes of the erosional–depositional system. Changes in the erosional area affecting the depositional area by causing changes in the stream connecting the two parts of the system. Bull (1964b) showed that changes in stream-channel gradient resulting from tectonic or climatic events in the mountains caused changes in the depositional slope of a fan.

Changes in fan slope can be observed in the radial topographical profiles of most fans. The overall profiles are gently concave, but they are not smooth curves. Instead, a radial profile comprises several straight or, less commonly, concave segments (Bull, 1961, 1964b; Denny, 1967; Hooke, 1972). The surfaces of the fan segments form bands of approximately uniform slope, which are concentric about the fan apex. The development of one type of fan segmentation is shown in Figure 18. Figure 18a shows an initial condition where alluvial-fan deposits are accumulating immediately adjacent to the mountain front. The steam issuing from the mountain front does not undergo an abrupt decrease in gradient where it enters the piedmont. Instead the stream and the depositional area on the fan have about the same gradient (Bull, 1964b, 100–2). The hypothetical fluvial system sketched in Figure 18a is changed by a period of tectonic activity during which several tens of metres of vertical differential uplift occurs at the mountain front as a result of either folding or faulting. The uplift induces trenching headward from the mountain front, leaving parts of the uplifted stream channel as paired terraces. As headward cutting by the stream proceeds into the drainage basin, the effects of the tectonic perturbation are lessened in that the stream gradient at the mountain front becomes less. However, the stream gradient is still steeper than before the uplift. Deposition on the fan apex is concurrent with accelerated downcutting of the stream channel in the mountains. Downcutting of the valley and raising of the fan surface continue until a common and uniform gradient results. The fan surface now (Figure 18b) has two segments that appear as

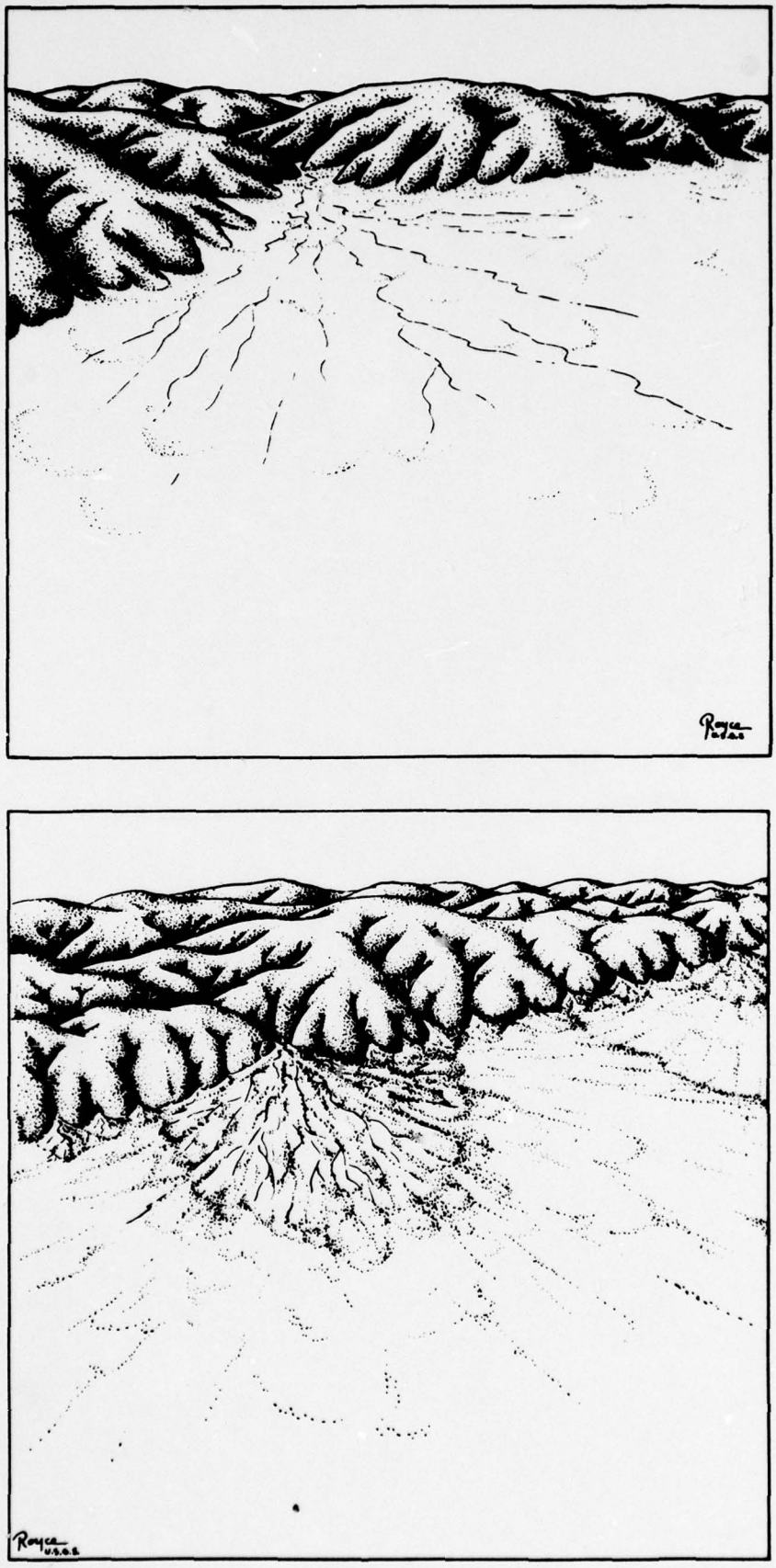

**Figure 18** Development of a segmented alluvial fan, where the area of deposition remains near the mountains. **a** Unentrenched alluvial fan before uplift of the mountain front. **b** Steeper fan segment deposited on the fanhead after uplift and headcutting had steepened the stream-channel and depositional gradients.

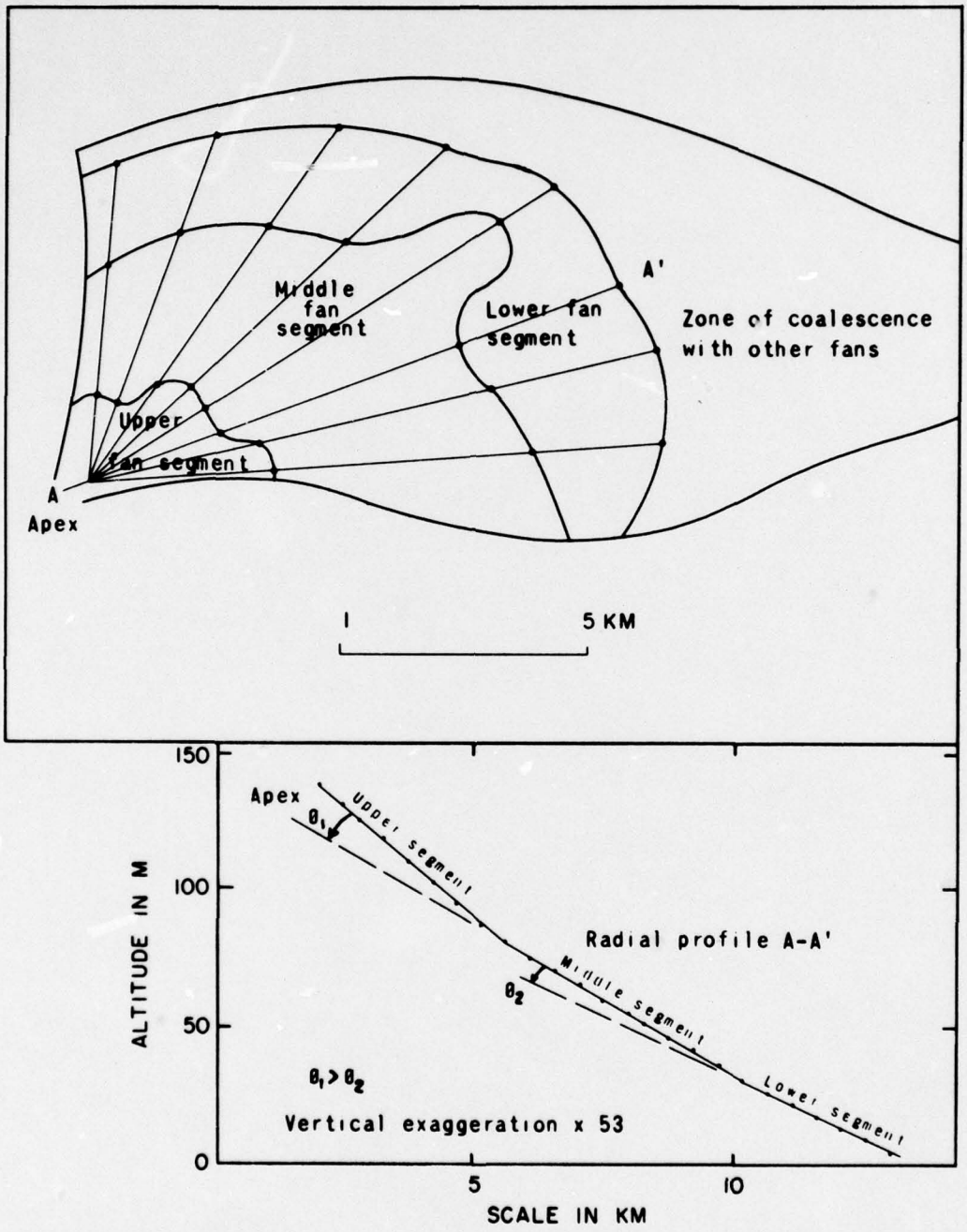


**Figure 19** Segmentation of the Tumey Gulch fan, western Fresno County, California. *After Bull, 1964b*

straight lines on a radial profile. If deposition should continue at the fan apex, the valley upstream from the apex might be aggraded in order to maintain a common gradient—provided that streamflow conditions, such as sediment load and size—favour additional deposition instead of channel downcutting. Segmentation of the type shown in Figure 18b is not generally obvious in the field, particularly where the change in slope the two fan segments is less than 2°.

Figure 19 shows a map and radial profile of a segmented alluvial fan of the type portrayed in Figure 18. The abrupt breaks in slope between the fan segments cannot represent tectonic hinge points, because the segment boundaries are strongly concave (more concentric than the contours) towards the fan apex. The concentric distribution shows that the fan segments are depositional features instead of purely tectonic forms. Each of the eight radial profiles of Figure 19 has three straight-line segments, and the angle, $\phi_1$, between the upper and middle segments is larger than the angle, $\phi_2$, between the middle and lower segments. The data of Figure 19 can be interpreted as evidence that the depositional slope was steepened twice as a result of stream-gradient steepening caused by intermittent uplift of the mountains. Differential uplift was greatest at the mountain front, which was the locus of initial headward stream erosion that resulted in a steeper-channel gradient than before uplift. The type of alluvial fan described in Figures 18 and 19 may have patches of older fan deposits with well-developed soil profiles on the lowest fan segment, but little or no soil-profile development will have occurred on the upper fan segment which is the area of maximum present deposition. Equation 5 describes the tectonic setting of the fan shown in Figure 19.

A different situation is portrayed in Figure 20. The initial condition portrayed in Figure 20a is similar to that of Figure 18a in that deposition of fan material occurs adjacent to the mountain front. If it is assumed that no further perturbations to the system, such as tectonic or climatic change, occur, the stream will continue to downcut and the loci of deposition will shift downfan. Uniform rates of channel downcutting will result in uniform rates of downfan shift in the area of deposition, and a concave fan profile will be formed.

Such uniform conditions are unlikely in nature. Instead, rapid downfan shifts in the area of deposition appear to be common, and may be the result of either tectonic or climatic changes.

In Figure 20b a hypothetical climatic change has caused an acceleration of stream-channel downcutting, which has rapidly shifted the area of deposition to a new downfan location. Deposition has ceased at the fan apex shown in Figure 20a and deposition at the fan apex shown in Figure 20b has created a new fan segment. The stream gradient immediately upslope from the new fan apex has a lesser gradient than the prior stream. Thus, both the new segment and stream-channel upstream from it have a more gentle gradient than before the downfan shift of the area of deposition. Stream-channel entrenchment of this type may be permanent, in which case the upper fan segment no longer receives streamflow and deposits, but undergoes weathering

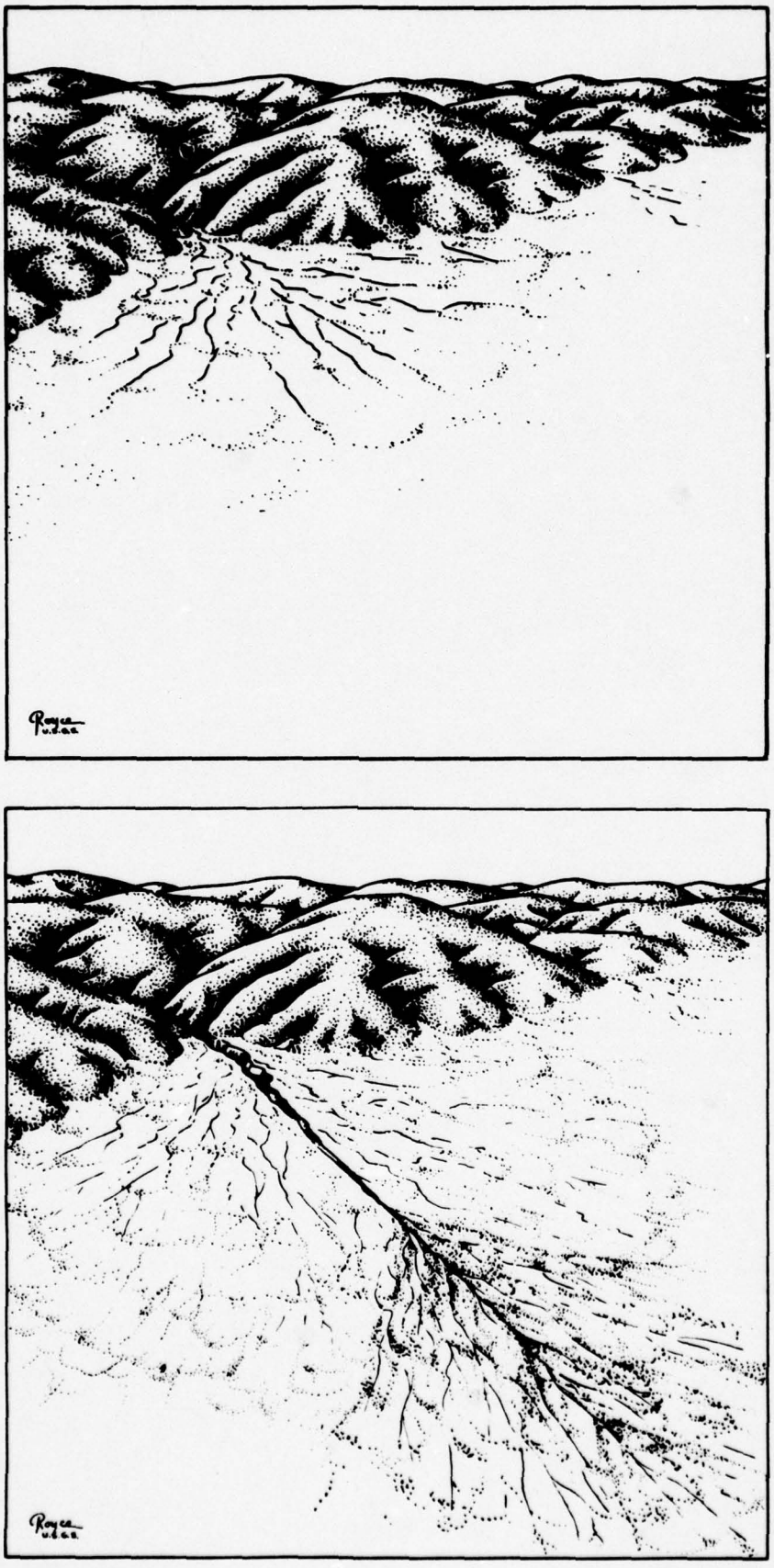

**Figure 20** Development of a segmented alluvial fan where the area of deposition has shifted downslope from the mountain front. **a** Unentrenched alluvial fan before period of accelerated stream-channel downcutting. **b** Entrenched alluvial fan, where the area of deposition has shifted downfan.

and is eroded by runoff originating on the upper fan segment. Assuming no change in sediment and water discharges, deposition cannot occur adjacent to the mountain front again until uplift is renewed and the total amount of uplift exceeds the amount of channel downcutting that has occurred at the mountain front during the time since the loci of deposition were last adjacent to the mountains. Because deposition does not occur on the upper part of the fan, stream terraces that formed within the drainage basin as a result of periods of accelerated erosion resulting from climatic or tectonic change commonly

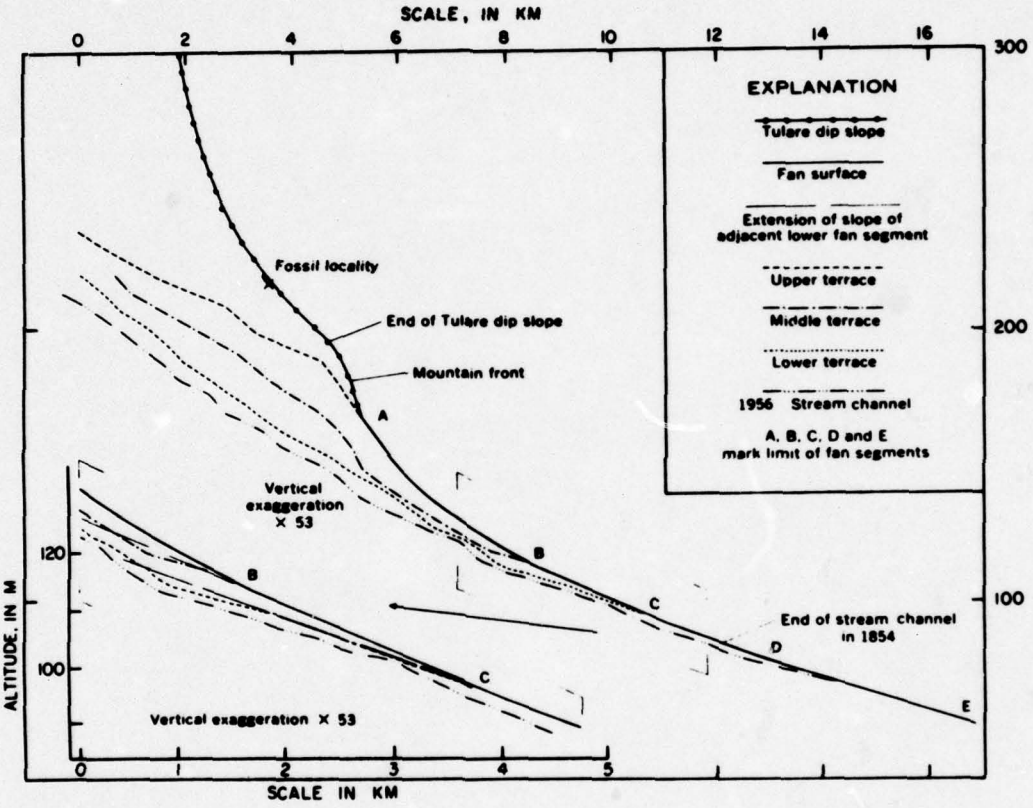


**Figure 21** Relation of stream terraces to fan segments for Little Panoche Creek, Western Fresno County, California.

extend down the channel incised into the fan, and terminate at the upslope end of the fan segments.

The relation of stream terraces to fan segments for a fan of the type portrayed in Figure 20 and described by Equation 6 is shown in Figure 21. Three paired terraces occur near the mouth of Little Panoche Creek. All three are underlain by a 1–6 m veneer of sand and gravel that was deposited on truncated sedimentary rocks. The mountain front has been subject to intermittent monoclinal folding. Terrace divergence occurs upstream from the zone of maximum differential uplift, and terrace convergence occurs downstream from the zone. The amount of uplift has been less than the amount of stream-channel down-

cutting; therefore, it has not been possible for fan deposition to remain immediately adjacent to the mountain front. Intermittent uplifts have accelerated the downcutting of the stream-channel in the mountains, and the overall effect has been to entrench the fanhead and extend the end of the channel further downfan. Each time this has happened, the area of deposition and the stream-channel upstream from it have developed a more gentle gradient than previously.

The slopes of the terraces are continuous with the slopes of the fan segments. The slope of the upper terrace continues onto segment A–B (Figure 21); the middle terrace ends at the upslope end of fan segment B–C; and the lower terrace ends at the upslope end of fan segment C–D. A gradient of the lower part of each terrace approximates the gradient of the adjacent lower fan segment (see the insert of Figure 21). A geomorphic map of the segments of the Little Panoche Creek fan has been published by Bull (1964b, 109).

## V Man and the alluvial-fan environment

The study of alluvial fans has many practical applications. Flooding by streams that traverse fans is of considerable interest to those farming and living on fans, and is an important source of water to recharge the groundwater reservoir. The alluvial-fan environment also provides clues to those interested in the Quaternary tectonic history of a given region.

Tectonic stability is important for engineering structures such as water-transport systems and nuclear generating plants. The presence of rapidly accumulating, thick alluvial-fan deposits next to a mountain front should be a warning sign to those who are looking for sites free of potential ground rupture, or which are distant from faults that may generate damaging earthquakes.

Consideration of the areas of tectonic activity in the southwestern United States, as indicated by earthquake epicentres, shows that western Nevada and much of California have had abundant epicentres. South-central Arizona has been almost free of earthquakes. The areas of abundant seismic epicentres have abundant alluvial fans, whereas pedimented landscapes are typical of the tectonically stable region of south-central Arizona.

The arid and semi-arid regions of the world are highly dependent on groundwater supplies. Alluvial-fan deposits are part of the groundwater reservoirs in basins filled with alluvium, and much of the recharge of the groundwater reservoirs is through the permeable fan deposits that fringe the basins. Examples would be the Los Angeles basin in southern California and the San Joaquin Valley of central California. Tucson, Arizona, is one of the largest cities in the world totally dependent on underground water supplies. Much of the water used in Tucson is pumped from an alluvial-fan deposit of late Cenozoic age. The fan deposits of mid-Cenozoic age are so impregnated with calcium carbonate cement that they yield little water.

Flood hazards on alluvial fans are different to those in valleys. Sheetflow is common on alluvial fans and stream-channel shifts can occur rapidly in the

alluvial-fan environment (Chawner, 1935; Troxell and Peterson, 1937; Woolley, 1946; Schick, 1971; Scott, 1973). Beaty (1968) has summarized the flood hazards to roads and ranches for a bajada along the west side of the White Mountains in California. Schick (1974) concluded that roads should be built on the same level as the fan surface. Roads that are lower than the surface tend to be buried, and roads that are higher may be destroyed by floods. The San Luis Canal–California Aqueduct that transports water 1000 km from the water-rich areas of northern California to the water-deficient areas of southern California crosses many alluvial fans, particularly in the San Joaquin Valley of California. Where the canal crosses each fan, provisions must be made to siphon flood waters under the canal or to let streamflows pass through overshoots that cross the canal.

The weathered sandy deposits on fans, particularly on the downslope parts of large fans, are commonly good agricultural soils. Of equal importance is the fact that these soils usually occur above the sands and gravels of the fan deposits that furnish well water in sufficient abundance to support the agricultural operations.

Not all aspects of alluvial fans are beneficial, Many of the basin fills—the deposits of alluvial fans, through-flowing rivers, and lakes—are areas that are subject to land subsidence (Schumann and Poland, 1969; Miller *et al.*, 1971; Bull 1975b). Pumping of groundwater from clayey sediments increases the forces squeezing the basin-fill deposits, and as water is expelled from the pores in the deposits the thickness of the groundwater reservoir becomes less and the surface of the land sinks. More than 2 m of subsidence has been measured in Arizona, and as much as 8 m of subsidence due to groundwater withdrawal from alluvial-fan and adjacent deposits has been measured in central California.

The occurrence of earth fissures in Arizona such as those described by Robinson and Peterson (1962) and Schumann and Poland (1969) appear to be associated with land subsidence. Both the subsidence and earth fissures are a potential danger to engineering structures, particularly nuclear generating plants, airport runways and water-transport systems. Quaternary alluvial-fan and other types of basin-fill deposits should be avoided for these purposes, particularly where the deposits contain large amounts of silt and clay.

Clayey alluvial-fan deposits may be susceptible to collapse when wetted, thus causing another type of land subsidence. In the west-central San Joaquin Valley of California several hundred square kilometres of farmlands have settled and cracked because irrigation has weakened the clay binder of fan deposits for the first time since the drying and burial of the Late Quaternary deposits (Bull, 1964a). In the same region, several thousand square kilometres of large fans were the sites of near-surface subsidence during the Holocene when streamflow wetted the deposits for the first time since the burial (Bull, 1972b).

## VI Summary

An alluvial fan is a deposit with a distinctive surface. The deposit is usually a fan-shaped segment of a cone that radiates downslope from an apex where a single-trunk stream leaves the source area.

Deposition is caused by decreases in depth and velocity where streamflow spreads out on a fan, and by infiltration of water into permeable surficial deposits. Changes in the hydraulic geometry of streamflow are accompanied by changes in stream-channel pattern on fans with little gravel. A common sequence is braided channels, complex channel flow and sheetflow, sheetflow and rillflow that enter headcut channels formed because decrease in sediment load creates conditions favourable for temporary channel incision.

Fans consist of water-laid sediments, debris-flow deposits, or both. Water-laid sediments occur as channel, sheetflood or sieve deposits. Entrenched stream channels are commonly backfilled with gravel that may be imbricated, massive or thick-bedded. Sieve deposits are overlapping lobes of permeable gravel. Debris-flow deposits generally consist of cobbles and boulders in a poorly sorted matrix. Low-viscosity debris flows have graded bedding, and a horizontal orientation of tabular particles. Highly viscous flows have uniform particle distribution, and a vertical preferred orientation normal to the flow direction.

A fan is deposited as a sequence of overlapping sheets (length/width ratio $\approx 10$) that may have abundant backfilled stream channels near the fan apex. Adjacent beds vary greatly in particle size, sorting and thickness. Beds extend for long distances along radial sections, and channel deposits are rare. Cross-fan sections reveal beds of limited extent that are interrupted by backfilled stream channels. The longitudinal shape of a fan may be lenticular, or a wedge that is thickest, or thinnest, near the mountains.

Several aspects of fans can be described mathematically. Troeh has derived a polynomial equation that describes the concave–convex curvature typical of most alluvial fans. A power function can be used to describe the relation between fan areas and their respective source areas. An exponent of about 0.9 for most suites of fans suggests that sediment output from large basins is less than that for small basins because of less steep hillslopes, and more opportunities for storage of alluvium in valleys. The coefficient of the power function is indicative of the relative areas of fans per unit source area for regressions of similar exponent. When compared with fans derived from quartzite areas, fans derived from granite, sandstone and mudstone source areas are roughly 5, 10 and 20 times as large respectively. Fan slope is less with increasing fan size and stream discharge, and with decreasing particle size and flow viscosity.

Thick alluvial fans are orogenic deposits, not only because uplift creates mountainous areas that provide debris and increased stream competence, but also because the loci of deposition on alluvial fans are controlled by the rates and magnitudes of uplift of the adjacent mountains. The loci of deposition are dependent on the interrelations of the rates of mountain front uplift ($\Delta u$/

$\Delta t$), stream-channel downcutting ($\Delta w/\Delta t$), and fan deposition ($\Delta s/\Delta t$) or erosion ($\Delta e/\Delta t$). two types of fans can be defined.

Fans that continue to aggrade adjacent to a mountain front occur in tectonically active areas, where the local base-level processes have the following relation

$$\frac{\Delta u}{\Delta t} \geqslant \frac{\Delta w}{\Delta t} + \frac{\Delta s}{\Delta t}$$

Although the overall radial profiles of such fans are gently concave, they generally consist of several straight segments. The surfaces of the fan segments form bands of approximately uniform slope that are concentric about the fan apex. Each pulse of uplift induces channel trenching headward from the mountain front that steepens the stream channel and the slope of the fan surface being aggraded by the stream.

Fans that are not actively aggrading next to the mountains occur where rates of channel downcutting exceed rates of uplift

$$\frac{\Delta u}{\Delta t} < \frac{\Delta w}{\Delta t} - \frac{\Delta e}{\Delta t}$$

Entrenchment of the trunk stream has removed the fanhead area as an area of possible deposition. Either tectonic or climatic perturbations may cause rapid downfan shifts in the loci of deposition, and result in a segmented alluvial fan with the youngest segment at the toe of the fan.

The alluvial-fan environment is important to man. Crops are grown on fans, and water is pumped from fan deposits. Floods that occur in channels and as sheetflow may damage roads, cities and agricultural operations on fans. Certain fan deposits may be susceptible to land subsidence caused by wetting of dry clayey deposits, or by pumping of water from confined aquifer systems. Many fans are indicative of active tectonism, and may be the sites of future ground rupture by faulting.

*University of Arizona*

## VII References

**Anderson, G. S.** and **Hussey, K. M.** 1962: Alluvial fan development at Franklin Bluffs, Alaska. *Proceedings of the Iowa Academy of Science* 69, 310–22.

**Anstey, R. L.** 1965: Physical characteristics of alluvial fans. Massachusetts: United States Army Natic Laboratories, Technical Report ES-20. (109 pp.)

1966: A comparison of alluvial fans in West Pakistan and the United States. *Pakistan Geographical Review* 21, 14–20.

**Arnold, B.** 1962: Proposed relics of coastal alluvial fans in southern California. *California Geographer* 3, 123–30.

**Bagnold, R. A.** 1954: Experiments on a gravity-free dispersion of large solid spheres in a Newtonian fluid under shear. *Proceedings of the Royal Society of London* 225, 49–63.

1956: The flow of cohesionless grains in fluids. *Philosophical Transactions of the Royal Society* 249, 235–97.

**Baker, C. L.** 1911: Notes on the Later Cenozoic history of the Mojave Desert Region in southeastern California. *University of California, Department of Geology, Published Bulletin* 6, 333–83.

**Beaty, C. B.** 1961: Topographic effects of faulting; Death Valley, California. *Annals of the Association of American Geographers* 51, 234–40.

1963: Origin of alluvial fans, White Mountains, California and Nevada. *Annals of the Association of American Geographers* 53, 516–35.

1968: *Sequential study of desert flooding in the White Mountains of California and Nevada.* United States Army Natic Earth Science Laboratory, Technical Report 68–31–ES. (96 pp.)

1970: Age and estimated rate of accumulation of an alluvial fan. White Mountains, California, USA. *American Journal of Science* 268, 50–77.

1974: Debris flows, alluvial fans, and a revitalized catastrophism. *Zeitschrift für Geomorphologie, Supplementband* 21, 39–51.

**Beaumont, P.** 1972: Alluvial fans along the foothills of the Elburz Mountains, Iran. *Palaeogeography, Palaeoclimatology, Palaeoecology* 12, 251–73.

**Beaumont, P.** and **Oberlander, T. M.** 1971: Observations on stream discharge and competence at Mosaic Canyon, Death Valley, California. *Bulletin of the Geological Society of America* 82, 1695–8.

**Berkey, C. P.** and **Morris, E. K.** 1927: Geology of Mongolia. *Natural History of Central Asia* 2.

**Blackwelder, E.** 1928: Mudflow as a geologic agent in semiarid mountains. *Bulletin of the Geological Scoeity of America* 39, 465–84.

1931: Desert plains. *Journal of Geology* 39, 133–40.

1954: Geomorphic processes in the desert. *California Division of Mines Bulletin* 170, chapter 5, 11–20.

**Blissenbach, E.** 1952: Relation of surface angle distribution to particle size distribution on alluvial fans. *Journal of Sedimentary Petrology* 22, 25–8.

1954: Geology of alluvial fans in semiarid regions. *Bulletin of the Geological Society of America* 65, 175–90.

**Bluck, B. J.** 1964: Sedimentation of an alluvial fan in southern Nevada. *Journal of Sedimentary Petrology* 34, 395–400.

1965: The sedimentary history of some Triassic congolmerates in Vale of Glamorgan, South Wales. *Sedimentology* 4, 225–45.

**Bond, G.** 1949: A preliminary account of the Pleistocene geology of the plateau tin fields region of northern Nigeria. *Proceedings of the Third West African Conference, Ibadan*, 187–201.

**Brune, G. M.** 1948: *Rates of sediment production in midwestern United States.* United States Department of Agriculture, Soil Conservation Service Technical Publication 65. (40 pp.)

**Bull, W. B.** 1961: Tectonic significance of radial profiles of alluvial fans in western Fresno County, California. *United States Geological Survey Professional Paper* 424-B, 182–4.

1962a: Relations of alluvial-fan size and slope to drainage-basin size and lithology in western Fresno County, California. *United States Geological Survey Professional Paper* 450-B, 51–3.

1962b: Relation of textural (CM) patterns of depositional environment of alluvial-fan deposits. *Journal of Sedimentary Petrology* 32, 211–16.

1964a: Alluvial fans and near-surface subsidence in western Fresno County, California. *United States Geological Survey Professional Paper* 437-A. (71 pp.)

1964b: Geomorphology of segmented alluvial fans in western Fresno County, California. *United States Geological Survey Professional Paper* 352-E, 89–129.

1968: Alluvial fans: *Journal of Geology* 16, 101–6.

1972a: Recognition of alluvial-fan deposits in the stratigraphic record. In Hamblin, W. K. and Rigby, J. K., editors, *Recognition of Ancient Sedimentary Environments*, Society of Economic Paleontologists and Mineralogists, *Special Publication* 16, 63–83.

1972b: Prehistoric near-surface subsidence cracks in Western Fresno County, California. *United States Geological Survey Professional Paper* 437-C. (86 pp.)

1973: Local base-level processes in arid fluvial systems. *Geological Society of America*, abstracts with programs.

1975a: Allometric change of landforms. *Bulletin of the Geological Society of America* 86, 1489–98.

1975b: Land subsidence in the Los Banos Kettleman City area, California; Part 2, Subsidence and compaction of deposits. *United States Geological Survey Professial Paper* 437-F. (90 pp.)

1976: Landforms that do not tend toward a steady state. *Sixth Annual Geomorphology Proceedings*, Binghamton, New York.

**Busche, D.** 1972: Untersuchungen zur pedimententwicklung im Tibesti-Gebirge. *Zeitschrift für Geomorphologie, Supplementband* 15, 21–38.

**Butzer, K. W.** 1965: *Environment and archaeology*, first edition. London: Methuen. (524 pp.)

**Buwalda, J. F.** 1951: Transportation of coarse material on alluvial fans. *Bulletin of the Geological Society of America* 62, 1497.

**Campbell, R. H.** 1975: Soil slips, debris flows, and rainstorms in the Santa Monica Mountains and vicinity, southern California. *United States Geological Survey Professional Paper* 851. (51 pp.)

**Carryer, S. J.** 1966: A note on the formation of alluvial fans. *New Zealand Journal of Geology and Geophysics* 9, 91–4.

**Chamberlain, T. C.** and **Salisbury, R. D.** 1909: *Geology*, second edition. London: John Murray.

**Chawner, W. D.** 1935: Alluvial-fan flooding, the Montrose, California flood of 1934. *Geographical Review* 25, 225–63.

**Church, M.** and **Ryder, J. M.** 1972: Paraglacial sedimentation: A consideration of fluvial processes conditioned by glaciation. *Geological Society of America* 83, 3059–72.

**Conway, W. M.** 1893: Exploration in the Mustang Mountains. *Geographical Journal* 2, 289–99.

**Cooke, R. U.** and **Reeves, R. W.** 1976: *Arroyos and environmental change in the American southwest*. Oxford: Clarendon Press. (213 pp.)

**Cooke, R. U.** and **Warren, A.** 1973: *Geomorphology in deserts*. London: Batsford. (374 pp.)

**Cotton, C. A.** 1918: The geomorphology of the coastal district of southwest Wellington. *Transactions of New Zealand Institute* 50, 212–22.

1922: Geomorphology of New Zealand, Part 1: Systematic. Wellington.

1948: *Landscape*. Christchurch, New Zealand: Whitcombe and Tombs (509 pp.)

**Crandell, D. R.** 1971: Postglacial Lahars from Mount Ranier Volcano, Washington. *United States Geological Survey Professional Paper* 677. (73 pp.)

**Crawford, A. C.** and **Thackwell, F. E.** 1931: Some aspects of the mudflows north of Salt Lake City, Utah. *Proceedings of the Utah Academy of Science* 8, 97–105.

**Crowell, J. C.** 1954: Geology of the Ridge Basin Area. *Bulletin of the California Division of Mines* 170, map sheet number 7.

1974: Sedimentation along the San Andreas Fault, California. *Society of Economic Paleontologic Minerals, Special Publication* 19, 202–3.

**Czajka, W.** 1958: Schwemmfacherbildung und schwemmfacherformen. *Mitteilungen der geologischem Gesellschaft in Wien* 100, 18–36.

**Dana, J. D.** 1880: *Manual of geology*, third edition. New York: American Book Company. (911 pp.)

**Davis, W. M.** 1905: The geographical cycle in an arid climate. *Journal of Geology* 13, 381–407.

**Denny, C. S.** 1965: Alluvial fans in the Death Valley region, California and Nevada. *United States Geological Survey Professional Paper* 466. (62 pp.)

1967: Fans and pediments. *American Journal of Science* 265, 81–105.

**Doeglas, D. J.** 1962: The structure of sedimentary deposits of braided rivers. *Sedimentology* 1, 167–90.

**Doehring, D. O.** 1970: Discrimination of pediments and alluvial fans from topographic maps. *Bulletin of the Geological Society of America* 811, 3109–16.

**Drew, F.** 1873: Alluvial and lacustrine deposits and glacial records of the upper Indus basin. *Geological Society of London Quarterly Journal* 29, 441–71.

**Drewes, H.** 1963: Geology of the Funeral Peak Quadrangle, California on the east flank of Death Valley. *United States Geological Survey Professional Paper* 413. (78 pp.)

**Dunbar, C. O.** 1949: *Historical geology*, New York: John Wiley. (573 pp.)

**Dutton, C. E.** 1880: *Report on the geology of the high plateaus of Utah.* United States Geographical and Geological Survey of the Rocky Mountain Region, Washington. (307 pp.)

**Eckis, R.** 1928: Alluvial fans in the Cucamonga district, Southern California. *Journal of Geology* 36, 111–41.

**Fenneman, N. M.** 1931: *Physiography of the western United States.* New York: McGraw-Hill. (534 pp.)

**Fisher, R. V.** 1971: Features of coarse-grained, high-concentration fluids and their deposits. *Journal of Sedimentary Petrology* 41, 916–27.

**Gansser, A.** 1964: *Geology of the Himalayas.* New York: John Wiley–Interscience. (289 pp.)

**Geikie, A.** 1886: *Class-book of geology*, first edition. London: Macmillan. (516 pp.)

**Gilbert, G. K.** 1875: Report on the geology of portions of Nevada, Utah, California and Arizona, 1871–72. In *Report upon Geolographical and Geological Explorations and Surveys West of the One Hundredth Meridian* 3, part 1, 21–187.

1877: *Report on the geology of the Henry Mountains.* United States Geographical Survey Rocky Mountain Region (160 pp.)

1890: Lake Bonneville. *United States Geological Survey Monograph* 1. (438 pp.)

**Haast, J.** 1864: *Report on the formation of the Canterbury Plains.* Christchurch.

1879: *Geology of the Provinces of Canterbury and Westland, New Zealand.* Christchurch. (486 pp.)

**Hack, J. T.** 1965: Geomorphology of the Shenandoah Valley, Virginia and West Virginia, and origin of residual ore deposits. *United States Geological Survey Professinal Paper* 484. (84 pp.)

**Hadley, R. F.** 1967: Pediments and pediment-forming processes. *Journal of Geological Education* 15, 83 9.

**Hawley, J. W.** 1965: Geomorphic surfaces along the Rio Grande Valley from El Paso, Texas to Caballo Reservoir, New Mexico. *New Mexico Geologic Society Guidebook of southwestern New Mexico* II, 188–98.

**Hawley, J. W.** and **Wilson, W. E.** 1965: Quaternary geology of the Winnemucca area, Nevada. *University of Nevada Desert Research Institute Technical Report* No. 5. (66 pp., 28 figures.)

**Hooke, R. L. B.** 1967: Processes on arid-region alluvial fans. *Journal of Geology* 75, 438–60.

1968: Steady-state relationships on arid-region alluvial fans in closed basins. *American Journal of Science* 266, 609–29.

1972: Geomorphic evidence for Late-Wisconsin and Holocene tectonic deformation, Death Valley, California. *Bulletin of the Geological Society of America* 83, 2073–98.

**Hoppe, G.** and **Ekman, S.** 1964: A note on the alluvial fans of Ladtjovagge, Swedish Lapland. *Geografiska Annaler* 46, 338–42.

**Howard, J. D.** 1966: Patterns of sediment dispersal in the Fountain Formation of Colorado. *Mountain Geologist* 3, 147–53.

**Hubert, J. F.** 1960: Petrology of the Fountain and Lyons Formations, Front Range, Colorado. *Colorado School of Mines Quarterly* 55, 1–242.

**Hunt, C. B.** 1975: *Death Valley; geology, archaeology, ecology.* Berkeley: University of California Press.

**Hunt, C. B.** and **Mabey, D. R.** 1966: Stratigraphy and structure, Death Valley, California. *United States Geological Survey Professional Paper* 494-A. (162 pp.)

**Hurelbrink, R. L.** and **Fehrenbacher, J. B.** 1970: Soils and stratigraphy of a portion of the Gola River. *Proceedings of the Soil Science Society of America* 34, 911–16.

**Jahns, R. H.** 1949: Desert floods. *Engineering and Scientific Monthly.* California Institute of Technology, May 10–14.

**Janda, R. J.** 1965: *Quaternary alluvium near Friant, California.* International Association of Quaternary Research, eighth Congress, USA, 1965. Guidebook for field conference I, 128–33.

**Johnson, A. M.** 1970: *Physical processes in geology.* San Francisco: Freeman Cooper. (577 pp)

**Johnson, A. M.** and **Rahn, P. H.** 1970: Mobilization of debris flows. *Zeitschrift für Geomorphologie, Supplementband* 9, 168–86.

**Karcz, I.** 1972: Sedimentary structures formed by flash floods in Southern Israel. *Sedimentary Geology* 7 161–82.

**Kesseli, J. E.** and **Beaty, J. B.** 1959: *Desert flood conditions in the White Mountains of California and Nevada.* United States Army Quartermaster Research and Engineering Command, Natic, Massachusetts, Environmental Protection Research Division Technical Report EP-108. (107 pp.)

**Klein, G. de V.** 1962: Triassic sedimentation, Maritime Provinces, Canada. *Bulletin of the Geological Society of America* 73, 1127–46.

**Knight, M. J.** *et al.*, 1973: Land resources and agricultural potential of the Markham Valley. Papua, New Guinea: *Bulletin of the Department of Agriculture Stock and Fisheries Resources* 10. (220 pp.)

**Krynine, P. D.** 1950: Petrology, stratigraphy, and origin of Triassic sedimentary rocks of Connecticut. *Bulletin of the Connecticut Geological and Natural History Survey* 73. (247 pp.)

**Landim, P. M. B.** and **Frakes, L. A.** 1968: Distinction between tills and other diamictons based on textural characteristics. *Journal of Sedimentary Petrology* 38, 1213–23.

**Lattman, L. H.** 1973: Calcium carbonate cementation of alluvial fans in southern Nevada. *Bulletin of the Geological Society of America* 84, 3013–28.

**Leggett, R. F., Brown, R. J. E.** and **Johnston, G. H.** 1966: Alluvial-fan formation near Aklavik, Northwest Territories, Canada. *Bulletin of the Geological Society of America* 77, 15–30.

**Leopold, L. B., Wolman, M. G.** and **Miller, J. P.** 1964: *Fluvial processes in geomorphology*. San Francisco: W. H. Freeman. (522 pp.)

**Lindsay, J. F.** 1968: The development of clast fabrics in mudflows. *Journal of Sedimentary Petrology* 38, 1242–53.

**Longwell, C. R.** 1930: Faulted fans west of the Sheep Range, southern Nevada. *American Journal of Science* 220, 1–13.

**Lustig, L. K.** 1965: Clastic sedimentation in Deep Springs Valley, California. *United States Geological Survey Professional Paper* 352-F, 131–92.

1974: Alluvial fans. In *Encyclopedia Britannica*, fifteenth edition, 611–17.

**Mabbutt, J. A.** 1966: Mantle-controlled planation of pediments. *American Journal of Science* 264, 78–91.

**McGee, W. J.** 1891: The Pleistocene history of northwestern Iowa: *United States Geological Survey eleventh Annual Report*, Part I, 189–577.

**McPherson, H. J.** and **Hirst, F.** 1972: Sediment changes on two alluvial fans in the Canadian Rocky Mountains. In Slaymaker and McPherson, H. J., editors, *Mountain Geomorphology. Geomorphological processes in the Canadian Cordillera. B. C. Geographical Series* 14, 161–75.

**Magleby, D. C.** and **Klein, I. E.** 1965: Ground-water conditions and potential pumping resources above the Corcoran Clay—an addendum to the ground-water geology and resources definite plan appendix, 1963. *United States Bureau of Reclamation open-file report.*

**Maycock, Jan** 1962: *The Torridonian Sandstone, Round Lock, Torridon, Wester Ross*. Unpublished Ph.D. thesis, University of Reading, England. (305 pp.)

**Medall, S. E.** 1962: A petrographic study of desert fanglomerate. *Compass* 39, 77–87.

**Melton, M. A.** 1965: The geomorphic and paleoclimatic significance of alluvial deposits in southern Arizona. *Journal of Geology* 73, 1–38.

**Mensching, H.** 1958: Glacis-Flussflache-pediment. *Zeitschrift für Geomorphologie* 2, 165–86.

**Miall, A. D.** 1970: Devonian alluvial fans, Prince of Wales Island, Arctic Canada. *Journal of Sedimentary Petrology* 40, 556–71.

**Miller, H.** 1883: River-terracing: its methods and their results. *Proceedings of the Royal Physical Society*, Edinburgh 7, 263–306.

**Miller, R. E., Green, J. H.** and **Davis, G. H.** 1971: Geology of the compacting deposits in the Los Banos–Kettleman City subsidence area, California. *United States Geological Survey Professional Paper* 497-E. (46 pp.)

**Morton, D. M.** and **Campbell, R. H.** 1974: Spring mudflows at Wrightwood, southern California. *Engineering Geology Quarterly Journal* 7, 377–84.

**Murata, T.** 1931a: Theoretical consideration on the shape of alluvial fans. *Geographical Review*, Japan 7, 569–86 (in Japanese).

1931b: Relation between a fan and its surrounding mountains. *Geographical Review*, Japan 7, 649–63 (in Japanese).

1966: A theoretical study of the forms of alluvial fans. Tokyo Metropolitan University, *Geographical Report*, 1, 33–43.

**Nilsen, T. H.** 1968a: *Old red sedimentation in the Solund District, western Norway*. International Symposium on the Devonian System, Calgary, Canada. September, 1967, 2, 1101–15.

1968b: *The relationship of sedimentation to tectonics in the Solund Devonian district of wouthwestern Norway*. Universitetsforaget, Olso Norges Geolgiske Undersokelse No. 359. (108 pp.)

1969: Old Red sedimentation in the Buelandet-Vaerlandet Devonian district, western Norway. *Sedimentary Geology* 3, 35–57.

**Oliferov, A. N.** 1970: Transport of large rocks by mudflows. *Soviet Hydrology, Selected Papers* 2, 121–3.

**Packard, F. A.** 1974: *The hydraulic geometry of a discontinuous ephermeral stream on a bajada near Tucson, Arizona.* University of Arizona Ph.D. dissertation. (127 pp.)

**Pain, C. F.** 1973: *The Late Quaternary geomorphic history of the Kangel Valley, Papua, New Guinea.* Unpublished Ph.D. thesis, Australian National University. (226 pp.)

**Pain, C. F.** and **Pullar, W. A.** 1968: Chronology of fans and terraces in the Galatea Basin. *Earth Science Journal* 2, 1–14.

**Pashaly, N. V.** 1967: Peculiarities of debris-cone formation in the Alazan–Agrichai Valley (Nekotorye osobennosti formiroyaniya knousov vynosa Alazano–Agrichaiskoi doliny). In *Materialy Nauchnoteoreticheskoi Konferentsii melodykh uchenykh, Akademiya nauk Azerbaidzhanskoi SSR* (*Proceedings of the Scientific and Theoretical Conference of Young Scientists. Academy of Science of the Azerbaidzhan SSR*). *Akademiya nauk Azerbaidzhanskoi SSR* (Baku) 3, 127–8 (in Russian).

**Pashley, E. F., Jr** 1966: *Structure and stratigraphy of the central, northern, and eastern parts of the Tucson basin, Arizona*, University of Arizona Ph.D. dissertation. (273 pp.)

**Pe, G. G.** and **Piper, D. J.** 1975: Textural recognition of mudflow deposits. *Sedimentary Geology* 13, 303–6.

**Picard, M. O.** and **High, L. R.** 1973: Sedimentary structures of ephemeral streams. *Developments in Sedimentology*, No. 17, Amsterdam: Elsevier.

**Price, W. E., Jr** 1974: Simulation of alluvial fan deposition by a random walk model. *Water Resources Research* 10, 263–74.

**Pumpelly, R.** 1905: Explorations in Turkestan with an account of the Basin of eastern Persia and Sistan; with contributions from W. M. Davis and E. Huntington. *Carnegie Institute of Washington, Publication* No. 26. (324 pp.)

**Rapp, A.** 1962: Karkevagge, some recordings of mass-movements in the northern Scandinavian Mountains. *Biuletyn Peryglacjalny* 11, 287–309.

**Reinemund, J. A.** 1955: Geology of the Deep River Coal Field, North Carolina. *United States Geological Survey Professional Paper* 246. (159 pp.)

**Riccio, J. F.** 1962: A geological and geographical appraisal of alluvial fans. *Compass* 39, 87–95.

**Rickmers, W. R.** 1913: *The Duab of Turkestan.* Cambridge University Press.

**Robinson, G. M.** and **Peterson, D. E.** 1962: Notes on earth fissures in southern Arizona. *United States Geological Survey, Circular* 466.

**Rodine, J. D.** and **Johnson, A. M.** 1976: The ability of debris, heavily freighted with coarse clastic materials, to flow on gentle slopes. *Sedimentology* 23, 213–34.

**Roed, M. A.** and **Wasylyk, D. G.** 1973: Age of inactive alluvial fans—Bow River Valley, Alberta. *Canadian Journal of Earth Sciences* 10, 1834–40.

**Ruhe, R. V.** 1964: Landscape and alluvial deposits in southern New Mexico. *Annals of the Association of American Geographers* 54, 147–59.

**Ryder, J. M.** 1971a: The stratigraphy and morphology of paraglacial alluvial fans in south central British Columbia. *Canadian Journal of Earth Sciences* 8, 279–98.

1971b: Some aspects of the morphometry of paraglacial alluvial fans in south-central British Columbia. *Canadian Journal of Earth Sciences* 8, 1252–64.

**Sato, H.** 1960: Geomorphology of the western lowlands of the Central Andes, 414–17. In *Andes, the Report of the University of Tokyo Scientific Expedition to the Andes in 1958* (in Japanese and English). (528 pp.)

**Schäfer, A.** and **Schwab, K.** 1975: Schlammströme in den Anden—sedimentation in der Quebrada del Toro, Ostkordillere, NW Argentinien. *Natur. u. Museum* 105, 305–11.

**Schick, A. P.** 1971: A desert flood; physical characteristics; effects of man, geomorphic

significance, human adaptation—a case study of the southern Arava watershed. *Jerusalem studies in Geography* 2, 91–155.

1974: Alluvial fans and desert roads—a problem in applied geomorphology. *Abhandlungen Akademie der Wissenschaften, Gottingen, Mathematisch-physikalische Kl.*, III F., 29, 418–25.

**Schumann, H.** and **Poland, J. F.** 1969: Land subsidence, earth fissures, and groundwater withdrawal in south-central Arizona. In Tison, L. J., editor, *Land subsidence*, AIHS–UNESCO Publication No. 88, 295–302.

**Schumm, S. A.** 1973: Geomorphic thresholds and complex response of drainage systems. In Morisawa, M., editor, *Fluvial geomorphology*, State University at New York, Binghamton, New York, Publications in Geomorphology, 299–310.

**Schumm, S. A.** and **Hadley, R. F.** 1957: Arroyos and the semi-arid cycle of erosion. *American Journal of Science* 255, 161–74.

**Scott, K. M.** 1973: Scour and fill in Tujunga Wash—fanhead valley in urban southern California—1969. *United States Geological Survey Professional Paper* 732-B. (29 pp.)

**Sharp, R. P.** 1942: Mudflow levees. *Journal of Geomorphology* 5, 222–7.

1948: Early Tertiary fanglomerate, Big Horn Mountains, Wyoming. *Journal of Geology* 56, 1–15.

**Sharp, R. P.** and **Nobles, L. H.** 1953: Mudflows of 1941 at Wrightwood, southern California. *Bulletin of the Geological Society of America* 64, 547–60.

**Smith, D. G.** 1972: Aggradation and channel patterns of the Alexandra–North Saskatchewan River, Banff National Park, Alberta. In Slaymaker, O. and McPherson, H. J., editors, *Mountain geomorphology. Geomorphological processes in the Canadian Cordillera. B. C. Geographical Series* 14, Tantalus Research Ltd, Vancouver, Canada, 177–85.

**Smith, G. I.** 1958: Late Quaternary geologic and climatic history of Searles Lake, southeastern California. In Morrison, R. B. and Wright, H. E., editors, *Means of correlation of Quaternary successions*, Salt Lake City: University of Utah Press, 293–310.

**Spearing, D. R.** 1974: Alluvial fan deposits. *Summary sheets of sedimentary deposits, Sheet 1, Boulder Colorado.* Geological Society of America.

**Steel, R. J.** 1974: New red sandstone floodplain and piedmont sedimentation in the Hebridean Province, Scotland. *Journal of Sedimentary Petrology* 44, 336–57.

**Suggate, R. P.** 1963: The fan surfaces of the central Canterbury Plain. *New Zealand Journal of Geology and Geophysics* 6, 281–7.

**Surell, A.** 1841: *Etude sur les torrents des hautes Alpes*, first edition. Paris.

**Suslov, S. P.** 1961: *Physical geography of Asiatic Russia.* San Francisco: Freeman.

**Teilhard de Chardin, P.** 1933: The significance of piedmont gravels in continental geology. *International Geological Congressional Session, XVI, USA* 2, 1031–9.

**Terra, H. de** and **Paterson, T. T.** 1939: *Studies on the Ice Age in India and associated human cultures.* Carnegie Institute, Washington. (354 pp.)

**Thomas, M. F.** 1974: *Tropical geomorphology.* London: Macmillan. (332 pp.)

**Thompson, J. T.** 1873: The glacial action and terrace formation of south New Zealand. *Transactions of the New Zealand Institute* 6, 309–32.

**Tieje, A. J.** 1923: The red beds of the Front Range of Colorado: a study in sedimentation. *Journal of Geology* 31, 192–207.

**Tricart, J.** 1966: Un Chott dans le desert Chilien, la Pampa del Tamarugal. *Revue de géomorphologie dynamique* 16, 12–22.

**Troeh, F. R.** 1965: Landform equations fitted to topographic maps. *American Journal of Science* 263, 616–27.

**Troxell, H. C.** and **Peterson, J. Q.** 1937: Flood in La Canada Valley, California. *United States Geological Survey Water-Supply Paper* 796-C, 53–98.

**Twenhofel, W. H.,** editor, 1932: *Treatise on sedimentation.* Baltimore: The Williams and Wilkins Company. (926 pp.)

**Vinogradov, Yu B.** 1969: Some aspects of the formation of mudflows and methods of computing them. *Soviet Hydrology* 5, 480–500.

**Vita-Finzi, C.** 1969: *The Mediterranean valleys.* Cambridge: Cambridge University Press. (140 pp.)

**Wasson, R. J.** 1974: Intersection point deposition on alluvial fans: An Australian example. *Geografiska Annaler* 56A, 83–92.

1975: *Evolution of alluvial fans in two areas of southeastern Australia.* Ph.D. dissertation, Macquarie University, New South Wales, Australia. (360 pp.)

**Weaver, E. W.** and **Schumm, S. A.** 1974: Fan-head trenching: an example of a geomorphic threshold. *Geological Society of America, Abstract with programs* 6. (481 pp.)

**Werner, D. J.** 1972: Beobachtungen an bergfussflächen in den trockenbebieten NW Argentina. *Zeitschrift für Geomorphologie, Supplementband* 15, 1–20.

**Williams, G. E.** 1966: Paleogeography of the Torridonian Applecross Group. *Nature* 209, 1303–6.

1969: Characteristics and origin of a Pre-Cambrian pediment. *Journal of Geology* 77, 183–207.

1970: Piedmont sedimentation and Late Quaternary chronology in the Biskra region of the northern Sahara. *Zeitschrift für Geomorphologie, Supplementband* 10, 40–63.

1973: Late Quaternary piedmont sedimentation, soil formation and paleoclimates in arid south Australia. *Zeitschrift für Geomorphologie, Supplementband* 17, 102–25.

**Winder, C. G.** 1965: Alluvial cone construction by alpine mudflow in a humid temperate region. *Canadian Journal of Earth Sciences* 2, 270–7.

**Woolley, R. R.** 1946: Cloudburst floods in Utah, 1850–1938. *United States Geological Survey Water-Supply Paper* 994. (128 pp.)

**Yazawa, D., Toya, H.** and **Kaizuka, S.** 1971: *Alluvial fans.* Kokon Shoin, Tokyo (318 pp.) (in Japanese).

# APPENDIX J

## TECTONIC GEOMORPHOLOGY NORTH AND SOUTH OF THE GARLOCK FAULT

BY

WILLIAM B. BULL

# TECTONIC GEOMORPHOLOGY NORTH AND SOUTH OF THE GARLOCK FAULT, CALIFORNIA

William B. Bull
Leslie D. McFadden

Geosciences Department
University of Arizona

ABSTRACT

Five differential equations that interrelate uplift, erosion, and deposition along stream systems that cross the mountain fronts of the northern Mojave Desert were used to appraise three classes of Quaternary tectonism. Class 1 (active tectonism) terrains are characterized by mountain-front sinuosities of 1.2 - 1.6, unentrenched alluvial fans, elongate drainage basins with narrow valley floors and steep hillslopes even in soft materials. Class 2 (moderate to slightly active tectonism) terrains are generally characterized by mountain-front sinuosities of 1.8 - 3.4, entrenched alluvial fans, large drainage basins that are more circular than class 1 basins in similar rock types, steep hillslopes and valley floors that are wider than their floodplains. Class 3 (tectonically inactive) terrains are characterized by mountain-front sinuosities of 2 to 7, pedimented mountain fronts and embayments, steep hillslopes only on resistant rock types, and few large integrated stream systems in the mountains.

Marked contrasts of landscapes, that are due to different relative rates of base level fall, are present north and south of the strike-slip Garlock fault. In a northern subarea, class 1 terrains generally occur on the west sides and class 2 terrains on the east sides of the eastward tilted

*The views and conclusions contained in this document are those of the authors and should not be interpreted as necessarily representing the official policies, either expressed or implied, of the U. S. government. Sponsored by the U. S. Geological Survey No. 14-08-0001-G-394.*

fault-block mountains. Extreme tectonic stability is shown by the dominance of class 3 terrains south of the fault. Pedimentation has left only remnants of the formerly more extensive mountain ranges and their drainage basins. Between the extremes of these two subareas is a transitional subarea north of the Garlock fault, where the magnitudes of Quaternary uplift of the mountain fronts decrease towards the south.

## INTRODUCTION

The hillslope, stream, and depositional subsystems of arid fluvial systems tend toward configurations that are the result of the interaction of many variables. One important independent variable is base level change. Tectonic base level fall partly determines the relief of a fluvial system, and a pulse of uplift along a mountain front will cause adjustments in the systems that flow across the front. For example, uplift can change a stream's erosional work from predominately lateral cutting to downcutting, which will leave the former floodplain as paired strath terraces. Of course, one also has to take into account the concurrent effects of other independent variables, such as climate (which varies with time) and rock type and structure (which varies with space). These independent variables largely determine the morphologies of hillslopes, valleys and drainage nets; and affect processes pertaining to soil and vegetation, sediment yield, and discharge of water and sediment from the erosional part of the system.

The subject of tectonic geomorphology deals with (1) the impact of tectonic base level fall on the processes and morphologies of fluvial systems and (2) assessment of the relative degrees of tectonic activity of mountain fronts, or other structural elements, during the Quaternary. These are the chief subjects of a book manuscript by W. B. Bull entitled, Climatic and Tectonic Geomorphology of Arid Fluvial Systems.

This article deals with the second type of study. We wish to report the results of an application of a tectonic geomorphology model to the landscape north and south of the Garlock fault in eastern California. This part of the Basin and Range Province (Figure 1) has some obvious differences in relief and continuity of mountain blocks. The purpose of this article is to quantify some of these differences in mountain fronts, and to evaluate areal variations in Quaternary tectonism. The scope of the article includes a brief outline of the tectonic geomorphology model, discussion of two landscape parameters that are useful in defining relative rates of uplift, and classification and discussion of the relative rates of Quaternary mountain front uplift in the study area. Uplift and/or erosion of the mountains during the Quaternary (the last 1.8 m.y.) accounts for most of the configuration of the landscape elements discussed in this article. Only major, localized tectonic processes will be considered. Broad warping and minor faulting of only a few meters are not easily accommodate by the model and only those mountain fronts that are more than 10 km long are analyzed. A mountain front is considered as being a zone that includes part of the mountains, the adjacent escarpment and part of the basin adjacent to the escarpment. The fronts studied are show in Figure 1 and the general rock types are shown in Figure 2.

The names of the mountains on Table 2 are not identical with geographic place names because the mountain fronts were selected for this study on the basis of topographic, lithologic, geomorphic and structural, continuity. For example, the Spangler Hills occur just north of the Garlock fault, but are part of the Argus Range structural-lithologic block. This block is named after the largest mountain mass within it and the fronts are numbered from north to south on both the east and west sides of the block.

The geomorphic characteristics of the mountain fronts do not change abruptly at the Garlock fault. Because of the transitional changes that are characteristic of the differ-

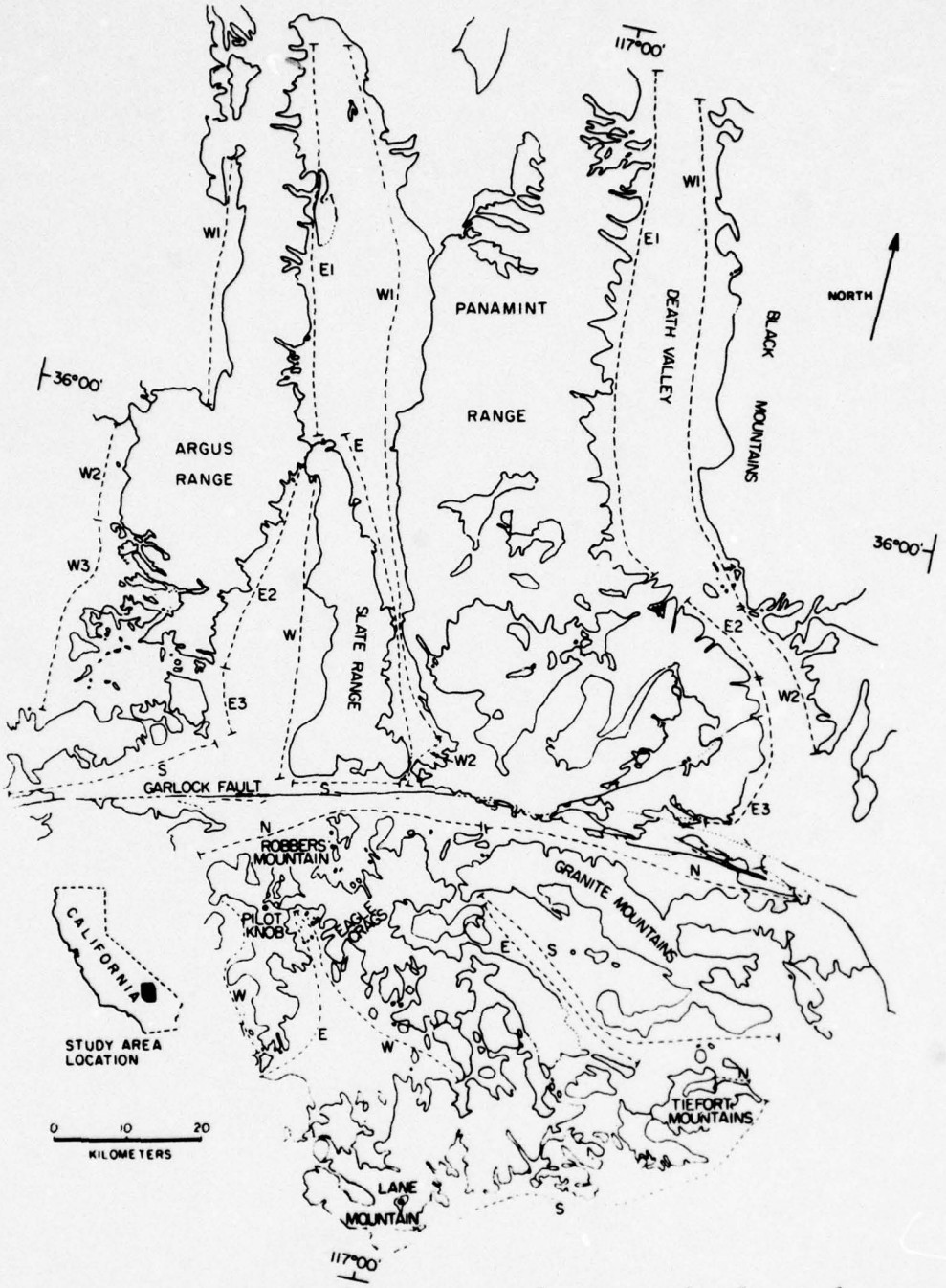


*Figure 1. Locations of the larger mountain ranges in the study area, and the mountain fronts analyzed.*


*Figure 2. Generalized geology of the study area, from Jennings and others (1962) and Jennings (1958).*

ent blocks, northern, transitional and southern subareas were separated for study and comparison (see Table 2).

The basins and low ranges receive less than 100 mm of precipitation during the average year, but the 3200 m high Panamint Range locally receives more than 300 mm. Most of the precipitation comes during the winter, although infrequent, but the intense rains from convective storms during the hot summers account for some of the major streamflow events.

### Earlier Studies

The eastward striking Garlock fault in the Mojave Desert has a left lateral displacement of at least 48-64 km (Smith, 1962; Smith and Ketner, 1970; Davis and Burchfiel, 1973) and separates markedly different landscapes to the north and south. "South of the Garlock is the Mojave Desert block of generally old, low mountain blocks, largely buried by basin deposits in the west. North of the Garlock fault is a region of high and exceedingly active fault-block ranges, the Sierra Nevada, Argus, Panamint, and Black Mountains" (Hamilton and Myers, 1966). Davis and Burchfiel conclude that the Garlock fault is an intracontinental transform structure that is related to the extensional origin of the Basin and Range Province north of the fault. Both strike-slip and vertical tectonic movements have occurred north of the Garlock fault. Wright and Troxel (1967) describe less than 8 km of right-lateral movement along the Death Valley fault zone, and Smith (1975) found that the right-lateral displacement of Quaternary landforms by the Panamint Valley fault zone exceeds the vertical offset of the landforms.

## THE EFFECTS OF VERTICAL TECTONIC MOVEMENTS ON FLUVIAL SYSTEMS

A process that changes the altitude of a point on a streambed is a local base level process. Base level processes include stream-channel downcutting in the mountains

(w) and erosion (e) or deposition (s) on the piedmont adjacent to the escarpment. These three interdependent processes are affected by the relative uplift (u) of the mountain front. The four base level processes noted above affect the processes and morphologies of the stream and hillslope subsystems, the loci of erosion and deposition and, therefore, the topography of the basins.

The effects of continued rapid uplift of mountains relative to the adjacent basins, by eitner continuous or pulsatory uplift, result in a distinctive suite of landforms. Figure 3 depicts the accumulation of thick alluvial fan deposits adjacent to a faulted mountain front. Either channel downcutting in the mountains and/or basin deposition will tend to cause the stream channel to become entrenched into the fan apex, which will shift the loci of fan deposition down the fan. Counteracting the tendency to trench the fanhead is the uplift of the erosional subsystem along the range-bounding fault. Continued channel downcutting will occur only when uplift equals or exceeds the sum of the two local base level processes that are tending to cause the fanhead trenching as shown by equation 1:

$$\Delta u/\Delta t \geq \Delta w/\Delta t + \Delta s/\Delta t \qquad (1)$$

Equation 1 is but one of five equations interrelating local base level processes for three different tectonic environments. The equations are shown in Table 1, and they form the basis of three classes of relative tectonic activity of mountain fronts within a given study area during the Quaternary.

The assignment of a tectonic activity class for a given mountain front is based on numerical parameters that describe diagnostic landform morphologies within both the erosional and depositional subsystems. The typical landform of Table 1 is but one of many diagnostic landforms for a given class. For example, class 1 landscapes, when compared to class 3 landscapes of similar total relief, climate, and rock type, have more convex ridgecrests, steeper footslopes, narrower and steeper valleys, less sinuous

mountain fronts, thicker basin deposits next to the mountains, and minimal soil profile development on the piedmont (Bull, 1973). Thus, the tectonic geomorphology model defines the interrelations of tectonic base level change to the other local base level processes by the equations of Table 1, and allows the assignment of an appropriate tectonic activity class by quantitative descriptions of selected landscape elements.

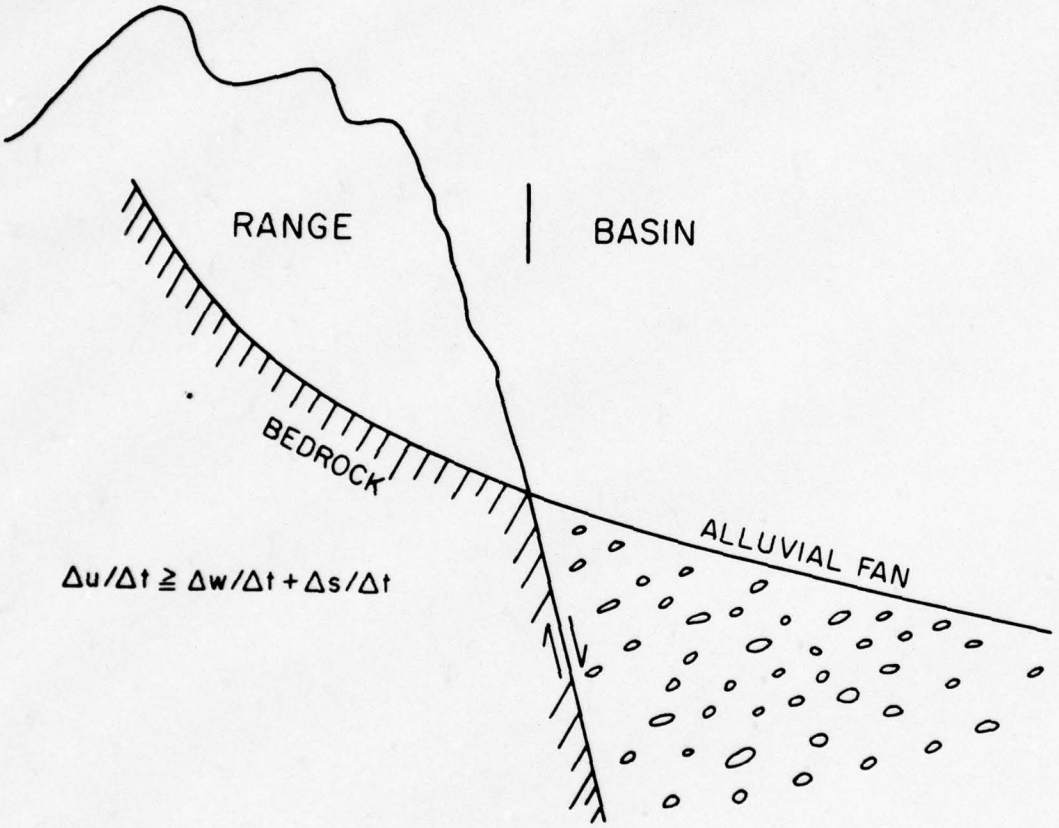


*Figure 3. Interrelations of local base level processes conducive for the accumulation of thick alluvial fan deposits next to a mountain front.*

## SELECTED PARAMETERS THAT DESCRIBE THE INTERACTION OF FLUVIAL SYSTEMS AND VERTICAL TECTONIC MOVEMENTS: THEORY AND RESULTS

For the purposes of this reconnaissance, two chief parameters were used that are reliable and easy to obtain.

Mountain-front sinuosity uses the two horizontal dimensions of the landscape at the junction between the erosional and depositional subsystems. The valley floor width-valley height ratio uses one vertical and one horizontal dimension at a given point along the stream in the erosional subsystem, and, thus, is affected by variables and perturbations both upstream and downstream from the measurement point.

## Mountain-Front Sinuosity

Many workers have used qualitative aspect of mountain fronts to make general assessments of the degree of tectonic activity present. A straight mountain front might be indicative of an active fault or fold while an embayed, pedimented front generally is considered to be representative of tectonic quiescence. Because the plan views of most faults and folds are gently curving or straight, the degree of erosional modification of tectonic structures can be measured by a mountain-front sinuosity index. Mountain-front sinuosity (S) is the ratio of the length along the edge of the mountain-piedmont junction (Lmf) to the overall length of the mountain front (Ls) as shown in equation 2.

$$S = \frac{Lmf}{Ls} \qquad (2)$$

The sinuosity of a mountain front at any given time is a balance between the tendency of uplift to maintain a fairly straight front that coincides with a tectonic structure and the work of streams that tend to erode irregularities into the front. Erosional retreat of the front from the range bounding tectonic structure also increases with time and is accompanied by increasing values of S.

Values of S are in part a function of the scale and detail of the maps and/or aerial photos. Small-scale topographic maps (1:250,000) provide only crude estimates of S, but aerial photographs, large scale (1:62,500) topographic maps, and 1:250,000 geologic maps generally are adequate. Results obtained from the different sources of data generally are about the same, but in some cases aerial photos or small scale topographic maps will give values of S that are 20-30%

higher than the 1:250,000 geologic maps. Geologic maps that depict intensive pedimentation cannot be used.

Studies made elsewhere in the Sonoran and Mojave deserts show that each of the tectonic activity classes of Table 1 has fairly distinctive ranges of mountain-front sinuosity. Class 1 fronts generally range from 1.0 to 1.6, class 2 from 1.4 to 3, and class 3 from 1.8 to more than 5. Sinuosities of more than 3 characteristically are associated with mountain fronts that are so embayed and pedimented that the range-bounding tectonic structure initially responsible for the mountain front may be more than 1 km from the present erosional front.

| Class of Relative Tectonic Activity | Local base level processes: u, uplift; w, channel downcutting; s, piedmont deposition; e, piedmont erosion; t, time. | Typical landform |
|---|---|---|
| 1. Active | $\Delta u/\Delta t \geq \Delta w/\Delta t + \Delta s/\Delta t$ | Alluvial fan that is receiving deposits on fanhead |
| 2. Slight | $\Delta u/\Delta t < \Delta w/\Delta t > \Delta e/\Delta t$ | Entrenched alluvial fan with old soils on fanhead |
| 3a. Inactive | $\Delta u/\Delta t << \Delta w/\Delta t > \Delta e/\Delta t$ | Dissected pediment or pediment terraces |
| 3b. Inactive | $\Delta u/\Delta t << \Delta w/\Delta t = \Delta e/\Delta t$ | Undissected pediment |
| 3c. Inactive | $\Delta u/\Delta t << \Delta w/\Delta t < \Delta e/\Delta t$ | Undissected pediment |

*Table 1. Mountain Front Tectonic Activity Classes (from Bull, 1973).*

The sinuosities for the mountain fronts of the study area are summarized in Table 2. They range from 1.2 to 7.2. The mean mountain-front sinuosities are 2.1, 4.1 and 3.8 for the northern, transitional and southern subareas respectively and the difference between the northern and southern sub-

| Mountain Front and Direction Front Faces | Mountain-Front Sinuosity | Mean Valley Morphologies Valley Floor Width/Valley Height Ratio ($V_f$) | Tectonic Activity Class* |
|---|---|---|---|
| NORTHERN SUBAREA | | | |
| Black Mountains W1[1] | 1.4 | 0.2[3] | 1 |
| Black Mountains W2[1] | 3.1 | 2.0 | 2 |
| Panamint Range E1 | 3.4 | 1.1 | 2 |
| Panamint Range E2 | 2.9 | 1.5 | 2 |
| Panamint Range W1[1] | 1.6 | 0.055[3] | 1 |
| Slate Range E | 1.8 | 2.3 | 2 |
| Slate Range W | 1.4 | 0.3[3] | 1 |
| Argus Range E1[1] | 2.5 | 3.6 | 2 |
| Argus Range E2[1] | 2.0 | 2.0 | 2 |
| Argus Range W1[1] | 1.2 | 0.9 | 1 |
| Argus Range W2[1] | 1.5 | 0.5[3] | 2 |
| TRANSITIONAL SUBAREA | | | |
| Panamint Range E3 | 3.5 | 8.4 | 3 |
| Panamint Range W2 | 2.9 | [2] | 3 |
| Slate Range S | 4.0 | 3.0 | 3 |
| Argus Range E3[1] | 4.1 | 6.2 | 3 |
| Argus Range W3[1] | 7.2 | 2.5 | 3 |
| Argus Range S[1] | 2.6 | 10.0 | 3 |
| SOUTHERN SUBAREA | | | |
| Granite Mountains N | 2.7 | 3.1 | 3 |
| Granite Mountains S | 3.4 | 4.0 | 3 |
| Tiefort Mountains S | 3.0 | 3.7 | 3 |
| Eagle Crags E | 1.8 | 2.1 | 3 |
| Eagle Crags W | 6.0 | 47.0 | 3 |
| Robbers Mountains N | 6.5 | 2.9 | 3 |
| Pilot Mountain E | 3.4 | 3.9 | 3 |
| Pilot Mountain W | 3.6 | 12.0 | 3 |

[1] *Mountain-front sinuosities derived from 1:250,000 scale 1° x 2° California Division of Mines Geologic Sheet.*

[2] *No major drainage basins along mountain front, therefore no $V_f$ values obtained.*

[3] *$V_f$ value is a maximum, width of valley floor <100 meters.*

* *See Table 1.*

*Table 2. Geomorphic Data for the Mountain Fronts*

areas is signficant at the .005 level (i.e. $\alpha = .005$). The mountain front is considered to coincide with the range-bounding geologic structure only for the class 1 fronts. For the class 3 fronts of the southern subarea, there are few geomorphic clues as to the locations of possible range-bounding structure that have been tectonically active in the past.

Valley Floor Width - Valley Height Ratio

Obvious differences in the transverse morphologies of valleys, such as v-shaped canyons and broad-floored pediment embayments can be described by a simple ratio, the valley floor width-valley height ratio. At a given distance upstream from the mountain front (1 km in this study), comparison of the width of the floor of the valley with the mean height of the valley, provides an index that indicates whether the stream is actively downcutting (being dominated by the influence of a base level fall at some point downstream) or is primarily eroding laterally into the adjacent hillslopes. If we let $V_{fw}$ be the width of the valley floor, and $E_{ld}$, $E_{rd}$, and $E_{sc}$ be the altitudes of the left and right divides and the stream respectively, then the valley floor width-valley height ratio ($V_f$) is defined as,

$$V_f = \frac{V_{fw}}{\frac{(E_{ld} - E_{sc}) + (E_{rd} - E_{sc})}{2}} . \qquad (3)$$

The location of the cross-valley transect within a drainage basin affects the values of $V_f$. Valley floors tend to become progressively narrower upstream from the mountain front and for a given stream system the values of $V_f$ tend to become progressively larger downstream from the headwaters. In this study the transects for determining $V_f$ were located 1 km upstream from the mountain front in the larger drainage basins for a given mountain range. The reason for working with a selected size range of drainage basins is that smaller streams tend to maintain the downcutting mode of operation longer than the more competent larger streams.

The dimensions for $V_f$ vary in their ease of measurement. Detailed topographic quadrangles provided accurate determinations of the altitudes of the divide above the stream channel, but the width of the valley floor could not be measured with equal accuracy, even where well defined by the topographic maps. In the narrow canyons that are typical of class 1 mountains, only maximum values of valley floor width could be estimated, which resulted in maximum values of $V_f$. However, even when one uses conservative methods, such as maximum values, highly significant differences in $V_f$ are present for the suites of mountain ranges north and south of the Garlock fault.

The valley floor width-valley height ratios are summarized in Table 2. They range from about 0.05 to 47. The mean ratios are 1.3, 6.1, and 11.0 for the northern transitional, and southern subareas, respectively; and the difference between the northern and southern subareas is significant at the .01 level. In the canyons of the class 1 landscapes the floodplain width and the valley-floor width are the same, but in class 2 valleys the floodplain width is less than the valley floor width. In class 3 terrains the ratio describes pediment embayments of the broad valleys upstream from the embayments. Drainage basins were best defined for class 1 fronts, while along some class 3 fronts, the scattered inselbergs so poorly defined mountainous drainage basins that no ratios were computed (see Figures 4 and 6). For most of the fronts, ratios were computed for one or two drainage basins, and for Robbers Mountain (north), three measurements were made.

## Drainage Basin Shape

The lack of well defined drainage basins in some of the class 3 terrains precluded extensive comparisons of drainage basin shape, but basin shape was compared for those drainage basins that extend from the divide to the mountain fronts on the east and west sides of the central Panamint Range.

*Figure 4. Class 1 mountain front on the west side of the Panamint Range at Redlands Canyon.*

The migration of drainage basin divides that occurs as adjacent basins compete for space results in planimetric shapes that can be described quantitatively. The typical basin of a tectonically active mountain range is elongate (Davis, 1909, p. 343) and basin shapes become progressively more circular with time after cessation of mountain uplift. The planimetric shape of a basin may be described by an elongation ratio (Cannon, 1976). (4)

$$Re = \frac{\text{diameter of circle with the same area as the basin}}{\text{distance between the two most distant points in basin}}$$

Although the Panamint Range is a block that has been tilted eastward (Maxson, 1950; Hunt and Mabey, 1966; Drewes, 1963; Denny, 1965 and Hooke, 1972), the drainage divide between the east and west flowing streams is in the central part of the range. The western margin of the range is a class 1 front, and the eastern margin is a class 2 front. The elongation ratios range from 0.39 to 0.65 (mean is 0.53) for the west-side basins, and from 0.66 to 0.74 (mean is 0.69) for the east-side basins. The difference between the means is significant at the .01 level. Drainage basin widths are much narrower near the mountain front on the tectonically active west side where the streams have directed much of their energies to downcutting. Apparently the lack of continuing rapid uplift along the east side has permitted widening of the basins upstream from the mountain front and the production of well-developed straths that extend far into the mountain range along the main streamcourses.

## QUATERNARY TECTONIC ACTIVITY OF THE MOUNTAIN FRONTS

The mountain fronts of the study area were assigned to appropriate relative tectonic activity classes (see Table 1) on the basis of, (1) the mountain-front sinuosities and valley floor width-valley height ratios, and (2) other features (such as entrenched or unentrenched alluvial fans) which were observed during trips to the study area and on flights over the area. All of the mountain fronts are considered to be class 3 except in the northern subarea where

four class 1 and seven class 2 fronts are present.

A typical class 1 landscape is shown in Figure 4. The rugged, narrow drainage basins have V-shaped cross-valley profiles and the valley floors are the same width as the floodplains. The canyons are being downcut into the Paleozoic sediments and are notched into an eroded fault scarp that comprises an unembayed mountain front. Thick alluvial fans are actively accumulating on the piedmont immediately downstream from the escarpment. This is an example of the type of landscape sketched in Figure 3.

An example of a class 2 terrain in granitic rocks is shown in Figure 5. Although rugged, the cross-valley profile of Wilson Canyon is more U-shaped than V-shaped. An embayment extends upstream from the topographic escarpment that marks the mountain front, and the terraces upstream from the embayment are clear evidence that the floodplain is much narrower than the valley floor. A fault scarp is not apparent and the embayments have created a more sinuous mountain front than probably was formerly present.

The unentrenched alluvial fan downslope from the mountain front shown in Figure 5 should not be considered as evidence for a class 1 front, particularly in view of the types of landscape elements noted above. The unentrenched nature of the fan is the result of the impact of the Pleistocene-Holocene climatic change on a rock type that is sensitive to climatic perturbations (Bull, 1976). Late Pleistocene climates in the Argus range were more conducive to denser plant growth on the hillslopes and for weathering of the hillslope materials than Holocene climates. The postulated decrease in vegetative density during the early Holocene resulted in rapid erosion of the unprotected materials on the slopes. Granitic colluvium responds more rapidly to such a perturbation because lower stresses are needed to move grus-size particles than blocks of rock that would be weathered from most metamorphic rocks. The resulting increase in sediment yield completely backfilled any entrenched stream channels in the valley or on the alluvial fan. In Homewood Canyon, 9 km to the north of Wilson Canyon

*Figure 5. Class 2 mountain front on the east side of the Argus Range at Wilson Canyon.*

the same sequence of events has occurred. The stratigraphy exposed in a streambank in the valley of Homewood Canyon consists of well-sorted, reddish-brown, clayey grus of apparent Pleistocene age that is overlain by 2 m of gray bouldery grus of apparent Holocene age. With continuing decreases in the amounts of colluvium left on the hillslopes during the Holocene, the stream systems in both drainage basins have changed their mode of operation and now are downcutting through the alluvium that accumulated on the valley floors.

Mountains that are typical of the class 3 landscape south of the Garlock fault are shown in Figure 6. In contrast to the class 1 setting of the Panamint Range, the topographic highs tend to be occupied by rock types that are resistant to weathering and erosion. Large drainage basins with mountainous areas are hard to define, and the defining of topographic mountain fronts that extend for more than 10 km can be made only on a highly subjective basis. Much of the terrain consists of inselbergs and small mountain masses that are spaced in such a way as to suggest the absence of larger intermontane valleys. Stream systems tend to be discontinuous, and the presence of dune sand on the west sides of some mountains is an additional complication in studying the fluvial systems.

A most useful parameter for assessing the relative tectonic activity of a given mountain front is the thickness of deposits in the basin immediately downslope from an escarpment. Alluvial fans that are thicker than 100 m most likely are the result of a tectonic perturbation, rather than being caused by climatic variations such as were described for the Argus Range. Class 3 terrains may have virtually no basin deposits next to the mountains or may have fans as thick as 10 m that are the result of climatic perturbations. Unfortunately, alluvium thickness data are difficult to obtain, the best sources being from boreholes, entrenched stream channels, and geophysical surveys.

A gravity map of much of the study region (Nilsen and Chapman, 1971) shows anomalies in the basins north of the

*Figure 6. Class 3 terrain southeast of the Tiefort Mountains. Soda Mountains are in the background.*

Garlock fault that are indicative of great thicknesses of deposits. South of the fault, gravity anomalies appear to be minor and are chiefly the result of local variations in the density of surficial rock types. Both the geomorphic and geophysical evidence suggest that the southern subarea may be a batholith with low relief that is capped locally with metasedimentary, volcanic, and Cenozoic terrestrial rocks. Quaternary faulting is minor or absent in the southern subarea. One exception appears to the north side of the Tiefort Mountains (Figure 1). Here a 7 km long, straight mountain front trends east-west and is associated with small V-shaped canyons and alluvial fans. This minor class 1 front may be a product of the stress field associated with either the Garlock fault, and/or the zone of northwest trending right-lateral strike-slip faults in the central Mojave Desert.

Another useful type of data is the age of the oldest alluvium downslope from the mountains. Active deposition of alluvial fans next to the mountains is indicative of class 1 tectonic conditions, except where such deposition has been caused by climatic perturbations (Figure 5). The presence of older alluvium next to the mountains provides clues as to the length of time that has passed since class 1 conditions last prevailed. Within the arid parts of the study area, Holocene soils lack the argillic horizons that are so common on the late and middle Pleistocene geomorphic surfaces. Early Pleistocene geomorphic surfaces generally have been dissected into a ridge and ravine topography that is not conducive to the preservation of soil profiles for long periods of time.

The oldest alluvium associated with class 1 fronts generally is of Holocene age. Late to mid-Pleistocene piedmont alluvium is associated with most class 2 fronts and patches of early Pleistocene alluvium in pediment embayments are typical of the class 3 fronts. Any front that is associated with a granitic drainage basin may have a piedmont that is dominated by Holocene alluvium, because of the sensitivity of granitic rocks to climatic variations.

## Areal Variations in Quaternary Tectonism

Pronounced contrasts in the rates and magnitudes of Quaternary uplift are reflected in the landscapes north and south of the Garlock fault. The northern subarea is the southern extent of one of the most tectonically active regions in North America. Class 1 and class 2 mountain fronts are typical of the northern subarea (Table 2) where the Panamint Range rises to more than 3200 m and Death Valley has been depressed to below sea level. In addition to the tilting of the fault blocks, the mean altitude of the northern subarea may be higher than the transitional subarea (significant at $\alpha = 0.20$). Hooke (1972) uses geomorphic criteria to estimate a maximum possible uplift rate for the west front of the Black Mountains at 7 m per 1,000 years, and Quaternary studies by Smith (1975) indicate that the central part of Panamint Valley is the most active tectonically. Fault scarps and faults in the piedmont alluvium also are common in the northern subarea (Hunt and Mabey, 1966; Smith and others, 1968).

Although the Garlock fault marks the southern extent of the prominent north-south structural blocks (see Figure 2) that have been associated with the extensional tectonics of the Basin and Range Province, the magnitudes of Quaternary uplift do not change abruptly at the fault. The north-south mountain fronts north of the Garlock fault have morphologies that reveal decreasing magnitudes of Quaternary uplift toward the south (see Table 2). Within the northern subarea the class 1 fronts change to class 2 fronts, which then change to the class 3 fronts of the transitional subarea. The north-south decrease in uplift rates is most apparent for the Argus Range block, which consists almost entirely of granitic rocks that are susceptible to pedimentation. The fact that the general locations of the mountain fronts are still discernible in the transition subarea, but are extremely poorly defined in the southern subarea is suggestive that the southern subarea has been even more inactive tectonically during the late Cenozoic

than the transitional subarea.

Another conclusion is that the general model of the Garlock fault being the result of extensional tectonics to the north of the fault may be too simple. A more complete model is needed to explain the north to south decrease in Quaternary uplift along the mountain fronts north of the fault, and the possibly greater mean altitudes of the northern subarea.

## REFERENCES CITED


Bull, W. B., 1973, Local base-level processes in arid fluvial systems: Geol. Soc. America Abstracts with Programs, v. 5, p. 562.

_____, 1976, Sensitivity of fluvial systems in hot deserts to climatic change: American Quat. Assoc. 4th Biennial Conf., discussant paper, p. 42-43.

Cannon, P. J., 1976, Generation of explicit parameters for a quantitative geomorphic study of the Mill Creek Drainage Basin: Oklahoma Geology Notes, v. 36 , no. 1, p. 3-16.

Davis, G. A., and Burchfiel, B. C., 1973, Garlock fault; an intracontinental transform structure, southern California: Geol. Soc. America Bull., v. 84, p. 1407-1422.

Davis, W. M., 1909, Geographical Essays, New York, Dover Publications, 777 p.

Denny, C. S., 1965, Alluvial fans in the Death Valley region, California and Nevada: U. S. Geol. Survey Prof. Paper 466, 62 p.

Drewes, Harald, 1963, Geology of the Funeral Peak quadrangle, California: U. S. Geol. Survey Prof. Paper 413, 78 p.

Hamilton, Warren, and Myers, W. B., 1966, Cenozoic tectonics of the western United States: Rev. Geophysics, v. 4, p. 509-549.

Hooke, R. LeB., 1972, Geomorphic evidence for late-Wisconsin and Holocene tectonic deformation, Death Valley, California: Geol. Soc. America Bull., v. 83, p. 2073-2098.

Hunt, C. B., and Mabey, D. R., 1966, Stratigraphy and structure Death Valley, California: U. S. Geol. Survey Prof. Paper 494-A, 162 p.

Jennings, C. W., (compiler), 1953, Death Valley sheet: California Div. Mines and Geology Map Sheet, scale, 1:250,000.

_____, Burnett, J. L., and Troxel, B. W., (compilers), 1962, Trona sheet: California Div. Mines and Geology Map sheet, scale, 1:250,000.

Maxson, J. H., 1950, Physiographic features of the Panamint Range, California: Geol. Soc. America Bull., v. 61, p. 99-114.

Nilsen, T. H., and Chapman, R. H. (compilers), 1971, Bouger gravity map of California, Trona Sheet: California Div. Mines and Geology Map Sheet, scale, 1:250,000.

Smith, G. I., 1962, Large lateral displacement on Garlock Fault, California, as measured from offset dike swarm: Am. Assoc. Petrol. Geologists Bull., v. 46, p. 85-104.

_____, Troxel, B. W., Gray, C. H., Jr., and von Huene, R. E., 1968, Geologic reconnaissance of the Slate Range, San Bernardino and Inyo Counties, California: California Div. Mines and Geology Spec. Rept. 96, 33 p.

_____, and Ketner, K. B., 1970, Lateral displacement on the Garlock fault, southeastern California, suggested by offset sections of similar metasedimentary rocks: U. S. Geol. Survey Prof. Paper 700-D, p. 1-9.

Smith, R. S. U., 1975, Late-Quaternary pluvial and tectonic history of Panamint Valley, Inyo and San Bernardino Counties, California: California Institue of Technology Unpub. Ph.D. Dissertation, 295 p.

Wright, L. A., and Troxel, B. W., 1967, Limitations on right-lateral strike-slip displacement, Death Valley and Furnace Creek fault zones, California: Geol. Soc. America Bull., v. 78, p. 933-950.

# APPENDIX K

## QUATERNARY SURFACE MAPPING

BY

LOUIS H. FLEISCHHAUER

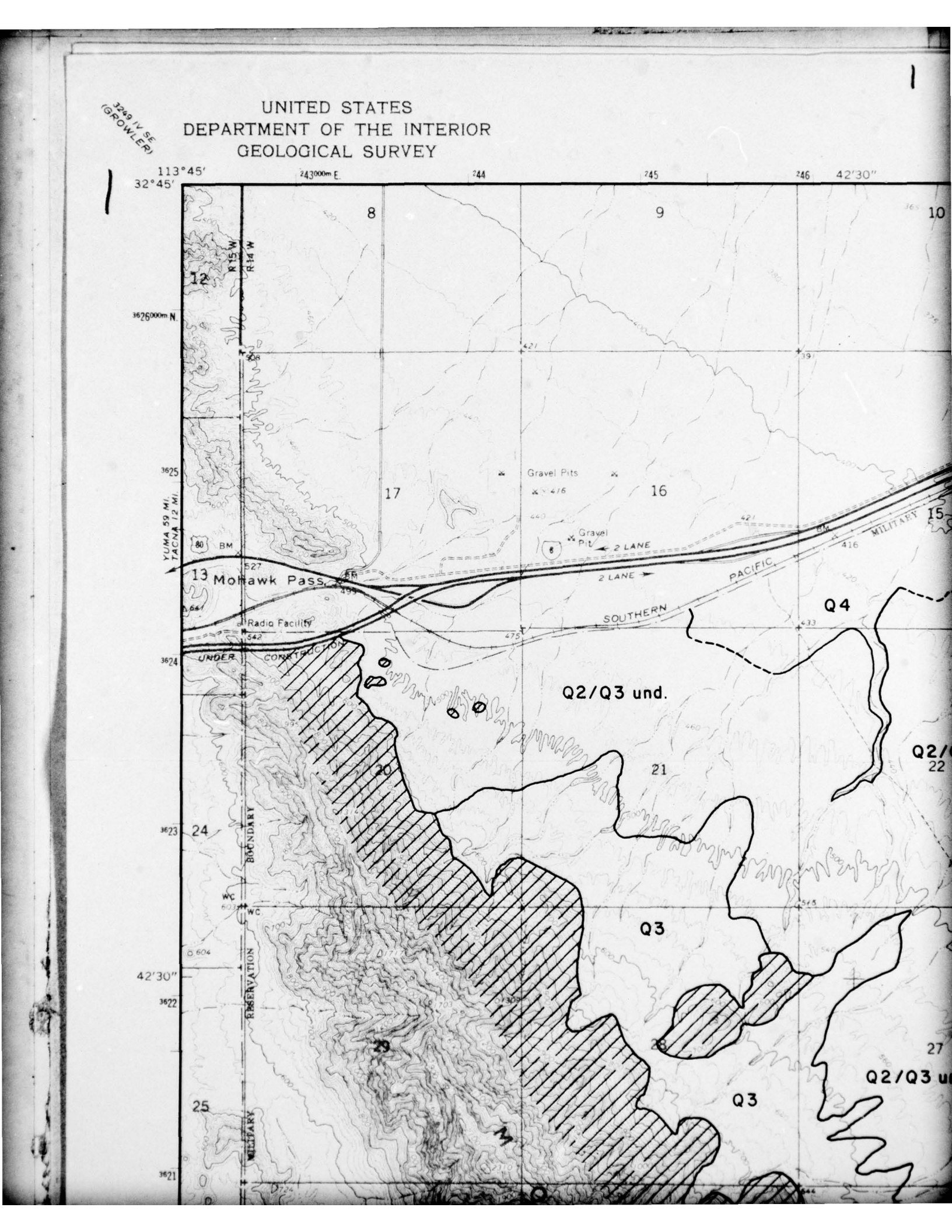
3249 IV SE (GROWLER)
UNITED STATES
DEPARTMENT OF THE INTERIOR
GEOLOGICAL SURVEY
113°45'
32°45'
243000m E.
244
245
246
42'30"
3626000m N.
3625
3624
3623
42'30"
3622
3621
R15W
R14W
8
9
10
12
17
16
15
13
24
25
Gravel Pits
Gravel Pit
2 LANE
2 LANE
MILITARY
PACIFIC
SOUTHERN
Mohawk Pass
Radio Facility
UNDER CONSTRUCTION
YUMA 59 MI.
TACNA 12 MI.
BM
80
8
INTERNATIONAL BOUNDARY
WC
RESERVATION
MILITARY
Q4
Q2/Q3 und.
Q3
Q3
Q2/Q3 u
20
21
22
27
29
28

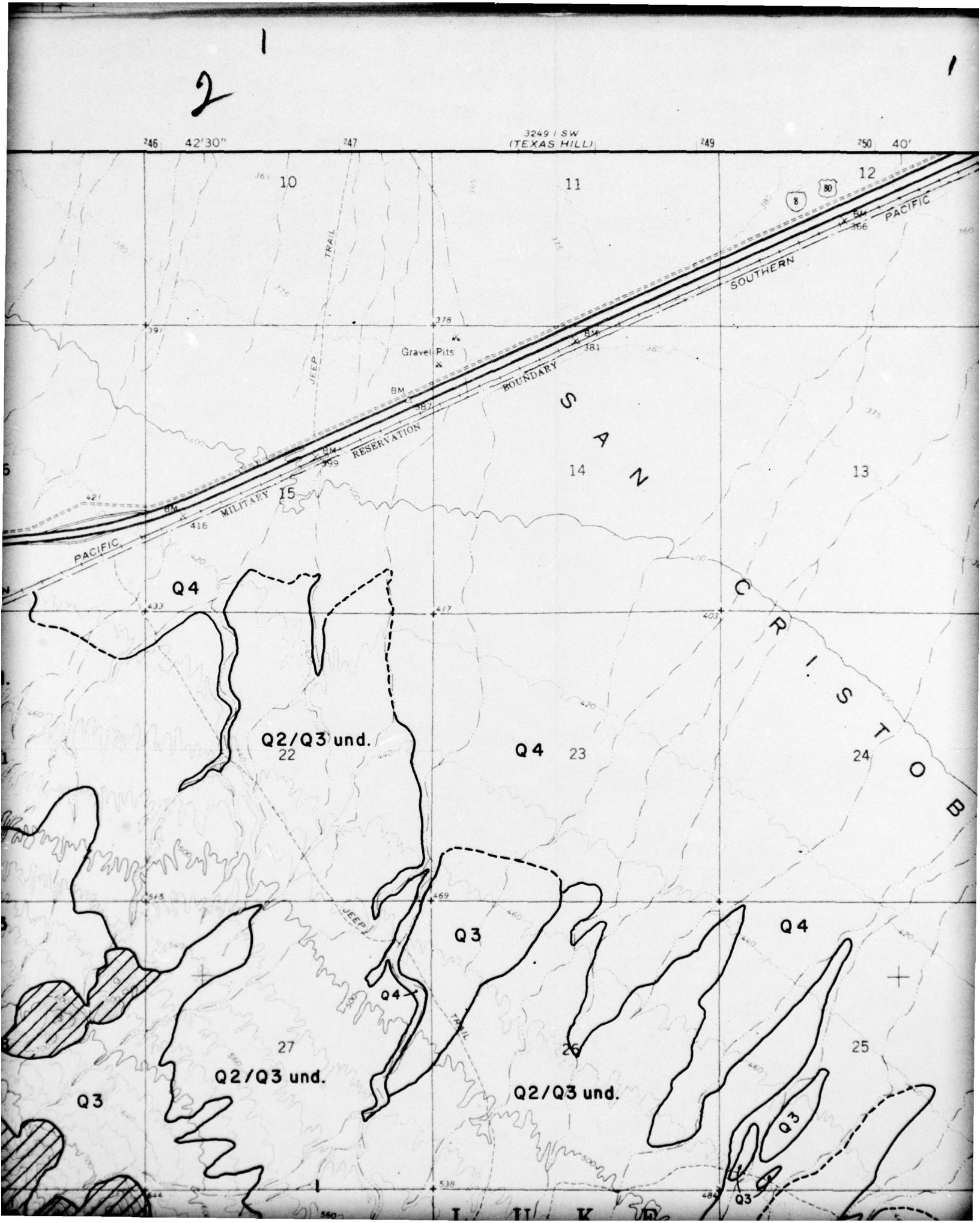
3249 I SW
(TEXAS HILL)
246
42'30"
247
249
250
40'
10
11
12
13
14
15
22
23
24
25
26
27
TRAIL
JEEP
SOUTHERN
PACIFIC
BOUNDARY
MILITARY
RESERVATION
Gravel Pits
BM
SAN CRISTOBAL
Q4
Q2/Q3 und.
Q3
Q4
Q2/Q3 und.
Q2/Q3 und.
Q3
Q3

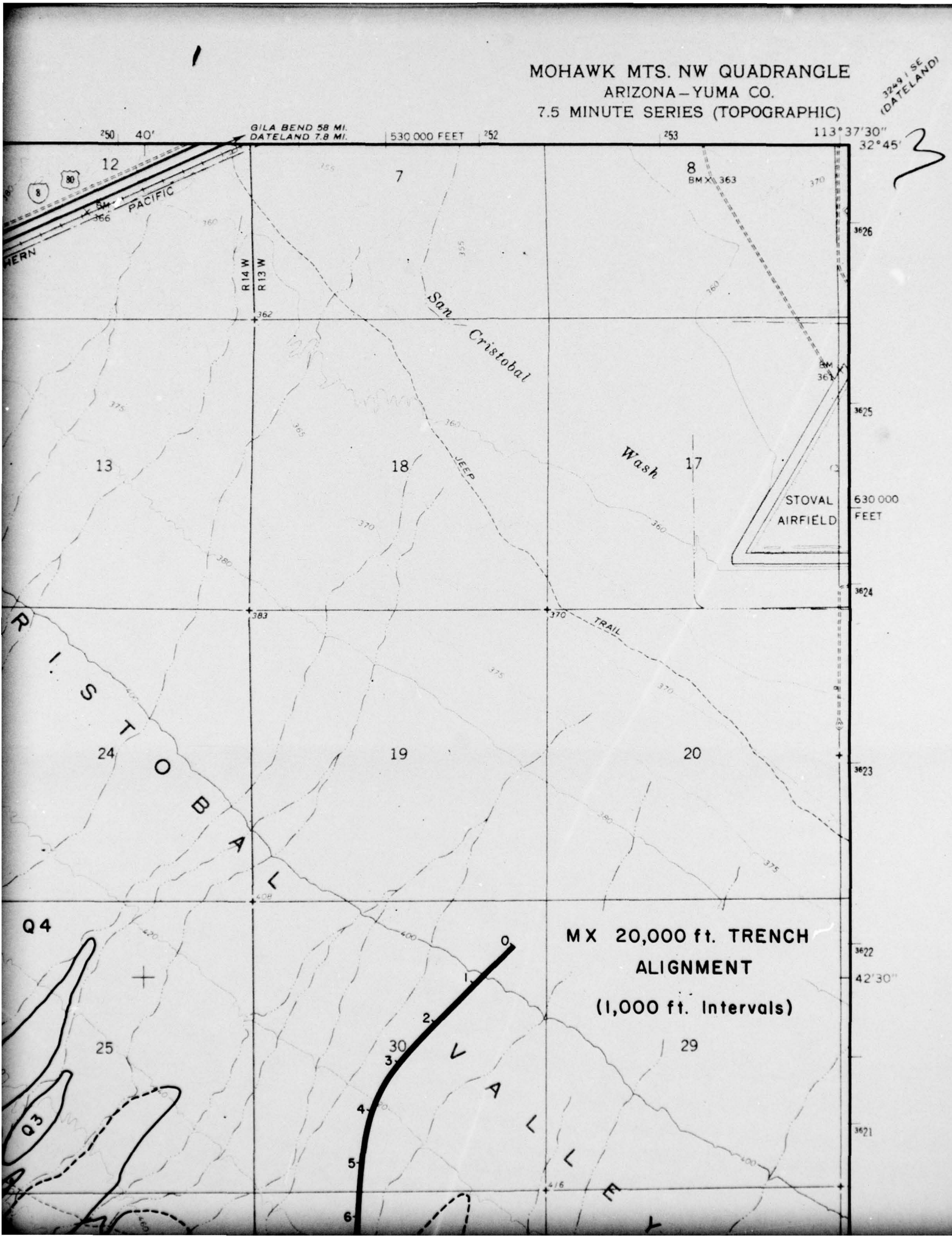
MOHAWK MTS. NW QUADRANGLE
ARIZONA – YUMA CO.
7.5 MINUTE SERIES (TOPOGRAPHIC)
3249 I SE (DATELAND)
GILA BEND 58 MI.
DATELAND 7.8 MI.
530 000 FEET
113°37'30"
32°45'
40'
R14W
R13W
PACIFIC
SOUTHERN
San Cristobal
Wash
JEEP TRAIL
STOVAL AIRFIELD
630 000 FEET
SAN CRISTOBAL VALLEY
MX 20,000 ft. TRENCH ALIGNMENT
(1,000 ft. Intervals)
0
1
2
3
4
5
6
Q4
Q3
12
7
8
BM X 363
13
18
17
24
19
20
25
30
29
3626
3625
3624
3623
3622
3621
42'30"

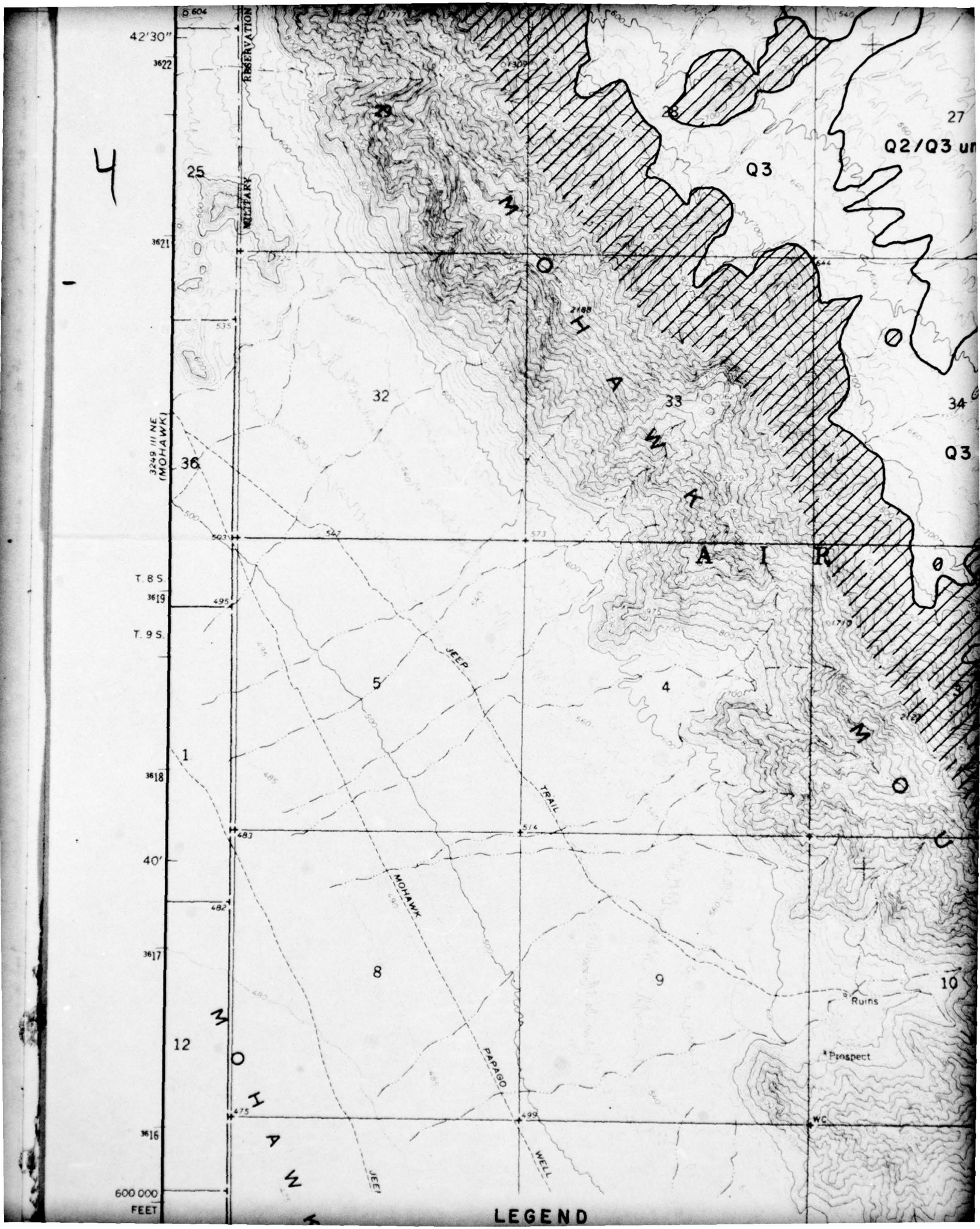
42'30"
3622
3621
3620
T. 8 S.
3619
T. 9 S.
3618
40'
3617
3616
600 000 FEET
RESERVATION
MILITARY
3249 III NE (MOHAWK)
25
32
33
34
36
5
4
1
8
9
12
10
27
Q3
Q2/Q3 ur
Q3
MOHAWK
HAWAIIAN
JEEP TRAIL
MOHAWK
PAPAGO
JEEP
WELL
Ruins
Prospect
WC
LEGEND


Q3
Q4
Q2/Q3 und.
Q2/Q3 und.
Q3
Q4
L U K E
A I R F O R C E R A N G E
Q3
Q2/Q3 und.
Q2
Q3
Q2?
Q3
Q4
Q4
Q3
Q2
Q3
Q2/Q3 und.
Q4
Q2
Q2/Q3 und.
Q3
Q3
M O U N T A I N S
Ruins
Prospect
Q3
Q2/Q3 und.
Q3
Q4
JEEP
TRAIL
JEEP
27
26
25
34
35
36
10
11
12
1
2
3
C
D
12
13
14
15
16
17
18
19
20

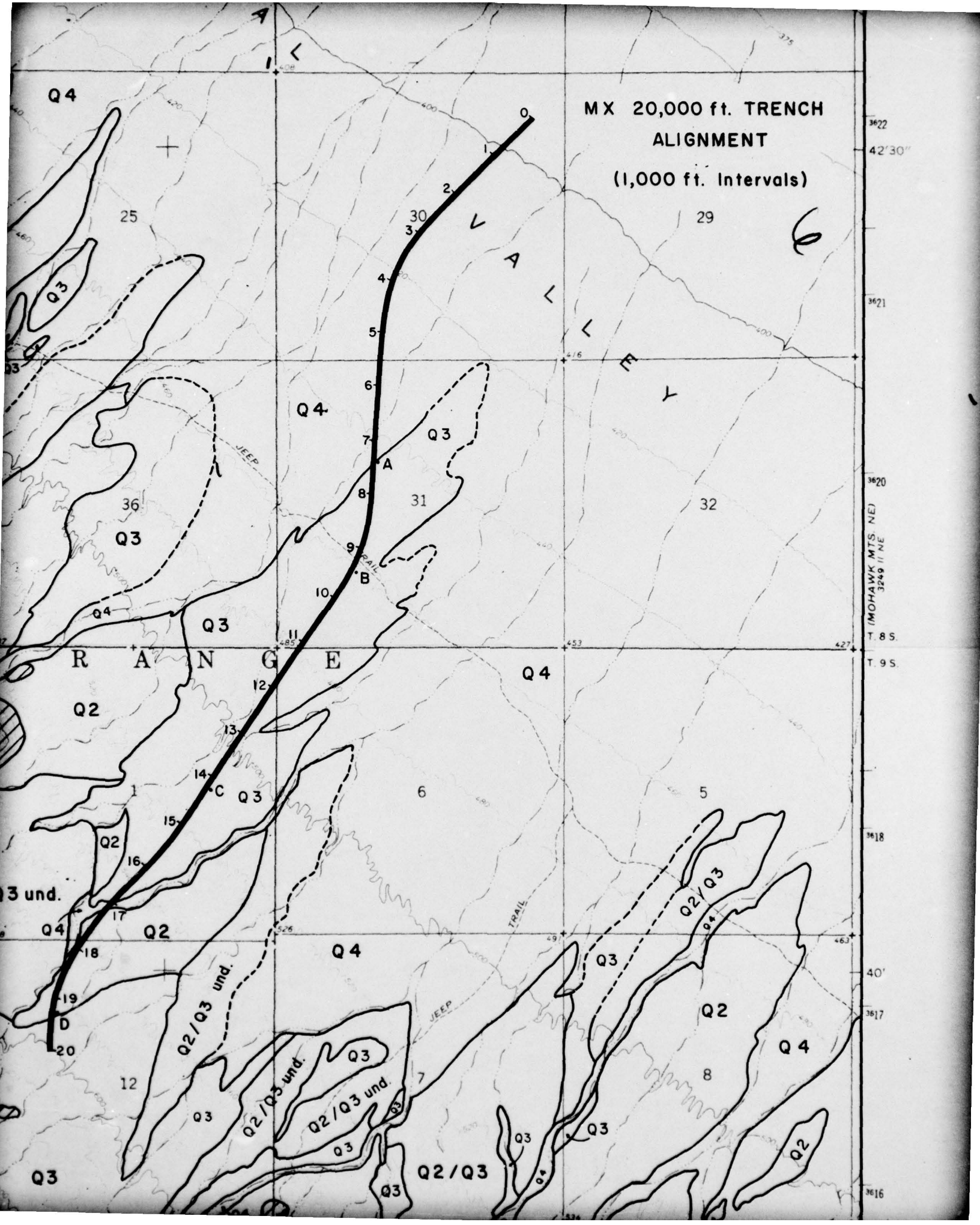
MX 20,000 ft. TRENCH ALIGNMENT
(1,000 ft. Intervals)
0
1
2
3
4
5
6
7
8
9
10
11
12
13
14
15
16
17
18
19
20
A
B
C
D
VALLEY
RANGE
Q4
Q3
Q2
Q2/Q3
Q2/Q3 und.
Q3 und.
JEEP TRAIL
TRAIL
25
30
29
36
31
32
1
6
5
12
7
8
T. 8 S.
T. 9 S.
3622
42'30"
3621
3620
3618
40'
3617
3616
T (MOHAWK MTS. NE)
3249 II NE

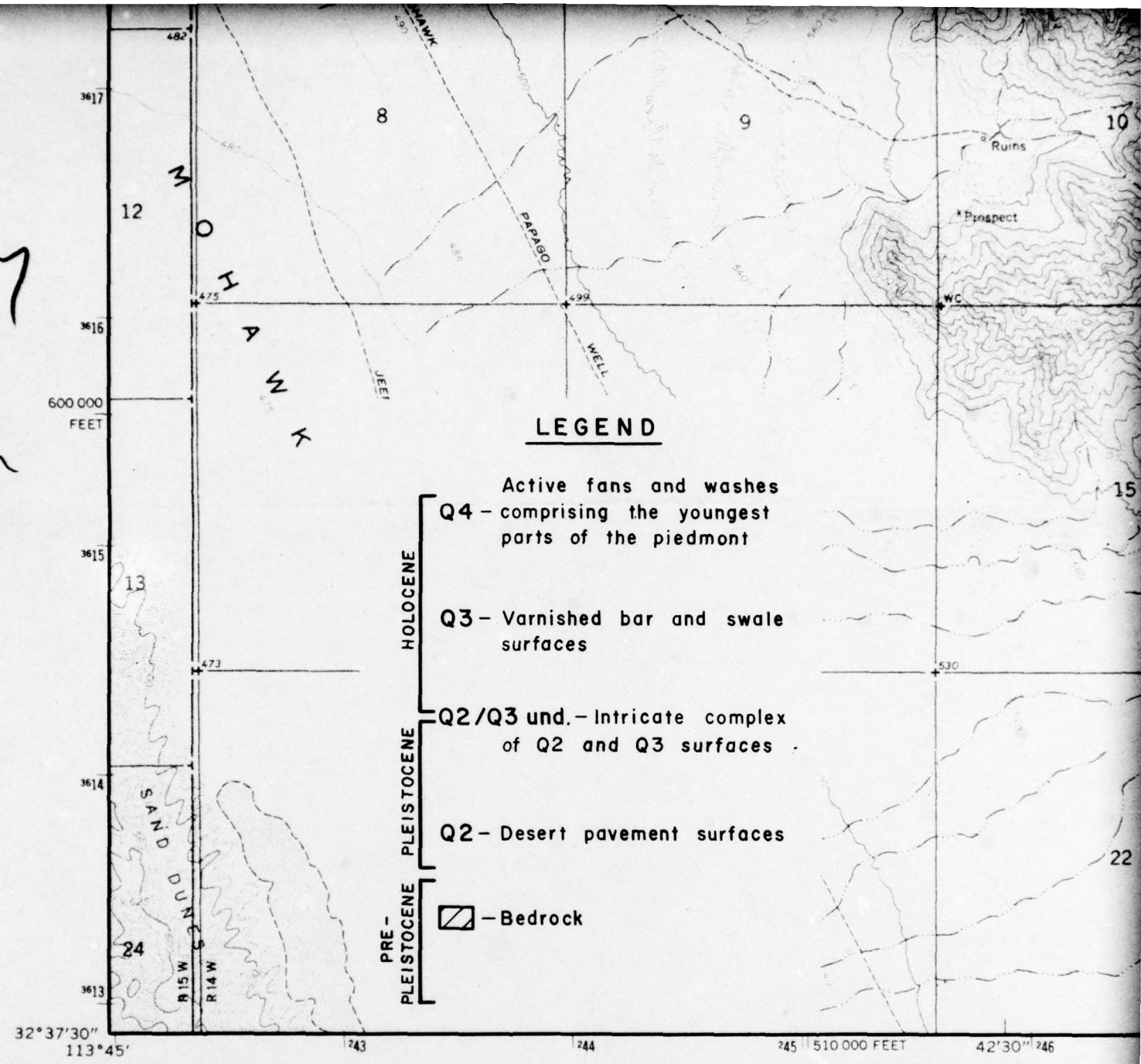


(MOHAWK SE)
3249 III SE

Mapped, edited, and published by the Geological Survey

Control by USGS and USC&GS

Topography by photogrammetric methods from aerial photographs taken 1961. Field checked 1965

Polyconic projection. 1927 North American datum
10,000-foot grid based on Arizona coordinate system, west zone
1000-meter Universal Transverse Mercator grid ticks,
zone 12, shown in blue

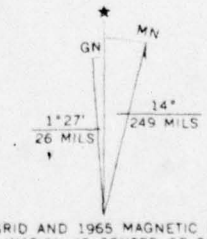


UTM GRID AND 1965 MAGNETIC NORTH
DECLINATION AT CENTER OF SHEET

**APPENDIX - K**

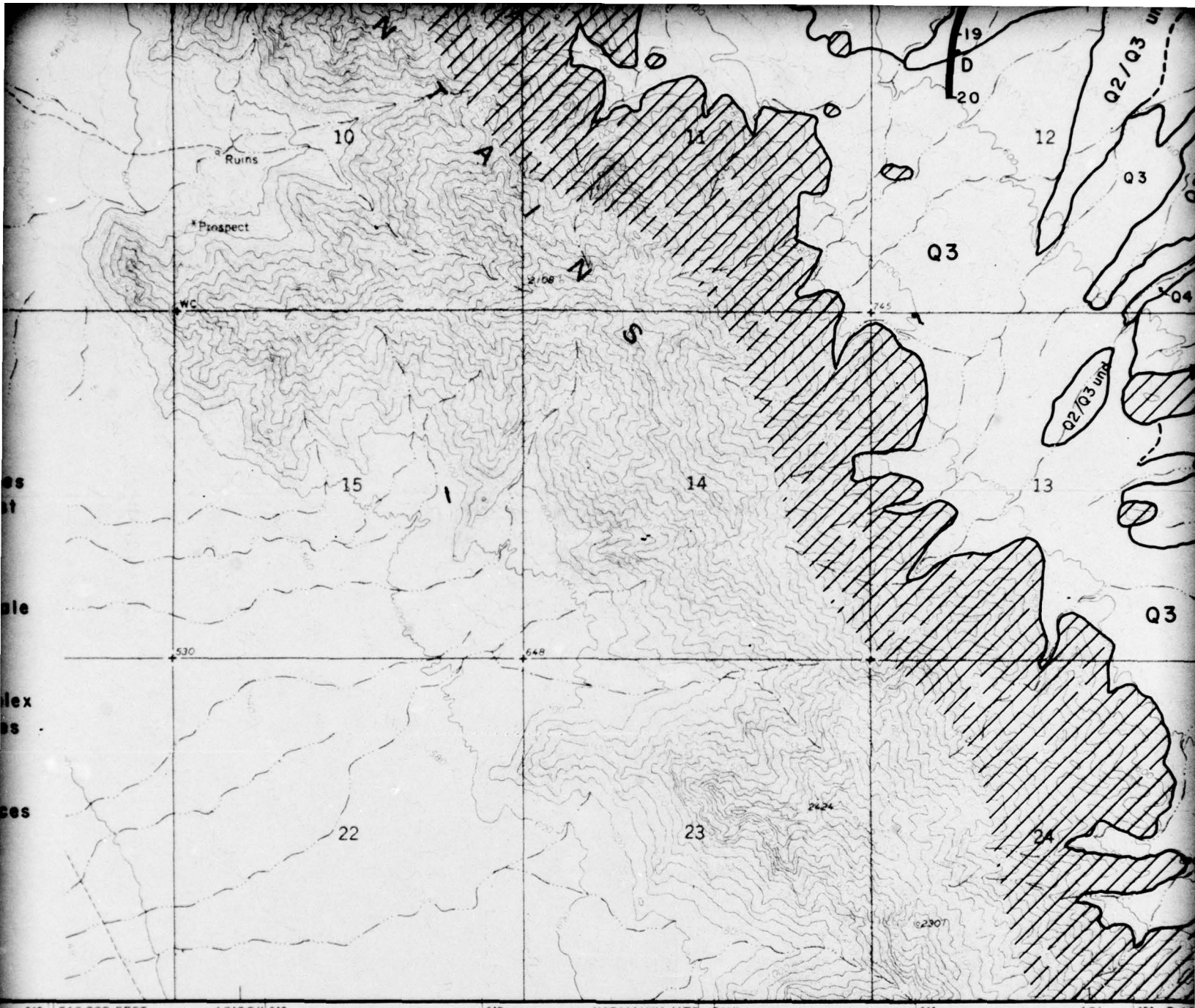


245 | 510 000 FEET | 42'30" | 246 | 247 | (MOHAWK MTS. SW) 3249 II SW | 249 | 40' | 250 R. 14

SCALE 1:24 000

1 0 1 MILE

1000 0 1000 2000 3000 4000 5000 6000 7000 FEET

1 .5 0 1 KILOMETER

CONTOUR INTERVAL 20 FEET
DOTTED LINES REPRESENT 5-FOOT CONTOURS
DATUM IS MEAN SEA LEVEL

GN MN

1°27' 26 MILS | 14° 249 MILS

RID AND 1965 MAGNETIC NORTH
INATION AT CENTER OF SHEET

THIS MAP COMPLIES WITH NATIONAL MAP ACCURACY STANDARDS
FOR SALE BY U. S. GEOLOGICAL SURVEY, DENVER, COLORADO 80225, OR WASHINGTON, D. C. 20242
A FOLDER DESCRIBING TOPOGRAPHIC MAPS AND SYMBOLS IS AVAILABLE ON REQUEST

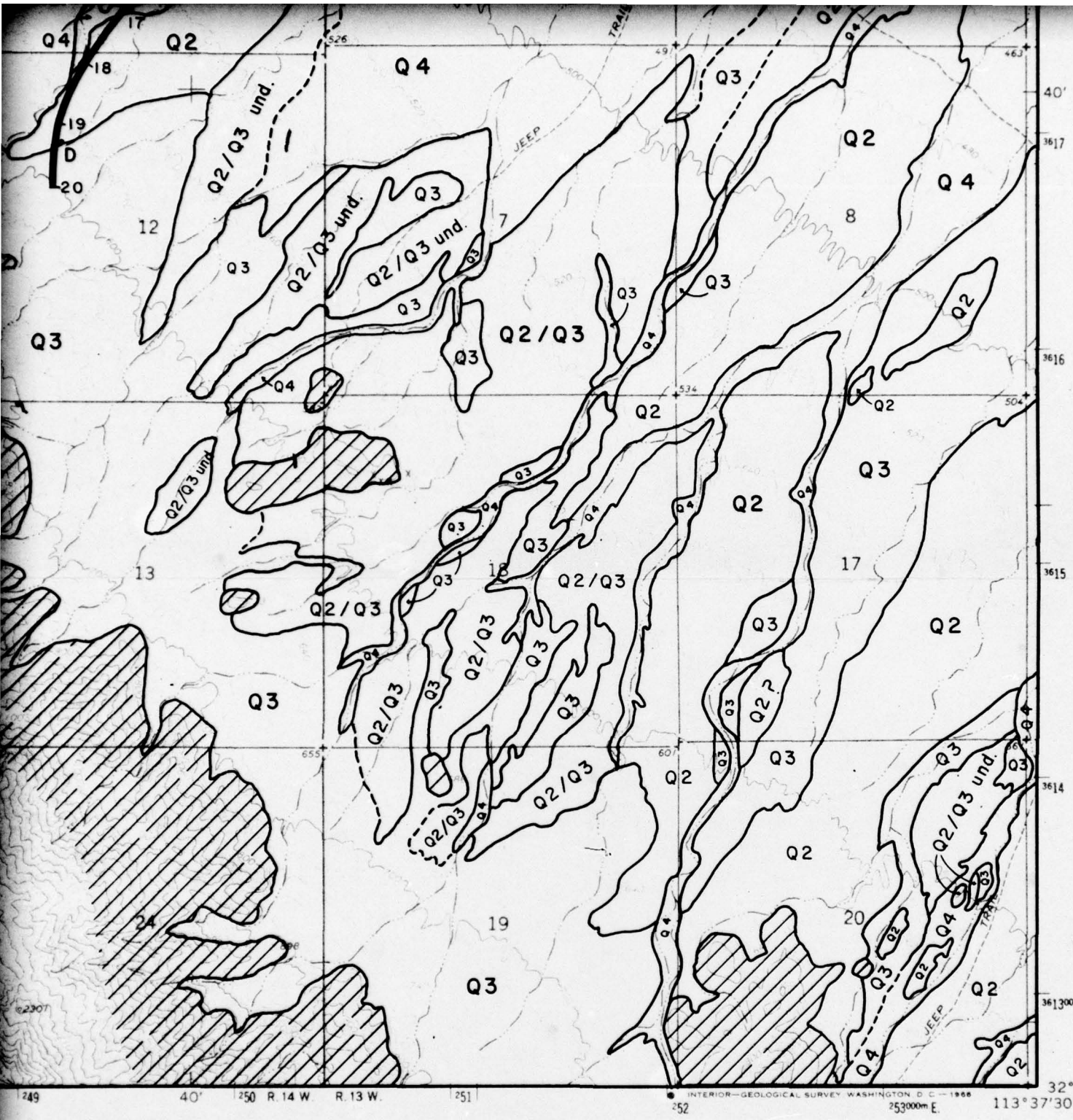


249 40' 250 R. 14 W. R. 13 W. 251 252 253000m E.

INTERIOR—GEOLOGICAL SURVEY, WASHINGTON, D. C.—1968

32°37'30"

113°37'30"

1 MILE

7000 FEET

ILOMETER

ROAD CLASSIFICATION

Heavy-duty ——— Light-duty ═══

Unimproved dirt - - - - - -

Interstate Route ⬡ U. S. Route

(MOHAWK MTS. SE)
3249 II SE

ARIZONA

QUADRANGLE LOCATION

HINGTON, D. C. 20242
REQUEST

# MOHAWK MTS. NW, ARIZ.

N3237.5—W11337.5/7.5

1965

AMS 3249 II NW—SERIES V898

9

1